



This work is protected by copyright and other intellectual property rights and duplication or sale of all or part is not permitted, except that material may be duplicated by you for research, private study, criticism/review or educational purposes. Electronic or print copies are for your own personal, non-commercial use and shall not be passed to any other individual. No quotation may be published without proper acknowledgement. For any other use, or to quote extensively from the work, permission must be obtained from the copyright holder/s.

# Outflows from galaxy nuclei: dynamics and implications for scaling relations

Rachael C. McQuillin  
BSc Hons

Doctor of Philosophy

Department of Physics, University of Keele.

February 2014

# Abstract

The  $M$ - $\sigma$  relations observed between the masses of central massive objects (CMOs: either a nuclear star cluster or a supermassive black hole) in galaxy nuclei and the stellar velocity dispersion of their host galaxy bulges strongly suggest that the evolution of CMOs and their host galaxies are closely related. Self-regulated feedback from CMOs sweeps the surrounding ambient medium into a shell and when the CMO is at a critical mass the shell is driven from the galaxy, cutting off fuel to the CMO for further growth and locking in the  $M$ - $\sigma$  relations. We investigate the  $M$ - $\sigma$  relations that result from either momentum- or energy-conserving feedback.

In the case of momentum-conserving feedback in an isothermal halo, we find the previously derived critical mass is not by itself sufficient to drive the shell to large radius and it takes a CMO with a mass three times the critical value to drive the shell to the escape speed of the halo. In non-isothermal haloes both of these issues are mitigated as the critical mass is sufficient to drive any shell to large radius where it will accelerate and escape the halo.

For energy-conserving feedback, we focus on the case that the CMO is a black hole and we find  $Mv_w \propto \sigma^5$ , where  $v_w$  is the black hole wind speed. This relation allows us to infer the wind speeds a sample of now quiescent galaxies would have had during an active phase, and we find good agreement with distributions of observed wind speeds in local active galaxies. We discuss the possibility of a transition from momentum- to energy-driving, the implications of relaxing the assumption of steady CMO winds and the effects these may have on the derived  $M$ - $\sigma$  relations.

# Acknowledgements

Someone once quoted Chairman Mao Tse-tung to me, “the journey of a thousand miles begins with a single step”. In their infinite wisdom this person also pointed out that by the time you take the final step you will be completely exhausted and will have been to hell and back. Here’s to the people who’ve made my thousand miles less hellish.

First of all, Dean McLaughlin, who through many hours of patience, confusion and frustration (on both our parts!), as well as a few laughs, has helped and guided me through the last four years to reach this point. My hat’s off to you.

Secondly, to my family. The love and support of my parents, my brother and my sister have been invaluable. Their ability to encourage me and occasionally shove me towards the finish line is outstanding and there is no doubt in my mind that I couldn’t have done this with out them. My extended family have also played their part. My Aunty Sue, Uncle Vince and much missed Aunty Barbara are just a few who have kept me going.

Finally, a few special friends. My comrades in arms from LJ 2.01, Adam and Kevin. We have kept each other sane, mostly through the media of alcohol and curry, which is not a bad thing! In all seriousness though, you have both supported me through some difficult times, providing a good laugh when it was most needed. On a softer note, Percy and Roy have provided support in a way nobody else could. And last, but certainly not least, Alison who just knows everything will be fabulous darling!

Rachael McQuillin

June 2013

# Contents

<b>Abstract</b> . . . . .	<b>iii</b>
<b>Acknowledgements</b> . . . . .	<b>iv</b>
<b>1 Introduction</b> . . . . .	<b>1</b>
1.1 Observational overview . . . . .	2
1.1.1 Supermassive black holes . . . . .	2
1.1.2 Nuclear star clusters . . . . .	12
1.1.3 Central massive objects . . . . .	19
1.2 Theoretical overview . . . . .	21
1.2.1 Physical concepts . . . . .	21
1.2.1.1 The Eddington luminosity . . . . .	21
1.2.1.2 Stellar winds and super bubbles . . . . .	23
1.2.1.3 Black hole winds . . . . .	23
1.2.2 The $M_{\text{CMO}} - \sigma$ relation . . . . .	25
1.3 Dark matter haloes . . . . .	28
<b>2 Outflow physics</b> . . . . .	<b>35</b>
2.1 Outflow structure . . . . .	35
2.2 Jump conditions . . . . .	39
2.3 Cooling mechanisms . . . . .	43
2.3.1 Atomic processes . . . . .	43
2.3.2 Inverse Compton scattering . . . . .	46
2.4 CMO outflows . . . . .	46
2.4.1 Nuclear star clusters . . . . .	46
2.4.2 Supermassive black holes . . . . .	48
2.4.3 Review of energy- vs. momentum-driven outflows . . . . .	50
2.5 Summary . . . . .	51
<b>3 Momentum-driven feedback and the <math>M - \sigma</math> relation in non-isothermal galaxies</b> . . . . .	<b>53</b>
3.1 Introduction . . . . .	55
3.2 Equation of motion . . . . .	59
3.3 The singular isothermal sphere . . . . .	61
3.4 Non-isothermal dark matter haloes . . . . .	66
3.4.1 General analysis . . . . .	66
3.4.1.1 Velocity fields at small and large radii . . . . .	68
3.4.1.2 Condition for the escape of a particular shell . . . . .	69
3.4.1.3 Sufficient condition for the escape of any shell . . . . .	71
3.4.1.4 $M - \sigma$ and $M - V_c$ relations . . . . .	73
3.4.2 Hernquist model haloes . . . . .	74

3.4.3	NFW model haloes . . . . .	79
3.4.4	Dehnen & McLaughlin model haloes . . . . .	82
3.5	Summary and discussion . . . . .	86
3.5.1	The singular isothermal sphere . . . . .	87
3.5.2	Non-isothermal haloes . . . . .	89
3.5.3	Observational implications . . . . .	92
3.A	The maximum critical CMO mass . . . . .	93
3.B	Sufficient condition for the escape of any shell II . . . . .	95
<b>4</b>	<b>Energy-driven outflows: black hole wind speeds and the <math>M</math>-<math>\sigma</math> relation</b>	<b>99</b>
4.1	Introduction . . . . .	100
4.2	Energy-driven outflows . . . . .	102
4.3	The Observed $M_{\text{BH}}$ - $\sigma$ relation . . . . .	110
4.4	Observed AGN outflow velocities . . . . .	114
4.5	Summary . . . . .	116
4.A	Terminal speeds of energy-driven shells . . . . .	117
<b>5</b>	<b>Energy-driven Outflows in Non-isothermal Galaxies</b>	<b>120</b>
5.1	Equation of motion . . . . .	121
5.1.1	Velocity fields at small radius . . . . .	122
5.1.2	Hernquist model haloes . . . . .	123
5.1.3	NFW model haloes . . . . .	126
5.1.4	Dehnen & McLaughlin model haloes . . . . .	128
5.2	Wind speeds and the $M$ - $\sigma$ relation . . . . .	130
5.3	Momentum and energy-driven outflows . . . . .	132
5.4	Summary . . . . .	136
<b>6</b>	<b>Summary and Discussion</b>	<b>138</b>
6.1	Summary . . . . .	138
6.2	Momentum- versus energy-driven outflows . . . . .	142
6.3	Observed $M$ - $\sigma$ relations . . . . .	147
6.4	Galaxy outflows . . . . .	150
6.5	Co-existing SMBHs and NCs . . . . .	152
6.6	Open questions and future work . . . . .	156
	<b>Publications</b> . . . . .	<b>160</b>
	<b>Bibliography</b> . . . . .	<b>161</b>

## List of Figures

1.1	A comparison of the spectra of a cD galaxy and an active galaxy (Schneider 2006). . . . .	4
1.2	The $M$ - $\sigma$ relations and $M$ - $M_{\text{bul}}$ relations for black holes. . . . .	9
1.3	Surface brightness profiles for nine galaxies of the ACS VCS sample from Côté et al. (2007). . . . .	17
1.4	The $M$ - $\sigma$ relations and $M$ - $M_{\text{bul}}$ relations for both black holes and nuclear star clusters. . . . .	18
1.5	Density profiles, $\rho(r)$ , mass profiles, $M(r)$ and circular speed profiles, $V_c^2(r)$ for a singular isothermal sphere and the dark matter profiles of Hernquist (1990), NFW, Dehnen & McLaughlin (2005) and Burkert (1995). . . . .	31
2.1	Schematic of a wind bubble. . . . .	37
2.2	Cooling functions of Sutherland & Dopita (1993). . . . .	45
3.1	Velocity fields for momentum-driven shells in a singular isothermal sphere with spatially constant gas fraction and $\widetilde{M}_{\text{CMO}} = 0.3, 1.01$ and 3. . . . .	62
3.2	The sufficient critical CMO mass, $\widetilde{M}_{\text{crit}}^{\text{max}}$ , that allows for the escape of any momentum-driven shell from a Hernquist halo (upper panel); and the radius $x_{\text{c,max}}$ , at which the slowest-moving shell driven by any such CMO starts to accelerate (lower panel) both as functions of $\widetilde{M}_{\text{pk}}$ . . . . .	76
3.3	Velocity fields for $\widetilde{M}_{\text{CMO}} = 0.3, 1, 3$ in a Hernquist dark matter halo with spatially constant gas fraction and $\widetilde{M}_{\text{pk}} = 4000$ which corresponds to a roughly Milky Way-sized halo. . . . .	77
3.4	The critical CMO mass, $\widetilde{M}_{\text{crit}}^{\text{max}}$ which is sufficient for the escape of any momentum-driven shell from an NFW halo (upper panel); and the radius $x_{\text{c,max}}$ at which the slowest-moving shell starts to accelerate (lower panel), both as functions of $\widetilde{M}_{\text{pk}}$ . . . . .	80
3.5	Velocity fields for $\widetilde{M}_{\text{CMO}} = 0.3, 1$ and 3 in an NFW halo with spatially constant gas fraction and $\widetilde{M}_{\text{pk}} = 4000$ . . . . .	82
3.6	The critical CMO mass, $\widetilde{M}_{\text{crit}}^{\text{max}}$ , that is sufficient to ensure the escape of any momentum-driven shell from a Dehnen & McLaughlin (2005) halo (upper panel); and the radius $x_{\text{c,max}}$ , at which the slowest moving shell begins to accelerate (lower panel) both as functions of $\widetilde{M}_{\text{pk}}$ . . . . .	84
3.7	Velocity fields for CMO masses $\widetilde{M}_{\text{CMO}} = 0.3, 1$ and 3 in a Dehnen & McLaughlin (2005) dark matter halo with a spatially constant gas fraction and $\widetilde{M}_{\text{pk}} = 4000$ . . . . .	85

3.8	An example of the velocity fields of momentum-driven shells in a non-isothermal halo (a Hernquist halo in this case), and the function $\tilde{v}_{\text{ex}}^2(x_{\text{ex}})$ that passes through all of the extrema. . . . .	97
4.1	Velocity fields for energy-driven shells in a singular isothermal sphere with spatially constant gas fraction and $\tilde{M}_{\text{BH}} \tilde{v}_w = 43/16, 6.5$ and $22$ . . .	107
4.2	<i>Left panel:</i> The $M_{\text{BH}}-\sigma$ relation from the compilation of Gültekin et al. (2009) with the $M_{\text{BH}}-\sigma$ relations from momentum- and energy-driven outflows. <i>Right panel:</i> The distribution of $v_w/c$ obtained from applying the condition for the escape of an energy-driven shell from an isothermal halo to the galaxy sample of Gültekin et al. (2009). . . . .	109
4.3	Inferred $v_w/c$ vs. observed $M_{\text{BH}}$ for the normal early-type galaxies and bulges in Gültekin et al. (2009). . . . .	112
4.4	Distribution of model (past) SMBH wind velocities for the normal galaxies in Gültekin et al. (2009), compared to the observed distributions of $v_w/c$ in local AGN, in samples measured by Tombesi et al. (2011) and by Gofford et al. (2013). . . . .	113
5.1	Velocity fields for energy-driven shells in a Hernquist (1990) dark matter halo with $\tilde{M}_{\text{pk}} = 4000$ , $\tilde{v}_w = 45$ and $\tilde{M}_{\text{BH}} = 0.01, 0.06$ and $0.49$ . . . . .	124
5.2	Velocity fields for energy-driven shells in an NFW dark matter halo with $\tilde{M}_{\text{pk}} = 4000$ , $\tilde{v}_w = 45$ and $\tilde{M}_{\text{BH}} = 0.01, 0.06$ and $0.49$ . . . . .	126
5.3	Velocity fields for energy-driven shells in a Dehnen & McLaughlin (2005) dark matter halo with $\tilde{M}_{\text{pk}} = 4000$ , $\tilde{v}_w = 45$ and $\tilde{M}_{\text{BH}} = 0.01, 0.06$ and $0.49$ . . . . .	129
5.4	Momentum- and energy-driven velocity fields for shells in an isothermal halo with $\tilde{M}_{\text{BH}} = 1$ and $\tilde{v}_w = 45$ . . . . .	132
5.5	Momentum- and energy-driven velocity fields for shells in a Hernquist halo with $\tilde{M}_{\text{pk}} = 4000$ , $\tilde{M}_{\text{BH}} = 1$ and $\tilde{v}_w = 45$ . . . . .	134
5.6	Momentum- and energy-driven velocity fields for shells in a Hernquist halo with $\tilde{M}_{\text{pk}} = 4000$ , $\tilde{M}_{\text{BH}} = 0.06$ and $\tilde{v}_w = 45$ . . . . .	135
6.1	The $M_{\text{BH}}-\sigma$ relation of McConnell & Ma (2013) and the four suggested $M_{\text{BH}}-\sigma$ relations of Zubovas & King (2012) depending on galaxy type and environment. Also shown are the four $M_{\text{BH}}-\sigma$ relations that would result for energy-driven outflows for the different galaxy types and environments considered by Zubovas & King. . . . .	149
6.2	The $M-\sigma$ relations of Ferrarese et al. (2006) and McConnell & Ma (2013) shown with a sample of galaxies that host both a nuclear cluster and a black hole in the nucleus, from Scott & Graham (2013). . . . .	154

# 1 Introduction

Most early-type galaxies and galaxy bulges with masses  $M \gtrsim 10^{10} M_{\odot}$  harbour a supermassive black hole (SMBH) at their centre with a mass  $M_{\text{BH}} \sim 10^6 - 10^{10} M_{\odot}$ . The black hole mass is found to correlate with galaxy properties such as total spheroid mass,  $M_{\text{sph}}$  (i.e., the bulge of a spiral galaxy or all of an elliptical galaxy; Kormendy & Richstone 1995; Magorrian et al. 1998) and even more tightly with the stellar velocity dispersion of the host galaxy spheroid,  $\sigma$  (e.g., Ferrarese & Merritt 2000; Gebhardt et al. 2000; Ferrarese & Ford 2005; Gültekin et al. 2009; McConnell & Ma 2013). These connections between the SMBH, which has a sphere of influence of a few tens of parsecs, and the global properties of the host galaxy on kiloparsec scales strongly suggest that the evolution of the SMBH and the host galaxy are closely related.

Self-regulated feedback from accreting black holes has been thought to play a key role in galaxy formation, including establishing correlations between the black hole and galaxy properties (e.g., Silk & Rees 1998; Fabian 1999). Observations of strong, fast outflows from the SMBHs powering active galactic nuclei (AGN; Pounds et al. 2003; Reeves et al. 2003; Tombesi et al. 2011) lend support to this theory. Black holes accreting at or above the Eddington limit are expected to drive strong winds back into their host galaxies (King & Pounds 2003). These winds move out into the host galaxy, pushing material outwards until at a critical SMBH mass the gas is cleared from the galaxy, cutting off further star formation and SMBH growth, ultimately locking in the observed  $M_{\text{BH}}-\sigma$  relation. In further support of the self-regulated feedback scenario are observations of galaxy scale outflows driven from AGN that could be responsible for quenching star formation (e.g., Bautista et al. 2010; Rupke & Veilleux 2011; Sturm et al. 2011).

The  $M_{\text{BH}}-\sigma$  relation is used in many areas of astrophysics such as in cosmological simulations as it is widely recognised as critical to galaxy formation due to the feedback processes between the black hole and the galaxy (i.e., Merritt & Ferrarese 2001; Yu & Tremaine 2002; Monaco, Salucci & Danese 2000)

Less massive galaxies,  $M \lesssim 10^{10} M_{\odot}$ , are host to massive nuclear star clusters (NCs) with masses  $M_{\text{NC}} \sim 10^5 - 10^8 M_{\odot}$ . Surprisingly, the NCs also follow scaling relations between their mass and galaxy properties such as total spheroid mass and stellar velocity dispersion (e.g., Ferrarese et al. 2006; Wehner & Harris 2006). A similar self-regulated feedback scenario can be applied to the nuclear cluster case where the combined winds and supernova explosions of stars in the cluster drive a superwind. There is again a critical mass at which the superwind can clear the galaxy of gas, thus quenching star formation and establishing an  $M_{\text{NC}}-\sigma$  relation. The close connection between both NCs and SMBHs with their host galaxies has led to them being grouped under the term central massive objects (CMOs).

Due to the connection between the CMOs and their host galaxies that is suggested by the observed correlations, it is of interest to investigate the physical origins of these relations so as to determine the effect they have on the formation and evolution of the galaxies as a whole.

Before looking at the  $M-\sigma$  relations that result from the feedback scenario, we briefly review the observational evidence for CMOs in galaxies and the relations observed between CMOs and their host galaxies. We then look at the physical concepts behind theoretical derivations of the  $M-\sigma$  relations, before looking at the scaling relations that result. Finally, we look at descriptions of the dark matter haloes in which the feedback scenario can be modelled.

## 1.1 Observational overview

### 1.1.1 Supermassive black holes

The Milky Way Galaxy in which we reside is a fairly typical large spiral galaxy with a luminosity of  $(3.0 \pm 1.0) \times 10^{10} L_{\odot}$  (Binney & Tremaine 2008). Many large galaxies ( $M_{\text{gal}} \gtrsim 10^{10} M_{\odot}$ ), both early- and late-type, harbour a supermassive black hole (SMBH) in their nucleus with masses  $M_{\text{BH}} \sim 10^6 - 10^{10} M_{\odot}$ . Our Galaxy harbours an

SMBH at its centre with a mass  $M_{\text{BH}} \simeq (4.1 \pm 0.6) \times 10^6 M_{\odot}$  (Ghez et al. 2008).

Though SMBHs are now detected in quiescent galaxies, the black hole paradigm originates from the study of active galactic nuclei (AGN).

Normal, i.e., non-active galaxies are composed of stars, gas and dust embedded in a halo of non-luminous matter known as a dark matter halo. The spectrum of a normal galaxy is the composite spectrum of the stars, gas and dust that make up the galaxy. The stars emit a thermal spectrum with absorption lines overlaid. The gas is partly visible in the form of HII regions, clouds of hot gas that are the site of ongoing star formation, prominent in spiral and irregular galaxies. The dust in galaxies is relatively cool and its main effect on an optical spectrum is the dimming of starlight. The broadband spectrum of a normal galaxy peaks at optical wavelengths and has more energy radiated at far-IR wavelengths than in X-rays.

Active galaxies have extra, non-stellar, features in their spectra in addition to those of normal galaxies. The optical spectrum of an active galaxy has emission lines that are stronger and broader than a normal galaxy. The temperatures implied by the broadening are hotter than the cores of all but the most massive stars and the alternative explanation implies bulk motions of several thousands of kilometres per second, which would mean large amounts of kinetic energy are tied up in the gas motions. The broadband spectrum of an active galaxy peaks in the X-ray and UV region. They emit the ‘normal’ amount of starlight at optical wavelengths and emit several times this at IR and other wavelengths. In many cases a large fraction of the luminosity is produced in the central regions of the galaxy, in the active galactic nucleus (AGN), giving active galaxies their name.

Figure 1.1 shows the broadband spectral energy distribution of a cD galaxy and a quasar (Schneider 2006). cD galaxies are extremely luminous and large galaxies found near the centres of dense galaxy clusters. The spectra of the cD galaxy covers only a few decades in frequency and peaks in the optical part of the spectrum as we would expect for a normal galaxy. Quasars are high redshift members of the family of active galaxies. Figure 1.1 shows that the quasar is much brighter than the cD galaxy and that emission from the quasar is observed over the full electromagnetic spectrum. This

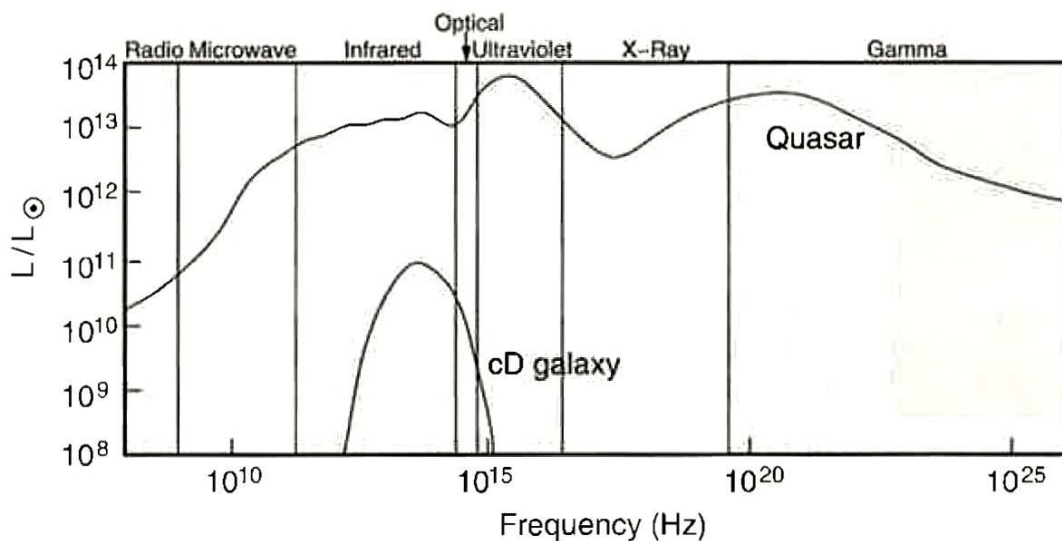


Figure 1.1: A comparison of the spectra of a cD galaxy and an active galaxy (Schneider 2006). The cD galaxy spans only a few decades in frequency and its spectrum peaks in the optical/IR wavelengths. The spectrum of an active galaxy (a quasar in this example) spans the whole EM spectrum and peaks in the higher energy UV, X-ray and  $\gamma$ -ray regions.

implies that the luminosity of the quasar is generated by some other, non-stellar source.

There is wide variety in the family of active galaxies, with different kinds of AGN discovered separately and seeming very different to each other, but they all show these spectral peculiarities.

Although unrealised at the time, the first study of AGN was made by Seyfert (1943) who identified 12 spiral galaxies with unusually bright, point like nuclei. The spectra of the nuclei showed emission lines of highly excited species and some very broad lines. The broadening of the hydrogen lines implied velocities of up to  $8,500\text{km s}^{-1}$  in several of the nuclei, whereas comparably bright knots of emission in the periphery of other galaxies showed no line broadening. It was also noted that the mean magnitude of these spirals was larger than the average spiral with no nuclear emission and that

the nuclei themselves had large luminosities, comparable to the sum of the stars in their host galaxy.

In the 1950's it was found that many of the strongest radio sources coincided with the nuclei of luminous elliptical galaxies. This, combined with the work of Seyfert (1943), made it clear that unfamiliar processes were occurring in the nuclei of many galaxies. Baade & Minkowski (1954b) catalogued discrete radio sources into four categories including "peculiar extragalactic nebulae". They associated the strong radio source Vir A with the giant elliptical galaxy M87, the dominant galaxy in the Virgo cluster. They noted that the galaxy does not differ significantly in size or brightness from other bright members of the cluster. However, a bright optical jet,  $\sim 1$  kpc in length, emanating from the nucleus and spectra of the nucleus showing line widths of several hundreds of kilometers per second implied that it was the radio source.

M87 was not an isolated case. Jennison & Das Gupta (1953) identified Cygnus A as being a double radio source, with Baade & Minkowski (1954a) later associating the radio source with a galaxy at the centre of a cluster at redshift  $z = 0.057$  ( $D \simeq 250$  Mpc for  $H_0 = 70 \text{ km s}^{-1} \text{ Mpc}^{-1}$ ). Baade & Minkowski (1954b) noted that the spectrum resembled to a certain degree those identified by Seyfert (1943) though there were some marked differences, most notably that the area of emission in Cygnus A was much larger than in the nuclei of Seyfert's galaxies. The source of emission was found to originate from two lobes on either side of the visible object. Like M87, the nucleus of the visible object associated with Cyg A showed strong extended emission with usual line strengths.

In the 1960's the first quasars were recognised. They were described as "quasi-stellar" because of their star-like appearance. However, their high redshifts ( $z > 0.1$ ) betrayed them as being incredibly luminous objects. It was soon recognised that a large number of radio sources were quasars at large redshifts.

Although all of these active nuclei seemed very different when their peculiarities were first observed, they all have several common properties. We can deduce that these sources are very long-lived. The radio sources in some objects are very large, several hundred kiloparsecs in extent. Even if the radio source were able to expand outwards

at the speed of light, the age of a source  $\sim 500$  kpc in extent would be of the order  $10^6$  yr, as a lower limit.

The high velocities observed in the nuclei imply that huge amounts of energy are generated in AGN. If we assume that the luminosity of the source does not change considerably over its lifetime then we can estimate the energy generated. A typical quasar has a bolometric luminosity  $L_{\text{bol}} \sim 10^{47}$  erg s $^{-1}$ , so over  $10^7$  yrs a total energy of  $E \sim 3 \times 10^{61}$  erg is generated. However, as we discuss below, the assumption of constant luminosity is not necessarily valid.

Another common property of all AGN types is how compact they are. Even the nearest AGN cannot be resolved, implying sizes  $< 1$  pc. They can be further constrained by the timescales on which their luminosities vary, for example, variability on the order of a day ( $\sim 10^5$  s) implies sizes  $\sim ct \simeq 10^{-3}$  pc.

It became widely accepted that the power supply in AGN is primarily gravitational, with various models involving dense clusters, supermassive stars and black holes (e.g., Salpeter 1964). However, these collections of objects in the compact regions implied from observations are found to be unstable. The most plausible candidate was found to be a supermassive black hole (SMBH). Thus it was suggested that the conversion of gravitational energy into radiation when matter accretes onto an SMBH produces the enormous luminosities observed in AGN. The variation in AGN types could then be caused by effects on larger scales where the emitted radiation is reprocessed by its environment, and by orientation effects.

There was still a long wait for the solid detections of SMBHs in galaxy nuclei. The giant elliptical galaxy M87 in the Virgo cluster was often the target in the search for SMBHs as an SMBH would be a plausible energy source for its relativistic jet and its relatively close proximity makes it a convenient candidate.

Sargent et al. (1978) analysed the stellar velocity dispersion as a function of radius for M87 and found the velocity dispersion showed a sharp increase in the central regions, consistent with a central mass concentration. Sargent et al. then deduced the mass distribution of M87 on general, model independent principles. Taking the first

moment of the spherical, isotropic, collisionless Boltzmann equations gives:

$$\frac{d}{dr} [\nu(r)\sigma_r^2(r)] = -\frac{GM(r)}{r^2}\nu(r) \quad , \quad (1.1)$$

where  $\nu(r)$  is the stellar mass density and  $\sigma_r(r)$  is the velocity dispersion of these stars. Equation (1.1) can be solved for the total mass interior to radius  $r$ ,  $M(r)$

$$M(r) = \frac{r\sigma_r^2(r)}{G} \left[ -\frac{d\ln\nu}{d\ln r} - \frac{d\ln\sigma_r^2}{d\ln r} \right] \quad . \quad (1.2)$$

Using their measured velocity dispersion and mass density (obtained from a luminosity density and assumed mass-to-light ratio), Sargent et al. (1978) found equation (1.2) implied a mass  $> 10^9 M_\odot$  inside the central 110pc of M87. However, it wasn't until the spectroscopic observations of Harms et al. (1994) that the presence of a  $(2.4 \pm 0.7) \times 10^9 M_\odot$  SMBH in the nucleus of M87 was firmly accepted.

It was found that the cumulative mass density of SMBHs required to power high redshift quasars is orders of magnitude higher than that required to power local AGN (Padovani, Burg & Edelson 1990). The total mass related to accretion in past quasars is not accounted for in local AGN and therefore must be present in quiescent galaxies. As such, recent SMBH searches have targeted quiescent galaxies where dormant SMBHs are expected to be found. Dormant SMBHs show little or no signs of unusual nuclear emission and, in the absence of an AGN, their presence must be detected by gravitational interactions with their surroundings. These Keplerian dynamical signatures can only be resolved in nearby galaxies.

The use of *Hubble Space Telescope* (*HST*) data greatly increased the number of galaxies in which the sphere of influence of a black hole could be resolved, leading to many more secure detections of black holes in quiescent galaxies.

Using these secure measurements of SMBH masses, work began to investigate the demographics of black holes. One of the first scaling relations identified for SMBHs was that between the SMBH mass,  $M_{\text{BH}}$ , and the absolute blue magnitude of the galaxy spheroid,  $M_{\text{B}}$  (i.e., the bulge for spiral galaxies or the whole of an elliptical galaxy) (Kormendy & Richstone 1995). The existence of a correlation between SMBHs and

the properties of their host galaxies suggests that the formation and evolution of the two could be related.

A connection between SMBH mass and stellar velocity dispersion of the host galaxy bulge,  $M_{\text{BH}} \propto \sigma^x$ , was first made observationally by Ferrarese & Merritt (2000) who found  $x = 4.8 \pm 0.5$ , and independently by Gebhardt et al. (2000) who found  $x = 3.75 \pm 0.3$ . There has been much debate over the “best fit” value of the slope of the  $M$ – $\sigma$  relation, with more recent works showing  $x = 4.24 \pm 0.41$  (Gültekin et al. 2009) and  $x = 5.65 \pm 0.32$  (McConnell & Ma 2013; they also show that if they split their sample into early- and late-type galaxies, both sub-samples have a slope of  $x = 5.01$  but with different intercepts). The difference in these results can be at least partially attributed to different groups’ definition of “the sigma”, specifically the choice of region across which it is measured. It is often measured at a fraction of the bulge effective radius<sup>1</sup>,  $R_e$ , though the fraction varies from group to group. However, this way of defining “the sigma” is inappropriate when considering galaxies with little or no bulge component.

In spite of these issues, the  $M$ – $\sigma$  relation is a remarkably tight correlation, with other relations showing much more scatter (e.g., see Ferrarese & Ford 2005 for a comparison between the  $M$ – $M_B$  and  $M$ – $\sigma$  relations). In either case, the correlation between SMBH masses and the global properties of their host galaxies is strong evidence for a connection between the formation and evolution of the two.

The tight correlation between SMBH mass and bulge velocity dispersion is shown in the left-hand panel of Figure 1.2 where the filled circles represent the SMBH data compiled by McConnell & Ma (2013) and the solid line has the equation

$$\log \left( \frac{M_{\text{BH}}}{M_{\odot}} \right) = (8.32 \pm 0.05) + (5.64 \pm 0.32) \log \left( \frac{\sigma}{200 \text{km s}^{-1}} \right), \quad (1.3)$$

which is their line of best fit to the data.

We expect this to be closely related to the correlation between black hole mass

---

<sup>1</sup>The effective radius of a source is that within which half of its luminosity is contained in projection.

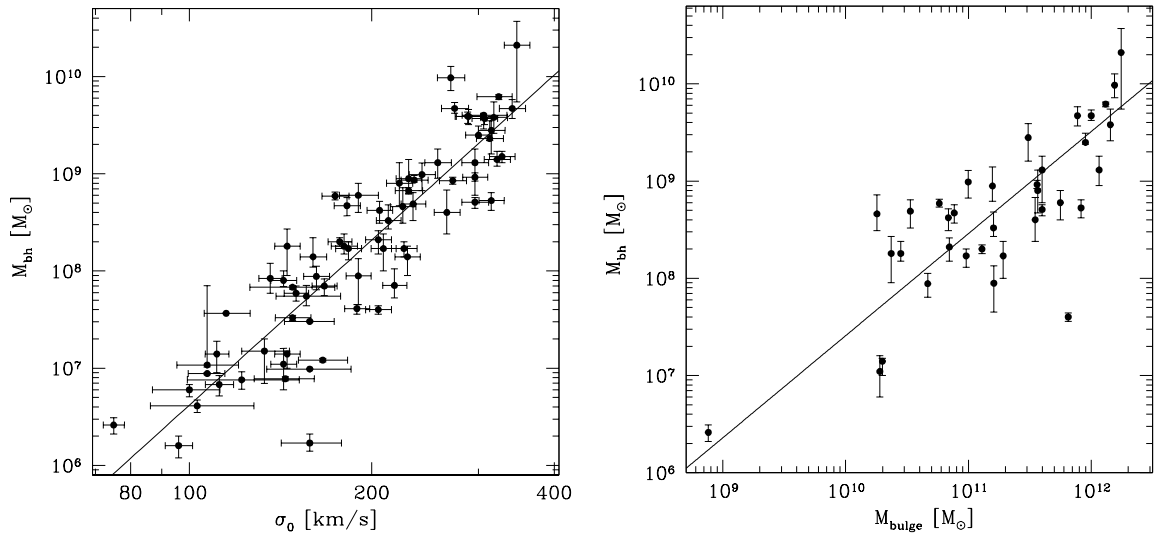


Figure 1.2: *Left:* The mass of the supermassive black holes,  $M_{\text{BH}}$ , plotted against the velocity dispersion,  $\sigma$ , of the galaxy bulges averaged within the effective radius,  $R_e$ . *Right:* The mass of the SMBH,  $M_{\text{BH}}$ , plotted against the mass of the host galaxy's bulge,  $M_{\text{bul}}$ . Data from McConnell & Ma (2013).

and the galaxy bulge mass,  $M_{\text{bul}}$ , because on dimensional grounds we have that

$$M_{\text{bul}} \propto \frac{\sigma^2 R_e}{G}, \quad (1.4)$$

where  $R_e$  is the effective radius of the galaxy. The filled points in the right-hand panel of Figure 1.2 show bulge masses for 35 galaxies in the compilation of McConnell & Ma (2013), found by multiplying the bulge luminosity by a mass-to-light ratio. The solid line there shows their best fit to the data which is given by

$$\log \left( \frac{M_{\text{BH}}}{M_{\odot}} \right) = (8.46 \pm 0.08) + (1.05 \pm 0.11) \log \left( \frac{M_{\text{bul}}}{M_{\odot}} \right). \quad (1.5)$$

As well as correlations between SMBHs and the baryonic component of their host galaxy, it has been proposed that black hole masses also scale with the properties of the dark matter halo in which their host galaxy resides. Ferrarese (2002) investigated the possibility of a relation between black hole mass and the total gravitational mass of

their host galaxy which is dominated by the dark matter mass,  $M_{\text{DM}}$ , using a sample of the 20 elliptical galaxies of Kronawitter et al. (2000) and 16 spiral galaxies of Gerhard et al. (2001). Ferrarese finds a tight correlation between the velocity dispersion,  $\sigma_c$ , measured inside  $R_e/8 \lesssim 0.5$  kpc, and the large scale circular speed,  $V_c$ , measured where the rotation curve is flat, at galactic radii  $R \sim 20 - 80$  kpc;

$$\log V_c = (0.84 \pm 0.09) \log \sigma_c + (0.55 \pm 0.19) . \quad (1.6)$$

In the simple case of a galaxy modelled as a singular isothermal sphere (see §1.3) we would expect  $V_c \propto \sigma$ , so a near linear relation is not unexpected. Combining this  $\sigma_c$ - $V_c$  relation with the  $M$ - $\sigma$  relation of Ferrarese & Merritt (2000) and using the cosmological simulations of Bullock et al. (2001) to connect  $V_c$  to  $M_{\text{DM}}$ , Ferrarese (2002) derives a relation between the black hole mass and the mass of the dark matter halo,

$$\frac{M_{\text{BH}}}{10^8 M_\odot} \sim 0.10 \left( \frac{M_{\text{DM}}}{10^{12} M_\odot} \right)^{1.65} . \quad (1.7)$$

Following this work, Baes et al. (2003) used  $\sigma_c$  and  $V_c$  measurements for an additional 12 spiral galaxies to ‘refine’ the  $\sigma_c$ - $V_c$  correlation. They found a similar relation to Ferrarese (2002) with

$$\log V_c = (0.96 \pm 0.11) \log \sigma_c + (0.32 \pm 0.25) . \quad (1.8)$$

Baes et al. also look explicitly at a relation between the black hole mass and large scale circular velocity, using the  $M$ - $\sigma$  relation of Tremaine et al. (2002) to estimate black hole masses based on their measurements of velocity dispersion. They find

$$\log \left( \frac{M_{\text{BH}}}{M_\odot} \right) = (4.21 \pm 0.60) \log \left( \frac{V_c}{200 \text{ km s}^{-1}} \right) + (7.24 \pm 0.17) , \quad (1.9)$$

which, because of the near linear relationship between  $V_c$  and  $\sigma$ , follows roughly the same relation as black hole mass and velocity dispersion. Baes et al. also look at the relation between black hole mass and dark matter mass, like Ferrarese (2002). They note however, that the uncertainties in an  $M_{\text{BH}}-M_{\text{DM}}$  relation are large, but an  $M_{\text{BH}}-V_c$  relation is based only on observable quantities, so has much smaller uncertainties.

With a much larger galaxy sample (792 galaxies, spanning a broad range of Hubble types) Ho (2007) found that the  $V_c$ - $\sigma$  relation exhibits much more scatter than previously shown. Ho also argues that the zero point of the relation varies with galaxy properties such as morphology, bulge-to-disk ratio and light concentration. Ho does note however that the  $M_{\text{BH}}-V_c$  relation still remains a useful tool in estimating black hole masses when  $\sigma_c$  is difficult to measure.

Part of the problem with the  $V_c$ - $\sigma_c$  relation can be traced back to the definition of the velocity dispersion. Ferrarese (2002) defines the velocity dispersion measured inside an aperture of size  $R_e/8$ . Ho (2007) use velocity dispersions that are generally measured inside an aperture that is smaller than  $R_e$ . In very late-type spirals which have little or no bulge component, Ho uses the velocity dispersion of the central star cluster (nuclear star cluster, see §1.1.2 below), which is a self-gravitating system, distinct from galaxy bulges and which has an effective radius of only a few parsecs.

More recently, Kormendy & Bender (2011) and Volonteri, Natarajan & Gültekin (2011) have argued against and for correlations between SMBHs and dark matter haloes respectively. Kormendy & Bender (2011) suggests that such a correlation requires exotic physics to control the black hole growth. They show that  $V_c$  does not correlate with  $\sigma_c$ , though the outliers are late-type spiral galaxies where the velocity dispersion of the nuclear star cluster is used.

Volonteri, Natarajan & Gültekin (2011) have argued that galaxies/bulges containing SMBHs show a correlation, of the form  $M_{\text{BH}} \propto V_c^y$  with  $y \approx 4$ , between black hole mass and the ‘asymptotic’ circular speed  $V_c$  at large radii where the dark matter is expected to dominate the total galaxy mass. They find that the  $M_{\text{BH}}-V_c$  relation is similar in scatter and slope to the  $M_{\text{BH}}-\sigma$  relation.

It is important to note that correlations between black holes and their dark matter haloes do not imply in any way that the dark matter feeds the growth of the black hole, as suggested by Kormendy & Bender (2011). It is clear the stellar velocity dispersion is connected to the dark matter distribution which dominates the potential of the galaxy. The circular speed at large radius probes the dark matter distribution so a correlation between  $\sigma$  and  $V_c$  is not unexpected, though the exact connection is

complex and model dependent.

The  $M$ – $\sigma$  relation for SMBHs, and other correlations, are in themselves interesting results warranting further investigation because of the links they show between parsec and kiloparsec scale structures in galaxies. They suggest that SMBHs co-evolve with their host galaxies, and play an important role in galaxy formation and evolution. These scaling relations are made all the more significant by the fact that analogous relations exist in lower mass galaxies that harbour nuclear star clusters (NCs) at their centres.

### 1.1.2 Nuclear star clusters

The Milky Way is a member of the Local Group which contains over 30 galaxies within a sphere  $\sim 1$ Mpc in radius, centred between the Milky Way and M31, the Andromeda galaxy. The majority of galaxies in the Local Group (around 85 %) are irregular galaxies, dwarf irregulars, dwarf ellipticals and dwarf spheroidals with luminosities less than  $10^9 L_{\odot}$ . The numerical dominance of these less luminous galaxies is demonstrated by the luminosity function, which describes the number of galaxies of different luminosities. It is known to depend upon both the galaxy type and environment, but it is observed that the number density of lower luminosity galaxies is much higher than that of massive galaxies, in all environments (Binney & Tremaine 2008).

The intrinsic faintness of these numerically dominant galaxies has made them difficult to study. The first data on the Local Group dwarf elliptical (dE) galaxy NGC 205 were collected by Redman & Shirley (1938) during their photometric study of M31 because of its close proximity to the larger galaxy as one of its satellites. Further work by Baade (1944) classified the dEs NGC 147 and NGC 185 as members of the Local Group. As such, they could be resolved into stars, leading Hodge (1963, 1973) to study their structure and content. In particular Hodge (1973) studied NGC 205 and by examining the colour gradient, a central population of young blue stars was identified, indicating a recent burst of star formation in the centre of the dE. Using the luminosity function of the observed stars, Hodge estimated the mass of the cluster

to be  $5 \times 10^5$  to  $5 \times 10^6 M_\odot$ . Then, assuming the brightest OB star in the cluster to be at the main sequence turn-off, Hodge estimated the age of the cluster as being of order  $5 \times 10^6$  years. This is much younger than expected for other, similarly massive star clusters in typical elliptical systems; for example, typical globular clusters in the Milky Way's halo have masses  $\sim 5 \times 10^5 M_\odot$  and ages of 13 Gyr.

Extensive studies of dEs beyond the Local Group came with large photographic surveys of the Virgo Cluster (the Virgo Cluster Catalogue, VCC; Binggeli, Sandage & Tammann 1985) and the Fornax Cluster (the Fornax Cluster Catalogue, FCC; Ferguson & Sandage 1990). Examples were found in Virgo and Fornax of bright dEs ( $L_B \lesssim 10^9 L_\odot$ ) showing unresolved spikes in luminosity in their centres, referred to as central nuclei (Sandage & Binggeli 1984; Bothun & Mould 1988). Of the 1277 members and 574 probable members of the Virgo Cluster in the VCC, Binggeli, Tammann & Sandage (1987) classified over 1600 of them to be dwarf galaxies, with 415 noted as having bright central nuclei. While studying the distribution of galaxies, it was found that the nucleated dEs (dE,Ns) are strongly concentrated toward the centre of the main substructure of the Virgo Cluster, whilst the non-nucleated dEs are more dispersed.

By examining the colours of dEs in the Fornax Cluster, Caldwell & Bothun (1987) noted that dE,Ns are redder at a given luminosity than non-nucleated dEs. This led them to hypothesize that some dEs may have been able to retain more of their enriched interstellar gas after an initial burst of star formation, and that this gas fell to the galaxy's centre triggering another burst of star formation. This second burst of star formation would have created not only the nucleus but also more stars throughout the galaxy, all of which would be metal-rich and hence redder. Caldwell & Bothun suggested that stellar winds and supernovae explosions in non-nucleated dEs may have been more efficient at sweeping out the residual gas, perhaps due to a shallower gravitational potential, leaving little metal-rich material from which to form new stars or a nucleus.

Babul & Rees (1992) proposed that faint blue objects (FBOs) seen in deep images of the sky are in fact dEs undergoing their initial bursts of star formation at redshifts  $z \sim 1$ . They suggest that the retention of gas in the dEs is dependent upon the

environment in which the galaxy evolves, i.e., the state of the intergalactic medium (IGM). In regions of low IGM density, the ram pressure of the supernovae driven gas outflow could overcome the pressure of the IGM allowing the gas to escape, whereas in higher density regions the IGM pressure would halt the wind. Retaining the supernovae ejecta could allow the dEs to undergo further episodes of star formation, in the way suggested by Caldwell & Bothun (1987), resulting in these dEs being nucleated. This theory ties in with the observation that dE,Ns are more centrally concentrated in both the Fornax and Virgo Clusters (Ferguson & Sandage 1989).

Other ideas for the formation of the nucleus hypothesized that dE,Ns and non-nucleated dEs *began* as morphologically distinct galaxies. Ferguson & Sandage (1989) proposed that non-nucleated dEs began as irregular galaxies that have been stripped of their gas whereas dE,Ns were always genuine ellipticals.

It came as some surprise when images from *HST* revealed that it is not just dEs that show central nuclei, but that galaxies all along the Hubble sequence show nuclear luminosity peaks (e.g., see Figure 1.3). While examining the centres of 20 nearby disk galaxies, from lenticulars to late type spirals, Phillips et al. (1996) found that they often exhibit unresolved nuclei, much like those found in dE galaxies. Further analysis of early type spiral galaxies with *HST* by Carollo et al. (1997) showed in a sample of 35 galaxies that central compact sources were found in 18 of them. With an additional 40 targets Carollo, Stiavelli & Mack (1998) found that the frequency of nucleation,  $f_n$  was still around 50%. Nuclei have also been found in the centres of very late type spiral galaxies, i.e. those with little or no bulge, with  $f_n \approx 75\%$  (Böker et al. 2002).

*HST* has been able to resolve these nuclei and has shown them to be massive star clusters with luminosities of order  $10^6 - 10^8 L_\odot$  (Böker et al. 2002), much brighter than the average globular cluster (GC) in our Galaxy which have luminosities of  $\lesssim 10^6 L_\odot$ . This luminosity difference could be in part due to the differing ages of the GCs and nuclear clusters. The average GC is  $\sim 13$  Gyr old, meaning they contain only faint, low-mass stars. On the other hand, nuclear clusters show evidence for multiple generations of stars (Rossa et al. 2006), and contain populations of young, massive, luminous stars. The dynamical masses of nuclear clusters,  $M_{nc} \sim 10^6 - 10^7 M_\odot$  (Walcher et al. 2005),

place them at the very high end of the GC mass function. Despite the higher masses and luminosities of the nuclear clusters they are comparable in size to GCs, both having effective radii of order a few parsecs (Böker et al. 2004).

The suggested formation mechanisms of a nuclear cluster can be broken down into two main categories. Either

1. The cluster formed in situ by gas infall which causes (possibly episodic) star formation, as envisioned by Caldwell & Bothun (1987). Or,
2. A dense cluster is formed elsewhere in the galaxy and falls into the centre by dynamical friction. The infall of gas onto this “migrated” star cluster would result in episodes of star formation.

There is some debate over which of these is the more viable formation mechanism. Böker et al. (2004) claim there is no explanation for high densities required for in-situ formation in late type spirals and suggest migration combined with a small amount of more recent star formation as a plausible alternative. Milosavljević (2004) takes the opposite stance, claiming the migratory scenario fails to place the clusters where they are observed in late type spirals and propose that gas is transported to the centre of the disk from elsewhere for in-situ formation. Emsellem & van de Ven (2008) construct models for the formation of clusters via tidal compression of gas. They find that the size of the regions in which the tidal forces are compressive correspond to the typical sizes of nuclear clusters in both early- and late-type galaxies.

The Advanced Camera for Surveys Virgo Cluster Survey (ACS VCS) was an *HST* program that imaged 100 early type members of the Virgo Cluster (Côté et al. 2004). Côté et al. (2006) examined the innermost structure of the galaxies in this survey. They found the frequency of nucleation to be much higher than previously believed from the VCC (Binggeli et al 1987). Of the 100 galaxies, there were 6 cases where a determination could not be made (due to either dust or the presence of an active galactic nucleus) and only 12 cases were classified with certainty as non-nucleated, posing an upper limit of  $f_n \lesssim 88\%$ . Of the remaining galaxies, 62 were classified as

definitely nucleated and 4 as likely nucleated, giving the overall frequency of nucleation as  $66\% \lesssim f_n \lesssim 88\%$ .

Côté et al. (2006) found the nuclear clusters that could be resolved in the early type cluster members to be a close match in terms of size and luminosity to those found in the late type spiral galaxies of Böker et al. (2002, 2004), suggesting that the formation mechanism of the clusters is largely insensitive to galaxy type.

Using a further 43 early type galaxies from the ACS Fornax Cluster Survey (ACS FCS; Jordán et al. 2007), Côté et al. (2007) show that central excesses of stellar light are present in the majority of low- and intermediate- luminosity early-type galaxies,  $L_{\text{gal}} \lesssim 10^{10} L_{\odot}$ . Figure 1.3 shows the surface brightness profiles of nine representative galaxies in the ACS VCS from Côté et al. (2007). When considering decreasing luminosity, the galaxies in the sample show a smooth transition from a central deficit with respect to inward extrapolation, possibly due to core evacuation by coalescing SMBH binaries, to an excess, i.e., a nuclear cluster.

With as many as 80% of low- and intermediate-luminosity galaxies of all Hubble types showing now-resolved nuclei (Carollo et al. 1997; Carollo, Stiavelli & Mack 1998; Böker et al 2002; Côté et al. 2006, 2007), much investigation into these nuclear clusters has taken place, uncovering two fundamental relations between the nuclear clusters and their host galaxies, analogous to the relations observed between SMBHs and their host galaxies.

The first of these is a tight correlation between the masses of the nuclear star clusters,  $M_{\text{nc}}$ , and the velocity dispersions of their host galaxy bulges,  $\sigma$ , the  $M_{\text{nc}} - \sigma$  relation. Ferrarese et al. (2006) use photometric data from the ACS VCS, with supplementary ground-based spectroscopy to show that

$$\log \left( \frac{M_{\text{nc}}}{M_{\odot}} \right) = (4.27 \pm 0.61) \log \left( \frac{\sigma}{54 \text{km s}^{-1}} \right) + (6.91 \pm 0.09), \quad (1.10)$$

which is shown as the dashed line in the left-hand panel Figure 1.4, where the open circles show the nuclear cluster data of Ferrarese et al.

As with SMBHs, the  $M_{\text{NC}} - \sigma$  relation is closely linked to a relationship between the nuclear cluster mass and the mass of the host galaxy bulge. Recalling  $M_{\text{bul}} \propto GR_{\text{e}}/\sigma^2$

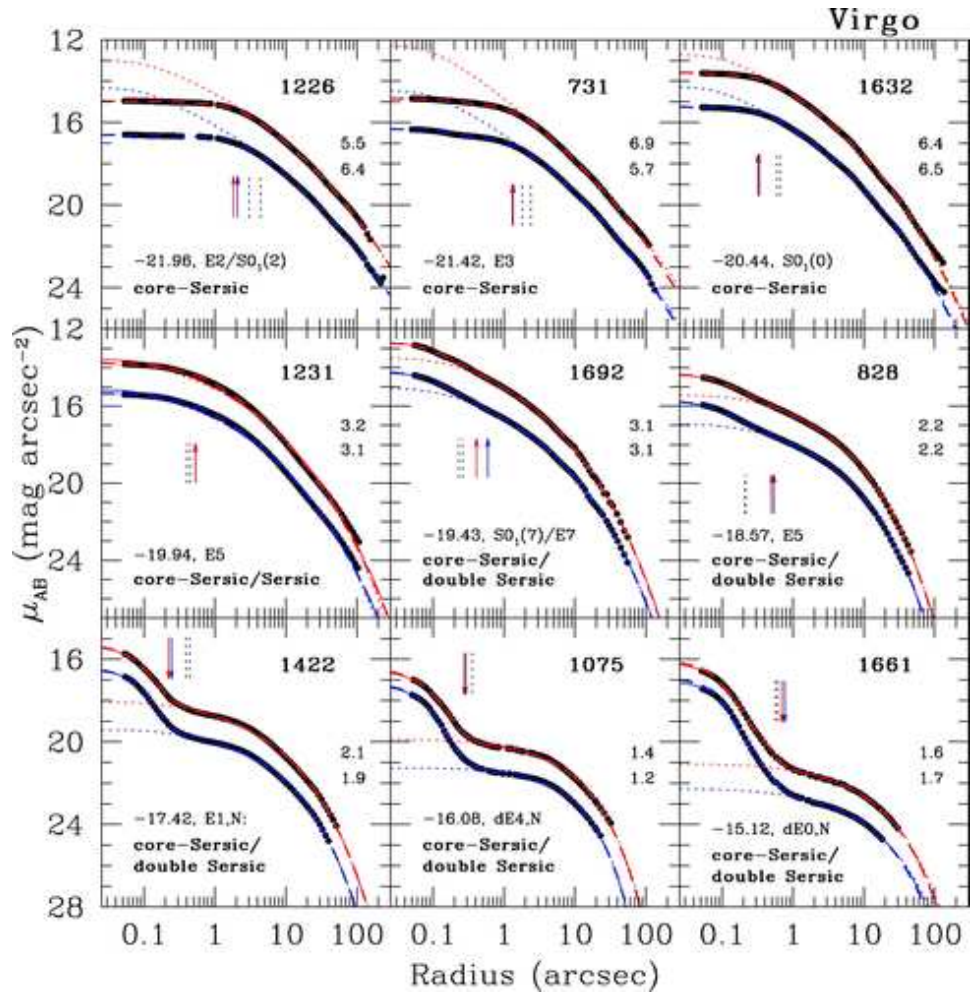


Figure 1.3: Surface brightness profiles for nine galaxies of the ACS VCS sample from Côté et al. (2007). The plots are ordered in terms of decreasing total luminosity with the total magnitude in the B-band,  $M_B$ , and the morphological type of each galaxy given along with the VCC catalogue number. The two lines (red-upper, blue-lower) represent magnitudes in the  $z$  and  $g$  bands respectively.

(equation [1.4]), Ferrarese et al. (2006) adopt a value for the constant of proportionality, known as the virial parameter, of  $\alpha = 5$  (from Cappellari et al. 2006) to estimate  $M_{\text{bul}}$

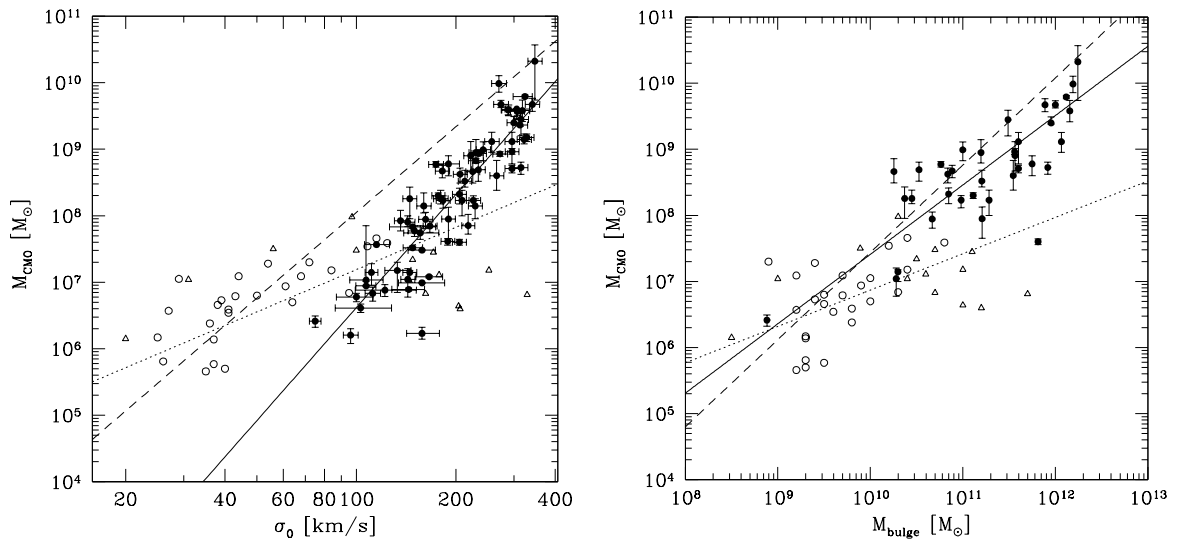


Figure 1.4: *Left:* The mass of the central massive object,  $M_{\text{CMO}}$ , plotted against the velocity dispersion,  $\sigma$ , of the galaxy bulges averaged within the effective radius,  $R_e$ . *Right:* The mass of the central massive object,  $M_{\text{CMO}}$ , plotted against the mass of the host galaxy's bulge,  $M_{\text{bul}}$ . In both cases the filled points represent data for black holes (McConnell & Ma 2013) and the open points represent the nuclear star clusters (Scott & Graham 2013). The bulge masses for the black holes are dynamical masses taken from McConnell & Ma (2013). For the nuclear star clusters, the bulge mass is defined as  $M_{\text{bul}} = 5r_e\sigma^2/G$ . The open circles represent the data of Ferrarese et al. (2006) in the compilation of Scott & Graham (2013).

and find

$$\log\left(\frac{M_{\text{nc}}}{M_{\odot}}\right) = (1.32 \pm 0.25) \log\left(\frac{M_{\text{bul}}}{10^{9.6} M_{\odot}}\right) + (6.91 \pm 0.09), \quad (1.11)$$

which is shown by the dashed line in the right panel of Figure 1.4, where again the open circles represent the Ferrarese et al. nuclear cluster data.

The parallels between the  $M$ - $\sigma$  and  $M$ - $M_{\text{bul}}$  relations for BHs and nuclear clusters suggest that the nuclear clusters may be the low mass analogues of SMBHs. As such, SMBHs and nuclear clusters have been grouped under the term central massive object (CMO), which we adopt here.

### 1.1.3 Central massive objects

Consider again the  $M$ - $\sigma$  relations shown in the left-hand panel of Figure 1.4. The SMBH data (McConnell & Ma 2013; filled circles, solid line) and the nuclear cluster data of Ferrarese et al. (2006) (open circles, dashed line) suggest that both types of CMO follow roughly the same scaling relation, though the exact slope of either relation is of some debate.

It has recently be argued that the nuclear cluster scaling relations have significantly shallower slopes than the relations defined by the sample of Ferrarese et al. (2006) and therefore, that BHs and nuclear clusters follow different scaling relations. With an additional 16 galaxies with  $M_{\text{NC}}$  and  $\sigma$  measurements, shown by the open triangles in Figure 1.4, Scott & Graham (2013) find

$$\log \left( \frac{M_{\text{nc}}}{M_{\odot}} \right) = (2.11 \pm 0.31) \log \left( \frac{\sigma}{54 \text{km s}^{-1}} \right) + (6.63 \pm 0.09) , \quad (1.12)$$

which is shown by the dotted line in the left-hand panel of Figure 1.4. Several of these galaxies appear to have under-massive star clusters at given velocity dispersions in comparison with the Ferrarese et al. (2006) data and best fit. However, many of these galaxies also harbour SMBHs with masses that are comparable to or larger than the nuclear clusters, which would put them in line with the black hole  $M$ - $\sigma$  relation.

Though black holes and nuclear clusters follow roughly the same scaling there is a clear offset between the Ferrarese et al. data and the data of McConnell & Ma in the sense that the nuclear clusters lie a factor of  $\sim 10$  above an extrapolation of the of the  $M_{\text{BH}}$ - $\sigma$  relation to lower masses.

When considering the  $M$ - $M_{\text{bul}}$  relations in the right-hand panel of Figure 1.4, there is very little overlap between the black hole data from McConnell & Ma (2013) and the nuclear cluster data of Ferrarese et al. (2006), which meet at galaxy masses of  $\sim 10^{10} M_{\odot}$ . Scott & Graham (2013) adopt the same method as Ferrarese et al. (2006) to calculate the bulge masses in their compilation (open triangles in the right panel of Figure 1.4), and again find a much shallower relation than Ferrarese et al., suggesting that BHs and nuclear clusters follow different scaling relations. Again, the BHs that

also reside in the additional galaxies in the Scott & Graham sample bring these galaxies in line with the  $M_{\text{BH}}-M_{\text{bul}}$  relation so that the BHs and nuclear clusters define a single  $M_{\text{CMO}}-M_{\text{bul}}$  relation. Wehner & Harris (2006) investigated the  $M_{\text{CMO}}-M_{\text{bul}}$  relation with bulge masses calculated using the observed galaxy magnitudes and mass-to-light ratios. They also find that the CMOs define a single, unbroken  $M_{\text{CMO}}-M_{\text{bul}}$  relation with the CMO masses almost directly proportional to the bulge masses.

As in the Scott & Graham (2013) data, there are cases where nuclear clusters and SMBH coexist, such as the low luminosity, active galaxy NGC 1042 (Shields et al. 2008); and other cases of nuclear clusters coexisting with AGN, and hence SMBHs, such as NGC 4395 (Filippenko & Ho 2003). Seth et al. (2008) studied a sample of galaxies of various types and masses, known to host nuclear star clusters, searching for signs of AGN activity to infer the presence of an SMBH. Of the 176 galaxies in the sample, it is suggested that  $\sim 10\%$  harbour an SMBH as well as a nuclear cluster. These cases of coexistence cover a wide range of galaxy masses ( $10^9 - 10^{11} M_{\odot}$ ) but the frequency of AGN detection increases with increasing galaxy and nuclear cluster mass. Seth et al. also find that the masses of the nuclear clusters and SMBHs are comparable in the galaxies where they coexist. The central few parsecs of our own Galaxy, the Milky Way, contains a dense star cluster with a very compact radio source, Sgr A\*, at its centre, only 3-10 light minutes in diameter. The orbits of  $\sim 30$  stars in the immediate vicinity of Sgr A\* imply an SMBH with  $M_{\text{BH}} \simeq (4.1 \pm 0.6) \times 10^6 M_{\odot}$ . Graham & Spitler (2009) speculate that the coexistence of SMBHs and nuclear clusters may be a common feature of galaxies with bulge masses  $10^8 - 10^{11} M_{\odot}$ , roughly the range covered by the galaxies in the Scott & Graham (2013) compilation.

The  $M_{\text{CMO}}-\sigma$  and  $M_{\text{CMO}}-M_{\text{bul}}$  relations suggest not only that SMBHs and nuclear clusters co-evolve with their host galaxies but also that the two types of CMO evolve with their host galaxies in similar ways. It is of interest to investigate the physical origins of these relations between CMOs and the properties of their host galaxies, and the effect they have on the formation and evolution of the galaxies as a whole.

## 1.2 Theoretical overview

### 1.2.1 Physical concepts

As discussed in §1.1, galaxies with masses greater than  $10^{10}M_{\odot}$  harbour SMBHs in their centres while those with masses less than  $10^{10}M_{\odot}$  host nuclear star clusters. In either case, it has been observed that these CMOs are closely connected to their host galaxies as can be seen through the  $M$ – $\sigma$  relations. The physical explanation of these relations has been an active area of research and it is now widely accepted that self-regulated feedback is key in establishing these correlations. The  $M$ – $\sigma$  relations can be used to probe the importance of feedback in galaxy formation and evolution, so it is of interest to investigate the physical origins of the relation.

The self-regulated feedback scenario, discussed in §1.2.2, utilises several key concepts: the Eddington luminosity, super wind bubbles and black hole winds.

#### 1.2.1.1 The Eddington luminosity

The Eddington luminosity is the maximum luminosity an object can sustain while radiation forces on free electrons outwards are balanced by gravitational force inwards. If we consider a fully ionised gas, the interaction of the radiation with the gas is due to photons scattering off free electrons, known as Thomson scattering.

The flux per unit area per unit time at radius  $r$  from a source of luminosity  $L$  is  $= L/(4\pi r^2)$ . The momentum of a photon is given by  $p = E/c$ , so that  $\dot{p} = L/c = F_{\text{rad}}$ . Thus the radiation force per unit area (i.e., the radiation pressure) is  $= L/(4\pi r^2 c)$ . The cross sectional area of an electron is given by the Thomson cross-section,  $\sigma_{\text{T}}$ , therefore the radiation force acting on an electron is

$$F_{\text{rad}} = \sigma_{\text{T}} \frac{L}{4\pi r^2 c} . \quad (1.13)$$

The gravitational force acting on an electron-proton pair by the source of the

luminosity which has mass  $M$ , is given by

$$F_{\text{grav}} = \frac{GM(m_{\text{p}} + m_{\text{e}})}{r^2} \simeq \frac{GMm_{\text{p}}}{r^2} \quad (1.14)$$

where we take the last equality because  $m_{\text{p}} \gg m_{\text{e}}$ .

Then the Eddington luminosity is found by equating the radiation force (equation 1.13) to the gravitational force (equation 1.14), giving

$$L_{\text{Edd}} = \frac{4\pi G m_{\text{p}} c}{\sigma_{\text{T}}} M \quad . \quad (1.15)$$

As can be seen from equation (1.15),  $L_{\text{Edd}}$  is directly proportional to the mass of the object in question. Objects with luminosities above their Eddington luminosity are unable to hold on to the material in their outer layers against the radiation pressure, resulting in a radiatively driven outflow.

In accretion-powered objects, such as AGN, the luminosity is produced by the conversion of rest mass,  $m$ , into energy at some efficiency,  $\eta$ , so that  $E = \eta mc^2$ . Differentiating this we find the luminosity of an object accreting masses  $m$  at a rate  $\dot{M}$ , is  $L = \eta \dot{M} c^2$ . For matter to fall on to an object, the radiation force must be smaller than the gravitational force, i.e., the object must be radiating at less than its Eddington limit. This places a limit on the accretion rate

$$\dot{M}_{\text{Edd}} = \frac{L_{\text{Edd}}}{\eta c^2} = \frac{4\pi GM}{\eta \kappa c} \quad (1.16)$$

where  $\eta$  is the accretion efficiency, i.e., the fraction of the gravitational potential energy of the accreted material that can be radiated away and  $\kappa = \sigma_{\text{T}}/m_{\text{p}}$ . When accreting above the Eddington rate (super-Eddington accretion), the object is unable to hold all the material it is gaining against radiation pressure, again resulting in a radiation driven outflow.

Although much more intense than the stellar winds of objects with luminosities less than their Eddington limits, these outflows interact with surrounding ambient medium in much the same way, driving a super bubble.

### 1.2.1.2 Stellar winds and super bubbles

It is well known from stellar wind theory (e.g., Lamers & Cassinelli 1999; Dopita & Sutherland 2003) that massive stars drive stellar winds that interact with their surrounding ambient medium. The wind sweeps up the ambient medium into a shell that it drives outwards. The material in the shell is hot and tries to expand both backwards and forwards, driving two shock fronts, one propagating into the ambient medium and one propagating back into the stellar wind. The resulting shock pattern is composed of four zones; 1) the freely flowing wind, 2) a region of shocked wind material, 3) a region of shocked ambient medium which also contains the original swept-up shell and 4) the undisturbed ambient medium.

The dynamics of the swept-up shell are determined by the behaviour of the shocked wind region immediately behind it. In a momentum-conserving phase the shocked wind region is able to cool efficiently, so it condenses and is geometrically thin. The swept-up shell is then effectively driven outwards by a direct transfer of momentum from the wind impacting on its inner side. In an energy-conserving phase the shocked wind does not cool and the region remains hot and expands. The shell is then driven by the thermal pressure in the shocked wind region.

In Chapter 2 we will discuss outflow physics in detail. For now we note that the same process occurs for the winds driven by SMBHs and nuclear star clusters. In the case of SMBHs and NCs, it is possible to connect the wind thrust to the Eddington luminosity using the black hole winds theory of King & Pounds (2003).

### 1.2.1.3 Black hole winds

Motivated by observations of high velocity outflows in AGN accreting at rates comparable to the Eddington value, King & Pounds (2003) outline a theory of black hole winds driven by radiation that is key in theoretical explanations of the  $M$ - $\sigma$  relation.

King & Pounds begin by looking at the electron scattering optical depth through

an outflow with density  $\rho = \dot{M}_{\text{out}}/(4\pi v_w br^2)$ , viewed from infinity down to radius  $r$

$$\tau = \int_r^\infty \kappa \rho dr = \frac{\kappa \dot{M}_{\text{out}}}{4\pi v_w br} = \frac{1}{2b\eta} \frac{r_s}{r} \frac{c}{v_w} \frac{\dot{M}_{\text{out}}}{\dot{M}_{\text{Edd}}}, \quad (1.17)$$

where  $r_s = 2GM_{\text{BH}}/c^2$  is the Schwarzschild radius,  $\dot{M}_{\text{Edd}}$  is the Eddington rate defined in equation (1.16),  $v_w$  is the outflow speed and the parameter  $b$  is a geometrical factor that allows for some collimation of the outflow. The photospheric radius,  $r_{\text{ph}}$ , is defined as the radius at which  $\tau = 1$ , giving

$$\frac{r_{\text{ph}}}{r_s} = \frac{1}{\tau_e \eta} \frac{c}{v} \frac{\dot{M}_{\text{out}}}{\dot{M}_{\text{Edd}}}, \quad (1.18)$$

where  $\tau_e = 2b\tau \sim 1$ . Since  $\tau_e \eta < 1$  and  $v/c < 1$ ,  $r_{\text{ph}} > r_s$  for outflows with  $\dot{M}_{\text{out}}$  of the order  $\dot{M}_{\text{Edd}}$ , i.e., these outflows are Compton thick. Inside  $r_{\text{ph}}$  the photons scatter off electrons and their momentum is transferred to the outflow. Outside  $r_{\text{ph}}$  the photons decouple from the matter. For the outflow to escape requires that  $r_{\text{ph}}$  lies close to the escape radius  $r_{\text{esc}} = (c/v_w)^2 r_s$ , so that

$$\frac{v_w}{c} = \tau_e \eta \frac{\dot{M}_{\text{Edd}}}{\dot{M}_{\text{out}}}. \quad (1.19)$$

or,

$$\tau_e \frac{L_{\text{Edd}}}{c} \simeq \dot{M}_{\text{out}} v_w. \quad (1.20)$$

McLaughlin, King & Nayakshin (2006) note that equation (1.20) can be extended to treat the nuclear cluster case as well as SMBHs by parameterizing the wind thrust as

$$\dot{M}_{\text{out}} v_w \simeq \lambda \tau_e \frac{L_{\text{Edd}}}{c} = \lambda \tau_e \frac{4\pi GM_{\text{CMO}}}{\kappa} \quad (1.21)$$

In the case the CMO is an SMBH the parameter  $\lambda \simeq 1$  and we return to equation (1.20), the case as argued by King & Pounds (2003). In the case the CMO is a nuclear cluster, the feedback is provided by the combined stellar winds and supernovae from stars in the cluster, which drive a superwind with a momentum flux that is much less than  $L_{\text{Edd}}/c$ , but still directly proportional to it. This proportionality comes from the fact the Eddington luminosity itself is directly proportional to mass. Only a fixed

fraction of stars in the cluster will contribute to the superwind, i.e., those massive enough to produce strong stellar winds and to result in supernovae. As such  $\lambda$  takes a value  $\ll 1$  related to the fraction of massive stars. McLaughlin, King & Nayakshin (2006) estimate the separate contributions of stellar winds and supernovae in a cluster with a Chabrier (2003) initial mass function and find  $\lambda \simeq 0.05$ .

With these concepts, we now move on to look at theoretical derivations of the  $M$ - $\sigma$  relations.

### 1.2.2 The $M_{\text{CMO}} - \sigma$ relation

Before the significance of the  $M - \sigma$  relation for SMBHs was established observationally (Ferrarese & Merritt 2000; Gebhardt et al. 2000), derivations of SMBH properties in relation to their host galaxies had already been the subject of much investigation (e.g. Haehnelt, Natarajan & Rees 1998; Magorrian et al. 1998; Merrifield, Forbes & Terlevich 2000). The works of Silk & Rees (1998) and Fabian (1999) are both concerned with the accretion of matter onto a seed black hole at the centre of a protogalaxy that is modelled as a singular isothermal sphere (see §1.3). This accretion of matter produces an outflow that sweeps the surrounding medium into a shell that expands into the galaxy. The key idea in both these works is that when the shell is able to escape the galaxy it will fragment and form the stars of the galaxy bulge, hence giving an  $M_{\text{BH}} - M_{\text{bul}}$  relation. By considering the velocity of the shell and when it can escape the galaxy, Silk & Rees find  $M_{\text{BH}} \propto \sigma^5$ . In a similar fashion, Fabian considers when the wind power is sufficient to eject the shell from the protogalaxy, finding  $M_{\text{BH}} \propto \sigma^4$ . In both Silk & Rees (1998) and Fabian (1999) the wind luminosity is taken to be an unspecified fraction of the Eddington luminosity of the SMBH, leaving the  $M_{\text{BH}} - \sigma$  relations in terms of a free parameter. Equation (1.20) has allowed more recent results to be derived with no free parameter.

It is the assumption of a momentum-driven outflow that leads to the scaling  $M_{\text{CMO}} \propto \sigma^4$  (e.g., Fabian 1999; King 2003, 2005; McLaughlin et al. 2006) as we can see by considering the ram pressure of the wind that drives the shell and the pressure of

the ambient medium. Using equation (1.20), the ram pressure of the wind is

$$\rho_w v_w^2 = \frac{\dot{M}_{\text{out}} v_w}{4\pi r^2} = \tau_e \frac{L_{\text{Edd}}}{4\pi r^2 c} = \tau_e \frac{GM_{\text{CMO}}}{\kappa r^2} \quad (1.22)$$

In order for the shell to escape, the ram pressure must be greater than the ambient pressure, which in a halo modelled as a singular isothermal sphere (see equation [1.26] below) is given by

$$\rho_{\text{amb}} \sigma_0^2 = \frac{f_g \sigma_0^4}{2\pi G r^2} \quad (1.23)$$

where  $\sigma_0$  is the velocity dispersion that characterizes a singular isothermal sphere and  $f_g$  is an ambient gas fraction,  $\sim 0.2$  at all radii in a halo where the gas traces the dark matter directly. Therefore, for the ram pressure to overcome the ambient pressure, i.e., for the shell to escape, gives a relation where  $M_{\text{CMO}} \propto \sigma^4$ .

In more detail, by considering the motion of the shell as it moves out against the gravity of the dark matter inside it, McLaughlin et al. (2006) find for the shell to reach large radius requires

$$M_{\text{CMO}} = \lambda^{-1} \frac{f_g \sigma_0^4}{\pi} \frac{\kappa}{G^2} \simeq 3.68 \times 10^8 M_{\odot} \lambda^{-1} \left( \frac{\sigma}{200 \text{ km s}^{-1}} \right)^4 \quad (1.24)$$

(see also Murray et al. 2005; King 2005). Taking values of  $\lambda = 1$  for SMBHs and  $\lambda = 0.05$  for nuclear clusters gives an offset of the same order as is observed between the  $M_{\text{BH}} - \sigma$  and  $M_{\text{nc}} - \sigma$  relations, as seen in the left-hand panel of Figure 1.4.

Once a CMO in an isothermal halo with a given  $\sigma_0$  has grown to the mass in equation (1.24), the CMO wind may drive a momentum-conserving shell with coasting speed  $v > 0$  at arbitrarily large radii in the galaxy. If the wind is strong enough to drive the shell to the escape speed of the halo then the galaxy is cleared of any remaining ambient gas, cutting off further star formation and CMO growth, and locking in an  $M_{\text{CMO}} - \sigma$  relation.

In their derivation, Silk & Rees (1998) find  $M_{\text{BH}} \propto \sigma^5$  because they assume that the outflow is energy-conserving.

In the energy-driven regime the shell is driven by the thermal pressure of the shocked wind region, into which energy is injected from the wind so that in that region

$$\frac{d}{dt} [r^3 P] \propto \dot{E}, \quad (1.25)$$

where  $\dot{E} = \dot{M}_{\text{out}} v_w^2 / 2$  is the kinetic energy flux of the wind. We note that the full energy equation of the shocked wind region includes work done by expanding the shell and work against the gravity of both the CMO and the dark matter inside the shell as we will discuss in Chapter 4.

Combining equation (1.25) with equation (1.20), we find the thermal pressure driving the shell outwards  $P \propto v_w M_{\text{CMO}} / [r^2 v(r)]$ , where  $v(r) = dr/dt$  is the velocity of the swept up shell. Then for the thermal pressure to overcome the ambient pressure (equation [1.23]) actually leads to  $M_{\text{CMO}} v_w \propto \sigma_0^5$ , for shell speeds  $v(r) \sim \sigma_0$ .

The explicit dependence of the energy-driven  $M_{\text{CMO}} - \sigma$  relation on  $v_w$  has not been made by previous authors (e.g., Silk & Rees 1998) who have assumed a constant  $v_w$  and found  $M_{\text{CMO}} \propto \sigma^5$ . The dependence on  $v_w$  is also lost in other related analyses of energy-driven shells (e.g., King 2005; Faucher-Giguère & Quataert 2012).

It has been argued that energy-driven outflows lead to too steep a slope in the  $M - \sigma$  relation. King (2003) suggests that as the shell moves out into the galaxy the cooling time of the shocked wind region increases. The shell then transitions from a momentum- to an energy-driven regime that allows it to accelerate and escape, while preserving the  $M_{\text{CMO}} \propto \sigma^4$  scaling of momentum-driven outflows. In that case, in its momentum-driven phase the CMO needs only to push the shell to the radius where the switch to energy-driving occurs. This could be done with a CMO less massive than the mass in equation (1.3), suggesting that this may be an upper limit for observed  $M - \sigma$  relations; and indeed, the equation lies above the current best fits to data by factors of a few. However, as discussed earlier, the slope of the observed  $M - \sigma$  relation is  $\sim 4 - 5$ , so it is not clear whether momentum-driven outflows ( $M_{\text{CMO}} \propto \sigma^4$ ) or energy-driven outflows ( $M_{\text{CMO}} v_w \propto \sigma^5$ ) provide better agreement with observations.

Whether the CMO outflow is energy- or momentum-driven is the subject of some debate, a discussion we will return to in Chapter 2.

As discussed above, much of the previous theoretical work on the  $M - \sigma$  relation has modelled momentum-driven outflows in galaxies with dark matter haloes modelled as singular isothermal spheres (SISs). The SIS is analytically tractable and has some features that relate to real dark matter haloes. The SIS provides a good first order

approximation of dark matter haloes but it does suffer from some drawbacks, perhaps most notably that its mass increases linearly with radius at all radii. A truncated isothermal halo is often used, where outside some radius the mass is zero, but there are also much more realistic models for dark matter haloes that we will consider here, though these are often not analytically tractable.

### 1.3 Dark matter haloes

There has been evidence for some time that galaxies include a large, non-luminous component of matter which we now call dark matter haloes. While tabulating galaxy masses as a function of radius Ostriker, Peebles & Yahil (1974) found that spiral galaxy masses increase linearly with radius, out to tens and hundreds of kpc, and the masses of galaxy groups increase linearly with radius out to almost  $\sim 1\text{Mpc}$ , implying masses of order  $10^{12}M_{\odot}$ . It has also been observed that the circular speed profiles of many galaxies remain flat, or even rise slightly, at large radii well beyond the extent of the luminous matter (e.g. Rubin, Ford & Thonnard 1980; Burstein 1982). The circular speed  $V_c^2(r) = GM(r)/r$ , so that a constant circular speed at large radius implies the galaxy mass,  $M(r)$  increases linearly with radius, as found by Ostriker et al. (1974).

Today, cold dark matter (CDM) is the favoured theory for how galaxies are formed from the initial smooth state of the Universe. In the CDM paradigm small objects are formed by the collapse of random fluctuations under gravity and galaxies form hierarchically by mergers of these small objects to form larger structures. Many simulations have been performed under this model, and the results are in general agreement with observations of large scale structures. Much has been learned about dark matter haloes from these simulations. One such result concerns the similarity of the density profiles of haloes of widely different masses (Navarro, Frenk & White 1996). There has been much work in fitting the ‘universal’ density profile of simulated dark matter haloes.

Before looking in detail at the density profiles used to fit simulated dark matter

haloes, we look at the density profile of a singular isothermal sphere (SIS). The SIS provides a good “zeroth-order” approximation for galaxy density profiles in theoretical work because it is simple to work with, but it does have some relevance to real galaxies and the structure of dark matter haloes.

The density of an SIS is given by

$$\rho_{\text{DM}}(r) = \frac{\sigma_0^2}{2\pi G r^2} \quad , \quad (1.26)$$

where  $\sigma_0$  is the velocity dispersion that characterizes the halo. This means that the mass inside radius  $r$  is given by

$$M_{\text{DM}}(r) = 4\pi \int_0^r \rho_{\text{DM}}(r') r'^2 dr' = \frac{2\sigma_0^2}{G} r \quad . \quad (1.27)$$

We then find that the circular speed profile of an SIS is constant at all radii:

$$V_c^2(r) = \frac{GM_{\text{DM}}(r)}{r} = 2\sigma_0^2 \quad . \quad (1.28)$$

Given the simplicity of the SIS model, this result matches well with the observations of real haloes as discussed above (Rubin et al. 1980 etc.) that the circular velocity remains constant at large radius.

However, the SIS has  $\rho_{\text{DM}} \propto r^{-2}$  at all radii, so that the mass increases linearly with radius to infinitely large radii, and similarly, the circular speed is constant out to infinitely large radii. More realistically, we are interested in dark matter haloes that have a finite extent, so that the mass and circular speed fall off at large radius, as is observed. As such, a truncated SIS is often used in analytic calculations, where outside some radius (often the virial radius) the mass is zero.

It is not entirely satisfactory to just chop off the outer extent of the halo. There are more sophisticated models that have been used to fit simulated dark matter haloes where the density falls off more steeply than  $r^{-2}$  at large radii. Simulated dark matter haloes generally have density profiles that are shallower than isothermal at small radii and steeper than isothermal at large radii.

The general fitting function most commonly applied to simulated dark matter haloes has the form

$$\rho(r) \propto \frac{1}{r^{-\alpha}(r_s + r)^{\alpha-\beta}} \quad (1.29)$$

where  $r_s$  is an appropriate scale length. This form for the density profile gives  $\rho(r) \propto r^{-\alpha}$  for  $r \ll r_s$ , and  $\rho(r) \propto r^{-\beta}$  for  $r \gg r_s$ . Density profiles used to fit simulated haloes commonly have  $\alpha < 2$  and  $\beta > 2$  (e.g, Hernquist 1990; Navarro, Frenk & White 1996, 1997), so that there is a single, well defined radius where the logarithmic density slope  $d \ln \rho / d \ln r = -2$ , which we denote  $r_{-2}$ . This form of density profile also gives circular speed profiles,  $V_c^2(r)$ , that have a single peak.

Figure 1.5 shows the density (*top panel*), mass (*middle panel*) and circular speed profiles (*bottom panel*) of several dark matter halo models with a scale radius  $r_s = r_{-2}$ . For comparison, the density, mass and circular velocity profile of an SIS are shown by dotted (black) lines in each panel. In all cases, the density, mass and circular speed are all scaled by their values at  $r_s$ , which we denote as  $\rho_{\text{DM}}(r_s) \equiv \rho_s$ ,  $M_{\text{DM}}(r_s) \equiv M_s$  and  $V_c^2(r_s) \equiv V_{c,s}^2$ .

The short-dashed (blue) lines in each panel of Figure 1.5 show the density, mass and circular speed profiles of Hernquist (1990), which was used by Dubinski & Carlberg (1991) to fit their simulated dark matter haloes. The properties of their simulated haloes, such as the rotation curves, were in reasonable agreement with observed rotation curves in spiral galaxies.

The Hernquist (1990) profile has

$$\rho_{\text{DM}}(r) = \frac{M_{\text{tot}}}{2\pi r_0^3} \left(\frac{r}{r_0}\right)^{-1} \left(1 + \frac{r}{r_0}\right)^{-3}, \quad (1.30)$$

where  $M_{\text{tot}}$  is the total halo mass and  $r_0$  is a scale radius. We can see this is shallower in the centre and steeper at larger radius than the SIS, shown by the dotted (black) lines. This means that the mass profile, given by

$$M_{\text{DM}}(r) = M_{\text{tot}} \left(\frac{r/r_0}{1 + r/r_0}\right)^2, \quad (1.31)$$

risers more steeply in the centre but tends to a finite mass at large radius, unlike the SIS which diverges at large radius. Unlike the SIS, the circular speed profile of Hernquist (1990) varies with radius as

$$V_c^2(r) = \frac{GM_{\text{tot}}}{r_0} \frac{r/r_0}{(1 + r/r_0)^2}, \quad (1.32)$$

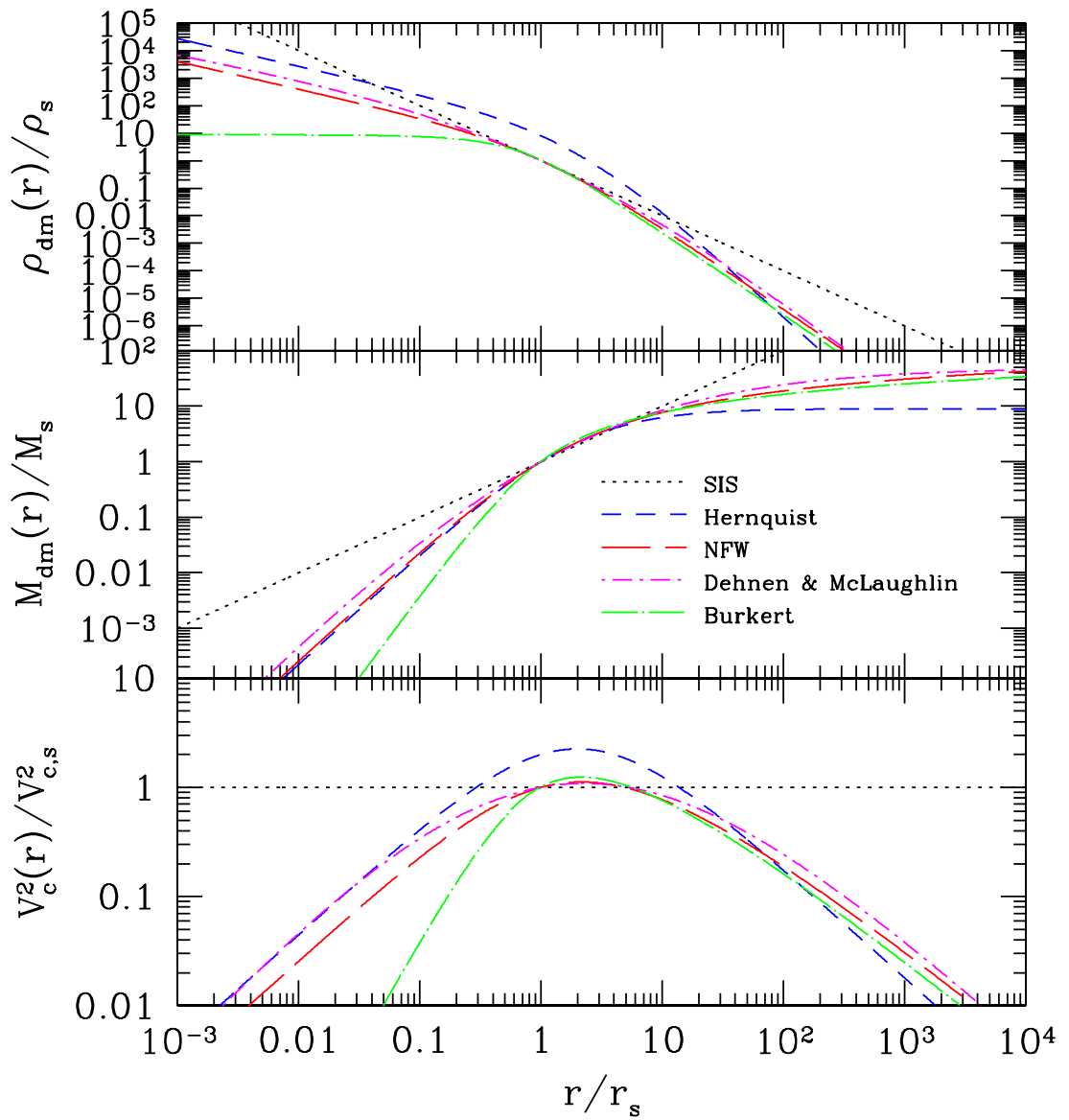


Figure 1.5: Density profile  $\rho(r)$  (*top panel*), mass profile  $M(r)$  (*middle panel*) and the circular speed profile  $V_c^2(r)$  (*lower panel*) for Hernquist (blue short-dashed lines), NFW (red long-dashed lines), Dehnen & McLaughlin (magenta dot-short-dashed lines) and Burkert (green dot-long-dashed lines).

so that the circular speed increases outward from the centre, reaches a peak and then declines towards larger radii.

Navarro, Frenk & White (1996) used high resolution simulations to investigate the formation of dark matter haloes with a wide range of halo masses. They found that the density profiles of haloes of different masses were all fitted well by the same model. The dark matter profile of Navarro, Frenk & White (1996, 1997, hereafter NFW) is given by

$$\rho_{\text{DM}}(r) = 4\rho_0 \left(\frac{r}{r_0}\right)^{-1} \left(1 + \frac{r}{r_0}\right)^{-2}, \quad (1.33)$$

where  $r_0$  is a scale radius and  $\rho_{\text{DM}}(r_0) \equiv \rho_0$ . This gives a mass profile

$$M_{\text{DM}}(r) = 16\pi\rho_0 r_0^3 \left[ \ln(1 + r/r_0) - \frac{r/r_0}{1 + r/r_0} \right], \quad (1.34)$$

which then gives a circular speed profile of

$$V_c^2(r) = 16\pi G\rho_0 r_0^2 \left[ \frac{\ln(1 + r/r_0)}{r/r_0} - \frac{1}{1 + r/r_0} \right]. \quad (1.35)$$

Like Hernquist (1990), the NFW profile has  $\rho_{\text{DM}} \propto r^{-1}$  at small radii, though  $\rho_{\text{DM}} \propto r^{-3}$  at large radii. It has also been shown that the NFW profile provides an equally good fit to the haloes simulated by Dubinski & Carlberg (1991) as the profile of Hernquist (1990) (Deimand & Moore 2009). The NFW profile is shown by the long-dashed (red) lines in Figure 1.5. We can see that in the inner regions the density, mass and circular speed profiles of the NFW match that of Hernquist (1990). At large radius however, the density of NFW is somewhat shallower than Hernquist (1990) and the mass of NFW actually diverges logarithmically at large radius. Like Hernquist (1990), the circular speed curve of NFW rises outwards to a single peak and then declines at large radius.

Dehnen & McLaughlin (2005) developed a family of halo models motivated by the result that the ratio  $\rho_{\text{DM}}(r)/\sigma^3(r)$  is a single power law in radius for simulated dark matter haloes. Their derived density profile for the case of velocity isotropy has

$$\rho_{\text{DM}}(r) = \frac{5}{9} \frac{M_{\text{tot}}}{\pi r_0^3} \left(\frac{r}{r_0}\right)^{-7/9} \left[ 1 + \left(\frac{r}{r_0}\right)^{4/9} \right]^6, \quad (1.36)$$

where again  $r_0$  is a scale radius and  $M_{\text{tot}}$  is the total mass of the halo. This gives a mass profile

$$M_{\text{DM}}(r) = M_{\text{tot}} \left[ \frac{(r/r_0)^{4/9}}{1 + (r/r_0)^{4/9}} \right]^5, \quad (1.37)$$

and circular speed profile

$$V_c^2(r) = GM_{\text{tot}} r_0 \frac{(r/r_0)^{11/9}}{[1 + (r/r_0)]^5}. \quad (1.38)$$

This profile matches current simulations at least as well as any other fitting function. The profile of Dehnen & McLaughlin (2005) is shown as the short dash-dot (magenta) lines in Figure 1.5. At small radius, the density goes as  $r^{-7/9}$  which is slightly shallower than both Hernquist (1990) and NFW. At large radius  $\rho_{\text{DM}} \propto r^{-20/9}$ , a slope between that of Hernquist (1990) and NFW. The mass profile of Dehnen & McLaughlin (2005) increases approximately in line with Hernquist and NFW and tends to a finite mass at large radius. Again, the circular speed profile increases outwards, peaks and then falls off at large radius.

In addition to the appearance of a ‘universal’ density profile for dark matter haloes, another result common to many simulated haloes is the absence of a well defined central ‘core’ of constant density. Several studies argue for a steeper central ‘cusp’ where the dark matter density grows without limit towards the centre of the halo, such as the profiles of Hernquist (1990), NFW and Dehnen & McLaughlin (2005). However, the resolution of current simulations can only resolve structure to within an appreciable fraction ( $\sim 10^{-3}$ ) of the virial radius, leaving the possibility that the density may still become shallower than  $r^{-1}$  at smaller radii.

There are several models for cored density profiles such as Burkert (1995), which has been used to model the dark matter haloes of dwarf galaxies. The density profile of this model is given by

$$\rho_{\text{DM}}(r) = \frac{4\rho_0}{(1 + r/r_0)(1 + r^2/r_0^2)}, \quad (1.39)$$

where  $r_0$  is the scale radius and  $\rho_{\text{DM}}(r_0) \equiv \rho_0$ . This leads to

$$M_{\text{DM}}(r) = 8\pi\rho_0 r_0^3 \left[ \ln(1 + r/r_0) + \frac{1}{2} \ln(1 + r^2/r_0^2) - \tan^{-1}(r/r_0) \right], \quad (1.40)$$

and

$$V_c^2(r) = 8\pi G\rho_0 r_0^2 \left(\frac{r}{r_0}\right)^{-1} \left[ \ln(1 + r/r_0) + \frac{1}{2} \ln(1 + r^2/r_0^2) - \tan^{-1}(r/r_0) \right]. \quad (1.41)$$

The Burkert (1995) density profile is still shallower than isothermal at small radii and steeper than isothermal at large radii, with  $\rho_{\text{DM}} \propto r^{-3}$  at large radius and a constant density at small radii, as can be seen by the long dash-dot (green) lines in Figure 1.5. It also has the most steeply increasing mass profile at small radius. As with the cuspy dark matter profiles, the circular speed profile of Burkert (1995) has a single, well defined peak.

As we have noted, all of these models, both cored and cuspy, have a single, well defined peak in their circular speed profiles,  $V_c^2(r) = GM(r)/r$ , as can be seen in the bottom panel of Figure 1.5. This peak, occurring at radius  $r_{\text{pk}}$ , so that  $V_c^2(r_{\text{pk}}) \equiv V_{c,\text{pk}}^2$ , provides a natural point of reference in all such haloes, which we will make use of later (see Chapters 3 and 5).

We will now look in detail at physics of momentum- and energy-driven outflows, and whether outflows from nuclear star clusters and supermassive black holes are momentum or energy-driven.

## 2 Outflow physics

As discussed in Chapter 1, it is widely accepted that the  $M_{\text{CMO}}-\sigma$  relations between CMO mass,  $M_{\text{CMO}}$ , and stellar velocity dispersion,  $\sigma$ , for both nuclear star clusters and supermassive black holes are the result of self-regulated feedback. In the self-regulated feedback scenario the CMO drives a wind that sweeps the surrounding ambient medium into a shell. A key question regarding CMO winds is whether the swept-up shell is momentum-driven, which leads to an  $M-\sigma$  relation of the form  $M_{\text{CMO}} \propto \sigma^4$ , or if it is energy-driven, which gives  $M_{\text{CMO}} \propto \sigma^5$ . There is an ongoing debate in the literature over which driving mechanism is responsible for the  $M-\sigma$  scaling, which couples with the observational discussion of the exact slope.

In this chapter we look in detail at outflow physics and at the dynamics of the shell. We will look at the shock structure generated by the outflow and at how the pre- and post-shock properties of the gas are related through the jump conditions. We use the jump conditions to find the temperature, density and velocity of the post-shock gas, which we subsequently use to determine the cooling time of the shocked gas. This allows us to address the question of whether the CMO driven outflows are momentum- or energy-driven.

### 2.1 Outflow structure

Outflows arise from a variety of astrophysical objects. Of interest in the context of outflows driven by nuclear clusters or black holes are;

1. Supernova explosions,
2. Radiatively driven stellar winds,
3. Outflows from active galactic nuclei.

Stars with initial main sequence masses of  $\gtrsim 8 M_{\odot}$  result in supernovae explosions. In a supernova explosion a large fraction of the star’s mass is ejected at high speed, depositing a large amount of kinetic energy into the surrounding region. The expansion of the supernova ejecta drives an outflow into the ambient medium.

All hot stars, including main sequence and evolved stars, produce winds driven by radiation pressure. Essentially, radiation from the star is scattered by the atmosphere, transferring momentum from the radiation field to the atmospheric gas, driving an outflow.

In nuclear star clusters the supernovae and the winds of individual stars in the cluster combine to drive a “superwind”.

Strong outflows in local AGN have been observed both on large scales and closer to the SMBH. As discussed in Chapter 1, an SMBH accreting at near- or super-Eddington rates is expected to drive a fast outflow back into the host galaxy.

The properties of these different objects cover a wide range of parameters including various wind speeds,  $v_w$ , (several thousands of  $\text{km s}^{-1}$  from massive stars, to  $\sim 0.1c$  from AGN) and a range of mass-loss rates,  $\dot{M}_{\text{out}}$ , ( $\sim 10^{-6} M_{\odot} \text{ yr}^{-1}$  for massive stars, to several  $M_{\odot} \text{ yr}^{-1}$  in AGN outflows). These combine to give a wide range of mechanical or wind luminosities,  $L_w = \frac{1}{2} \dot{M}_{\text{out}} v_w^2$  ( $\sim 10^{35} \text{ erg s}^{-1}$  for massive stars, e.g., Lamers & Cassinelli 1999; to  $\sim 10^{45} \text{ erg s}^{-1}$  for AGN outflows, e.g., Tombesi et al. 2013). Despite the range of mechanical luminosities, these winds interact with their surrounding ambient media in much the same way.

The basic theory outlining the interaction of stellar winds with their surrounding ambient media was developed by Castor, McCray & Weaver (1975), and in more detail by Weaver et al. (1977). In our cases, the CMO wind sweeps the surrounding ambient medium into a shell which it drives outwards. The swept-up shell is hot and tries to expand both backwards, into the freely flowing wind, and forwards into the undisturbed ambient medium. This expansion drives two shock fronts, an inner shock that propagates into the wind material, and an outer shock that propagates into the ambient medium. The resulting shock pattern, shown in Figure 2.1, has four distinct regions:

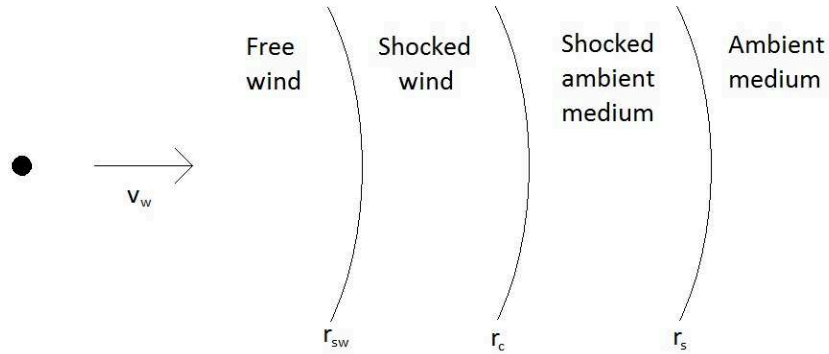


Figure 2.1: Schematic of a wind bubble. Here, the source emits a wind of constant velocity  $v_w$  which passes through the wind shock at radius  $r_{sw}$ . The shocked wind region is separated from the shocked ambient medium by the contact surface at radius  $r_c$ . The region of shocked ambient medium also contains the original shell of swept-up material and is bounded by the ambient shock at radius  $r_s$ .

- Zone 1 — The free wind, of constant velocity  $v_w$ , with density  $\rho_w(r) = \dot{M}_w / (4\pi r^2 v_w)$ , forms the innermost region and is bounded only by the inner or wind shock at radius  $r_{sw}$ .
- Zone 2 — The shocked wind region is bounded by the wind shock and the contact surface, at radius  $r_c$ , which separates material that originates from the wind and material originally from the ambient medium. This region gathers mass from the wind material that passes through the inner shock.
- Zone 3 — The region of shocked ambient medium is bounded by the contact

surface and the outer or ambient shock, at radius  $r_s$ . This region contains the shell of swept-up material and gathers mass as the outer shock passes through the undisturbed ambient medium.

- Zone 4 — The undisturbed ambient medium is the outermost region and is bounded only on the inner side by the ambient shock at  $r_s$ .

The wind shock and ambient shock have velocities of  $v_{sw}$  and  $v_s$  respectively, in the stationary frame. The shell continues to gain mass as it is driven outwards, which causes the expansion of the shell to slow down. As such we have that  $v_{sw} \ll v_{in}$  and  $v_s \ll v_{in}$ . Then the velocity of the wind relative to the wind shock is  $u_0 \equiv v_{in} - v_{sw} \approx v_{in}$

In their study of the dynamics of wind bubbles and superbubbles, Koo & McKee (1992) explain that the behaviour of the bubble, or shock pattern, depends on three timescales (see also, Faucher-Giguère & Quataert 2012):

- $t_{flow} = r_s/v_s$  — the flow time of the shell, where  $r_s$  is the radius of the shell and  $v_s$  is the shell velocity.
- $t_{cool,sw} \sim E/\dot{E}$  — the cooling time of the shocked wind region, where  $E$  is the energy in the shocked wind and  $\dot{E}$  is the energy loss rate in the region.
- $t_{dyn} = r_{sw}/v_w$  — the dynamical time of the wind, where  $r_{sw}$  is the radius of the wind shock and  $v_w$  is a constant wind velocity.

If  $t_{cool,sw} \ll t_{dyn}$ , then the shock is radiative, i.e., the shocked wind region is able to cool in the time it takes new wind material (i.e., more energy input) to reach the shock front from the source. Thus, the shocked wind region cools efficiently and condenses so it is geometrically thin. The swept-up shell is then effectively driven outwards by a direct transfer of momentum from the wind impacting on its inner side, defining a momentum-driven outflow.

If instead  $t_{cool,sw} \gg t_{flow}$ , then the shocked wind material is unable to cool in the time it takes to reach the shell. Hence the region is hot and geometrically thick, driving the swept up shell outwards with its thermal pressure, so the outflow is energy-driven.

If  $t_{\text{dyn}} \lesssim t_{\text{cool,sw}} \lesssim t_{\text{age}}$  then the bubble is in a partially radiative regime. In this case, most of the shocked wind cools, but the most recently shocked portion remains hot and occupies most of the volume of the bubble. In this intermediate state the outflow conserves neither energy or momentum.

Thus, the nature of the outflow is determined by whether or not the shocked wind region is able to cool efficiently. Although properties such as density and velocity can change discontinuously as the material passes through the shock front, mass, momentum and energy must also be conserved across the shock. These conservation laws place constraints upon how the properties of the material can change by relating the pre- and post-shock conditions of the flow, known as adiabatic jump conditions. Using these jump conditions, we can find the temperature and density of the gas in the shocked wind region immediately after it has been shocked and determine whether or not the material is able to cool efficiently, and thus whether the outflow is momentum- or energy-conserving.

We note that the behaviour of the shocked ambient medium does not greatly impact the results. If the shocked ambient medium cools efficiently then both the shocked wind and the shocked ambient medium are confined to a thin shells. If the shocked ambient medium does not cool then it is still confined to a relatively thin shell because is it being continually compressed by the shocked wind region (Koo & McKee 1992).

## 2.2 Jump conditions

We follow Dopita & Sutherland (2003) in our derivation of the jump conditions and take a frame of reference where the shock front is stationary. The fluid motion must obey the conservation of mass, momentum and energy. The flow is also subject to an equation of state relating pressure, density and temperature. We consider a radiationless, or adiabatic shock where the material does not lose or gain energy when passing through the shock front. We will consider the cooling process of the material immediately after

it has been shocked in §2.3.

The conservation equations are given by

$$\frac{\partial \rho}{\partial t} + \nabla \cdot (\rho \mathbf{u}) = 0 \quad (2.1)$$

$$\rho \left[ \frac{\partial \mathbf{u}}{\partial t} + (\mathbf{u} \cdot \nabla) \mathbf{u} \right] = \mathbf{F} - \nabla P \quad (2.2)$$

$$\frac{\partial}{\partial t} \left( \frac{\rho u^2}{2} + \rho U + \rho \Phi \right) + \nabla \cdot \left[ \rho \mathbf{u} \left( \frac{u^2}{2} + H + \Phi \right) \right] = 0, \quad (2.3)$$

where  $\rho$  is the mass density of the fluid,  $\mathbf{u}$  is the velocity,  $\mathbf{F}$  represents any external force (i.e., gravity) per unit volume,  $P$  is the internal fluid pressure,  $\Phi$  is the potential,  $U$  is the internal energy and  $H = U + P/\rho$  is the enthalpy per unit mass, which represents the total amount of energy per mass available to the gas, including the specific internal energy and the energy required to establish its volume and pressure.

Equation (2.1) is the continuity equation, which states that the rate of change of mass in a region (i.e., the density) is determined by the difference in the rate of flow into and out of that region.

Equation (2.2) gives the conservation of momentum, which states that the rate of change of momentum in a region is balanced by the flux of momentum into that region and the net force acting upon the material in that region, i.e.,  $\partial \mathbf{p} / \partial t = \mathbf{F}$  per unit volume.

The conservation of energy is given by equation (2.3), which requires that the rate of change of energy in a region equates to the net flux of energy through the surface that bounds that region.

In the spherical systems that we are considering, we can reduce equations (2.1)–(2.3) to one dimension so the conservation of mass, momentum and energy are given by

$$\frac{\partial \rho}{\partial t} + \frac{\partial}{\partial x} (\rho u) = 0 \quad (2.4)$$

$$\rho \frac{\partial u}{\partial t} + \rho u \frac{\partial u}{\partial x} = -\frac{\partial P}{\partial x} \quad (2.5)$$

$$\frac{\partial}{\partial t} \left( \frac{\rho u^2}{2} + \rho U \right) + \frac{\partial}{\partial x} \left[ \frac{\rho u^3}{2} + \frac{\gamma}{\gamma - 1} P u + F \right] = 0 \quad (2.6)$$

We can simplify this further by assuming a potential-free (i.e.,  $\Phi = 0$ ), steady flow, and we can substitute  $U = P/\rho(\gamma - 1)$  where  $\gamma$  is the ratio of specific heats. For a steady flow the time derivatives vanish, and we have

$$\frac{d}{dx}(\rho u) = 0 \quad (2.7)$$

$$\frac{d}{dx}(P + \rho u^2) = 0 \quad (2.8)$$

$$\frac{d}{dx} \left[ \frac{\rho u^3}{2} + \frac{\gamma}{\gamma - 1} P u + F \right] = 0 \quad (2.9)$$

Equations (2.7), (2.8) and (2.9) provide a complete description of a one dimensional, potential-free, steady-state flow. We can integrate the equations between two points, a region with variables  $u_0$ ,  $\rho_0$  and  $P_0$  and a later region in the flow with variables  $u_1$ ,  $\rho_1$  and  $P_1$ , where  $u_0$  and  $u_1$  are the velocities relative to the shock front. This gives us the *Rankine-Hugoniot jump conditions*:

$$[\rho u]_0^1 = 0 \quad (2.10)$$

$$[P + \rho u^2]_0^1 = 0 \quad (2.11)$$

$$\left[ \frac{u^2}{2} + \frac{\gamma}{\gamma - 1} \frac{P}{\rho} \right]_0^1 = 0 \quad (2.12)$$

As noted previously, the quantity  $\rho u$  is constant in the flow and equation (2.12) follows from dividing equation (2.9) by  $\rho u$ .

We now use equations (2.10)-(2.12) to relate the pre- and post-shock variables.

Expanding equations (2.10) and (2.11), we find that

$$\rho_0 u_0 = \rho_1 u_1, \quad (2.13)$$

and

$$P_0 + \rho_0 u_0^2 = P_1 + \rho_1 u_1^2. \quad (2.14)$$

We then use equation (2.13) to eliminate  $\rho_1$  and equation (2.14) to eliminate  $P_1$  from the expansion of equation (2.9) giving

$$\left( \frac{\gamma + 1}{\gamma - 1} \right) u_1^2 - \frac{2\gamma}{\gamma - 1} \frac{(P_0 + \rho_0 u_0^2)}{\rho_0 u_0} u_1 + \left( \frac{2\gamma}{\gamma - 1} \frac{P_0}{\rho_0} + u_0^2 \right) = 0. \quad (2.15)$$

We can simplify this further by using the definition of the adiabatic sound speed

$$c_s^2 = \gamma \frac{P}{\rho} , \quad (2.16)$$

to eliminate  $P_0$ . Then, defining  $\beta = u_1/u_0$ , we have

$$\left(\frac{\gamma+1}{\gamma-1}\right) \beta^2 - \frac{2}{\gamma-1} \left[ \left(\frac{c_0}{u_0}\right)^2 + \gamma \right] \beta + \left[ \frac{2}{\gamma-1} \left(\frac{c_0}{u_0}\right)^2 + 1 \right] = 0 . \quad (2.17)$$

We can simplify this one step further by noting that the Mach number  $\mathcal{M} \equiv u/c_s$ , finally giving

$$\left(\frac{\gamma+1}{\gamma-1}\right) \beta^2 - \frac{2}{\gamma-1} (\mathcal{M}_0^{-2} + \gamma) \beta + \left(\frac{2\mathcal{M}_0^{-2}}{\gamma-1} + 1\right) = 0 , \quad (2.18)$$

where  $\mathcal{M}_0 = u_0/c_0$  is the pre-shock Mach number.

In the limit of a strong shock, where the velocity of the gas is much higher than the sound speed,  $\mathcal{M}_0 \gg 1$  so the  $\mathcal{M}_0^{-2}$  terms become negligible. Therefore, in a monatomic gas where  $\gamma = 5/3$ , equation (2.18) becomes

$$4\beta^2 - 5\beta + 1 = 0 , \quad (\mathcal{M}_0 \gg 1) \quad (2.19)$$

which has solutions

$$\beta = 1 \implies u_0 = u_1 , \quad (2.20)$$

$$\beta = \frac{1}{4} \implies u_1 = \frac{u_0}{4} . \quad (2.21)$$

The first of these simply implies that nothing happens to the fluid. Since  $\rho_0 u_0 = \rho_1 u_1$ , the second implies that in the limit of a strong shock the fluid can be compressed by at most a factor of four. Since we have considered the shock to be stationary in the frame of reference,  $u_0 = v_w - v_{sw} \simeq v_w$  where  $v_{sw}$  is the wind shock velocity relative to the source of the wind, and the last equality follows because the wind speed is much higher than the shock velocity, as discussed above. The full set of post-shock variables is then found

$$\begin{aligned} u_1 &= \frac{v_w}{4} , \\ \rho_1 &= 4\rho_0 , \\ P_1 &= \frac{3}{4}\rho_0 v_w^2 . \end{aligned} \quad (2.22)$$

Finally, because we have the equation of state,  $P = \rho kT/(\mu m_p)$ , we can obtain the post-shock temperature of the gas in the strong shock limit

$$T_1 = \frac{3}{16} \frac{\mu m_p}{k} v_w^2 . \quad (2.23)$$

With these jump conditions we can estimate the properties of the shocked wind material in outflows driven by nuclear clusters and black holes. We can use this to find the gas cooling times, which depend on the density, velocity and temperature of the shocked material. This will allow us to address the question of whether these outflows are momentum- or energy-driven.

## 2.3 Cooling mechanisms

The dynamics of the shell depends upon whether or not the shocked wind material is able to cool efficiently. We can now find the properties of the immediate post-shock material, such as density and temperature, through the jump conditions derived above. We look next at the mechanisms by which this material may be able to cool.

### 2.3.1 Atomic processes

We adopt the cooling function of Sutherland & Dopita (1993) for cooling by atomic process and follow Dopita & Sutherland (2003) in our discussion of this cooling function.

The rate of energy lost by a plasma is the sum of the various cooling and heating rates. In general, cooling and heating rates are functions of density  $n$ , temperature  $T$  and metallicity  $A$ . Sutherland & Dopita (1993) investigated the cooling function of a non-relativistic, thermal plasma over a range of temperatures ( $T = 10^4 - 10^{8.5}$  K) and metallicities. They use the following cooling function (in units  $\text{erg cm}^3 \text{s}^{-1}$ ) in their calculations:

$$\Lambda_N(T, A) = \Lambda_{\text{lines}} + \Lambda_{\text{cont}} \pm \Lambda_{\text{rec}} - \Lambda_{\text{photo}} + \Lambda_{\text{coll}} \pm \Lambda_{\text{Compton}} . \quad (2.24)$$

It is a function of the electron temperature,  $T$ , and the metallicity of the plasma,  $A$ . It accounts for collisional line radiation ( $\Lambda_{\text{lines}}$ ), continuum emission ( $\Lambda_{\text{cont}}$ ), recombination processes ( $\Lambda_{\text{rec}}$ ), photoionisation heating ( $\Lambda_{\text{photo}}$ ), collisional ionisation ( $\Lambda_{\text{coll}}$ ) and Compton heating (or cooling,  $\Lambda_{\text{Compton}}$ ).

$\Lambda_{\text{line}}$ ,  $\Lambda_{\text{cont}}$  and  $\Lambda_{\text{coll}}$  all represent processes by which the gas loses energy. Line radiation is emitted when an ion becomes excited and then decays back to the ground state, emitting photons, hence losing energy. The continuum processes include free-free radiation, also known as Bremsstrahlung, and free-bound radiation. Free-free radiation is emitted when a charged particle, such as an electron, is deflected by other charged particles, such as protons. Free-bound emission arises by the capture of a free electron into a bound state and describes the recombination process. When an electron strikes an ion with enough energy to knock out a bound electron, i.e., the collisional ionisation, the incoming electron loses energy.

Photoionisation represents a heating process as energy is transferred from a photon to an electron during the ionisation process.

The Compton term can represent heating or cooling. It is a heating process when high-energy photons excite low-energy electrons, transferring energy from the photon field to the electrons. It is a cooling process when low-energy photons are scattered by high-energy electrons, transferring energy from the electrons to the photon field. We will discuss Compton cooling in more detail below.

Sutherland & Dopita (1993) note that recombinations (giving rise to free-bound radiation), may be a heating or cooling process and so treat the radiation from recombinations separately in  $\Lambda_{\text{rec}}$ .

Figure 2.2 shows the cooling function for a plasma as a function of the heavy metal abundance, from Sutherland & Dopita (1993).

Line cooling and collisional ionisation are the dominant processes in the temperature range  $4 \lesssim \log T(\text{K}) \lesssim 7$ . In the range  $5 \lesssim \log T(\text{K}) \lesssim 7$ , the cooling rate decreases with increasing temperature because the material becomes increasingly ionised.

At still higher temperatures ( $\log T(\text{K}) > 7.5$ ), all plasmas are totally ionised and electron free-free, or bremsstrahlung, emission is the dominant process. Sutherland &

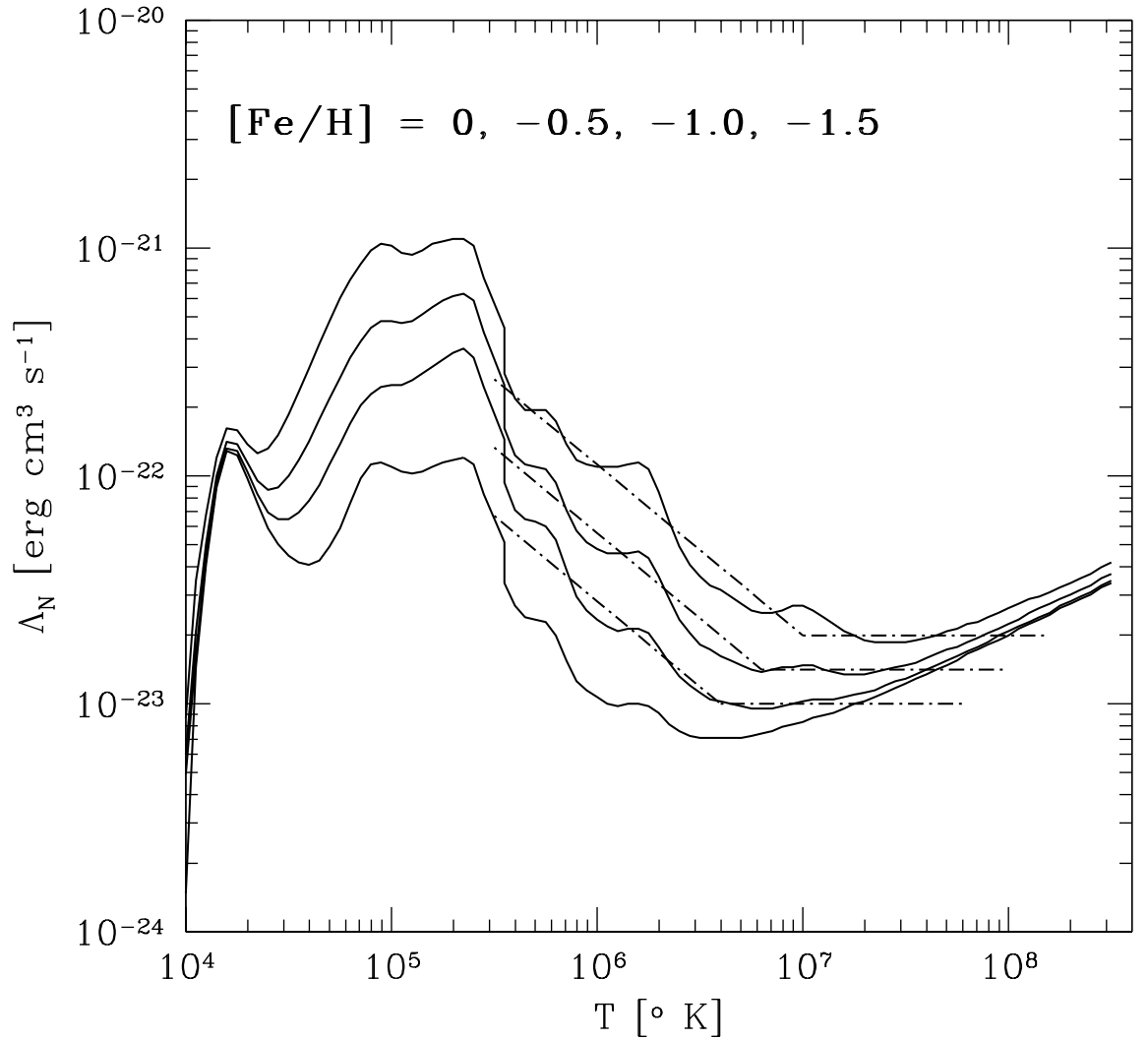


Figure 2.2: Cooling functions calculated by Sutherland & Dopita (1993) for (top to bottom curve)  $[Fe/H] = 0.0, -0.5, -1.0$  and  $-1.5$ . The dot-dashed lines show the approximation of the cooling function from McLaughlin et al. (2006) that is used to calculate the cooling time of the shocked wind region in the case of outflows driven by nuclear clusters (see §2.4.1).

Dopita (1993) note that the free-free power law can be extrapolated to higher temperatures with a fair level of accuracy, up to  $\log T(K) \sim 9$  when relativistic effects become

important, and Compton cooling becomes dominant.

### 2.3.2 Inverse Compton scattering

In the Compton scattering process high energy photons collide with electrons and transfer some of their energy and momentum to the electron, reducing the energies and momenta of the scattered photons, as discussed above.

In inverse Compton scattering ultra-relativistic electrons scatter low energy photons to higher energies, i.e., the photons gain energy from the kinetic energy of the electrons, so this cools the electron gas. In this case the energy loss rate of an electron is (Longair 2011)

$$\left(\frac{dE}{dt}\right)_{\text{IC}} = \frac{4}{3} \sigma_{\text{T}} c u_{\text{rad}} \left(\frac{v_{\text{e}}}{c}\right)^2 \gamma^2 \quad (2.25)$$

where  $v_{\text{e}}$  is the velocity of the electron,  $u_{\text{rad}}$  is the radiation density and  $\sigma_{\text{T}}$  is the Thomson cross section. The electron loses energy when it interacts with photons, therefore the energy loss rate is dependent upon the density of the photon field.

## 2.4 CMO outflows

We look now at the behaviour of the shocked wind region in outflows driven by nuclear clusters and black holes to determine whether the outflows are momentum- or energy-driven. We treat the two cases separately because as we have seen above, the temperature of the shocked gas depends on the wind velocity, which varies greatly between the two cases.

### 2.4.1 Nuclear star clusters

In the case that the CMO is a nuclear star cluster the super wind is driven by the combined winds and supernovae of stars in the cluster and is far from relativistic.

Using equation (2.23) we find that the temperature of the post-shock wind material in this case is

$$T_{\text{sw}} = \frac{3}{16} \frac{\mu m_{\text{p}}}{k} v_{\text{w}}^2 = 1.23 \times 10^6 \text{ K} \left( \frac{v_{\text{w}}}{300 \text{ km s}^{-1}} \right)^2 \left( \frac{\mu}{0.6} \right). \quad (2.26)$$

This falls into the regime of the cooling by atomic processes calculated by Sutherland & Dopita (1993), shown in Figure 2.2. We follow McLaughlin, King & Nayakshin (2006) in approximating the cooling function by

$$\Lambda_{\text{N}} \simeq 3.55 \times 10^{-18} \left( \frac{Z}{Z_{\odot}} \right)^{0.6} T^{-0.75} \text{ erg cm}^3 \text{ s}^{-1}, \quad (2.27)$$

which is applicable for  $(Z/Z_{\odot}) = 0.1 - 1$  and  $T \simeq (0.5 - 5) \times 10^6 \text{ K}$ , shown by the dot-dashed lines in Figure 2.2 for  $(Z/Z_{\odot}) = 0.1, 0.3$  and  $1$ .

We use equation (2.27) to calculate the cooling time of the post-shock wind material which is given by

$$t_{\text{cool}} = \frac{\mu m_{\text{p}} k T}{\rho_{\text{sw}} \Lambda_{\text{N}}}. \quad (2.28)$$

Recalling the post-shock density given by the adiabatic jump conditions,  $\rho_{\text{sw}} = 4\rho_{\text{w}}$  (equation 2.22), calculating the wind density  $\rho_{\text{w}} = \dot{M}_{\text{w}}/(4\pi r^2 v_{\text{w}})$  and recalling  $\dot{M}_{\text{w}} v_{\text{w}} = \lambda L_{\text{Edd}}/c$  (equation [1.20] with  $\tau_{\text{e}} \sim 1$ ), we find that the cooling time for the shocked wind in the nuclear cluster case is given by

$$\begin{aligned} t_{\text{cool}} &= 1.77 \times 10^{-32} \text{ s } \lambda^{-1} v_{\text{w}}^{5.5} M_{\text{CMO}}^{-1} r^2 \left( \frac{Z}{Z_{\odot}} \right)^{-0.6} \left( \frac{\mu}{0.6} \right)^{2.75} \\ &\simeq 3600 \text{ yr } \lambda^{-1} \left( \frac{v_{\text{w}}}{300 \text{ km s}^{-1}} \right)^{5.5} \left( \frac{M_{\text{CMO}}}{10^8 M_{\odot}} \right)^{-1} \left( \frac{r}{\text{kpc}} \right)^2 \left( \frac{\mu}{0.6} \right)^{2.75} \left( \frac{Z}{Z_{\odot}} \right)^{-0.6}. \end{aligned} \quad (2.29)$$

We can see immediately that this cooling timescale will be very short when the shell is at small radii, demonstrating that the shell is initially momentum-driven.

The shell is momentum-driven when the cooling time is shorter than the dynamical time of the wind,  $t_{\text{dyn}} = r_{\text{sw}}/v_{\text{w}}$ , or at radii

$$r_{\text{sw}} \lesssim 900 \text{ kpc } \lambda \frac{M_{\text{CMO}}}{10^8 M_{\odot}} \left( \frac{v_{\text{w}}}{300 \text{ km s}^{-1}} \right)^{-6.5} \left( \frac{Z}{Z_{\odot}} \right)^{0.6} \left( \frac{\mu}{0.6} \right)^{-2.75}. \quad (2.30)$$

When the wind shock is inside this radius the shocked wind region cools efficiently and is thin so  $r_{\text{sw}} \sim r_s$ . Thus, we find that in the case of outflows driven by nuclear clusters the shocked wind region can cool efficiently out to radii of order 50 kpc (for  $\lambda = 0.05$ ), meaning that the outflow is predominantly momentum-driven, the case as considered by McLaughlin et al. (2006).

The shell becomes energy-driven when  $t_{\text{cool}} \gtrsim t_{\text{flow}} = r_s/v_s$ , or at radii

$$r_s \simeq 1350 \text{ kpc } \lambda \left( \frac{M_{\text{CMO}}}{10^8 M_\odot} \right) \left( \frac{v_s}{200 \text{ km s}^{-1}} \right)^{-1} \left( \frac{v_w}{300 \text{ km s}^{-1}} \right)^{-5.5} \left( \frac{\mu}{0.6} \right)^{-2.75} \left( \frac{Z}{Z_\odot} \right)^{0.6}. \quad (2.31)$$

Hence, the shell can become energy-driven at radii  $\sim 70$  kpc, again for  $\lambda = 0.05$ .

## 2.4.2 Supermassive black holes

In the case that the central object is a supermassive black hole, the temperature of the shocked wind material exceeds the range considered by Sutherland & Dopita (1993) for cooling by atomic processes,

$$T_{\text{sw}} = \frac{3}{16} \frac{\mu m_p}{k} v_w^2 \simeq 1.10 \times 10^9 \text{ K} \left( \frac{v_w}{0.03c} \right)^2. \quad (2.32)$$

Sutherland & Dopita (1993) state that extrapolating their results to higher temperatures breaks down at  $\log T \sim 9$  because of relativistic effects. This temperature corresponds to electron velocities  $v_e \sim 0.8c$ , thus in the case of SMBHs we consider the case where the shocked wind material is cooled by inverse Compton scattering. We recall the electron energy loss rate from equation (2.25) depends on the density of the radiation field, which in this case is given by

$$u_{\text{rad}} = \frac{L_{\text{Edd}}}{4\pi r^2 c}. \quad (2.33)$$

The energy loss rate also depends upon the post-shock energy of the electrons, which is given by

$$E = 3kT = \frac{9}{16} m_p \mu (v_w - v_{\text{ws}})^2 \simeq \frac{9}{16} m_p \mu v_w^2. \quad (2.34)$$

We use equation (2.34) to find the velocity of the electrons by noting that

$$E_{e,\text{kin}} = (\gamma - 1) m_e c^2 = \frac{9}{16} \mu m_p v_w^2 \quad (2.35)$$

or

$$\gamma - 1 = \frac{9}{16} \frac{m_p v_w^2}{m_e c^2} \quad (2.36)$$

where in this case  $\gamma = (1 - v^2/c^2)^{-1/2}$  (not the ratio of specific heats). This implies that the electrons are very relativistic with velocities  $v_e \simeq 0.85c$ .

With the above, the cooling timescale of the post-shock wind material by inverse Compton scattering is given by (King 2003)

$$\begin{aligned} t_{\text{cool}} = \frac{E}{dE/dt} &= \frac{4}{3} \frac{cr^2}{GM_{\text{bh}}} \left(\frac{m_e}{m_p}\right)^2 \left(\frac{v_w}{c}\right)^{-2} \left(\frac{v_e}{c}\right)^{-2} \\ &\simeq 4.29 \times 10^8 \text{ yr} \left(\frac{r}{\text{kpc}}\right)^2 \left(\frac{v_w}{0.03c}\right)^{-2} \left(\frac{v_e}{0.85c}\right)^{-2}. \end{aligned} \quad (2.37)$$

The dynamical time of the wind is simply

$$t_{\text{dyn}} = r_{\text{sw}}/v_w \simeq 1.09 \times 10^5 \text{ yr} \frac{r}{\text{kpc}} \left(\frac{v_w}{0.03c}\right)^{-1}. \quad (2.38)$$

Again, the outflow is momentum-driven when the cooling timescale (equation 2.37) is shorter than the dynamical timescale of the wind (equation 2.38), or at radii

$$\begin{aligned} r_{\text{sw}} &= \frac{3}{4} \frac{GM_{\text{BH}}}{c^2} \left(\frac{m_p}{m_e}\right)^2 \left(\frac{v_w}{c}\right) \left(\frac{v_e}{c}\right)^2 \\ &\simeq 0.26 \text{ pc} \frac{M_{\text{BH}}}{10^8 M_\odot} \frac{v_w}{0.03c} \left(\frac{v_e}{0.85c}\right)^2. \end{aligned} \quad (2.39)$$

When the wind shock is inside this radius  $r_{\text{sw}} \sim r_s$  and the outflow is momentum-driven, which implies that in the case of outflows driven by black holes, the shocked wind region is only able to cool at very small radii.

The outflow is energy-driven when the cooling time exceeds the flow time of the shell,  $t_{\text{flow}} = r_s/v_s$ , at radii

$$\begin{aligned} r_s &\gtrsim \frac{3}{4} \frac{GM_{\text{BH}}}{cv_s} \left(\frac{m_p}{m_e}\right)^2 \left(\frac{v_w}{c}\right)^2 \left(\frac{v_e}{c}\right)^2 \\ &\simeq 11 \text{ pc} \left(\frac{v_s}{200 \text{ km s}^{-1}}\right)^{-1} \left(\frac{M_{\text{BH}}}{10^8 M_\odot}\right) \left(\frac{v_w}{0.03c}\right)^2 \left(\frac{v_e}{0.85c}\right)^2 \end{aligned} \quad (2.40)$$

for typical shell velocities  $v_s \sim \sigma \sim 200 \text{ km s}^{-1}$ . Outside of this radius, the shell is energy-driven. This radius is comparable to the sphere of influence of a  $10^8 M_\odot$  SMBH in a halo with  $\sigma = 200 \text{ km s}^{-1}$ , so the outflow can be predominantly energy-driven, in contrast to previous discussion of momentum- versus energy-driven outflows.

### 2.4.3 Review of energy- vs. momentum-driven outflows

There has been much debate in the literature about whether the  $M$ - $\sigma$  relation between CMO mass and stellar velocity dispersion is the result of momentum- or energy-driven feedback. This couples with an ongoing debate about the slope of the observed  $M$ - $\sigma$  relations for both black holes and nuclear clusters.

As discussed in Chapter 1, the first results relating black hole mass to stellar velocity dispersion were part of calculations aimed at deriving a relation between the black hole mass and bulge mass. Silk & Rees (1998) found a relation of the form  $M_{\text{BH}} \propto \sigma^5$  by considering a swept-up shell that is energy-driven, though the normalization of their relation places it well below the relation observed between black hole mass and velocity dispersion. Fabian (1999) found the shallower relation  $M_{\text{BH}} \propto \sigma^4$  as the result of a momentum-conserving outflow.

King (2003) considered an outflow from a black hole which cools by inverse Compton scattering, as discussed above, and found that the outflow is at least initially momentum-driven. This results in an  $M$ - $\sigma$  relation with  $M_{\text{BH}} \propto \sigma^4$ , with a normalisation a factor of a few above the observed relation. Following King (2003), McLaughlin, King & Nayakshin (2006) looked at the case of outflows driven by nuclear cluster with cooling by atomic transitions and also concluded that the outflows are momentum-driven.

It is expected that outflows from black holes will transition to an energy-conserving regime as they move outwards into the protogalaxy. King (2005) and King, Zubovas & Power (2011) look at energy-driving in the specific case that the black hole has reached the critical mass found by King (2005) during a momentum-driven phase and then transitions to an energy-driven regime. They find that the large radius coasting speed

of energy-driven shells is higher than the speed of momentum-driven shells driven by the same  $M_{\text{BH}}$  in an isothermal halo with the same velocity dispersion. They suggest that the initial momentum-driven phase establishes the  $M_{\text{BH}} \propto \sigma^4$  scaling, though more recent fits favour a steeper slope, and that the switch to energy-driving causes the shell to accelerate to this higher coasting speed, which allows the shell to clear the galaxy bulge.

More recent work has focussed on the evolution of the shell once it has transitioned to an energy-driven regime, connecting explicitly to observations of large-scale outflows driven by AGN. King, Zubovas & Power (2011) investigate the properties of large scale, energy-driven outflows, considering the case where the AGN “switches off” before the shell has cleared the galaxy. They find that the residual thermal pressure behind the shell is capable of driving the shell further out and possibly to escape, which could explain why massive outflows are sometimes observed when there is little or no AGN activity.

It is clear that an energy-driven phase is of importance, but in a more detailed analysis of the cooling of shocked AGN winds, Faucher-Giguère & Quataert (2012) show that energy-driving may be the dominant form of feedback in more circumstances than previously.

## 2.5 Summary

We have looked at the nature of outflows driven by both nuclear star clusters and by supermassive black holes. We used the adiabatic jump conditions, derived in §2.2, to calculate the properties of the post-shock wind material which determines the dynamics of the shell by whether or not it is able to cool. We considered the cooling mechanisms relevant in the cases of nuclear clusters and black holes separately, due to the difference in wind speed in each case.

We have shown that outflows driven by nuclear clusters may be able to cool efficiently, and thus momentum-driven, out to several 10 kpc, whereas outflows driven

by black holes may only be efficiently cooled inside a few parsecs, implying they may be energy-driven for most of their lifetime.

Motivated by these results we look at the two extremes of outflows that are purely momentum- and purely energy-driven. We consider momentum-driven outflows for both black holes and nuclear star clusters in haloes modelled as singular isothermal spheres and non-isothermal haloes in Chapter 3. We look at energy-driven outflows driven by black holes in a halo modelled as a singular isothermal sphere in Chapter 4, and in non-isothermal haloes in Chapter 5. In Chapter 6 we present a summary and discussion of these results.

### 3 Momentum-driven feedback and the $M$ – $\sigma$ relation in non-isothermal galaxies

We showed in Chapter 2 that outflows from nuclear star clusters may be momentum-driven for most of their evolution and that outflows from black holes are at least initially momentum-driven, though perhaps only at very small radii. As discussed in Chapter 1, momentum-driven outflows have been modelled in galaxies described by singular isothermal spheres, resulting in  $M_{\text{CMO}}-\sigma$  relations where  $M_{\text{CMO}} \propto \sigma^4$ .

Presented in this chapter is the paper ‘Momentum-driven outflows and the  $M$ – $\sigma$  relation in non-isothermal galaxies’ (McQuillin & McLaughlin 2012), where we look in detail at the effect on the  $M_{\text{CMO}}-\sigma$  relations of relaxing the assumption that galaxies are isothermal spheres.

We solve for the velocity fields of momentum-conserving supershells driven from galaxy centres by steady winds from either a supermassive black hole or a nuclear star cluster. We look for the critical CMO mass that allows such a shell to escape from its host galaxy. In the case that the host galaxy dark matter halo is a singular isothermal sphere, we find that the critical CMO mass derived by King, which scales with the halo velocity dispersion as  $M_{\text{crit}} \propto \sigma^4$ , is necessary, but not by itself sufficient, to drive shells to large radii in the halo. Furthermore, a CMO mass at least 3 times the King value is required for a steady wind to drive the shell to the escape speed of the halo. In the case of CMOs embedded in protogalaxies with non-isothermal dark matter haloes, which we treat here for the first time, we find a critical CMO mass that *is sufficient* to drive *any* shell (under a steady wind) to escape *any* galaxy with a peaked circular speed profile. In the limit of large halo mass, relevant to real galaxies, this critical CMO mass depends only on the value of the peak circular speed of the halo, scaling as  $M_{\text{crit}} \propto V_{\text{c,pk}}^4$ . Our results therefore relate to observational scalings between black hole mass and asymptotic circular speed in galaxy spheroids. They also suggest a natural way of extending analyses of  $M$ – $\sigma$  relations for black holes in massive bulges, to include similar relations for nuclear clusters in lower-mass and disc galaxies.

McQuillin & McLaughlin (2012) was written by R. C. McQuillin with drafts of sections 3.1, 3.4.1.3, 3.4.1.4 and 3.5 completed by D. E. McLaughlin.

Appendix 3.B contains an alternative method of finding the critical CMO mass that enables the escape of a momentum-driven shell from any non-isothermal halo with a singly peaked circular speed profile (from §3.4.1.3), which is not included McQuillin & McLaughlin (2012)

### 3.1 Introduction

Most early-type galaxies and bulges with  $M \gtrsim 10^{10} M_{\odot}$  harbour a supermassive black hole (SMBH) at their centre (Kormendy & Richstone 1995); while observations with the *Hubble Space Telescope* have revealed the presence of massive nuclear star clusters (NCs) in the majority of less massive galaxies (both early- and late-type: Phillips et al. 1996; Carollo et al. 1997; Böker et al. 2002; Côté et al. 2006, 2007). The properties of these central massive objects (CMOs) correlate tightly with properties of their host galaxies, perhaps most notably in terms of CMO mass,  $M_{\text{CMO}}$ , versus (bulge) stellar velocity dispersion,  $\sigma$ :  $M_{\text{CMO}} \propto \sigma^x$ , with  $x \simeq 4$  (for SMBHs, see, e.g., Ferrarese & Merritt 2000, Gebhardt et al. 2000, Tremaine et al. 2002, Ferrarese & Ford 2005, or Gültekin et al. 2009; for NCs, see Ferrarese et al. 2006; also relevant are Wehner & Harris 2006 and Rossa et al. 2006). Though essentially parallel, there is an offset between the  $M$ – $\sigma$  relations of NCs and SMBHs, in the sense that the NC masses in intermediate- and low-mass galaxies tend to be  $\sim 10\times$  larger than if they followed a simple extrapolation of the SMBH  $M$ – $\sigma$  relation for higher-mass spheroids (Ferrarese et al. 2006; see also McLaughlin et al. 2006).

Recently, Volonteri, Natarajan, & Gültekin (2011; cf. Ferrarese 2002) have argued that galaxies/bulges containing SMBHs also show a correlation, of the form  $M_{\text{bh}} \propto V_c^y$  with  $y \approx 4$ , between black hole mass and the “asymptotic” circular speed  $V_c$  at large radii where dark matter is expected to dominate the total galaxy mass. There is some debate (e.g., see Ho 2007; Kormendy & Bender 2011) over how the stellar velocity dispersions in the  $M$ – $\sigma$  relation, which are measured inside a fraction of the bulge effective radius, connect *empirically* to asymptotic circular speeds, which normally refer to many times the effective radius defined by stars. This can be a difficult question (with a model-dependent answer), especially in “hot” stellar systems where circular speeds—that is,  $V_c^2(r) = GM(r)/r$ —are not observed simply as net rotation. However, the existence of *some* kind of connection, and at least the possibility of an  $M_{\text{bh}}$ – $V_c$  relation in addition to  $M_{\text{bh}}$ – $\sigma$ , is clear in principle: The stellar velocity dispersion at *any* radius in a dark-matter dominated galaxy depends on the dark matter distribution, which is

precisely what  $V_c$  probes at large radii.

Self-regulated feedback from growing CMOs is thought to play a key role in establishing the  $M$ - $\sigma$  relation and associated scalings. Though through different mechanisms, either an NC or an SMBH will drive an outflow, which sweeps the ambient gas in a protogalaxy into a shell that, at least initially, is able to cool rapidly and is therefore momentum-driven (King 2003; McLaughlin et al. 2006; see also §3.2 below). There is then a critical CMO mass above which the outwards force of the wind on the shell may overcome the inwards gravitational pull of the CMO plus the dark matter halo of the parent galaxy.

The only case that has been considered in detail analytically is that of a steady wind, in which the CMO mass (and associated wind thrust) is constant throughout the motion of the shell (Silk & Rees 1998; Fabian 1999; King 2003, 2005, 2010a; Murray et al. 2005; McLaughlin et al. 2006, Silk & Nusser 2010). In this case, *and* assuming a halo modelled as a singular isothermal sphere, King (2005) found a critical CMO mass of

$$M_{\text{crit}} = \frac{f_0 \kappa}{\lambda \pi G^2} \sigma_0^4 \simeq 4.56 \times 10^8 M_\odot \sigma_{200}^4 f_{0.2} \lambda^{-1} , \quad (3.1)$$

(see also McLaughlin et al. 2006; Murray et al. 2005). In this expression  $f_0$  is an average gas mass fraction ( $\approx 0.2$ , so  $f_{0.2} = f_0/0.2$ ) and  $\sigma_{200} = \sigma_0/200 \text{ km s}^{-1}$ . The parameter  $\lambda$  is related to the feedback efficiency for each type of CMO; it has a value  $\lambda \approx 1$  for SMBHs, and  $\lambda \approx 0.05$  for NCs (McLaughlin et al. 2006). Once a CMO in an isothermal halo with a given  $\sigma_0$  has grown to at least the mass in equation (3.1), the CMO wind may drive a momentum-conserving shell with coasting speed  $v > 0$  at arbitrarily large radii in the galaxy. This then admits the possibility of a blow-out clearing the galaxy of any remaining ambient gas, choking off further star formation and CMO growth, and locking in an  $M_{\text{CMO}}$ - $\sigma$  relation.

As a momentum-driven shell moves outwards from a CMO, gas cooling times increase and a switch to an energy-driven phase is expected, at which point the shell can accelerate to escape the galaxy (King 2003). Momentum-driving may then need only push a shell out to where the switch to energy-driving occurs; and this can be

done with a CMO less massive than the  $M_{\text{crit}}$  in equation (3.1), which is necessary for momentum-driving to *arbitrarily* large radii. This suggests that equation (3.1) may actually predict an upper limit for observed  $M$ - $\sigma$  relations; and indeed, the equation lies above current best fits to data by factors of a few.

Distributed star formation in a protogalaxy bulge is expected to provide additional momentum input to the feedback (Murray et al. 2005; Power et al. 2011). This would also reduce the CMO mass required for the feedback to escape, again suggesting that the  $M_{\text{CMO}}-\sigma$  relation in equation (3.1) is an upper limit.

Silk & Nusser (2010) have shown that, in a truncated isothermal sphere specifically, a momentum-conserving shell driven solely by a steady black-hole wind can reach large radius with fast enough speed to escape directly (that is, with  $v \gtrsim 2\sigma_0$ ), only if the SMBH mass is at least a few times *larger* than the critical value in equation (3.1) (which is necessary just to have  $v > 0$  at large  $r$ ). This would put the predicted normalization of an  $M_{\text{CMO}}-\sigma$  relation above the observed normalization by a full order of magnitude. Silk & Nusser argue from this that the real key to a feedback origin for  $M_{\text{CMO}}-\sigma$  is momentum input from distributed bulge-star formation that is triggered by the outflow from a CMO. However, Power et al. (2011) counter that a switch from momentum- to energy-driving of the CMO feedback is still inevitable and will alleviate some of the difficulty identified by Silk & Nusser.

In this chapter, we investigate how this basic feedback scenario for  $M$ - $\sigma$  relations depends on the simplifying assumption that dark matter haloes are singular isothermal spheres. We analyze aspects of the dynamics of supershells in spherical but non-isothermal haloes, while retaining some other simplifying assumptions (steady winds and purely momentum-driven shells) in common with previous work.

Our main result is a generalization of the critical CMO mass that suffices to blow momentum-driven feedback entirely out of *any* realistic, non-isothermal dark matter halo that has a *well-defined maximum in its circular speed profile*,  $V_c^2(r) = GM_{\text{DM}}(r)/r$ .

For large halo masses, this critical CMO mass tends to the limiting value,

$$\begin{aligned} M_{\text{crit}} &\longrightarrow \frac{f_0 \kappa}{\lambda \pi G^2} \frac{V_{\text{c,pk}}^4}{4} \\ &= 1.14 \times 10^8 M_{\odot} \left( \frac{V_{\text{c,pk}}}{200 \text{ km s}^{-1}} \right)^4 f_{0.2} \lambda^{-1} , \end{aligned} \quad (3.2)$$

where  $V_{\text{c,pk}}$  is the peak value of the circular speed.

In a singular isothermal sphere, which has a constant  $V_c = \sqrt{2}\sigma_0$ , our new equation (3.2) clearly reduces to equation (3.1). However—as we discuss in detail in §3.3 and §3.4.1 below—in an *isothermal* halo this  $M_{\text{crit}}$  is *necessary but not sufficient*, in general, to guarantee the escape of a momentum-driven CMO wind. By contrast, in the more realistic, *non-isothermal* cases that we consider, equation (3.2) gives the  $M_{\text{CMO}}$  that *is sufficient* for the escape of any such feedback.

Any momentum-conserving shell driven by a steady wind from a CMO with the mass in equation (3.2) will eventually accelerate at large radii and exceed the escape speed of any non-isothermal halo with a peaked  $V_c(r)$  profile, even without a possible change to energy-driving, additional momentum feedback from star formation or growth of the CMO (none of which we include in our analysis). Thus, the objection of Silk & Nusser (2010) to equation (3.1) as the basis for observed  $M$ – $\sigma$  relations applies *only* if dark matter haloes are strictly isothermal.

Equation (3.2) defines the “characteristic” velocity dispersion that needs to be considered when interpreting observed  $M_{\text{CMO}}$ – $\sigma$  relations in non-isothermal galaxies:  $\sigma_0 \equiv V_{\text{c,pk}}/\sqrt{2}$ . It also gives the first direct, quantitative prediction of an  $M_{\text{CMO}}$ – $V_c$  relation such as that discussed by Volonteri et al. (2011). The result may still be an upper limit to observed relations since we do not consider any transition to energy-conserving feedback, nor any sources of feedback other than steady CMO winds, in this work.

We begin in §3.2 by looking at the general equation of motion of a momentum-driven shell as it moves out into a gaseous protogalaxy. In §3.3 we develop, in more detail than before, the case of the singular isothermal sphere. In §3.4.1, we analyze the motion of a momentum-driven shell in a general, non-isothermal halo with a peaked

circular-speed curve, and derive equation (3.2). In the rest of §3.4, we illustrate our general results using three particular dark-matter halo models as examples (those of Hernquist 1990; Navarro, Frenk, & White 1996, 1997; and Dehnen & McLaughlin 2005). In §3.5 we summarize the chapter and give a brief discussion.

## 3.2 Equation of motion

An SMBH accreting at near- or super-Eddington rates in a gaseous protogalaxy is expected to drive a fast wind back into the galaxy (King & Pounds 2003), with quasi-spherical (i.e., *not* highly collimated) geometries indicated by observations of strong outflows from local AGN (e.g., Tombesi et al. 2010). Similarly, the combined winds and supernovae from massive stars in a very young (still forming) NC will drive a superwind into its host protogalaxy. In a spherical approximation to either case, the wind sweeps up the surrounding ambient gas into a shell. The material in this shell is hot and tries to expand both backwards and forwards, giving rise to two shock fronts, one propagating forwards into the ambient medium and one backwards into the wind. Initially, the shocked wind region can cool efficiently, by inverse Compton scattering for SMBHs (King 2003) and by atomic processes for NCs (McLaughlin et al. 2006). As such, this region is geometrically thin and the shell is effectively driven outwards by a transfer of momentum from the wind impacting on its inside.

The thrust on the shell from the CMO wind is proportional to the Eddington luminosity of the CMO (King & Pounds 2003; McLaughlin et al. 2006):

$$\frac{dp_{\text{wind}}}{dt} = \lambda \frac{L_{\text{Edd}}}{c} = \lambda \frac{4\pi GM_{\text{CMO}}}{\kappa}, \quad (3.3)$$

where  $M_{\text{CMO}}$  is the CMO mass and  $\kappa$  is the electron scattering opacity. For SMBHs,  $\lambda \sim 1$  (King & Pounds); for NCs,  $\lambda \sim 0.05$ , a value related to the mass fraction of the massive stars that contribute to the superwind (McLaughlin et al.).

As the shell moves outwards, the cooling time of the shocked wind material behind the shell eventually becomes longer than the dynamical time of the wind. This region

then cannot cool before more material/energy is injected (King 2003; McLaughlin et al. 2006). As such, it expands and the shell becomes driven by the thermal pressure in the shocked wind region. If the shell can reach a galactocentric radius where this switch from momentum- to energy-driving occurs, then it may accelerate from that point to escape the galaxy (King 2003).

In this chapter, we consider only the momentum-conserving phase of the feedback, in the form of a spherical supershell moving outwards into a spherical, dark-matter dominated protogalaxy, driven entirely by a steady wind from a central point mass that may be thought of as either an SMBH or an NC. Our aim is primarily to explore the effects of relaxing the assumption of isothermal dark matter distributions, so we leave to one side all issues around any transition to energy-driving, additional feedback from bulge-star formation, and evolution of the CMO mass.

The equation of motion that we consider for the shell is

$$\frac{d}{dt} [M_g(r)v] = \lambda \frac{L_{\text{Edd}}}{c} - \frac{GM_g(r)}{r^2} [M_{\text{CMO}} + M_{\text{DM}}(r)] \quad , \quad (3.4)$$

where  $r$  is the instantaneous radius of the shell;  $v = dr/dt$  is the velocity of the shell;  $M_{\text{DM}}(r)$  is the dark matter mass inside radius  $r$ ; and  $M_g(r)$  is the ambient gas mass originally inside radius  $r$  (i.e., the mass that has been swept up into the shell when it has radius  $r$ ). The first term on the right-hand side of equation (3.4) is the wind thrust acting on the shell, from equation (3.3). The second and third terms on the right-hand side are the gravity of the CMO and the dark matter inside the shell (see also King 2005).

In general, we write  $M_g(r) = f_0 h(r) M_{\text{DM}}(r)$ , where  $f_0$  is a fiducial gas fraction ( $\approx 0.2$ ) and  $h(r)$  is a function that describes how the gas traces the dark matter; when  $h(r) \equiv 1$ , the gas directly traces the dark matter. It is also convenient to define characteristic mass and radius scales,  $M_\sigma$  and  $r_\sigma$ , in terms of a characteristic velocity dispersion  $\sigma_0$  in the dark matter halo:

$$\begin{aligned} M_\sigma &\equiv f_0 \kappa \sigma_0^4 / (\lambda \pi G^2) \simeq 4.56 \times 10^8 M_\odot \sigma_{200}^4 f_{0.2} \lambda^{-1} \\ r_\sigma &\equiv GM_\sigma / \sigma_0^2 \simeq 49.25 \text{ pc } \sigma_{200}^2 f_{0.2} \lambda^{-1}, \end{aligned} \quad (3.5)$$

where  $\sigma_{200} = \sigma_0/200 \text{ km s}^{-1}$  and  $f_{0.2} = f_0/0.2$ . Referring back to equation (3.1), the unit  $M_\sigma$  is just the critical CMO mass found by King (2005).

Then, defining  $\widetilde{M} \equiv M/M_\sigma$ ,  $\widetilde{r} \equiv r/r_\sigma$  and  $\widetilde{v} \equiv v/\sigma_0$  equation (3.4) can be written

$$\frac{d}{d\widetilde{r}} \left[ h^2 \widetilde{M}_{\text{DM}}^2 \widetilde{v}^2(\widetilde{r}) \right] = 8\widetilde{M}_{\text{CMO}} h(\widetilde{r}) \widetilde{M}_{\text{DM}}(\widetilde{r}) - \frac{2h^2(\widetilde{r}) \widetilde{M}_{\text{DM}}^2(\widetilde{r})}{\widetilde{r}^2} \left[ \widetilde{M}_{\text{CMO}} + \widetilde{M}_{\text{DM}}(\widetilde{r}) \right]. \quad (3.6)$$

We aim to solve this equation for the velocity fields of momentum-driven shells,  $\widetilde{v}^2(\widetilde{r})$ , rather than  $\widetilde{r}(t)$  explicitly.

If the wind thrust is great enough, then equation (3.6) will have solutions that allow shells to reach arbitrarily large  $\widetilde{r}$  with non-zero  $\widetilde{v}$ —the minimum requirement for escape of the feedback. If the wind thrust is unable to overcome the combined gravity of the CMO and dark matter then the shell will *stall* with  $\widetilde{v}^2 = 0$  at some finite radius, and subsequently collapse. Equation (3.6) cannot describe such a collapse, since that would involve a shell with fixed mass rather than one that continually gathers mass [ $M_{\text{g}}(r) = f_0 h(r) M_{\text{DM}}(r)$ ] as it moves outwards into a galaxy.

The form of equation (3.6) allows us to select any density profile for the host galaxy dark matter and also allows for the segregation of gas and dark matter through the function  $h(r)$ . Throughout this chapter, we consider only the case that  $h(r) \equiv 1$ , but we investigate various halo mass distributions.

### 3.3 The singular isothermal sphere

We look first at the dark matter density profile of a singular isothermal sphere, with  $h(\widetilde{r}) \equiv 1$  so that gas traces the dark matter directly. Aspects of this case have been considered previously by several authors (Silk & Rees 1998; Fabian 1999; King 2003, 2005, 2010a; McLaughlin et al. 2006; Murray et al. 2005). King (2005, 2010a) looked at the behaviour of a shell that is far from an SMBH, so that the mass of dark matter inside the shell dominates over the SMBH gravity. King (2005, 2010a) find that the

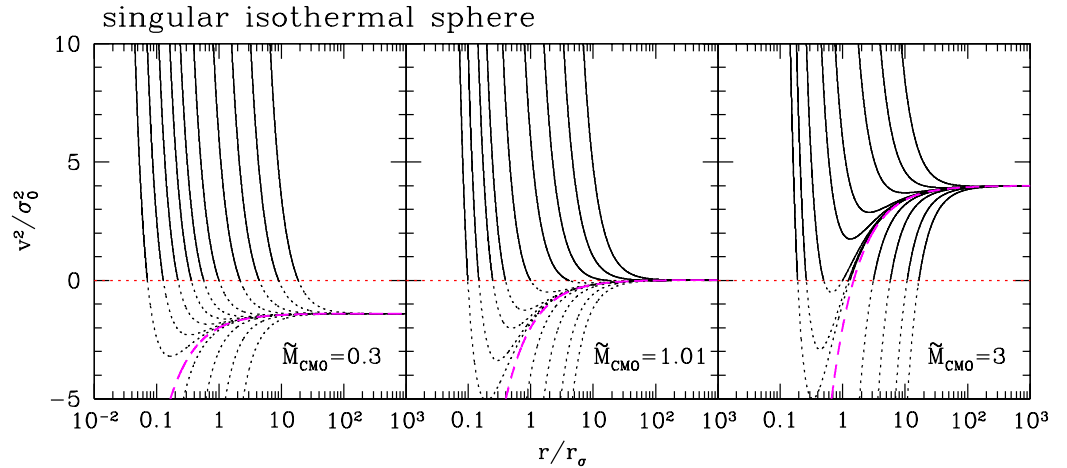


Figure 3.1: Velocity fields  $\tilde{v}^2$  versus  $\tilde{r}$  for momentum-driven shells in a singular isothermal sphere with spatially constant gas fraction and  $\tilde{M}_{\text{CMO}} = 0.3, 1.01$  and  $3$ . In each case, the solution with  $C = [\tilde{r} \tilde{v}(0)]^2 = 0$  is shown by a long-dashed (magenta) line. The physical ( $\tilde{v}^2 \geq 0$ ) parts of other solutions are shown as solid lines. All solutions with  $C < 0$  are unphysical at small radii, but if  $\tilde{M}_{\text{CMO}} > 1$  they will achieve  $\tilde{v}^2 \geq 0$  at large  $\tilde{r}$ , corresponding to launches. All solutions with  $C > 0$  decelerate from small radii. If one hits  $\tilde{v}^2 = 0$  at some point, then it generally becomes unphysical at larger radii, and the shell it describes must stall and collapse. This can occur even if  $\tilde{M}_{\text{CMO}} > 1$ . Formally, solutions with  $C > 0$  and  $\tilde{M}_{\text{CMO}} > 1$  that stall can have second physical parts with  $\tilde{v}^2 > 0$  at still larger  $\tilde{r}$ . These parts of such solutions again correspond to launches, though not of the same shells that stall at smaller radii.

shell can reach arbitrarily large radii only if the black hole has the critical mass given in equation (3.1). However, as we now show, this condition does not actually guarantee that a momentum-driven shell will be able to make it to large enough radii that the CMO gravity becomes negligible compared to the dark matter.

The density of a singular isothermal sphere is given by

$$\rho_{\text{DM}}(r) = \frac{\sigma_0^2}{2\pi G r^2}, \quad (3.7)$$

so that

$$M_{\text{DM}}(r) = 4\pi \int_0^r \rho_{\text{DM}}(r') r'^2 dr' = \frac{2\sigma_0^2}{G} r. \quad (3.8)$$

In terms of the characteristic mass and radius defined in equation (3.5), this means

$$\widetilde{M}_{\text{DM}}(\widetilde{r}) = 2\widetilde{r} . \quad (3.9)$$

Then, with  $h(\widetilde{r}) \equiv 1$ , equation (3.6) for the motion of the shell becomes

$$\frac{d}{d\widetilde{r}} [\widetilde{r}^2 \widetilde{v}^2] = 4\widetilde{M}_{\text{CMO}}\widetilde{r} - 2\widetilde{M}_{\text{CMO}} - 4\widetilde{r} , \quad (3.10)$$

which has solution

$$\widetilde{v}^2 = 2\widetilde{M}_{\text{CMO}} - 2 - \frac{2\widetilde{M}_{\text{CMO}}}{\widetilde{r}} + \frac{C}{\widetilde{r}^2} . \quad (3.11)$$

The constant of integration,  $C$ , represents (the square of) the shell's momentum,  $[M_{\text{g}}(r)v(r)]^2 \propto \widetilde{r}^2 \widetilde{v}^2$ , at  $\widetilde{r} = 0$ .

In the limit of very large radius, equation (3.11) shows that the shell approaches a constant coasting speed:

$$\widetilde{v}^2 \longrightarrow 2\widetilde{M}_{\text{CMO}} - 2 . \quad (\widetilde{r} \gg 1) \quad (3.12)$$

Equations (3.11) and (3.12) are implicit in King (2005) (multiply his eq. [2] by  $\dot{R}R$  and integrate). Equation (3.12) specifically is only physical if  $\widetilde{v}^2 > 0$ . Thus, for the shell to have any chance of escaping we must have  $\widetilde{M}_{\text{CMO}} > 1$ , which is exactly the result of King (2005, 2010a).

In the limit of small radius, the last term of equation (3.11) for  $\widetilde{v}^2$  becomes dominant, and the initial momentum of the shell (i.e.,  $C$ ) determines the behaviour of the shell.

If  $C \leq 0$ , then  $\widetilde{v}^2$  is large and negative at small radii, which is unphysical. However,  $d\widetilde{v}^2/d\widetilde{r} > 0$ , so it may happen that  $\widetilde{v}^2 = 0$  at some larger radius and increases further outwards. The  $\widetilde{v}^2 \geq 0$  part of such a solution *is* physical, and the point at which  $\widetilde{v}^2 = 0$  can be considered as a ‘‘launch’’ radius for a (pre-existing) shell initially at rest.

A launch solution has  $\widetilde{v}^2 = 0$  and  $d\widetilde{v}^2/d\widetilde{r} \geq 0$  at some  $\widetilde{r}_{\text{launch}}$ . From equation (3.11), this requires

$$\widetilde{r}_{\text{launch}}(\widetilde{M}_{\text{CMO}} - 1) \geq \frac{\widetilde{M}_{\text{CMO}}}{2} . \quad (3.13)$$

Thus, such solutions are only possible for  $\widetilde{M}_{\text{CMO}} > 1$ , and then only starting from radii

$$\widetilde{r}_{\text{launch}} \geq \frac{\widetilde{M}_{\text{CMO}}}{2(\widetilde{M}_{\text{CMO}} - 1)} > \frac{1}{2}. \quad (3.14)$$

As  $\widetilde{M}_{\text{CMO}} \rightarrow 1$ ,  $\widetilde{r}_{\text{launch}} \rightarrow \infty$ , so launches are not possible when  $\widetilde{M}_{\text{CMO}} = 1$ .

If  $C > 0$ ,  $\widetilde{v}^2$  is large and positive at small radii but  $d\widetilde{v}^2/d\widetilde{r} < 0$ , so the shell decelerates but keeps moving out into the galaxy, unless and until  $\widetilde{v}^2 = 0$  is reached at some finite  $\widetilde{r}$ . If this happens, then the shell stalls and is not able to escape. If  $\widetilde{v}^2 = 0$  is never realised, then the shell is formally able to escape to large radii while purely momentum-driven.

The stall radius, at which  $\widetilde{v}^2 = 0$ , is found from equation (3.11) as

$$\widetilde{r}_{\text{stall}} = \frac{\widetilde{M}_{\text{CMO}} - \sqrt{\widetilde{M}_{\text{CMO}}^2 - 2C(\widetilde{M}_{\text{CMO}} - 1)}}{2(\widetilde{M}_{\text{CMO}} - 1)}, \quad (3.15)$$

where we have taken the root with the minus sign since this corresponds to the first instance of  $\widetilde{v}^2 = 0$  as the shell moves outwards. If  $\widetilde{r}_{\text{stall}}$  is positive and finite, the shell cannot move out beyond this radius while purely momentum driven.

In the case that  $\widetilde{M}_{\text{CMO}} < 1$ ,  $\widetilde{r}_{\text{stall}} > 0$  for any  $C > 0$ . We can see this by noting that when  $\widetilde{M}_{\text{CMO}} < 1$  the discriminant in equation (3.15) is always positive and  $> \widetilde{M}_{\text{CMO}}^2$  so that both the numerator and denominator are negative, leading to a positive  $\widetilde{r}_{\text{stall}}$ . As there are no physical launch solutions and the shell always stalls when  $\widetilde{M}_{\text{CMO}} < 1$ , no shell can ever escape while purely momentum-driven if  $\widetilde{M}_{\text{CMO}} < 1$ .

In the limit that  $\widetilde{M}_{\text{CMO}} \rightarrow 1$ , we find that

$$\widetilde{r}_{\text{stall}} = \frac{\widetilde{M}_{\text{CMO}} - \widetilde{M}_{\text{CMO}} \sqrt{1 - \frac{2C(\widetilde{M}_{\text{CMO}} - 1)}{\widetilde{M}_{\text{CMO}}^2}}}{2(\widetilde{M}_{\text{CMO}} - 1)} \rightarrow \frac{C}{2}, \quad (3.16)$$

so  $\widetilde{r}_{\text{stall}}$  occurs at some positive and finite radius when  $C > 0$  and, because  $\widetilde{r}_{\text{launch}}$  is infinite (equation [3.14]), when  $\widetilde{M}_{\text{CMO}} = 1$  exactly no shell can escape.

When  $\widetilde{r}_{\text{stall}}$  does not exist (formally, when equation [3.15] is complex),  $\widetilde{v}^2 = 0$  is never realised (for solutions with  $C > 0$ ) and the shell is able to reach arbitrarily large

radii while being purely momentum-driven. This requires

$$\widetilde{M}_{\text{CMO}}^2 - 2C(\widetilde{M}_{\text{CMO}} - 1) < 0 \quad , \quad (3.17)$$

which, for  $\widetilde{M}_{\text{CMO}} > 1$  (as we know this is the only case where purely momentum-driven escape is possible), means that escape requires

$$C > \frac{\widetilde{M}_{\text{CMO}}^2}{2(\widetilde{M}_{\text{CMO}} - 1)} \quad . \quad (3.18)$$

If the value of  $C$  does not satisfy this constraint, then the shell will stall before ever reaching the radii where it could coast at the speed given by equation (3.12), even if  $\widetilde{M}_{\text{CMO}} > 1$ . This is one reason why the critical CMO mass of King (2005, 2010a) is a *necessary but not sufficient* condition for the escape of momentum-driven CMO feedback from an isothermal sphere.

Figure 3.1 plots  $\widetilde{v}^2$  versus  $\widetilde{r}$  from equation (3.11) for  $\widetilde{M}_{\text{CMO}} = 0.3, 1.01$  and  $3$ , with a range of  $C$  values in each case. The long-dashed (magenta) curve in each panel is the solution with  $C = 0$  for that  $\widetilde{M}_{\text{CMO}}$ . The physical parts of solutions with  $C \neq 0$  are shown as solid lines

The left-hand panel of Figure 3.1 shows solutions for  $\widetilde{M}_{\text{CMO}} = 0.3$ . No solution can escape in this case. Those with  $C > 0$  all stall at some finite radius (beyond which  $\widetilde{v}^2 < 0$ ), while those with  $C \leq 0$  never give physical values of  $\widetilde{v}^2 > 0$ .

Since we know that  $\widetilde{M}_{\text{CMO}} = 1$  exactly also has no escape, the middle panel shows solutions for  $\widetilde{M}_{\text{CMO}} = 1.01$ . In this case, only a few realistic solutions can “escape,” and those that do tend to a coasting speed of just  $v \sim 0.14 \sigma_0$  at large radii (eq. [3.12]). In order even to reach the radii where this applies, shells must have very large velocity at small radii ( $C \gtrsim 51$  from equation [3.18], which corresponds to  $v \sim 0.2c$  at a distance of 1 pc from the CMO if  $\sigma_0 = 200 \text{ km s}^{-1}$ ), or else be launched somehow from very large radius ( $\widetilde{r}_{\text{launch}} > 50.5$  from equation [3.14], which corresponds to  $r \gtrsim 2.5 \text{ kpc}$  if  $\sigma_0 = 200 \text{ km s}^{-1}$ ).

Finally, the right-hand panel of Figure 3.1 illustrates solutions for  $\widetilde{M}_{\text{CMO}} = 3$ . Formally, all solutions now have a significant coasting speed of  $2\sigma_0$  at large radii, but

those with  $C < 9/4$  (or  $v \lesssim 15,000 \text{ km s}^{-1}$  at  $r = 1 \text{ pc}$  when  $\sigma_0 = 200 \text{ km s}^{-1}$ ) still stall before they are able to make it to large radius. Several of the solutions that escape are those with a launch radius; these require  $\tilde{r}_{\text{launch}} > 3/4$  ( $r \gtrsim 40 \text{ pc}$  for  $\sigma_0 = 200 \text{ km s}^{-1}$ ).

The escape speed from a truncated isothermal sphere is  $v_{\text{esc}} \gtrsim 2\sigma_0$  at large radius. Our results for a shell driven by a CMO of constant mass (i.e., a steady wind, equation [3.12] in particular) show that to achieve this escape speed requires  $\tilde{M}_{\text{CMO}} \geq 3$ . This is another reason why the condition of King (2005, 2010a), i.e., simply  $\tilde{M}_{\text{CMO}} > 1$ , is necessary but not sufficient for the escape of a purely momentum-driven shell from an isothermal sphere. It is also, in essence, the same as the objection raised by Silk & Nusser (2010) against explanations of observed  $M_{\text{CMO}}-\sigma$  relations as the result of outflows driven by the central objects alone. However, these and all other prior results have come from modelling protogalaxies only as singular isothermal spheres. We look now at the effect of allowing more realistic descriptions of dark-matter (and ambient gas) density profiles.

## 3.4 Non-isothermal dark matter haloes

### 3.4.1 General analysis

Simulated dark matter haloes have density profiles that are shallower than that of an isothermal sphere at small radii and steeper than isothermal at large radii. Dubinski & Carlberg (1991) originally fitted haloes with the profile of Hernquist (1990), which has  $\rho_{\text{DM}} \propto r^{-1}$  at small radii and  $\rho_{\text{DM}} \propto r^{-4}$  at large radii. The dark-matter profile of Navarro, Frenk & White (1996, 1997) also has  $\rho_{\text{DM}} \propto r^{-1}$  at small radii, but  $\rho_{\text{DM}} \propto r^{-3}$  at large radii. Dehnen & McLaughlin (2005) develop a family of physically motivated halo models that, with  $\rho_{\text{DM}}(r)$  slightly shallower than  $r^{-1}$  at small radii and slightly steeper than  $r^{-3}$  at large radii, match current simulations at least as well as any other fitting function.

The circular speed corresponding to all such density profiles,  $V_c^2(r) = GM(r)/r$ ,

increases outwards from the centre, has a well-defined peak, and then declines towards larger radii. This suggests the peak of the circular speed curve as a natural point of reference for velocities, radii, and masses in realistically non-isothermal haloes.

We denote the location of the peak in  $V_c(r)$  by  $r_{\text{pk}}$  and the value  $V_c(r_{\text{pk}}) \equiv V_{c,\text{pk}}$ , and we define

$$\sigma_0^2 \equiv V_{c,\text{pk}}^2/2 \quad (3.19)$$

as a characteristic velocity dispersion in order to specify unique mass and radius units,  $M_\sigma$  and  $r_\sigma$ , as in equation (3.5) above. Then, recalling that  $\widetilde{M} \equiv M/M_\sigma$ ,  $\widetilde{r} \equiv r/r_\sigma$ , and  $\widetilde{v} \equiv v/\sigma_0$ , so that  $\widetilde{V}_c^2(\widetilde{r}) = \widetilde{M}_{\text{DM}}(\widetilde{r})/\widetilde{r}$ , we have

$$\widetilde{V}_{c,\text{pk}}^2 = 2 \quad (3.20)$$

and

$$\widetilde{M}_{\text{DM}}(\widetilde{r}_{\text{pk}}) \equiv \widetilde{M}_{\text{pk}} = 2\widetilde{r}_{\text{pk}} \quad . \quad (3.21)$$

We now refer all radii to the peak of the circular speed curve, defining  $x \equiv r/r_{\text{pk}}$ ; and we introduce a dimensionless mass profile,  $m(x)$ , such that

$$\widetilde{M}_{\text{DM}}(x) \equiv \widetilde{M}_{\text{pk}} m(x) \quad . \quad (3.22)$$

By construction, then,

$$\widetilde{M}_{\text{DM}}(1) \equiv \widetilde{M}_{\text{pk}} \quad \implies \quad m(1) = 1 \quad . \quad (3.23)$$

Moreover,  $\widetilde{V}_c^2 = \widetilde{M}_{\text{DM}}(\widetilde{r})/\widetilde{r} = 2m(x)/x$ , and thus,

$$\left( \frac{d\widetilde{V}_c^2}{dx} \right)_{x=1} = 0 \quad \implies \quad \left( \frac{d \ln m}{d \ln x} \right)_{x=1} = 1 \quad . \quad (3.24)$$

These generic properties of  $m(x)$  are important later in our analysis (see especially Appendix 3.A).

With these definitions, equation (3.6) for the motion of a momentum-driven shell becomes

$$\frac{d}{dx} [h^2 m^2 \widetilde{v}^2(x)] = 4\widetilde{M}_{\text{CMO}} h(x)m(x)$$

$$-4 \frac{\widetilde{M}_{\text{CMO}}}{\widetilde{M}_{\text{pk}}} \frac{h^2(x)m^2(x)}{x^2} - 4 \frac{h^2(x)m^3(x)}{x^2} . \quad (3.25)$$

The formal solution of this, when  $h(x) \equiv 1$  for protogalactic gas that traces the dark matter directly, is

$$m^2(x) \tilde{v}^2(x) = C + 4\widetilde{M}_{\text{CMO}} \int_0^x m(u) du - 4 \frac{\widetilde{M}_{\text{CMO}}}{\widetilde{M}_{\text{pk}}} \int_0^x \frac{m^2(u)}{u^2} du - 4 \int_0^x \frac{m^3(u)}{u^2} du , \quad (3.26)$$

where  $C \equiv m^2(0) \tilde{v}^2(0)$  is again a constant of integration representing (the square of) the momentum of the shell at the origin.

### 3.4.1.1 Velocity fields at small and large radii

In the limit of small  $x$ , we can assume to leading order that

$$m(x) \longrightarrow A x^p , \quad (x \ll 1, p > 1) \quad (3.27)$$

where  $p > 1$  because we consider only halo density profiles that are shallower than isothermal at the centre. Equation (3.26) then gives

$$\tilde{v}^2 \longrightarrow \frac{C}{A^2} x^{-2p} , \quad (x \ll 1, C \neq 0) \quad (3.28)$$

so, as with the singular isothermal sphere, the integration constant, or (the square of) the momentum of the shell at  $r = 0$ , determines the behaviour of the shell.

If  $C > 0$ , then  $\tilde{v}^2 > 0$  and  $d\tilde{v}^2/dx < 0$  at small radii, and the shell decelerates outwards unless and until  $\tilde{v}^2 = 0$ , at which point the shell stalls and then collapses.

If  $C < 0$ , then  $\tilde{v}^2 < 0$  at small radii, which is unphysical; but  $d\tilde{v}^2/dx > 0$ , so  $\tilde{v}^2$  may become positive at some non-zero ‘‘launch’’ radius.

When  $C = 0$ , from equation (3.26),

$$\tilde{v}^2 \longrightarrow \frac{4\widetilde{M}_{\text{CMO}}}{A} \frac{x^{1-p}}{p+1} - \frac{4\widetilde{M}_{\text{CMO}}}{\widetilde{M}_{\text{pk}}} \frac{x^{-1}}{2p-1} ,$$

$$(x \ll 1, C = 0) \quad (3.29)$$

and the behaviour of the shell depends on the specific values of  $A$  and  $p$ , which in turn depend upon the specific choice of dark matter density profile. The solution with  $C = 0$  corresponds to a shell having zero momentum at  $x = 0$  and is also the value of  $C$  that separates initially decelerating solutions that either escape or stall ( $C > 0$ ), from solutions that are launched from rest at a non-zero radius ( $C < 0$ ).

Since we consider only haloes that are steeper than isothermal at large radii, we must have that  $d \ln m / d \ln x < 1$  for  $x > 1$ . At large radius, the second term from the right-hand side of equation (3.26) then dominates, so that

$$\tilde{v}^2 \longrightarrow \frac{4\widetilde{M}_{\text{CMO}}}{m^2(x)} \int_0^x m(u) du \quad . \quad (x \gg 1) \quad (3.30)$$

The velocity field in the limit  $x \rightarrow \infty$  is therefore completely independent of initial conditions (i.e., no  $C$  dependence). To leading order,  $\tilde{v}^2 \rightarrow \mathcal{O}(x^{1-q})$  with  $q < 1$ . Thus, if the shell can make it to large radii at all in a non-isothermal halo it must eventually accelerate. This is in contrast to the singular isothermal sphere, where a shell at very large radius can only coast at a constant speed. It is the steeper-than-isothermal gradient of  $\rho_{\text{DM}}(r)$  at large radii in realistic dark matter haloes that leads to the acceleration.

### 3.4.1.2 Condition for the escape of a particular shell

Any momentum-driven shell with a velocity field given by equation (3.26), and with  $C > 0$ , decelerates as it moves outwards from small radii according to equation (3.28). The same is true of shells with  $C = 0$ , if the small- $x$  value of  $\tilde{v}^2$  from equation (3.29) is positive. Some shells with  $C < 0$  and relatively small launch radii can also have  $\tilde{v}^2 > 0$  and  $d\tilde{v}^2/dx < 0$  over some range of radius (see below). Meanwhile, any solution to equation (3.25) [with  $h(x) \equiv 1$ ] accelerates at large radii according to equation (3.30). Therefore, there is a large class of solutions that go through local minima in  $\tilde{v}^2$  at intermediate radii. We want to know the CMO mass required for a particular shell in this class to escape a given galaxy. (The only solutions not in this class are some, with

$C < 0$ , which are launched from large enough radii that they only accelerate outwards, and so always escape.)

If a local minimum in  $\tilde{v}^2$  exists for a particular solution, we denote the radius where it occurs by  $x_{\min}$ , and the value of the minimum by  $\tilde{v}_{\min}^2$ . Putting  $h(x) \equiv 1$  in equation (3.25) and setting  $d\tilde{v}^2/dx = 0$  at  $x = x_{\min}$ , we then obtain

$$\begin{aligned} \tilde{v}_{\min}^2 \frac{d \ln m^2(x_{\min})}{d \ln x_{\min}} &= 4\widetilde{M}_{\text{CMO}} \frac{x_{\min}}{m(x_{\min})} \\ &\quad - 4 \frac{\widetilde{M}_{\text{CMO}}}{\widetilde{M}_{\text{pk}}} \frac{1}{x_{\min}} - 4 \frac{m(x_{\min})}{x_{\min}} . \end{aligned} \quad (3.31)$$

If a shell with a given initial momentum (value of  $C$ ) is to escape a dark-matter halo with given  $m(x)$ ,  $\widetilde{M}_{\text{pk}}$ , and  $\sigma_0 \equiv V_{\text{c,pk}}/\sqrt{2}$ , then we must have  $\tilde{v}_{\min}^2 \geq 0$  so the shell does not stall (i.e., cross  $\tilde{v}^2 = 0$ ) before it can start accelerating outwards. We refer to the case that  $\tilde{v}_{\min}^2 = 0$  exactly as the *critical* case, and we denote the values of  $\widetilde{M}_{\text{CMO}}$  and  $x_{\min}$  in this case by  $\widetilde{M}_{\text{crit}}$  and  $x_{\text{crit}}$ . Then, from equation (3.31),

$$\widetilde{M}_{\text{crit}} = \frac{m^2(x_{\text{crit}})}{x_{\text{crit}}^2} \left[ 1 - \frac{1}{\widetilde{M}_{\text{pk}}} \frac{m(x_{\text{crit}})}{x_{\text{crit}}^2} \right]^{-1} . \quad (3.32)$$

Also, setting  $x = x_{\text{crit}}$ ,  $\tilde{v}^2 = 0$ , and  $\widetilde{M}_{\text{CMO}} = \widetilde{M}_{\text{crit}}$  in equation (3.26), and using equation (3.32) to eliminate  $\widetilde{M}_{\text{pk}}$ , yields

$$\widetilde{M}_{\text{crit}} = \frac{\int_0^{x_{\text{crit}}} [m(x_{\text{crit}}) - m(u)] [m(u)/u]^2 du + C/4}{\int_0^{x_{\text{crit}}} [x_{\text{crit}}^2/m(x_{\text{crit}}) - u^2/m(u)] [m(u)/u]^2 du} . \quad (3.33)$$

Equating the right-hand sides of equation (3.32) and (3.33) allows us to solve for  $x_{\text{crit}}$ , and then  $\widetilde{M}_{\text{crit}}$ , in terms of  $C$  and the dark-matter halo parameters. The *necessary* condition for the escape of a purely momentum-driven shell with a particular value of  $C$  is just  $\widetilde{M}_{\text{CMO}} \geq \widetilde{M}_{\text{crit}}$ .

Equation (3.32) can give a sensible (positive) value for  $\widetilde{M}_{\text{crit}}$  only for shell-and-dark matter combinations such that  $\widetilde{M}_{\text{pk}} > m(x_{\text{crit}})/x_{\text{crit}}^2$ . This is not a problem in general.  $\widetilde{M}_{\text{pk}}$  is the dark matter mass inside the peak of the dark-matter circular-speed

curve, in units of  $M_\sigma \simeq 4.6 \times 10^8 M_\odot \sigma_{200}^4$  (equation [3.5]), and so will be a large number in real galaxies. Meanwhile, the function  $m(x)/x^2$  is always equal to 1 at  $x = 1$  (equation [3.23]), so that having  $\widetilde{M}_{\text{pk}} > m(x_{\text{crit}})/x_{\text{crit}}^2$  at some reasonable value of  $x_{\text{crit}}$  is usually assured.

The density profiles of realistic dark-matter halo models are such that  $d \ln m / d \ln x < 2$  in the main, the only exception being in the very innermost regions of some models (see below). Thus, for most values of  $x_{\text{crit}}$ , the integral in the denominator of equation (3.33) is positive; while the integral in the numerator is always positive. Therefore, this equation implies  $\widetilde{M}_{\text{crit}} > 0$  for any shell with  $C \geq 0$ . Launch solutions with *modest*  $C < 0$  can also have  $\widetilde{M}_{\text{crit}} > 0$ , so long as the numerator in equation (3.33) is still positive. If  $C$  is too large and negative, then formally  $\widetilde{M}_{\text{crit}} < 0$ , which means that such solutions do not actually go through minima in  $\widetilde{v}^2$ . These correspond to shells, launched from large radii, which accelerate monotonically outwards to escape regardless of the CMO mass.

Below, we will find the necessary  $\widetilde{M}_{\text{crit}}$  for shells that have  $C = 0$  (i.e., zero momentum at zero radius) in some specific dark-matter haloes. We emphasize, however, that this is not the only physically meaningful solution. Solutions with  $C > 0$  would describe shells that receive an impulse at the centre. Solutions with  $C < 0$  could be of interest for shells that stall at some radius inside a galaxy during an early phase of CMO growth, and are later “re-launched” by feedback from the CMO when it is more massive.

### 3.4.1.3 Sufficient condition for the escape of any shell

Momentum-driven shells with different initial conditions ( $C$  values) have different values of  $x_{\text{crit}}$  and  $\widetilde{M}_{\text{crit}}$ , given by equations (3.32) and (3.33). To compare these values between different shell solutions, we differentiate equation (3.32) with respect to  $x_{\text{crit}}$ , for a fixed dark matter mass  $\widetilde{M}_{\text{pk}}$ :

$$\frac{d\widetilde{M}_{\text{crit}}}{dx_{\text{crit}}} = \frac{2 m^2(x_{\text{crit}}) x_{\text{crit}}}{\left[ x_{\text{crit}}^2 - m(x_{\text{crit}})/\widetilde{M}_{\text{pk}} \right]^2} \times$$

$$\left\{ \left[ \frac{d \ln m(x_{\text{crit}})}{d \ln x_{\text{crit}}} - 1 \right] - \frac{1}{2 \widetilde{M}_{\text{pk}}} \frac{1}{x_{\text{crit}}} \frac{dm(x_{\text{crit}})}{dx_{\text{crit}}} \right\}. \quad (3.34)$$

By definition,  $(d \ln m / d \ln x - 1) = d \ln V_c^2 / d \ln x$ , which is positive at  $x < 1$  and negative for  $x > 1$  (recall equation [3.24]). Hence,  $d \widetilde{M}_{\text{crit}} / dx_{\text{crit}} > 0$  among shells with sufficiently small  $x_{\text{crit}}$ , and  $d \widetilde{M}_{\text{crit}} / dx_{\text{crit}} < 0$  among shells with sufficiently large  $x_{\text{crit}}$ . Setting  $d \widetilde{M}_{\text{crit}} / dx_{\text{crit}} = 0$  for a given dark-matter  $m(x)$  and  $\widetilde{M}_{\text{pk}}$  therefore identifies the momentum-driven shell that has the *largest* critical CMO mass required for escape,  $\widetilde{M}_{\text{crit}}^{\text{max}}$ .

To find  $\widetilde{M}_{\text{crit}}^{\text{max}}$ , we first solve the equation  $d \widetilde{M}_{\text{crit}} / dx_{\text{crit}} = 0$  for the radius  $x_{c,\text{max}}$  at which the shell with exactly this critical mass begins to accelerate,

$$\left. \frac{d \ln m}{d \ln x} \right|_{x=x_{c,\text{max}}} = 1 + \frac{1}{2 \widetilde{M}_{\text{pk}}} \frac{1}{x_{c,\text{max}}} \left. \frac{dm}{dx} \right|_{x=x_{c,\text{max}}}, \quad (3.35)$$

and then use this value in equation (3.32):

$$\widetilde{M}_{\text{crit}}^{\text{max}} = \frac{m^2(x_{c,\text{max}})}{x_{c,\text{max}}^2} \left[ 1 - \frac{1}{\widetilde{M}_{\text{pk}}} \frac{m(x_{c,\text{max}})}{x_{c,\text{max}}^2} \right]^{-1}. \quad (3.36)$$

The *sufficient* condition for the escape of *any* momentum-driven shell is simply  $\widetilde{M}_{\text{CMO}} \geq \widetilde{M}_{\text{crit}}^{\text{max}}$ . This trivially includes any launch solutions of the type, mentioned above, that do not go through local minima in  $\tilde{v}^2$  but only ever accelerate outwards.

We analyse equations (3.35) and (3.36) further in Appendix 3.A. There we show that, in the observationally relevant limit of large halo mass  $\widetilde{M}_{\text{pk}}$ ,

$$\begin{aligned} x_{c,\text{max}} &\longrightarrow 1 + \frac{1}{2 \widetilde{M}_{\text{pk}}} \left( \left. \frac{d^2 m}{dx^2} \right|_{x=1} \right)^{-1} \\ \widetilde{M}_{\text{crit}}^{\text{max}} &\longrightarrow 1 + \frac{1}{\widetilde{M}_{\text{pk}}} \quad (\widetilde{M}_{\text{pk}} \gg 1) \end{aligned} \quad (3.37)$$

to first order in  $(1/\widetilde{M}_{\text{pk}})$ . That is, in very massive, non-isothermal dark matter haloes, the CMO mass that suffices to ensure the escape of any momentum-driven shell tends to the value  $\widetilde{M}_{\text{crit}}^{\text{max}} \rightarrow 1$ ; and the radius where the slowest-moving shell driven by a CMO with this mass begins to accelerate tends to  $x_{c,\text{max}} \rightarrow 1$ , which is the peak of the dark-matter circular-speed curve.

### 3.4.1.4 $M$ - $\sigma$ and $M$ - $V_c$ relations

The dimensional CMO mass that guarantees the escape of any momentum-driven shell from a non-isothermal halo follows from recalling the definition of the mass unit  $M_\sigma$  (equation [3.5]) and our identification of a characteristic velocity dispersion in terms of peak circular speed in the halo (equation [3.19]). For very massive haloes in particular ( $M_{\text{pk}} \gg M_\sigma$ ), equation (3.37) gives approximately

$$M_{\text{crit}}^{\text{max}} \longrightarrow M_\sigma \equiv \frac{f_0 \kappa}{\lambda \pi G^2} \sigma_0^4 \equiv \frac{f_0 \kappa}{\lambda \pi G^2} \frac{V_{\text{c,pk}}^4}{4} . \quad (3.38)$$

Numerically,

$$M_{\text{crit}}^{\text{max}} \longrightarrow 1.14 \times 10^8 M_\odot \left( \frac{V_{\text{c,pk}}}{200 \text{ km s}^{-1}} \right)^4 f_{0.2} \lambda^{-1} , \quad (3.39)$$

in which  $\lambda \sim 1$  describes CMOs that are supermassive black holes, while  $\lambda \sim 0.05$  applies for nuclear star clusters (King & Pounds 2003; McLaughlin et al. 2006).

This result reduces to the  $M$ - $\sigma$  relation obtained by King (2005) for singular isothermal spheres, in which  $V_c = \sqrt{2} \sigma_0$  is constant with radius. However, there are significant distinctions between previous work and our new analysis.

First, as we have emphasized,  $M_{\text{crit}}^{\text{max}}$  corresponds in the isothermal case to a CMO mass that is *necessary but not sufficient* for momentum-driven feedback to break out of a galaxy; while in the non-isothermal case it is a *sufficient but not always necessary* CMO mass. The CMO masses required for the escape of most momentum-driven shells in a given dark-matter halo (as obtained from equations [3.32] and [3.33] above) will be smaller than  $M_{\text{crit}}^{\text{max}}$ . On these grounds alone, theoretical  $M_{\text{crit}}^{\text{max}}-\sigma_0$  or  $M_{\text{crit}}^{\text{max}}-V_{\text{c,pk}}$  relations from our work are expected to be something of upper limits to observed  $M$ - $\sigma$  or  $M$ - $V_c$  relations.

Second, our general treatment shows that the value of  $M_{\text{crit}}^{\text{max}}$  in equation (3.38) or (3.39) applies only *in the limit of very large dark-matter halo mass*,  $M_{\text{pk}} \gg M_\sigma$ . The exact value of the sufficient CMO mass  $M_{\text{crit}}^{\text{max}}$  for a specific value of  $M_{\text{pk}}$  must be obtained from equations (3.35) and (3.36).

Third, our results are the first to incorporate explicitly and rigorously the peak value of a dark-matter circular-speed curve (and associated velocity dispersion), which

is a well-defined quantity in *any* realistic non-isothermal halo. This provides a new basis from which to begin addressing observational claims of correlations between CMO masses and dark-matter halo properties (e.g., Volonteri et al. 2011; Ferrarese 2002).

In the rest of this section, we illustrate the general results we have obtained, by looking in detail at their application to three specific dark-matter halo models.

### 3.4.2 Hernquist model haloes

The first non-isothermal density profile we consider is that of Hernquist (1990). This model has been used to fit dark-matter haloes from N-body simulations (e.g., Dubinski & Carlberg 1991) and also has the advantage that, with it, our problem remains analytically tractable.

The density of a Hernquist sphere is given by

$$\rho_{\text{DM}}(r) = \frac{M_{\text{tot}}}{2\pi r_0^3} \left(\frac{r}{r_0}\right)^{-1} \left(1 + \frac{r}{r_0}\right)^{-3}, \quad (3.40)$$

where  $r_0$  is a scale radius and  $M_{\text{tot}}$  is the total halo mass. In terms of the characteristic mass and radius of equation (3.5), the mass enclosed inside radius  $\tilde{r}$  is

$$\tilde{M}_{\text{DM}}(\tilde{r}) = \tilde{M}_{\text{tot}} \left(\frac{\tilde{r}/\tilde{r}_0}{1 + \tilde{r}/\tilde{r}_0}\right)^2. \quad (3.41)$$

The circular-speed curve for this model,  $\tilde{V}_c^2 = \tilde{M}_{\text{DM}}(\tilde{r})/\tilde{r}$ , peaks at  $\tilde{r}_{\text{pk}} = \tilde{r}_0$ , so that the mass inside this radius is

$$\tilde{M}_{\text{DM}}(\tilde{r}_{\text{pk}}) \equiv \tilde{M}_{\text{pk}} = \frac{\tilde{M}_{\text{tot}}}{4}. \quad (3.42)$$

Defining  $x \equiv r/r_{\text{pk}} = r/r_0$ , we therefore write

$$\tilde{M}_{\text{DM}}(x) = \tilde{M}_{\text{pk}} \frac{4x^2}{(1+x)^2} \equiv \tilde{M}_{\text{pk}} m(x). \quad (3.43)$$

With the above definitions and  $h(x) \equiv 1$  again, equation (3.25) for the motion of

a momentum-driven shell has the general solution

$$\begin{aligned} \tilde{v}^2 = & \widetilde{M}_{\text{CMO}} \left( \frac{1+x}{x} \right)^4 \left[ 1+x - \frac{1}{1+x} - 2 \ln(1+x) \right] \\ & - \frac{4}{3} \frac{\widetilde{M}_{\text{CMO}}}{\widetilde{M}_{\text{pk}}} \frac{1+x}{x} - \frac{16}{5} \frac{x}{1+x} + \frac{C}{16} \left( \frac{1+x}{x} \right)^4 . \end{aligned} \quad (3.44)$$

In the limit that  $x \rightarrow 0$ ,  $m(x) \rightarrow 4x^2$ , and from equation (3.28) we have

$$\tilde{v}^2 \longrightarrow \frac{C}{16} x^{-4} , \quad (x \ll 1, C \neq 0) \quad (3.45)$$

or, if  $C = 0$ , equation (3.29) instead gives

$$\tilde{v}^2 \longrightarrow \left[ \frac{\widetilde{M}_{\text{CMO}}}{3} - \frac{4}{3} \frac{\widetilde{M}_{\text{CMO}}}{\widetilde{M}_{\text{pk}}} \right] x^{-1} . \quad (x \ll 1, C = 0) \quad (3.46)$$

Thus, for halo masses  $\widetilde{M}_{\text{pk}} > 4$ , all shell solutions with  $C \geq 0$  decelerate from large, positive  $\tilde{v}^2$  at small radii.

In the large- $x$  limit,  $m(x) \rightarrow 4$  and equation (3.30) gives

$$\tilde{v}^2 \longrightarrow \widetilde{M}_{\text{CMO}} x . \quad (x \gg 1) \quad (3.47)$$

All solutions tend to the same form at large radii, corresponding to acceleration outwards that is independent of  $C$ , as we expect from the general discussion in §3.4.1

The solid lines in Figure 3.2 show, as functions of  $\widetilde{M}_{\text{pk}}$ , the sufficient CMO mass,  $\widetilde{M}_{\text{crit}}^{\text{max}}$ , that provides for the escape of *any* momentum-driven shell from a Hernquist halo (upper panel); and the radius,  $x_{\text{c,max}}$  at which the slowest-moving shell begins to accelerate towards larger radii (lower panel). These quantities have been calculated from equations (3.35) and (3.36), with  $m(x)$  defined in equation (3.43). As expected on general grounds (see equation [3.37]; also Appendix 3.A),  $\widetilde{M}_{\text{crit}}^{\text{max}} \rightarrow 1$  and  $x_{\text{c,max}} \rightarrow 1$  (denoting the peak of the circular-speed curve in the halo) for large  $\widetilde{M}_{\text{pk}} \gg 1$ .

The dashed lines in Figure 3.2 show the necessary CMO mass,  $\widetilde{M}_{\text{crit}}$ , that allows for the escape from a Hernquist halo of shells with  $C = 0$  [ $m^2 \tilde{v}^2 \rightarrow 0$  as  $x \rightarrow 0$ ] specifically; and the radius,  $x_{\text{crit}}$ , at which this particular shell begins to accelerate outwards. In this case,  $\widetilde{M}_{\text{crit}}$  and  $x_{\text{crit}}$  have been calculated from equations (3.32) and

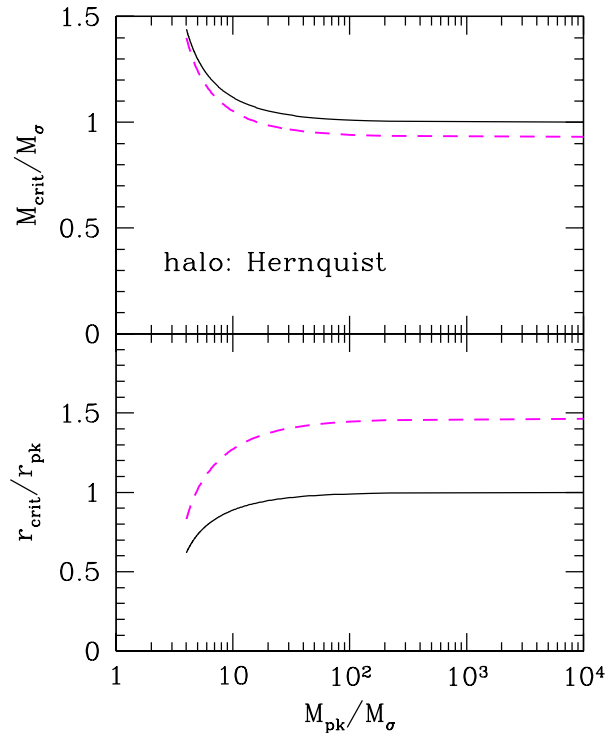


Figure 3.2: Solid lines show, as functions of  $\widetilde{M}_{\text{pk}}$ , the sufficient critical CMO mass,  $\widetilde{M}_{\text{crit}}^{\text{max}}$ , that allows the escape of any momentum-driven shell from a Hernquist halo (upper panel); and the radius,  $x_{\text{c,max}}$ , at which the slowest-moving shell driven by such a CMO begins to accelerate to escape (lower panel). Dashed lines show the necessary  $\widetilde{M}_{\text{crit}}$  and associated  $x_{\text{crit}}$  for the escape of the particular solution with  $C = 0$ . We show results only for halo masses  $\widetilde{M}_{\text{pk}} > 4$ , above which  $x_{\text{crit}}$  and  $x_{\text{c,max}}$  are single-valued functions of  $\widetilde{M}_{\text{pk}}$ .

(3.33), with  $C$  set to zero and  $m(x)$  taken from equation (3.43). Now, the necessary  $\widetilde{M}_{\text{crit}} \rightarrow 0.93$  in the limit  $\widetilde{M}_{\text{pk}} \rightarrow \infty$  (versus the *sufficient*  $\widetilde{M}_{\text{crit}}^{\text{max}} \rightarrow 1$ ), and the acceleration begins at  $x_{\text{crit}} \rightarrow 1.46$  (just beyond the corresponding radius for  $\widetilde{M}_{\text{CMO}} = \widetilde{M}_{\text{crit}}^{\text{max}}$ ).

Parameters that give a reasonable, model-independent summary of the circular-speed curve of the Milky Way dark-matter halo are  $r_{\text{pk}} \approx 50$  kpc and  $V_{\text{c,pk}} \approx$

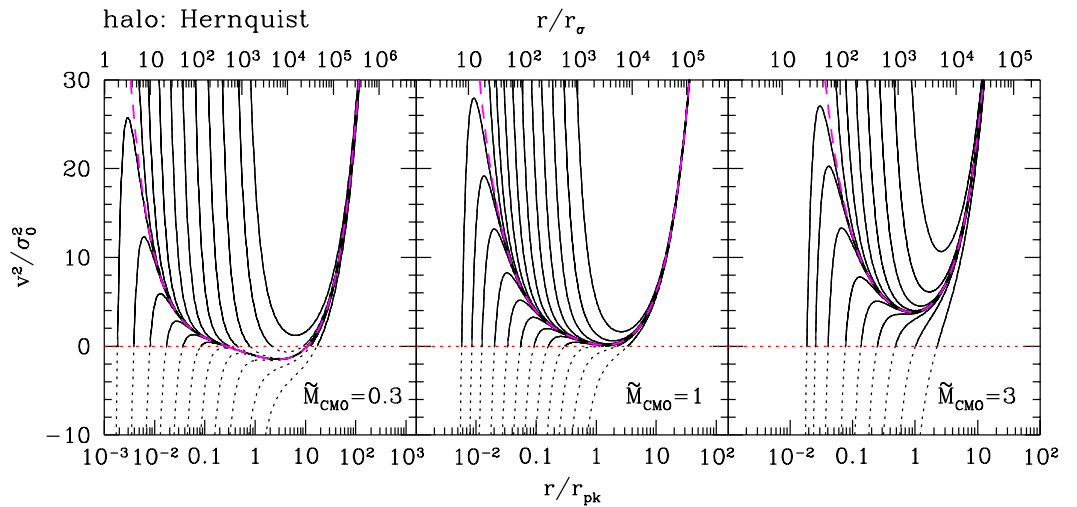


Figure 3.3: Velocity fields  $\tilde{v}^2(x)$  for  $\tilde{M}_{\text{CMO}} = 0.3, 1, 3$  in a Hernquist dark-matter halo with spatially constant gas fraction and dimensionless  $\tilde{M}_{\text{pk}} = 4000$ . This corresponds to a roughly Milky Way-sized halo with  $r_{\text{pk}} \approx 50$  kpc,  $M_{\text{pk}} \approx 4.7 \times 10^{11} M_{\odot}$ , and  $\sigma_0 \approx 140$  km s $^{-1}$ . The top axis gives the radius in units of  $r_{\sigma} \approx 25$  pc  $\sigma_{140}^2 f_{0.2} \lambda^{-1}$ , where  $f_{0.2} = f_0/0.2$ . The magenta curve represents the solution with  $C = 0$  for each value of CMO mass illustrated. As in Figure 3.1, the physical part(s) of each solution are shown by the solid lines.

200 km s $^{-1}$  (see, e.g., Dehnen, McLaughlin & Sachania 2006; McMillan 2011). Thus,  $M_{\text{pk}} = r_{\text{pk}} V_{\text{c,pk}}^2 / G \approx 4.7 \times 10^{11} M_{\odot}$ ;  $\sigma_0 \equiv V_{\text{c,pk}} / \sqrt{2} \approx 140$  km s $^{-1}$ ; and  $M_{\sigma} \approx 1.1 \times 10^8 M_{\odot} f_{0.2} \lambda^{-1}$ , so that  $\tilde{M}_{\text{pk}} \approx 4300$ .

Figure 3.3 shows the solutions from equation (3.44) for  $\tilde{M}_{\text{CMO}} = 0.3, 1$  and 3 in a Hernquist halo with  $\tilde{M}_{\text{pk}} = 4000$ . In each panel the dashed (magenta) curve shows the solution with  $C = 0$ . As in Figure 3.1, the physical parts of each solution (i.e., those with  $\tilde{v}^2 \geq 0$ ) are shown as solid lines.

The left panel shows solutions with  $\tilde{M}_{\text{CMO}} = 0.3$ . Most of these represent shells that stall and cannot escape. Unlike the singular isothermal sphere however, it is possible to have launch solutions when  $\tilde{M}_{\text{CMO}} < 1$ . Solutions with  $C < 0$  but very close to zero are launched from inside  $\tilde{r}_{\text{pk}}$  and initially accelerate, then reach a maximum

velocity and decelerate. When  $\widetilde{M}_{\text{CMO}} = 0.3$ , these solutions all stall at a finite radius. Solutions launched from outside  $\widetilde{r}_{\text{pk}}$  either correspond to large and negative  $C$  or are the formal continuations of solutions that stall at smaller radii, go into the unphysical  $\widetilde{v}^2 < 0$  regime, but then later recover to  $\widetilde{v}^2 > 0$ . All launch solutions of this type accelerate monotonically towards larger radii and therefore escape; but, for this value of  $\widetilde{M}_{\text{CMO}}$ , they all start from infeasibly large launch radii of order  $x \sim 10$  (i.e.,  $r \sim 10 r_{\text{pk}} \sim 500$  kpc) or more. For large enough *positive* values of  $C$  it is possible for a shell to escape without stalling (or being launched from a large radius) when  $\widetilde{M}_{\text{CMO}} = 0.3$ , although this is again a formal result that is not physically plausible. The uppermost curve in the left panel of Figure 3.3 shows one solution that evidently only requires  $\widetilde{M}_{\text{crit}} < 0.3$  to escape this halo; but it has  $C \gtrsim 10$ , which, given that  $r_{\text{pk}} \approx 50$  kpc and  $\sigma_0 \approx 140$  km s<sup>-1</sup>, corresponds to a shell velocity of  $\sim 10^6 c$  at a radius of 1 pc.

The middle panel of Figure 3.3 shows solutions for  $\widetilde{M}_{\text{CMO}} = 1$ . All of the solutions shown are able to escape the halo. However, from equation (3.37), we know that, with  $\widetilde{M}_{\text{pk}} = 4000$ , the CMO mass sufficient to ensure escape is actually  $\widetilde{M}_{\text{CMO}}^{\text{max}} \approx 1.00025$ . Thus, there are some shells in a (narrow) range of  $C$  values very close to 0 that stall rather than escape; these are simply not shown here. Several solutions are shown that have  $C < 0$  but close to 0. These are launched from inside the peak of the circular-speed curve and, though they come very close to stalling, those shown manage eventually to accelerate and escape to large radii. Several launch solutions with large and negative  $C$  are also shown, all starting from radii  $r > r_{\text{pk}}$  and all accelerating to escape. The solution with  $C = 0$  exactly is seen to escape (as do all solutions above it with  $C > 0$ ), which is expected since our calculations above (see Figure 3.2) gave  $\widetilde{M}_{\text{crit}} \simeq 0.93$  for this solution.

The right-hand panel of Figure 3.3 shows velocity-field solutions for  $\widetilde{M}_{\text{CMO}} = 3$ . This is well above the value of the sufficient  $\widetilde{M}_{\text{crit}}^{\text{max}}$  given by equations (3.35) and (3.36) above (or, approximately, equation [3.37]). As a result, and in contrast to the singular isothermal sphere, all shells are able to escape and there are no stalls, regardless of the initial shell momentum.

### 3.4.3 NFW model haloes

We next consider the dark matter density profile of Navarro, Frenk & White (1996, 1997; NFW), which has

$$\rho_{\text{DM}}(r) = 4\rho_s \left(\frac{r}{r_s}\right)^{-1} \left(1 + \frac{r}{r_s}\right)^{-2}, \quad (3.48)$$

where  $r_s$  is a scale radius and  $\rho_s$  is the density at  $r_s$ . From this,

$$M_{\text{DM}}(r) = 16\pi r_s^3 \rho_s \left[ \ln(1 + r/r_s) - \frac{r/r_s}{1 + r/r_s} \right], \quad (3.49)$$

and it follows that the circular-speed curve,  $V_c^2 = GM_{\text{DM}}(r)/r$ , peaks at  $\mathcal{R} \equiv r_{\text{pk}}/r_s \simeq 2.16258$ . Thus, with  $x \equiv r/r_{\text{pk}}$  we have

$$\widetilde{M}_{\text{DM}}(x=1) \equiv \widetilde{M}_{\text{pk}} = 16\pi r_s^3 \rho_s \left[ \ln(1 + \mathcal{R}) - \frac{\mathcal{R}}{1 + \mathcal{R}} \right], \quad (3.50)$$

and

$$\widetilde{M}_{\text{DM}}(x) = \widetilde{M}_{\text{pk}} \frac{\ln(1 + \mathcal{R}x) - \mathcal{R}x/(1 + \mathcal{R}x)}{\ln(1 + \mathcal{R}) - \mathcal{R}/(1 + \mathcal{R})} \equiv \widetilde{M}_{\text{pk}} m(x). \quad (3.51)$$

At small radii, then, the dimensionless mass profile tends to

$$m(x) \longrightarrow \frac{\mathcal{R}^2 x^2}{2} \left[ \ln(1 + \mathcal{R}) - \frac{\mathcal{R}}{1 + \mathcal{R}} \right]^{-1}, \quad (x \ll 1) \quad (3.52)$$

implying for the velocity field, from equation (3.28) for  $C \neq 0$ ,

$$\tilde{v}^2 \longrightarrow \frac{4C}{\mathcal{R}^4} \left[ \ln(1 + \mathcal{R}) - \frac{\mathcal{R}}{1 + \mathcal{R}} \right]^2 x^{-4}, \quad (x \ll 1, C \neq 0) \quad (3.53)$$

or from equation (3.29) for  $C = 0$ ,

$$\tilde{v}^2 \longrightarrow \left( \frac{8}{3} \left[ \ln(1 + \mathcal{R}) - \frac{\mathcal{R}}{1 + \mathcal{R}} \right] \frac{\widetilde{M}_{\text{CMO}}}{\mathcal{R}^4} - \frac{4}{3} \frac{\widetilde{M}_{\text{CMO}}}{\widetilde{M}_{\text{pk}}} \right) x^{-1}. \quad (x \ll 1, C = 0) \quad (3.54)$$

For  $\widetilde{M}_{\text{pk}} \gtrsim 5.001$ ,  $\tilde{v}^2$  tends to a positive value in the limit of small  $x$  for  $C = 0$ , and then all shells with  $C \geq 0$  decelerate from large, positive velocities at small radii.

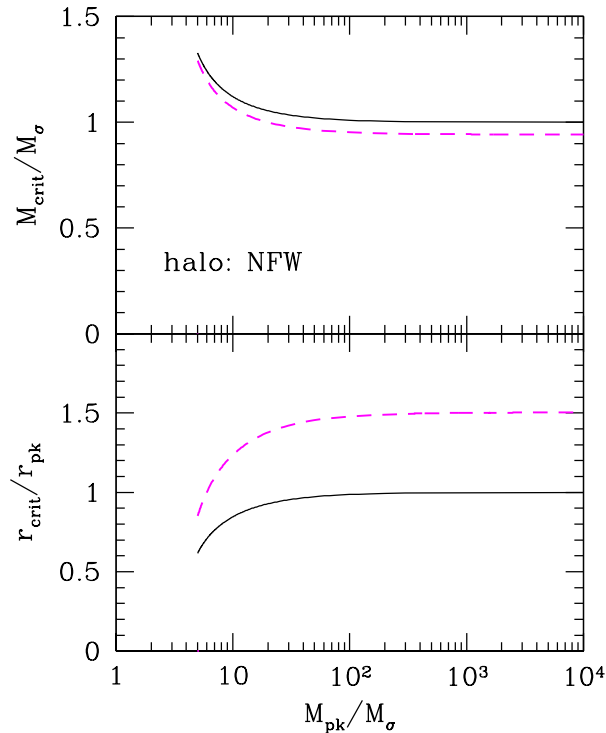


Figure 3.4: Solid lines show, as functions of  $\widetilde{M}_{\text{pk}}$ , the CMO mass  $\widetilde{M}_{\text{crit}}^{\text{max}}$ , which is sufficient for the escape of any momentum-driven shell from an NFW halo (upper panel); and the radius  $x_{\text{c,max}}$ , at which the slowest-moving shell begins to accelerate to escape (lower panel). Dashed lines show the necessary values of  $\widetilde{M}_{\text{crit}}$ , and the associated radii  $x_{\text{crit}}$ , for the escape of the particular solution with  $C = 0$ . Results are shown for  $\widetilde{M}_{\text{pk}} \gtrsim 5$ , above which  $x_{\text{crit}}$  and  $x_{\text{c,max}}$  are single-valued functions of  $\widetilde{M}_{\text{pk}}$ .

In the limit that  $x \rightarrow \infty$ , the NFW mass profile diverges logarithmically,

$$m(x) \longrightarrow \left[ \ln(1 + \mathcal{R}) - \frac{\mathcal{R}}{(1 + \mathcal{R})} \right]^{-1} \ln(\mathcal{R}x) \quad (x \gg 1) \quad (3.55)$$

and, from equation (3.30), all shell velocities tend to

$$\tilde{v}^2 \longrightarrow \frac{4\widetilde{M}_{\text{CMO}}}{[\ln(\mathcal{R}x)]^2} \left[ \ln(1 + \mathcal{R}) - \frac{\mathcal{R}}{1 + \mathcal{R}} \right] [x \ln(\mathcal{R}x) - x] \quad (x \gg 1) \quad (3.56)$$

The solid lines in Figure 3.4 show, as functions of  $\widetilde{M}_{\text{pk}}$ , the sufficient CMO mass

that allows for the escape of *any* momentum-driven shell from an NFW halo (upper panel); and the radius,  $x_{c,\max}$ , at which the slowest-moving shell begins to accelerate (lower panel). These are again calculated from equations (3.35) and (3.36), now with  $m(x)$  given by equation (3.51). In the limit of large  $\widetilde{M}_{\text{pk}}$ ,  $\widetilde{M}_{\text{crit}}^{\max} \rightarrow 1$  and  $x_{c,\max} \rightarrow 1$  again, just as found for the Hernquist halo in Figure 3.2 and as expected in general from equation (3.37) and Appendix 3.A.

The dashed lines in Figure 3.4 show the critical CMO mass that is necessary for the escape from NFW haloes of shells with  $C = 0$  specifically; and the radii,  $x_{\text{crit}}$  at which these particular shells begin to accelerate for a given  $\widetilde{M}_{\text{pk}}$ . In this case,  $\widetilde{M}_{\text{crit}}$  and  $x_{\text{crit}}$  are calculated from equations (3.32) and (3.33). In the limit of large  $\widetilde{M}_{\text{pk}}$ , we have  $\widetilde{M}_{\text{crit}} \rightarrow 0.94$ , again slightly smaller than the CMO mass sufficient to ensure the escape of any shell. The acceleration begins at  $x_{\text{crit}} \rightarrow 1.50$ , again somewhat larger than  $x_{c,\max}$  in the sufficient case.

Given  $m(x)$  in equation (3.51), equation (3.26) for the velocity fields of momentum-driven shells in NFW haloes must be evaluated numerically. Figure 3.5 shows several of the solutions for dimensionless CMO masses  $\widetilde{M}_{\text{CMO}} = 0.3, 1$  and  $3$ , and with  $\widetilde{M}_{\text{pk}} = 4000$  for a Milky Way-sized halo (see §3.4.2). In each panel of this figure, the dashed (magenta) line shows the solution with  $C = 0$ . As in Figures 3.1 and 3.3, the physical parts of solutions with  $C \neq 0$  are shown by solid lines.

Figure 3.5 is qualitatively similar to Figure 3.3 for shells in Hernquist (1990) haloes. The left-hand panel, which plots solutions for a modest  $\widetilde{M}_{\text{CMO}} = 0.3$ , shows all physically plausible shells with  $C \geq 0$  stalling and unable to escape the halo. (The one such solution shown that is able to escape, given this CMO mass, has  $C \gtrsim 20$ , corresponding to  $v \sim 10^6 c$  at  $r = 1$  pc.) Solutions with  $C < 0$  include those that are launched from within  $r < r_{\text{pk}}$ , which first accelerate but then decelerate and stall; and those launched from outside  $r > r_{\text{pk}}$ , which accelerate monotonically outwards and always escape, but which all start from large  $r \gtrsim 500$  kpc.

The middle panel shows solutions for  $\widetilde{M}_{\text{CMO}} = 1$ . All of those shown escape, including those with  $C < 0$  but near zero, which are launched from  $r < r_{\text{pk}}$ . There are solutions within a narrow range of  $C$  values near zero that cannot escape. These are

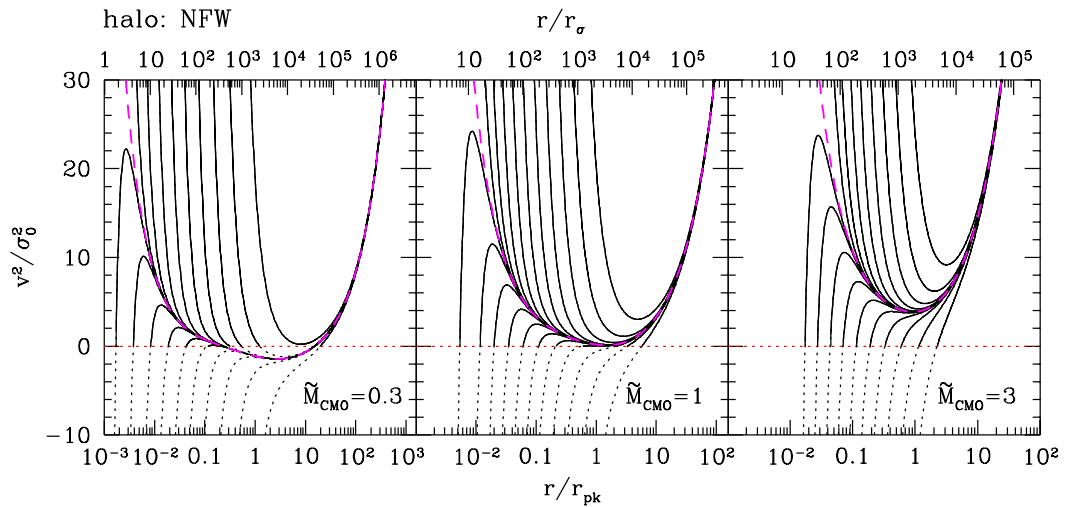


Figure 3.5: Velocity fields  $\tilde{v}^2(x)$  for  $\tilde{M}_{\text{CMO}} = 0.3, 1$  and  $3$  in an NFW halo with spatially constant gas fraction and  $\tilde{M}_{\text{pk}} = 4000$ . Radius is shown in units of  $r_\sigma \approx 25 \text{ pc } \sigma_{140}^2 f_{0.2} \lambda^{-1}$  along the top axis, and in units of  $r_{\text{pk}} \approx 50 \text{ kpc}$  along the bottom axis. The dashed, magenta curve in each panel represents the solution with  $C = 0$  for that value of  $\tilde{M}_{\text{CMO}}$ . The physical part(s) of all other solutions are shown as solid lines.

not shown, but they exist because, given that  $\tilde{M}_{\text{pk}} = 4000$  here, the critical CMO mass required for the escape of all possible solutions is  $\tilde{M}_{\text{crit}}^{\text{max}} \approx 1.00025 > 1$ , according to equation (3.37). The solution with  $C = 0$  is able to escape, as the CMO mass necessary to expel it from such a massive halo is  $\tilde{M}_{\text{crit}} \simeq 0.94 < 1$  (see Figure 3.4).

The right-hand panel of Figure 3.5 confirms again that all shells escape easily when  $\tilde{M}_{\text{CMO}} > \tilde{M}_{\text{crit}}^{\text{max}}$ .

### 3.4.4 Dehnen & McLaughlin model haloes

Finally, we consider a dark-matter density profile from the family developed by Dehnen & McLaughlin (2005). Their models are analytical solutions to the spherical Jeans equation, which have “pseudo” phase-space density profiles,  $\rho(r)/\sigma^3(r)$ , that are power

laws in radius and closely match those found in cosmological  $N$ -body simulations. They also allow for radially varying anisotropy in the dark-matter velocity dispersion; and they fit the spherically averaged density profiles of simulated haloes as well as, or better than, any other fitting function proposed to date.

The halo model of Dehnen & McLaughlin that is isotropic at its centre has the density distribution

$$\rho_{\text{DM}}(r) = \frac{5}{9} \frac{M_{\text{tot}}}{\pi r_0^3} \left(\frac{r}{r_0}\right)^{-7/9} \left[1 + \left(\frac{r}{r_0}\right)^{4/9}\right]^{-6}, \quad (3.57)$$

where  $r_0$  is a scale radius and  $M_{\text{tot}}$  is the total halo mass. This gives the enclosed mass profile,

$$M_{\text{DM}}(r) = M_{\text{tot}} \left[ \frac{(r/r_0)^{4/9}}{1 + (r/r_0)^{4/9}} \right]^5. \quad (3.58)$$

The circular-speed curve in this case peaks at  $r_{\text{pk}}/r_0 = (11/9)^{9/4}$ , so now we set  $x \equiv \tilde{r}/\tilde{r}_{\text{pk}} = (9/11)^{9/4}(r/r_0)$ . Then,

$$\tilde{M}_{\text{DM}}(x=1) \equiv \tilde{M}_{\text{pk}} = \left(\frac{11}{20}\right)^5 \tilde{M}_{\text{tot}} \quad (3.59)$$

and

$$\tilde{M}_{\text{DM}}(x) = \tilde{M}_{\text{pk}} \left(\frac{20}{11}\right)^5 \left(\frac{\frac{11}{9}x^{4/9}}{1 + \frac{11}{9}x^{4/9}}\right)^5 \equiv \tilde{M}_{\text{pk}} m(x). \quad (3.60)$$

When  $x$  is small,  $m(x) \rightarrow (20/9)^5 x^{20/9}$ , and from equation (3.28) the momentum-driven shell velocity field for  $C \neq 0$  tends to

$$\tilde{v}^2 \rightarrow C \left(\frac{9}{20}\right)^{10} x^{-40/9}; \quad (x \ll 1, C \neq 0) \quad (3.61)$$

or, from equation (3.29) if  $C = 0$ ,

$$\tilde{v}^2 \rightarrow \frac{36}{29} \left(\frac{9}{20}\right)^5 \tilde{M}_{\text{CMO}} x^{-11/9}. \quad (x \ll 1, C = 0) \quad (3.62)$$

When  $x$  is large,  $m(x) \rightarrow (20/11)^5$  and equation (3.30) gives

$$\tilde{v}^2 \rightarrow 4 \left(\frac{11}{20}\right)^5 \tilde{M}_{\text{CMO}} x. \quad (x \gg 1) \quad (3.63)$$

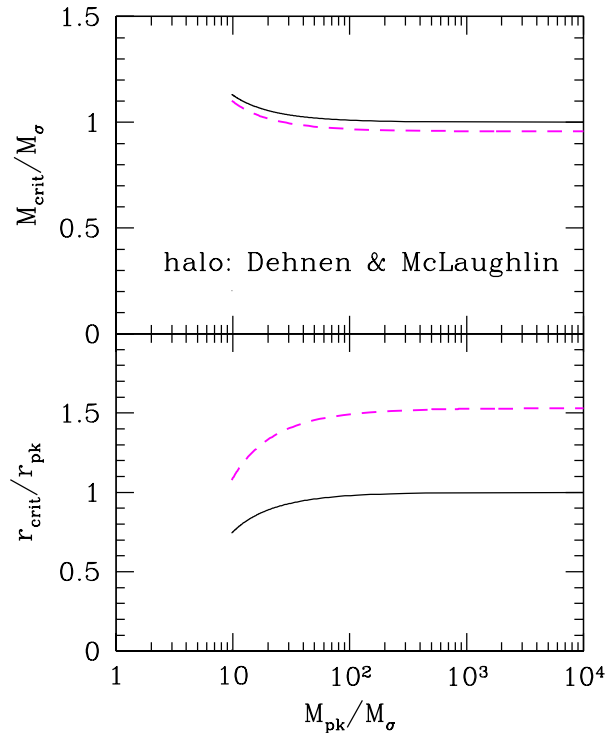


Figure 3.6: Solid lines show, as functions of  $\widetilde{M}_{\text{pk}}$ , the CMO mass,  $\widetilde{M}_{\text{crit}}^{\text{max}}$ , that is sufficient to ensure the escape of any momentum-driven shell from a Dehnen & McLaughlin (2005) halo (upper panel); and the radius,  $x_{c,\text{max}}$ , at which the slowest-moving shell begins to accelerate to escape (lower panel). Dashed lines show the necessary  $\widetilde{M}_{\text{crit}}$ , and the associated  $x_{\text{crit}}$ , for the escape of shells with  $C = 0$  specifically. Results are shown for  $\widetilde{M}_{\text{pk}} \gtrsim 10$ , since then  $x_{\text{crit}}$  and  $x_{c,\text{max}}$  are single-valued functions of  $\widetilde{M}_{\text{pk}}$ .

The solid lines in Figure 3.6 show, as functions of  $\widetilde{M}_{\text{pk}}$ , the CMO mass  $\widetilde{M}_{\text{crit}}^{\text{max}}$ , which is sufficient for the escape of any momentum-driven shell from this halo (upper panel); and the radius  $x_{c,\text{max}}$  at which the slowest-moving shell driven by a CMO with the sufficient mass begins to accelerate outwards (lower panel). These are calculated as usual from equations (3.35) and (3.36), with  $m(x)$  in equation (3.60). As for the other haloes we have looked at, and as will always be true in general,  $\widetilde{M}_{\text{crit}}^{\text{max}} \rightarrow 1$  and  $x_{c,\text{max}} \rightarrow 1$  for  $\widetilde{M}_{\text{pk}} \gg 1$ .

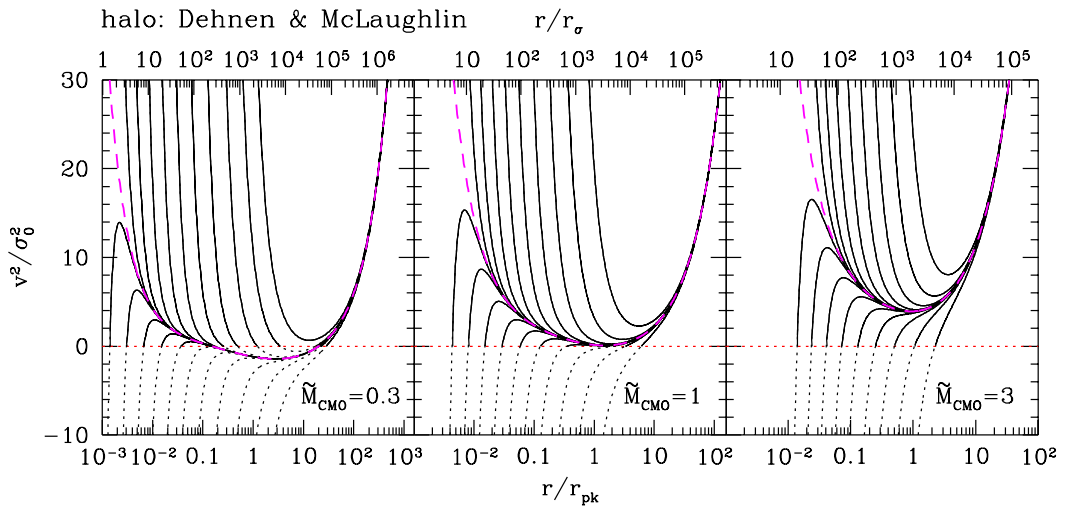


Figure 3.7: Velocity fields  $\tilde{v}^2(x)$  for CMO masses  $\tilde{M}_{\text{CMO}} = 0.3, 1$  and  $3$  in a Dehnen & McLaughlin (2005) dark-matter halo with spatially constant gas fraction and  $\tilde{M}_{\text{pk}} = 4000$ . Radius is in units of  $r_\sigma \approx 25 \text{ pc } \sigma_{140}^2 f_{0.2} \lambda^{-1}$  along the top axis, and in units of  $r_{\text{pk}} \approx 50 \text{ kpc}$  (for a Milky Way-sized halo) along the bottom axis. The solution with  $C = 0$  is shown by a dashed (magenta) line in each panel. As in Figures 3.1, 3.3, and 3.5, the physical part(s) of all other solutions are shown as solid lines.

The dashed lines in Figure 3.6 show the necessary CMO mass  $\tilde{M}_{\text{crit}}$ , and the radius  $x_{\text{crit}}$  at which acceleration begins, for the escape of shells with  $C = 0$ , calculated from equations (3.32) and (3.33). In the limit of large  $\tilde{M}_{\text{pk}}$ ,  $\tilde{M}_{\text{crit}} \rightarrow 0.96$  in this case, and  $x_{\text{crit}} \rightarrow 1.53$ .

With  $m(x)$  in equation (3.60), the solutions to equation (3.25) with  $h(x) \equiv 1$  must again be obtained numerically. Figure 3.7 shows solutions for several shells in a Dehnen & McLaughlin (2005) halo with  $\tilde{M}_{\text{pk}} = 4000$  (again as in §3.4.2), for each of the CMO masses  $\tilde{M}_{\text{CMO}} = 0.3, 1$  and  $3$ . The solution with  $C = 0$  in each case is shown by a dashed (magenta) line, and the physical part(s) of  $C \neq 0$  solutions are drawn as solid lines.

Figure 3.7 is similar in all respects to Figures 3.3 and 3.5 for the other non-isothermal halo models we have examined. The left-hand panel of the figure shows

again that with  $\widetilde{M}_{\text{CMO}} < 1$ , all physically interesting solutions correspond to shells that stall. Launch solutions with  $C < 0$  that escape must start from impractically large  $r \gtrsim 500$  kpc. Solutions with  $C > 0$  require  $C \gtrsim 30$  to escape, which implies unphysical shell speeds at small radii (i.e.,  $v \gtrsim 10^6 c$  at 1 pc). The middle panel of Figure 3.7 confirms that  $\widetilde{M}_{\text{CMO}} = 1$  is *almost* sufficient for the escape of all momentum-driven shells; there are a few solutions with a narrow range of  $C$  values near  $C = 0$  that cannot escape (because in fact  $\widetilde{M}_{\text{crit}}^{\text{max}} \approx 1 + 1/\widetilde{M}_{\text{pk}} = 1.00025$  here), but which are not shown. The right-hand panel finally illustrates again how any shell, with any initial conditions, can escape the halo when  $\widetilde{M}_{\text{CMO}}$  exceeds the sufficient  $\widetilde{M}_{\text{crit}}^{\text{max}}$  given by equations (3.35) and (3.36) in general.

### 3.5 Summary and discussion

We have analyzed the motion of momentum-conserving supershells driven into isothermal and non-isothermal protogalaxies by steady (time-independent) winds from central massive objects (CMOs: either supermassive black holes or nuclear star clusters). Our main goal has been to find the critical CMO mass that can drive a supershell to escape a galaxy, essentially clearing it of ambient gas and stopping further CMO growth. Having such a critical CMO mass as a function of a characteristic dark-matter halo velocity dispersion then gives a theoretical  $M_{\text{CMO}}-\sigma$  relation.

We assumed that the CMO wind thrust is proportional to  $M_{\text{CMO}}$  (through the Eddington luminosity: King & Pounds 2003; McLaughlin et al. 2006) to obtain a general equation of motion for momentum-driven shells (equation [3.6] or [3.25]) that allows for any dark-matter halo mass profile and also for the segregation of gas and dark matter. We solved this equation for  $v^2(r)$ , the (square of the) shell velocity as a function of radius in the CMO's host galaxy, for a number of different dark-matter density profiles, though only ever considering the case that gas traces dark matter directly. This analysis extends and generalizes others in the literature, which have only considered dark-matter haloes described as singular isothermal spheres, and which have

not presented full solutions for the velocity fields of momentum-driven supershells.

Since our main aim was to clarify the effect on theoretical  $M$ – $\sigma$  relations of relaxing the simplifying assumption that CMOs are embedded in singular isothermal dark matter haloes, we retained some other simplifications also adopted by previous authors. One of these is the assumption that the wind driving the CMO feedback is time-independent—in essence, that the CMO mass is constant throughout the motion of a momentum-conserving supershell.

In reality, of course, if the CMO is a black hole emitting at the Eddington limit, then it is also accreting mass at the Eddington rate. The growth of the black hole and thus the wind thrust which is proportional to  $M_{\text{CMO}}$ , are governed by the Salpeter timescale, defined by

$$t_{\text{Salp}} = \frac{M_{\text{BH}}}{\dot{M}_{\text{Edd}}} = \frac{M_{\text{BH}} \eta c^2}{L_{\text{Edd}}} = 4.5 \times 10^7 \text{ yr} \left( \frac{\eta}{0.1} \right). \quad (3.64)$$

If the CMO is a nuclear star cluster, then the duration and strength of a superwind from it is tied to the star-formation history and to the main-sequence lifetime of supernova progenitors.

The other simplification we made was to consider only the momentum-driven phase of supershell evolution, ignoring any eventual transition to the energy-driven regime. Further work is needed to incorporate gas cooling properly into a fuller treatment of *time-dependent* feedback, which will also account for the impact of variable CMO masses and wind strengths on  $M$ – $\sigma$  relations.

### 3.5.1 The singular isothermal sphere

Revisiting the case of a galaxy modelled as a singular isothermal sphere (SIS), we showed in §3.3 that at large radii a momentum-driven shell tends to a constant coasting speed given by equation (3.12):

$$v^2 \longrightarrow v_\infty^2 \equiv 2\sigma_0^2 \left[ \frac{M_{\text{CMO}}}{M_\sigma} - 1 \right], \quad (r \rightarrow \infty, \text{ SIS}) \quad (3.65)$$

in which (cf. King 2005)

$$M_\sigma \equiv \frac{f_0 \kappa}{\lambda \pi G^2} \sigma_0^4 \simeq 4.56 \times 10^8 M_\odot \sigma_{200}^4 f_{0.2} \lambda^{-1} , \quad (3.66)$$

where  $\sigma_0$  is the velocity dispersion of the halo and  $\sigma_{200} \equiv \sigma_0/(200 \text{ km s}^{-1})$ ;  $f_0 \approx 0.2$  is a fiducial gas mass fraction; and the parameter  $\lambda \simeq 1$  if the CMO is a supermassive black hole (SMBH), or  $\lambda \approx 0.05$  if the CMO is a nuclear star cluster (NC; McLaughlin et al. 2006). This shows that a momentum-conserving shell can reach arbitrarily large radii in an isothermal sphere, and potentially escape, only if the CMO driving the shell has a mass  $M_{\text{CMO}} > M_\sigma$  (so that  $v_\infty^2 > 0$ ). Otherwise, any shell must stall at some finite radius, and subsequently collapse, until the CMO grows in mass and drives a stronger wind (see also King 2005).

The critical  $M_{\text{CMO}}$  value in equation (3.66) has previously been obtained by methods that did not include solving explicitly for  $v^2(r)$  (see King 2003, 2005, 2010a; Murray et al. 2005; McLaughlin et al. 2006). By solving for the full velocity fields  $v^2(r)$  of momentum-driven shells, we have shown that, while  $M_{\text{CMO}} \geq M_\sigma$  is *necessary*, it is *not sufficient* to guarantee the escape of momentum-driven CMO winds from isothermal spheres.

First, as discussed in §3.3,  $M_{\text{CMO}}$  and the initial momentum of a shell very near a CMO *together* determine whether the shell can reach large enough radii to achieve the asymptotic coasting speed,  $v_\infty$ ; if it cannot, then the value of  $v_\infty$ , which is determined by  $M_{\text{CMO}}$  alone, is immaterial. As an example, when  $M_{\text{CMO}} = 1.01M_\sigma$ , a shell will stall at a finite radius, and re-collapse, unless its launch from the CMO gives it an exceedingly fast velocity of  $v \gtrsim 0.2 c \sigma_{200}$  at a radius of  $r \simeq 1 \text{ pc } \sigma_{200}^2$ .

Second, if a shell is to coast at large radii with the nominal “escape” velocity from an isothermal sphere—that is, with  $v_\infty > 2\sigma_0$ —then our work shows that  $M_{\text{CMO}} > 3M_\sigma$  is required. This would mean CMO masses almost an order of magnitude higher, at a given  $\sigma_0$ , than those provided by the observed  $M$ – $\sigma$  relations for either SMBHs or NCs. This is, in essence, the objection raised by Silk & Nusser (2010) to the idea that momentum-driven CMO winds are the sole source of  $M$ – $\sigma$ . However, the objection—and detailed answers to it, whether involving additional feedback from

bulge-star formation triggered by the CMO outflow (Silk & Nusser 2010) or a transition to energy-conserving evolution at some large shell radius (Power et al. 2011; King et al. 2011)—applies *only* if the host galaxy of a CMO is an isothermal sphere.

### 3.5.2 Non-isothermal haloes

More realistic descriptions of dark-matter haloes have density profiles that are shallower at small radii than the  $r^{-2}$  profile of an isothermal sphere, and steeper than  $r^{-2}$  at large radii. Therefore, they have circular-speed curves,  $V_c^2(r) = GM(r)/r$ , with well-defined peaks. We showed that, in *any* such non-isothermal halo, any momentum-driven shell must begin to accelerate beyond some large radius and will eventually exceed the halo escape velocity, just so long as the CMO wind driving the shell can push it to the radius where it starts accelerating. We obtained equations that can be solved for the critical CMO mass,  $M_{\text{crit}}$ , required for the escape of a shell with a given initial momentum in any halo with a peaked  $V_c(r)$  curve (§3.4.1.2; equations [3.32] and [3.33]). We then showed that there is a largest critical CMO mass,  $M_{\text{crit}}^{\text{max}}$ , in any such halo. Once a CMO exceeds this mass, *any* momentum-driven shell can escape the halo (§3.4.1.3). Our equations (3.35) and (3.36) allow the calculation of  $M_{\text{crit}}^{\text{max}}$  in general and provide a *sufficient* condition for the escape of momentum-driven feedback from non-isothermal haloes.

In this general analysis, a basic mass unit  $M_\sigma$  is defined in terms of the peak circular speed in a halo:

$$\begin{aligned} M_\sigma &\equiv \frac{f_0 \kappa}{\lambda \pi G^2} \frac{V_{\text{c,pk}}^4}{4} \\ &= 1.14 \times 10^8 M_\odot f_{0.2} \lambda^{-1} \left( \frac{V_{\text{c,pk}}}{200 \text{ km s}^{-1}} \right)^4. \end{aligned} \quad (3.67)$$

In the most relevant case that haloes are much more massive than  $M_\sigma$ , the sufficient condition for the escape of momentum-driven feedback is (equation [3.37])

$$M_{\text{CMO}} \geq M_{\text{crit}}^{\text{max}} = M_\sigma \left[ 1 + \frac{M_\sigma}{M_{\text{pk}}} + \mathcal{O} \left( \frac{M_\sigma^2}{M_{\text{pk}}^2} \right) \right], \quad (M_{\text{pk}} \gg M_\sigma) \quad (3.68)$$

where  $M_{\text{pk}} = r_{\text{pk}} V_{c,\text{pk}}^2 / G$  is the mass of dark matter inside the radius where the halo circular speed peaks. For the Milky Way,  $M_{\text{pk}} \approx 4000 M_\sigma$ , so this condition is  $M_{\text{CMO}} \gtrsim M_\sigma$  to a good approximation in intermediate and massive galaxies.

In a singular isothermal sphere,  $V_c = \sqrt{2} \sigma_0$  is constant and, in effect,  $M_{\text{pk}}$  is infinitely large, so formally  $M_{\text{crit}}^{\text{max}}$  and  $M_\sigma$  reduce to equation (3.66). Although important differences remain between the isothermal and non-isothermal cases, this suggests that the most appropriate single velocity dispersion to use to characterize an entire non-isothermal halo, at least in discussions of  $M$ - $\sigma$  relations, is simply  $\sigma_0 \equiv V_{c,\text{pk}} / \sqrt{2}$ .

We illustrated the application of our general results by solving for the velocity fields of momentum-driven shells in three specific models of non-isothermal dark-matter haloes (Hernquist 1990—§3.4.2; Navarro et al. 1996, 1997—§3.4.3; Dehnen & McLaughlin 2005—§3.4.4). We noted that there are two main types of  $v^2(r)$  solutions, corresponding to shells that decelerate from small radii close to the CMO (going on to accelerate further out if  $M_{\text{CMO}}$  is large enough, or to stall at a finite radius if not), and shells that are launched from zero velocity at non-zero radii (and may then either stall or escape at larger radii). We also saw that the radius at which any particular shell starts to accelerate to escape a halo is typically within a factor of order unity times the radius at which the dark-matter circular speed peaks (which is some tens of kpc in a Milky Way-sized halo).

Since  $M_{\text{CMO}} \geq M_{\text{crit}}^{\text{max}} \approx M_\sigma$  is a *sufficient* condition for the escape of momentum-driven feedback from non-isothermal haloes, it generally *exceeds* the minimally *necessary* condition for the escape of any one particular shell. In the specific haloes that we looked at, shells with zero initial momentum reach large radii and accelerate to escape for any  $M_{\text{CMO}} \gtrsim (0.93\text{--}0.96) M_\sigma$ . Different initial conditions may enable escape for still (slightly) lower CMO masses.

The fact that  $M_{\text{CMO}} \geq M_{\text{crit}}^{\text{max}}$  allows all purely momentum-conserving shells in non-isothermal haloes to *accelerate* at large radii—rather than just to coast as in isothermal spheres, at potentially sub-escape speeds even if  $M_{\text{CMO}} > M_\sigma$ —effectively answers the main objection of Silk & Nusser (2010) to momentum-driven feedback from CMO winds as the direct cause of observed  $M$ - $\sigma$  relations.

Again, these results are for time-independent winds from CMOs with fixed masses. We have integrated  $v(r)$  to find  $r(t)$  for the  $C = 0$  momentum-driven shells in each of the non-isothermal haloes calculated in §§3.4.2–3.4.4. For  $M_{\text{CMO}} = M_{\text{crit}}^{\text{max}}$ , these shells take  $\sim 3-4 \times 10^8$  yrs to move from  $r = 0$  to  $r \sim r_{\text{pk}}$ , from where they can accelerate to escape the galaxy. In the case that the CMO is an SMBH, this corresponds to  $\sim 7-8$  Salpeter times. Thus, if a critical mass black hole were to launch a momentum-driven shell from  $r = 0$ , the hole would be a factor of  $\sim e^{7-8}$  times more massive by the time the shell escapes. Our expression for the sufficient  $M_{\text{crit}}^{\text{max}}$  as a function of  $V_{\text{c,pk}}$  (eq. [67]) would then presumably estimate a *lower limit* to observed SMBH  $M$ - $\sigma$  relations. However, this apparent difficulty will be mitigated by two effects.

First, if SMBHs grew from much smaller seeds, then even in the case of purely momentum-driven feedback the supershells of swept-up ambient gas will have already been driven to large radii by the time the black hole reaches the critical mass. The question then becomes, for a given mass-accretion history, how near to  $r = r_{\text{pk}}$  is a supershell at the time that the black hole attains our critical mass; and can the shell subsequently move out to  $r_{\text{pk}}$ , and start to accelerate, within less than another Salpeter time? To answer this will require solving a fully time-dependent problem including CMO masses and wind thrusts that (in the SMBH case at least) increase monotonically with time. Whatever the final result, it is clear that any upwards “correction” to our  $M_{\text{crit}}$  for steady winds and momentum-conserving shells will be substantially *less* than a factor of  $\sim e^{7-8}$ .

Second, the time required for a shell to reach a radius at which it can accelerate to escape a galaxy will be *less* than any time we derive, whether for steady or time-dependent winds, if the shell transitions from momentum-conserving to energy-conserving at some radius (say,  $r_{\text{trans}}$ ), inside  $r_{\text{pk}}$ . This will happen if the cooling time of the shocked gas in the shell exceeds the dynamical time of the wind at  $r = r_{\text{trans}}$  (cf. King 2003; McLaughlin et al. 2006). The issue then becomes to find the CMO mass at the time when  $r = r_{\text{trans}}$ , rather than the mass when  $r = r_{\text{pk}}$ .

These considerations emphasize the need to include both cooling processes and time-dependent winds in future, more sophisticated analyses of CMO feedback-regulated

galaxy formation. Meanwhile, it is worth noting how tantalizingly close the  $M$ - $\sigma$  relations contained in our present work already are to the observed scalings.

### 3.5.3 Observational implications

Although subject to the indicated caveats about time-dependent winds and pure momentum-driving, our results directly predict a relation between SMBH (or NC) masses and the dark-matter haloes of their host galaxies, through the peak circular speed of the haloes (equations [3.67] and [3.68], for the large- $M_{\text{pk}}$  limit specifically). This provides a basis for understanding relations between SMBH mass and dark-matter halo mass or asymptotic circular speed, which have been claimed (e.g., Ferrarese 2002; Volonteri et al. 2011), though also contested (Ho 2007; Kormendy & Bender 2011), on empirical grounds. It is important to recognize the physical content of such a CMO–dark matter relation, in a feedback context. It does *not* suggest that dark matter in any way feeds the growth of either black holes or nuclear star clusters (cf. Kormendy, Bender & Cornell 2011). Rather, it reflects the fact that the gravity of a host galaxy, which is dominated by its dark matter halo, is what ultimately determines whether the feedback from a CMO can escape. The more familiar  $M$ - $\sigma$  relation has the same fundamental interpretation in this picture.

Making explicit the connection between a theoretical halo  $V_{\text{c, pk}}$  and an observed stellar  $\sigma$ , or even an asymptotic circular speed in real galaxies (which will include contributions from baryons as well as dark matter), is a non-trivial task and beyond the scope of our current discussion. We simply recall here that the observed relation between SMBH mass and the stellar velocity dispersion averaged over one effective radius in a sample of early-type galaxies and bulges analyzed by Gültekin et al. (2009) is

$$M_{\text{bh}} \simeq (1.32 \pm 0.24) \times 10^8 M_{\odot} \left( \frac{\sigma_{\text{eff}}}{200 \text{ km s}^{-1}} \right)^{4.24 \pm 0.41}; \quad (3.69)$$

while the relation inferred by Volonteri et al. (2011) between SMBH mass and the

*asymptotic* circular speed in a subset of the same systems is

$$M_{\text{bh}} \simeq (2.45 \pm 0.80) \times 10^7 M_{\odot} \left( \frac{V_{\text{c,a}}}{200 \text{ km s}^{-1}} \right)^{4.22 \pm 0.93}. \quad (3.70)$$

If we were to associate our  $V_{\text{c,pk}}$  and  $\sigma_0 \equiv V_{\text{c,pk}}/\sqrt{2}$  in non-isothermal haloes directly with observational estimates of  $V_{\text{c,a}}$  and  $\sigma_{\text{eff}}$ , then we might conclude that the normalizations of the predicted  $M_{\text{CMO}}-V_{\text{c,pk}}$  and  $M_{\text{CMO}}-\sigma$  relations exceed the observed normalizations by factors of  $\approx 3-4$ . This point has previously been made, from comparisons only with an isothermal-sphere analysis, by King (2010).

However, before too much is made of any normalization offset, or even the caveats associated with steady winds and pure momentum-driving, it is crucial that the correct relationships be worked out in detail (within specific dark-matter halo models, and accounting properly for the segregation of dark matter and stars) between  $V_{\text{c,pk}}$  and  $V_{\text{c,a}}$ , and between  $\sigma_0 \equiv V_{\text{c,pk}}/\sqrt{2}$  and the stellar  $\sigma_{\text{eff}}$ . It is probably also relevant that we (like other authors) have worked with the assumption that the gas in protogalaxies directly traces the dark matter. The consequences of relaxing this assumption remain unclear, although our general equation of motion for momentum-driven shells (eq. [3.6] or eq. [3.25]) offers a way to investigate the question.

Even with these issues, recognizing the non-isothermal structure of real galaxies and dark-matter haloes, and working in terms of an  $M_{\text{CMO}}-V_{\text{c,pk}}$  relation, could provide a way to extend and unify discussions and analyses to include correlations between CMO masses and host-galaxy properties in systems with significant rotational support as well as (or even instead of) pressure support. This could be of particular interest in connection with nuclear star clusters in intermediate-mass ellipticals and bulges, and even in very late-type Sc/Sd discs.

### 3.A The maximum critical CMO mass

Equation (3.35) in §3.4.1.3 is a general expression for the radius,  $x_{\text{c,max}}$ , marking the onset of acceleration of the momentum-driven shell that has the maximum critical

(necessary) CMO mass required to escape a non-isothermal dark-matter halo with a given mass profile  $m(x)$  and normalization  $\widetilde{M}_{\text{pk}}$ :

$$\left. \frac{d \ln m}{d \ln x} \right|_{x=x_{\text{c,max}}} = 1 + \frac{1}{2 \widetilde{M}_{\text{pk}}} \frac{1}{x_{\text{c,max}}} \left. \frac{dm}{dx} \right|_{x=x_{\text{c,max}}} . \quad (3.71)$$

Once this is solved for  $x_{\text{c,max}}$ , then equation (3.36) gives the value of the maximum critical CMO mass for the halo in question:

$$\widetilde{M}_{\text{crit}}^{\text{max}} = \frac{m^2(x_{\text{c,max}})}{x_{\text{c,max}}^2} \left[ 1 - \frac{1}{\widetilde{M}_{\text{pk}}} \frac{m(x_{\text{c,max}})}{x_{\text{c,max}}^2} \right]^{-1} . \quad (3.72)$$

In the limit that  $\widetilde{M}_{\text{pk}} \rightarrow \infty$ , the second term on the right-hand side of equation (3.71) tends to zero, so that

$$\left. \frac{d \ln m}{d \ln x} \right|_{x=x_{\text{c,max}}} \longrightarrow 1 \quad \text{as} \quad \widetilde{M}_{\text{pk}} \longrightarrow \infty . \quad (3.73)$$

But  $m(x)$  is defined such that (see equations [3.23] and [3.24])

$$m(1) = 1 \quad \text{and} \quad \left. \frac{d \ln m}{d \ln x} \right|_{x=1} = \frac{x}{m} \left. \frac{dm}{dx} \right|_{x=1} = 1 , \quad (3.74)$$

so we conclude that  $x_{\text{c,max}} \rightarrow 1$  (the peak of the circular speed curve) for large halo masses  $\widetilde{M}_{\text{pk}} \rightarrow \infty$ . We therefore look for the dependence of  $x_{\text{c,max}}$ , and then  $\widetilde{M}_{\text{crit}}^{\text{max}}$ , on  $\widetilde{M}_{\text{pk}}$  for large but finite  $\widetilde{M}_{\text{pk}}$  (which is the observationally relevant situation; see the discussion before Figure 3.3 in §3.4.2), which also means for values of  $x_{\text{c,max}}$  close to 1.

We define

$$m_1'' \equiv \left. \frac{d^2 m}{dx^2} \right|_{x=1} , \quad (3.75)$$

so expanding  $m(x)$  in a Taylor series about  $x = 1$  leads to

$$m(x) = x + \frac{1}{2} m_1'' (x-1)^2 + \mathcal{O}(x-1)^3 \quad (3.76)$$

$$\frac{dm}{dx} = 1 + m_1'' (x-1) + \mathcal{O}(x-1)^2 \quad (3.77)$$

$$\frac{d \ln m}{d \ln x} = 1 + m_1'' (x-1) + \mathcal{O}(x-1)^2 , \quad (3.78)$$

where we have again used the facts (in equation [3.74]) that  $m = 1$  and  $dm/dx = 1$  at  $x = 1$  always. Equation (3.71) in the limit  $|x_{c,\max} - 1| \ll 1$  is then

$$\begin{aligned} (x_{c,\max} - 1) \left[ m_1'' - \frac{1}{2\widetilde{M}_{\text{pk}}} (m_1'' - 1) \right] \\ = \frac{1}{2\widetilde{M}_{\text{pk}}} + \mathcal{O}(x_{c,\max} - 1)^2 \end{aligned} \quad (3.79)$$

Since the limit  $x_{c,\max} \rightarrow 1$  corresponds to  $\widetilde{M}_{\text{pk}} \rightarrow \infty$ , terms in  $(x_{c,\max} - 1)/\widetilde{M}_{\text{pk}}$  are of the same order as terms in  $(x_{c,\max} - 1)^2$  or terms in  $1/\widetilde{M}_{\text{pk}}^2$ . With this in mind, solving equation (3.79) for  $x_{c,\max}$  as a function of  $\widetilde{M}_{\text{pk}}$  gives

$$x_{c,\max} = 1 + \frac{1}{2m_1''} \frac{1}{\widetilde{M}_{\text{pk}}} + \mathcal{O}\left(\frac{1}{\widetilde{M}_{\text{pk}}^2}\right). \quad (\widetilde{M}_{\text{pk}} \gg 1) \quad (3.80)$$

Finally, putting this into equation (3.72) yields

$$\widetilde{M}_{\text{crit}}^{\max} = 1 + \frac{1}{\widetilde{M}_{\text{pk}}} + \mathcal{O}\left(\frac{1}{\widetilde{M}_{\text{pk}}^2}\right). \quad (\widetilde{M}_{\text{pk}} \gg 1) \quad (3.81)$$

As discussed further in §3.4, this is the CMO mass that is *sufficient* to ensure the escape of *any* momentum-driven shell in *any* non-isothermal halo that has a well-defined peak in its circular-speed curve. In general, it is larger than the CMO mass that is *necessary* for the escape of any particular shell.

## 3.B Sufficient condition for the escape of any shell II

As noted in §3.4.1.3, momentum-driven shells with different initial conditions (i.e., different values of  $C$ ) have different  $x_{\text{crit}}$  and  $\widetilde{M}_{\text{crit}}$ , given by equations (3.32) and (3.33). In §3.4.1.3 we compared these values between different shell solutions by differentiating equation (3.32) with respect to  $x_{\text{crit}}$  for a fixed dark matter mass  $\widetilde{M}_{\text{pk}}$ . We then showed that setting  $d\widetilde{M}_{\text{crit}}/dx_{\text{crit}} = 0$  identifies the momentum-driven shell that has the *largest* critical CMO mass required for escape.

Here, we will derive the same condition sufficient for the escape of any momentum-driven shell in an alternative way than was presented in McQuillin & McLaughlin (2012).

To compare the values of  $x_{\text{crit}}$  and  $\widetilde{M}_{\text{crit}}$  between different shell solutions we look at where the shells start to accelerate, or equivalently at the extrema of all the curves. The extrema of a set of  $\widetilde{v}^2(x)$  curves can be found from equation (3.25) for the motion of a shell by setting  $d\widetilde{v}^2/dx = 0$  at the radius  $x_{\text{ex}}$  at which the extremum occurs. With  $h(x) \equiv 1$  so that the gas traces the dark matter directly, this gives:

$$\widetilde{v}_{\text{ex}}^2 = \left[ \frac{d \ln m^2(x_{\text{ex}})}{d \ln x_{\text{ex}}} \right]^{-1} \left( 4\widetilde{M}_{\text{CMO}} \frac{x_{\text{ex}}}{m(x_{\text{ex}})} - 4 \frac{\widetilde{M}_{\text{CMO}}}{\widetilde{M}_{\text{pk}}} \frac{1}{x_{\text{ex}}} - 4 \frac{m(x_{\text{ex}})}{x_{\text{ex}}} \right). \quad (3.82)$$

where  $\widetilde{v}_{\text{ex}}^2 = \widetilde{v}^2(x_{\text{ex}})$ .

The curve  $\widetilde{v}_{\text{ex}}^2(x_{\text{ex}})$  passes through *all* the extrema of any family of solutions. For example, Figure 3.8 shows a set of  $\widetilde{v}^2(x)$  curves for fixed  $\widetilde{M}_{\text{CMO}}$  and  $\widetilde{M}_{\text{pk}}$  and a range of  $C$  values in a halo with a given  $m(x)$ . The dashed (blue) curve in the figure shows the corresponding  $\widetilde{v}_{\text{ex}}^2(x_{\text{ex}})$  curve.

By finding the minimum value of  $\widetilde{v}_{\text{ex}}^2$ , we know where the lowest extremum of the family of solutions occurs, or physically where the slowest moving shell starts to accelerate. If the minimum  $\widetilde{v}_{\text{ex}}^2 \geq 0$  then the slowest moving shell can accelerate and escape, and all other shells represented by that family of solutions will be able to escape. We identify the case where the minimum in  $\widetilde{v}_{\text{ex}}^2 = 0$  as the critical case and denote the CMO mass required for escape as  $\widetilde{M}_{\text{crit}}^{\text{max}}$  because escape is generally possible for particular solutions with smaller CMO masses, so  $\widetilde{M}_{\text{crit}}^{\text{max}}$  represents the *largest* critical CMO mass required for escape. We also denote the radius at which a shell driven by a CMO with this critical mass begins to accelerate as  $x_{\text{c,max}}$ .

To find the minimum of  $\widetilde{v}_{\text{ex}}^2$ , we differentiate equation (3.82) with respect to  $x_{\text{ex}}$

$$\begin{aligned} \frac{d\widetilde{v}_{\text{ex}}^2}{dx_{\text{ex}}} \frac{d \ln m^2}{d \ln x_{\text{ex}}} + \widetilde{v}_{\text{ex}}^2 \frac{d}{dx_{\text{ex}}} \left( \frac{d \ln m^2}{d \ln x_{\text{ex}}} \right) = \\ 4 \frac{\widetilde{M}_{\text{CMO}}}{m(x_{\text{ex}})} \left[ 1 - \frac{d \ln m}{d \ln x_{\text{ex}}} \right] + \frac{4}{x_{\text{ex}}^2} \frac{\widetilde{M}_{\text{CMO}}}{\widetilde{M}_{\text{pk}}} - 4 \frac{m(x_{\text{ex}})}{x_{\text{ex}}^2} \left[ \frac{d \ln m}{d \ln x_{\text{ex}}} - 1 \right]. \end{aligned} \quad (3.83)$$

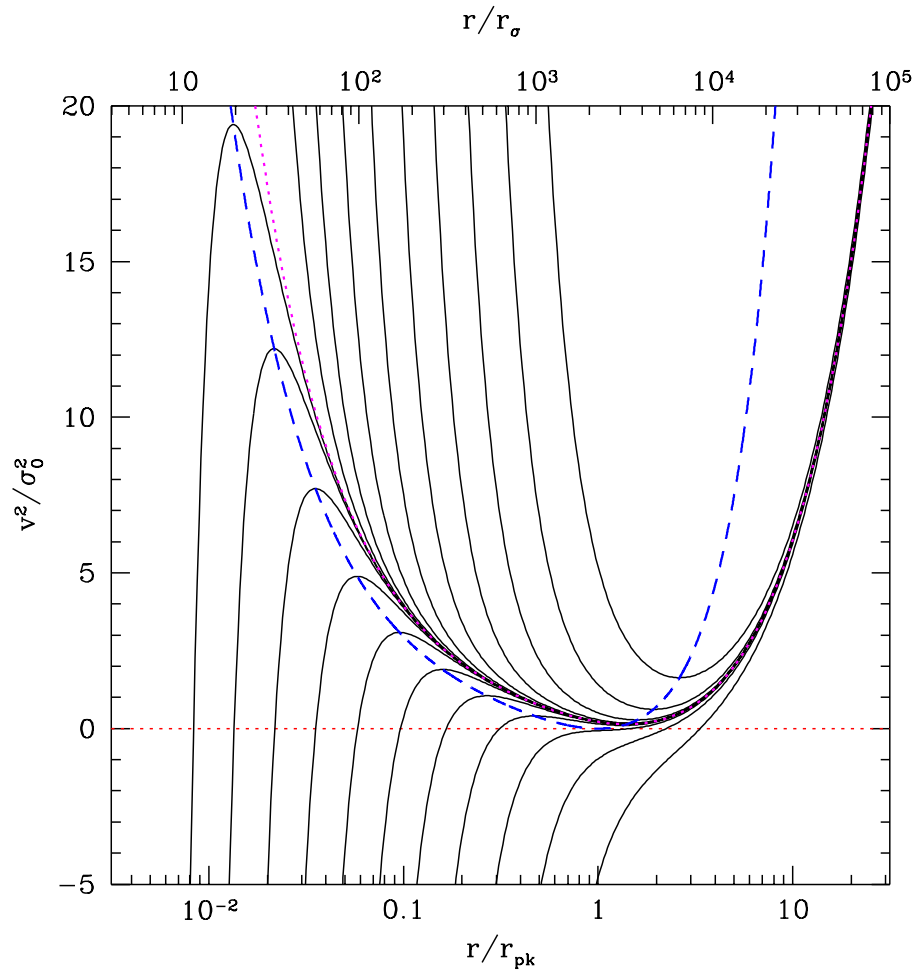


Figure 3.8: The solid lines show examples of  $\tilde{v}^2(x)$  in a non-isothermal halo (a Hernquist halo with  $\widetilde{M}_{\text{CMO}} = 1$  and  $\widetilde{M}_{\text{pk}} = 4000$  is used in this example). The dotted (magenta) curve shows the solutions with  $C = 0$ . The dashed (blue) line shows the curve  $\tilde{v}_{\text{ex}}^2(x_{\text{ex}})$  which passes through all the extrema.

The extremum in  $\tilde{v}_{\text{ex}}^2$  occurs when  $d\tilde{v}_{\text{ex}}^2/dx_{\text{ex}} = 0$ , and in the critical case we also require  $\tilde{v}_{\text{ex}}^2 = 0$ . From equation (3.82),  $\tilde{v}_{\text{ex}}^2 = 0$  gives

$$\widetilde{M}_{\text{crit}}^{\text{max}} = \frac{m^2(x_{\text{ex}})}{x_{\text{ex}}^2} \left[ 1 - \frac{1}{\widetilde{M}_{\text{pk}}} \frac{m(x_{\text{ex}})}{x_{\text{ex}}^2} \right]^{-1} \quad (3.84)$$

which combines with equation (3.83),  $d\tilde{v}_{\text{ex}}^2/dx = 0$  and  $\tilde{v}_{\text{ex}}^2 = 0$  to give

$$\tilde{M}_{\text{crit}}^{\text{max}} = \frac{m^2(x_{\text{ex}})}{x_{\text{ex}}^2} \frac{d \ln m(x_{\text{ex}})}{d \ln x_{\text{ex}}} \left[ 2 - \frac{d \ln m(x_{\text{ex}})}{d \ln x_{\text{ex}}} \right]^{-1} \quad (3.85)$$

We equate the right-hand sides of equations (3.84) and (3.85) to find that  $\tilde{v}_{\text{ex}}^2 = 0$  and  $d\tilde{v}_{\text{ex}}^2/dx = 0$  at  $x_{\text{c,max}}$  such that

$$\left. \frac{d \ln m(x_{\text{ex}})}{d \ln x_{\text{ex}}} \right|_{x_{\text{ex}}=x_{\text{c,max}}} = 1 + \frac{1}{2\tilde{M}_{\text{pk}}} \frac{1}{x_{\text{c,max}}} \left. \frac{dm(x_{\text{ex}})}{dx_{\text{ex}}} \right|_{x_{\text{ex}}=x_{\text{c,max}}}. \quad (3.86)$$

This is the same expression that is given for  $x_{\text{c,max}}$  in equation (3.35), and the same analysis following equation (3.35) can be applied to find  $\tilde{M}_{\text{crit}}^{\text{max}}$ .

## 4 Energy-driven outflows: black hole wind speeds and the $M-\sigma$ relation

We have looked at purely momentum-driven outflows in galaxies modelled as singular isothermal spheres and in non-isothermal haloes. As discussed in Chapter 2, outflows driven by black holes are initially momentum-driven, but it may be that these outflows become energy-driven within the sphere of influence of the black hole, meaning that the energy-driven regime dominates the evolution of the outflow.

Presented in this chapter is the paper ‘Black hole wind speeds and the  $M-\sigma$  relation’ (McQuillin & McLaughlin 2013), where we look at purely energy-driven outflows driven by black hole winds into galaxies modelled as isothermal spheres.

We derive an  $M_{\text{BH}}-\sigma$  relation between supermassive black hole mass and stellar velocity dispersion in galaxy bulges, that results from self-regulated, energy-conserving feedback. The relation is of the form  $M_{\text{BH}}v_w \propto \sigma^5$ , where  $v_w$  is the velocity of the wind driven by the black hole. We take a sample of quiescent early-type galaxies and bulges with measured black hole masses and velocity dispersions and use our model to infer the wind speeds they would have had during an active phase. This approach, in effect, translates the scatter in the observed  $M_{\text{BH}}-\sigma$  relation into a distribution of  $v_w$ . There are some remarkable similarities between the distribution of black hole wind speeds that we obtain and the distributions of outflow speeds observed in local AGN, including a comparable median of  $v_w = 0.035c$ .

In Appendix 4.A, which is not included in McQuillin & McLaughlin (2013), we discuss how our result for the terminal coasting speed of an energy-driven shell compares with other analyses (Silk & Rees 1998; King 2005; King et al. 2011; Faucher-Giguère & Quataert 2012).

## 4.1 Introduction

Self-regulated feedback from accreting supermassive black holes (SMBHs) in gaseous protogalaxies is thought to play a key role in establishing the  $M_{\text{BH}}-\sigma$  relation observed in local quiescent galaxies, between SMBH mass and bulge-star velocity dispersion:  $M_{\text{BH}} \propto \sigma^x$  with  $x = 4-5$  (Ferrarese & Merritt 2000; Gebhardt et al. 2000; Ferrarese & Ford 2005; Gültekin et al. 2009; McConnell & Ma 2013). The accreting SMBH drives a wind, which sweeps the surrounding ambient medium into a shell. There is then a critical SMBH mass above which the wind thrust pushing the shell outwards (proportional to  $M_{\text{BH}}$ ) can overcome the inward gravitational pull of the dark matter (related to  $\sigma$ ) and the SMBH itself. At this critical mass, the shell may be blown out of the galaxy, cutting off fuel to the SMBH and locking in an  $M_{\text{BH}}-\sigma$  relation (Silk & Rees 1998; Fabian 1999; King 2003, 2005; Murray, Quataert & Thompson 2005). Supporting this scenario are observations of strong outflows in local active galactic nuclei (AGN), both on large scales (e.g., Sturm et al. 2011) and closer to the SMBHs (e.g., Pounds et al. 2003; Tombesi et al. 2011; Gofford et al. 2013). The latter in particular have speeds and mechanical luminosities similar to those needed for SMBH winds to have cleared the gas from now-normal spheroids at high redshift, when the systems were active.

The dynamics of a swept-up shell of gas depend on whether or not the region of shocked wind material immediately behind the shell is able to cool. If the shocked gas cools efficiently then the region is geometrically thin and the swept-up shell is pushed outwards by the ram pressure of the wind. This momentum-driven regime is expected to be the case initially in the case of SMBH feedback (King 2003), and thus many authors have considered the  $M_{\text{BH}}-\sigma$  relation that results if the feedback is entirely momentum-driven (e.g., Fabian 1999; King 2003, 2005; McQuillin & McLaughlin 2012). In McQuillin & McLaughlin (2012) we considered shells moving outwards in non-isothermal, spherical dark matter haloes that have peaked circular speed curves. We showed that the critical SMBH mass above which any shell can escape tends to the limiting value (for haloes much more massive than the SMBH, independent of any

further details of the dark matter density profile)

$$M_{\text{crit}} = \frac{f_0 \kappa}{\pi G^2} \frac{V_{\text{c,pk}}^4}{4} \simeq 1.14 \times 10^8 M_{\odot} \left( \frac{f_0}{0.2} \right) \left( \frac{V_{\text{c,pk}}}{200 \text{ km s}^{-1}} \right)^4. \quad (4.1)$$

Here,  $V_{\text{c,pk}}$  is the peak value of the circular speed in the dark matter halo;  $\kappa$  is the electron scattering opacity; and  $f_0$  is a spatially constant gas-to-dark matter mass fraction. The peak circular speed defines a natural ‘‘characteristic’’ velocity dispersion for a non-isothermal galaxy:  $\sigma_0 \equiv V_{\text{c,pk}}/\sqrt{2}$ . Equation (4.1) then implies an  $M_{\text{BH}}-\sigma$  relation, which has a slope and an intercept that are near the observed values (see Figure 4.2 below).

If the shocked gas cannot cool then the region behind the shell is geometrically thick and hot. The outflow is energy-driven and the shell is pushed outwards by the thermal pressure of the shocked material. In the context of SMBH feedback, an initially momentum-driven shell is expected to transition to energy-driven, probably quite early on when the shell is still at relatively small galactocentric radius (§4.2 below; cf. King 2003, Zubovas & King 2012). Thus, in this chapter we investigate the implications of *purely* energy-driven feedback for the  $M_{\text{BH}}-\sigma$  relation.

In §4.2 we derive the large-radius coasting speed,  $v_{\infty}$ , of an energy-conserving shell in a dark-matter halo modelled as a singular isothermal sphere with velocity dispersion  $\sigma_0$ . We find that for the shell to coast at the escape speed of a truncated isothermal halo (i.e.,  $v_{\infty} = 2\sigma_0$ ) requires

$$\left( \frac{M_{\text{BH}}}{10^8 M_{\odot}} \right) \left( \frac{v_{\text{w}}}{c} \right) \simeq 6.68 \times 10^{-2} \left( \frac{f_0}{0.2} \right) \left( \frac{\sigma_0}{200 \text{ km s}^{-1}} \right)^5, \quad (4.2)$$

where  $M_{\text{BH}}$  is the (fixed) SMBH mass driving a wind of speed  $v_{\text{w}}$ . This  $M_{\text{BH}}-\sigma$  relation differs from that resulting from momentum-driven outflows (equation [4.1]), both in the power on  $\sigma_0$  and in the explicit dependence on  $v_{\text{w}}$ .

In §4.3 we apply our escape condition for energy-conserving feedback to the  $M_{\text{BH}}-\sigma$  relation defined observationally by a standard sample of low-redshift, quiescent early-type galaxies and bulges (Gültekin et al. 2009). We use equation (4.2) to infer the black hole wind speeds that would have had to occur during the main epoch of galaxy and

SMBH formation, if this simple model is to account for the individual  $M_{\text{BH}}$  and  $\sigma$  values for each galaxy or bulge in the Gültekin et al. sample. This gives a distribution of  $v_w/c$  for these galaxies in the past. In §4.4 we compare this distribution directly to the distributions of  $v_w/c$  observed for fast outflows in different samples of local AGN (Tombesi et al. 2011; Gofford et al. 2013). Our main result is a remarkable similarity between these distributions. In particular, the median SMBH wind speed we infer for the normal galaxies of Gültekin et al. is  $v_w = 0.035c$ , while the median of the outflow speeds in low-redshift AGN is  $v_w = 0.1c$  according to Tombesi et al. or  $v_w = 0.056c$  according to Gofford et al.

## 4.2 Energy-driven outflows

In the self-regulated feedback scenario the black hole wind sweeps up a shell of ambient gas as it moves outwards. This gives rise to two shock fronts, one propagating forwards into the ambient medium and one propagating back into the wind material. The resulting shock pattern has a four-zone structure: 1) the freely flowing wind; 2) the shocked wind region lying between the wind shock and the contact surface that separates material originally in the wind from material originating in the ambient medium; 3) the shocked ambient medium, lying between the contact surface and the ambient shock, also containing the original swept-up shell that gave rise to the shock fronts; and 4) the undisturbed ambient medium.

In detail, the dynamics of the swept-up shell depend on three timescales: the flow time of the shell,  $t_{\text{flow}} = r_s/v_s$ , where  $r_s$  is the radius of the shell and  $v_s$  is the shell velocity; the dynamical time of the wind,  $t_{\text{dyn}} = r_{\text{sw}}/v_w$ , where  $r_{\text{sw}}$  is the radius of the wind shock and  $v_w$  is the wind velocity; and the cooling time of the shocked wind,  $t_{\text{cool}}$  (Koo & McKee 1992; Faucher-Giguère & Quataert 2012).

If  $t_{\text{cool}} \ll t_{\text{dyn}}$ , then the shocked wind region cools before more energy is injected into the region from the freely flowing wind. The material in the region is then confined to a thin shell (so  $r_{\text{sw}} \sim r_s$ ) and the shell is effectively driven outwards by a transfer of

momentum from the wind impacting on its inner side, corresponding to a momentum-driven outflow.

If, instead,  $t_{\text{cool}} \gg t_{\text{flow}}$ , then the most recently shocked material cannot cool in the time it takes to travel across the shocked wind region. The region is thick and hot and drives the shell outwards with its thermal pressure, corresponding to an energy-driven outflow.

In the intermediate case,  $t_{\text{dyn}} \lesssim t_{\text{cool}} \lesssim t_{\text{flow}}$ , the shell is in a partially radiative phase where most of the material cools and condenses into a thin shell but the most recently shocked material has not cooled and occupies most of the volume of the region. In this regime the outflow conserves neither energy nor momentum.

For a wind from an SMBH, with cooling primarily by inverse Compton scattering (King 2003), the cooling rate is (e.g., Longair 2011)

$$\frac{dE}{dt} = \frac{4}{3} \kappa m_{\text{p}} c u_{\text{rad}} \left(\frac{v_{\text{e}}}{c}\right)^2 \left(\frac{E}{m_{\text{e}} c^2}\right)^2, \quad (4.3)$$

where  $v_{\text{e}}$  is the velocity of a post-shock electron;  $E$  is the post-shock electron energy;  $u_{\text{rad}}$  is the radiation energy density; and  $\kappa$  is the electron-scattering opacity. We take  $u_{\text{rad}} = L_{\text{Edd}}/(4\pi r^2 c)$ , where  $L_{\text{Edd}} = 4\pi G M_{\text{BH}} c/\kappa$  is the Eddington luminosity of a black hole of mass  $M_{\text{BH}}$ , and  $E \simeq (9/16)m_{\text{p}} v_{\text{w}}^2$  for the electron energy. Then, the cooling time,  $t_{\text{cool}} \equiv E/(dE/dt)$ , is less than the dynamical time of the wind,  $t_{\text{dyn}} \equiv r_{\text{sw}}/v_{\text{w}}$ , at radii

$$\begin{aligned} r_{\text{sw}} &\lesssim \frac{3}{4} \frac{G M_{\text{BH}}}{c^2} \left(\frac{m_{\text{p}}}{m_{\text{e}}}\right)^2 \left(\frac{v_{\text{w}}}{c}\right) \left(\frac{v_{\text{e}}}{c}\right)^2 \\ &\simeq 0.26 \text{ pc} \left(\frac{M_{\text{BH}}}{10^8 M_{\odot}}\right) \left(\frac{v_{\text{w}}}{0.03c}\right) \left(\frac{v_{\text{e}}}{0.85c}\right)^2. \end{aligned} \quad (4.4)$$

When the wind shock is inside this radius, the shocked wind region is thin, so  $r_{\text{sw}} \sim r_{\text{s}}$  and the shell is momentum-driven.

The cooling time exceeds the flow time of the shell,  $t_{\text{flow}} \equiv r_{\text{s}}/v_{\text{s}}$ , at radii

$$\begin{aligned} r_{\text{s}} &\gtrsim \frac{3}{4} \frac{G M_{\text{BH}}}{c v_{\text{s}}} \left(\frac{m_{\text{p}}}{m_{\text{e}}}\right)^2 \left(\frac{v_{\text{w}}}{c}\right)^2 \left(\frac{v_{\text{e}}}{c}\right)^2 \\ &\simeq 11 \text{ pc} \left(\frac{v_{\text{s}}}{200 \text{ km s}^{-1}}\right)^{-1} \left(\frac{M_{\text{BH}}}{10^8 M_{\odot}}\right) \left(\frac{v_{\text{w}}}{0.03c}\right)^2 \left(\frac{v_{\text{e}}}{0.85c}\right)^2, \end{aligned} \quad (4.5)$$

for typical shell velocities  $v_s \sim \sigma_0 \sim 200 \text{ km s}^{-1}$ . This is in rough agreement with Zubovas & King (2012; see their equation [6]), although they replace  $v_s$  with an estimate for the terminal velocity of a momentum-driven shell and normalize to a higher fiducial  $v_w$  than we do (see Sections 4.3 and 4.4 below for more about typical wind speeds). In any case, the radius in equation (4.5) is comparable to the sphere of influence of a  $10^8 M_\odot$  black hole in a stellar distribution with velocity dispersion  $200 \text{ km s}^{-1}$ . As such, SMBH outflows can be energy-conserving over much of their evolution, and accordingly we focus on *purely* energy-driven feedback in what follows.

McLaughlin, King & Nayakshin (2006) noted that a self-regulated feedback scenario can also be applied to nuclear star clusters in galaxy centres to explain the  $M_{\text{NC}}-\sigma$  relation observed by Ferrarese et al. (2006). In that case, cooling by atomic processes gives a shorter cooling timescale with a strong dependence on the wind speed (equation [9] of McLaughlin et al. ), and a slower wind speed results in a longer dynamical time. Thus, outflows from nuclear clusters can cool efficiently and be momentum-driven to much larger radii than in the black hole case.

Whether momentum- or energy-driven, the equation of motion for a shell of swept-up gas moving out into the dark-matter halo of a protogalaxy against the inwards gravitational pull of both the SMBH and the dark matter behind the shell can be written as (see also King 2005)

$$\frac{d}{dt} [M_g(r)v(r)] + \frac{G M_g(r)}{r^2} [M_{\text{BH}} + M_{\text{DM}}(r)] = 4\pi r^2 P \quad . \quad (4.6)$$

Here  $r$  is the instantaneous radius of the shell;  $M_{\text{DM}}(r)$  is the dark matter mass inside radius  $r$ ;  $M_g(r)$  is the mass of ambient gas initially inside radius  $r$  (i.e., the mass that has been swept up into the shell when it has radius  $r$ );  $v(r) = dr/dt$  is the velocity of the shell; and  $P$  is the outwards pressure on the shell.

We adopt the simple description by King & Pounds (2003) of a wind driven by radiation (continuum scattering) from an accreting SMBH, such that the wind thrust is

$$\dot{M}_{\text{out}} v_w = \tau \frac{L_{\text{Edd}}}{c} \quad . \quad (4.7)$$

Here  $\dot{M}_{\text{out}}$  is the mass outflow rate in the wind and  $v_w$  is the wind velocity when it

escapes the black hole; these are distinct from the mass growth rate  $dM_g/dt$  and the expansion speed  $v$  of the shell of swept-up ambient gas that the wind drives. The parameter  $\tau$  is the electron-scattering optical depth in the wind, measured down to its escape radius from the black hole (thus,  $\tau \sim 1$  in the single-scattering limit), multiplied by a geometrical factor (which is also  $\sim 1$ ) allowing for some non-sphericity in the wind; as discussed in Chapter 1, see §1.2.1.3 for more detail. In what follows, we retain  $\tau$  in our calculations, although ultimately we assume that  $\tau \approx 1$ .

The pressure on the right-hand side of equation (4.6) is just the wind ram pressure,  $4\pi r^2 P = \dot{M}_{\text{out}} v_w \approx L_{\text{Edd}}/c$ , for a momentum-driven shell. This is the case we solved in McQuillin & McLaughlin (2012) for isothermal and non-isothermal dark-matter halo models. For an energy-conserving shell, the driving pressure is instead the thermal pressure of the shocked-wind region behind the shell. In this case,  $P$  in equation (4.6) satisfies the energy equation,

$$\frac{d}{dt} \left[ \frac{4}{3} \pi r^3 \frac{P}{\gamma - 1} \right] = \dot{E} - P \frac{d}{dt} \left[ \frac{4}{3} \pi r^3 \right] - \frac{G M_g(r) v(r)}{r^2} [M_{\text{BH}} + M_{\text{DM}}(r)] . \quad (4.8)$$

In this equation,  $\gamma$  on the left-hand side is the ratio of specific heats. The last three terms on the right-hand side give the rates of work done by the expanding shell (both  $PdV$  work and the work against the gravity of the SMBH and the dark matter behind the shell; cf. King 2005). The first term on the right-hand side is the rate of energy input to the shocked wind region, which is given by the kinetic energy flux of the wind:

$$\dot{E} = \frac{1}{2} \dot{M}_{\text{out}} v_w^2 = \tau \frac{v_w}{c} \frac{L_{\text{Edd}}}{2} . \quad (4.9)$$

Note that this differs slightly from, e.g., King (2005, 2010) and King, Zubovas & Power (2011), where it is either stated or implied that  $\dot{E} = \eta L_{\text{Edd}}/2$  with  $\eta$  the radiative efficiency of accretion onto the black hole. These other papers make the *additional* assumption that  $\dot{M}_{\text{out}} = \dot{M}_{\text{Edd}} = L_{\text{Edd}}/(\eta c^2)$ . In combination with equation (4.7) above, this requires  $v_w/c = \eta\tau$ ; and putting this plus  $\tau \equiv 1$  into equation (4.9) is what gives  $\dot{E} = \eta L_{\text{Edd}}/2$ . However, in this work we do *not* assume that  $\dot{M}_{\text{out}} = \dot{M}_{\text{Edd}}$ , nor that  $v_w/c = \eta\tau$  necessarily; thus,  $v_w/c$  remains as an explicit parameter in our analysis.

Now we specialise to the case of a shell expanding into a dark-matter halo modelled as a singular isothermal sphere (SIS), with the ambient protogalactic gas tracing the dark matter exactly. The density of an SIS is given by  $\rho_{\text{DM}}(r) = \sigma_0^2/(2\pi Gr^2)$ , so that the mass inside radius  $r$  is

$$M_{\text{DM}}(r) = \frac{2\sigma_0^2 r}{G}, \quad (4.10)$$

and  $M_{\text{g}}(r) = f_0 M_{\text{DM}}(r)$  with a fiducial (cosmic)  $f_0 \approx 0.2$ . As in McQuillin & McLaughlin (2012), we then define characteristic mass and radius units in terms of the characteristic velocity dispersion of the halo,  $\sigma_0$ :

$$M_\sigma \equiv \frac{f_0 \kappa \sigma_0^4}{\pi G^2} \simeq 4.56 \times 10^8 M_\odot \left( \frac{f_0}{0.2} \right) \left( \frac{\sigma_0}{200 \text{ km s}^{-1}} \right)^4$$

and

$$r_\sigma \equiv \frac{GM_\sigma}{\sigma_0^2} \simeq 49.25 \text{ pc} \left( \frac{f_0}{0.2} \right) \left( \frac{\sigma_0}{200 \text{ km s}^{-1}} \right)^2.$$

With the identification  $\sigma_0 \equiv V_{\text{c,pk}}/\sqrt{2}$ , the mass unit  $M_\sigma$  is just the critical SMBH mass from equation (4.1) for the breakout of momentum-driven shells from non-isothermal dark matter haloes with peaked circular speed curves. In singular isothermal spheres, the critical mass required for momentum-driven shells to coast at large radii with the escape speed  $2\sigma_0$  is  $3M_\sigma$  (McQuillin & McLaughlin 2012; see also Silk & Nusser 2010).

We eliminate  $P$  from equation (4.8) using equation (4.6), then combine with the dark-matter and gas mass profiles of an SIS from equation (4.10) and the energy input from equation (4.9), together with  $L_{\text{Edd}} = 4\pi GM_{\text{BH}} c/\kappa$ . Also, we write  $d/dt = v d/dr$  in order to solve for the velocity fields of shells,  $v(r)$ , rather than for  $r(t)$  explicitly. Then, defining dimensionless variables

$$\widetilde{M} \equiv M/M_\sigma, \quad \widetilde{r} \equiv r/r_\sigma \quad \text{and} \quad \widetilde{v} \equiv v/\sigma_0,$$

the equation of motion for energy-driven shells in an SIS is

$$\begin{aligned} \frac{d^2}{d\widetilde{r}^2} [\widetilde{r}^2 \widetilde{v}^2(\widetilde{r})] + \frac{3(\gamma-1)}{\widetilde{r}} \frac{d}{d\widetilde{r}} [\widetilde{r}^2 \widetilde{v}^2(\widetilde{r})] \\ + 12(\gamma-1) \frac{\widetilde{M}_{\text{BH}}}{\widetilde{r}} - 6(\gamma-1) \frac{\tau \widetilde{M}_{\text{BH}} \widetilde{v}_{\text{w}}}{\widetilde{v}(\widetilde{r})} = -4(6\gamma-5). \end{aligned} \quad (4.11)$$

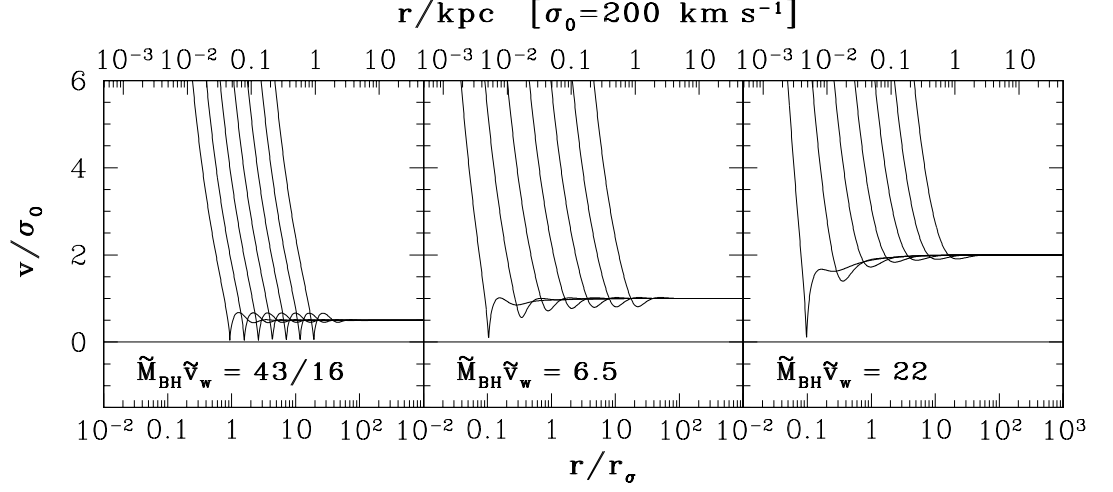


Figure 4.1: Velocity fields  $\tilde{v}$  versus  $\tilde{r}$  that solve equation (4.11) for energy-driven shells in an SIS with spatially constant gas fraction and  $\tilde{M}_{\text{BH}}\tilde{v}_w = 43/16$  ( $\simeq 2.7$ ), 6.5 and 22, leading to large-radius coasting speeds of  $v_\infty/\sigma_0 = 0.5$ , 1 and 2 for the shells (equation [4.13], with  $\gamma = 5/3$  and  $\tau = 1$ ). Solutions with a range of initial conditions are shown in each case. The radius unit  $r_\sigma = 49.25$  pc for a gas mass fraction  $f_0 = 0.2$  and  $\sigma_0 = 200 \text{ km s}^{-1}$ .

In the limit of large radius, the term  $\tilde{M}_{\text{BH}}/\tilde{r} \rightarrow 0$  in equation (4.11), and the remaining terms imply that the velocity of the shell tends to a constant:

$$\tilde{v} \longrightarrow \tilde{v}_\infty, (\tilde{r} \gg 1) \quad (4.12)$$

where  $\tilde{v}_\infty$  satisfies

$$(3\gamma - 2)\tilde{v}_\infty^3 + 2(6\gamma - 5)\tilde{v}_\infty = 3(\gamma - 1)\tau\tilde{M}_{\text{BH}}\tilde{v}_w. \quad (4.13)$$

Thus, any energy-conserving shell at sufficiently large radius tends to a coasting speed that depends on the black hole mass, the velocity dispersion of the halo *and* the velocity of the black hole wind.

If the values of  $\tilde{M}_{\text{BH}}$  and  $\tilde{v}_w$  are such that  $\tilde{v}_\infty$  from equation (4.13) is very small, then the feedback may not be able to escape on a timescale that allows that observed

$M$ - $\sigma$  relation to be locked in. A natural criterion for the escape of the feedback is that it reach a coasting speed equal to the escape speed from a truncated isothermal sphere,  $v_{\text{esc}} = 2\sigma_0$ . Thus, we set  $\tilde{v}_\infty = 2$  in equation (4.13) and obtain a critical value for the product of black hole mass and wind speed:

$$\left[ \tilde{M}_{\text{BH}} \tilde{v}_w \right]_{\text{crit}} = \frac{1}{\tau} \frac{4(4\gamma - 3)}{(\gamma - 1)} \quad (4.14)$$

or, with all units restored,

$$\left[ M_{\text{BH}} v_w \right]_{\text{crit}} = \frac{1}{\tau} \frac{4(4\gamma - 3)}{(\gamma - 1)} \frac{\kappa f_0}{\pi G^2} \sigma_0^5. \quad (4.15)$$

Setting  $\gamma = 5/3$  then gives

$$\left( \frac{M_{\text{BH}}}{10^8 M_\odot} \right) \left( \frac{v_w}{c} \right) = 6.68 \times 10^{-2} \frac{1}{\tau} \left( \frac{f_0}{0.2} \right) \left( \frac{\sigma_0}{200 \text{ km s}^{-1}} \right)^5. \quad (4.16)$$

This is what we will compare to the observed  $M_{\text{BH}}$ - $\sigma$  relation in §4.3 below.

Equation (4.16) shows explicitly how the escape of energy-conserving shells from an isothermal galaxy requires  $M_{\text{BH}} v_w \propto \sigma_0^5$  in general. If  $v_w$  were effectively the same in all galaxies (or at least uncorrelated with SMBH mass or halo velocity dispersion), then the implication is an observable relation  $M_{\text{BH}} \propto \sigma^5$ , as has been argued many times (e.g., Silk & Rees 1998; King 2005). In more detail, however, if  $v_w$  *did* in fact depend on black hole mass as, say,  $v_w \propto M_{\text{BH}}^y$ , then equation (4.16) would actually imply

$$M_{\text{BH}} \propto \sigma_0^{5/(1+y)}. \quad (4.17)$$

That is, if  $v_w$  and  $M_{\text{BH}}$  were correlated by even a weak power, the logarithmic slope of the  $M_{\text{BH}}$ - $\sigma$  relation from energy-driven outflows could differ measurably from 5.

In the limit of small radius, equation (4.11) admits solutions of the form

$$\tilde{v}^2 \tilde{r}^2 \longrightarrow C - 4\tilde{M}_{\text{BH}} \tilde{r} - \frac{2(6\gamma - 5)}{(3\gamma - 2)} \tilde{r}^2 + \mathcal{O}(\tilde{r}^3), \quad (\tilde{r} \ll 1) \quad (4.18)$$

where the constant  $C$  represents the square of the shell momentum,  $[M_g(r) v(r)]^2 \propto \tilde{v}^2 \tilde{r}^2$ , at  $\tilde{r} = 0$ . In order for equation (4.16) to apply, a shell moving out from  $\tilde{r} = 0$

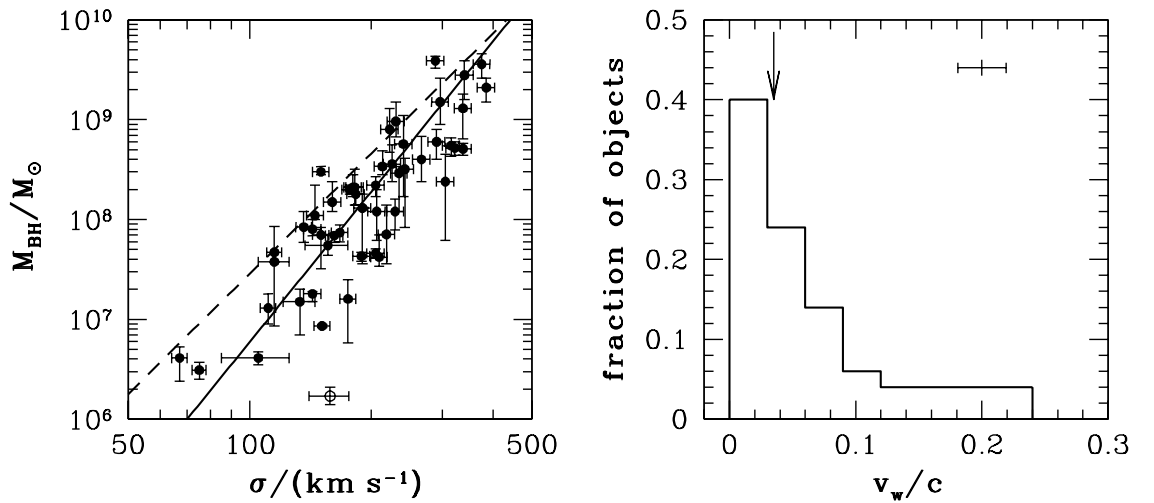


Figure 4.2: *Left-hand panel:* The  $M_{\text{BH}}-\sigma$  relation from the compilation of Gültekin et al. (2009). The dashed line shows  $M_{\text{BH}} = M_{\text{crit}}$  from equation (4.1), the sufficient condition for the escape of purely momentum-driven shells from non-isothermal haloes McQuillin & McLaughlin (2012). The solid line shows the condition for the escape of an energy-driven shell from an SIS from equation (4.16), with  $f_0 = 0.2$ ,  $\tau = 1$  and a typical SMBH wind speed of  $v_w = 0.035c$ . *Right-hand panel:* The distribution of  $v_w/c$  obtained from applying equation (4.16) to the measured  $M_{\text{BH}}$  and  $\sigma$  of the Gültekin et al. galaxies (excluding Circinus; see text). The median of the distribution,  $v_w = 0.035c$ , is indicated by the arrow. The errorbar represents the median uncertainty,  $\Delta(v_w/c) \simeq \pm 0.02$ .

must have an initial momentum large enough to keep  $\tilde{v}^2 \tilde{r}^2 > 0$  and avoid stalling before it reaches the large radii where the coasting speed in equation (4.13) applies.

Figure 4.1 shows the velocity fields,  $\tilde{v}(\tilde{r})$ , that solve equation (4.11) with  $\gamma = 5/3$ ,  $\tau = 1$  and dimensionless  $\tilde{M}_{\text{BH}} \tilde{v}_w = 43/16 (\simeq 2.7)$ , 6.5 and 22. The different curves in each panel represent different initial shell momenta, i.e., different values of  $C$  in equation (4.18). We have specified a fixed wind speed in all cases:  $\tilde{v}_w = 45$ , which corresponds to  $v_w = 0.03c$  for  $\sigma_0 = 200 \text{ km s}^{-1}$ . The dimensionless black hole masses are then (again, assuming  $\tau = 1$ )  $\tilde{M}_{\text{BH}} \simeq 0.06$ , 0.14 and 0.49. These are all below the critical SMBH masses for the escape of momentum-conserving shells from either non-

isothermal haloes ( $\widetilde{M}_{\text{crit}} = 1$ ) or an SIS ( $\widetilde{M}_{\text{crit}} = 3$ ). Given any of the black hole masses represented in Figure 4.1, all purely momentum-driven shells would stall at relatively small radii and go into collapse until the SMBH grew substantially (see Figure 1 of McQuillin & McLaughlin 2012).

With  $\gamma = 5/3$  and  $\tau = 1$ , equation (4.13) gives the final coasting speeds of the energy-driven shells illustrated in Figure 4.1 as  $v_\infty/\sigma_0 = 0.5, 1$  and  $2$  (independent of initial conditions) in the three panels from left to right. These are confirmed by our numerical solutions for the full  $\widetilde{v}(\widetilde{r})$ . In particular, all of the energy-driven solutions in the case  $\widetilde{M}_{\text{BH}}\widetilde{v}_w = 22$  eventually attain the speed for escape from a truncated SIS,  $v_\infty = 2\sigma_0 = v_{\text{esc}}$ . Energy-conserving feedback can blow out of an isothermal halo if driven by a wind at speed  $v_w \sim 0.03c$  (of the order of the nuclear outflows observed in local AGN; see below) from an SMBH significantly less massive than that required to expel momentum-conserving shells from isothermal or non-isothermal haloes.

### 4.3 The Observed $M_{\text{BH}}-\sigma$ relation

The left-hand panel of Figure 4.2 shows  $M_{\text{BH}}$  versus bulge-star velocity dispersion  $\sigma$  for 51 normal (quiescent) early-type galaxies and bulges in Table 1 of Gültekin et al. (2009).<sup>1</sup> The dashed line on the plot traces the relation

$$\left(\frac{M_{\text{BH}}}{10^8 M_\odot}\right) = 4.56 \left(\frac{f_0}{0.2}\right) \left(\frac{\sigma}{200 \text{ km s}^{-1}}\right)^4. \quad (4.19)$$

This represents the SMBH mass  $M_{\text{crit}}$  of equation (4.1) above, which is sufficient for the escape of any purely momentum-driven shell from any non-isothermal dark-matter halo, *if* the peak circular speed in the halo of an observed galaxy can be estimated as  $V_{\text{c,pk}} = \sqrt{2}\sigma$  (McQuillin & McLaughlin 2012). In a singular isothermal sphere,

---

<sup>1</sup>The main outlier in Figure 4.2, marked by an open circle, is Circinus, which is in the plane of the Milky Way. Ferrarese & Ford (2005) note that  $M_{\text{BH}}$  in this case may be in error, possibly because the inclination of the maser disc used to find  $M_{\text{BH}}$  is unconstrained. Gültekin et al. (2009) discuss this further.

for a momentum-driven shell to reach the escape speed of  $2\sigma$  at large radii requires  $M_{\text{BH}} \geq 3 M_{\text{crit}}$ —that is, SMBH masses a further 0.5 dex above the dashed line in Figure 4.2, which already represents an upper limit to the data. Relaxing the isothermal assumption alleviates some of this difficulty, and additional momentum input from bulge-star formation triggered by the outflow could further reduce the requirement on  $M_{\text{BH}}$  from that in equation (4.19) (see, e.g., Silk & Nusser 2010; and further discussion in McQuillin & McLaughlin 2012).

By contrast, the solid line running through the data in Figure 4.2 is the SMBH mass required for energy-driven shells to escape singular isothermal spheres, from equation (4.16) with a fixed SMBH wind speed of  $v_w/c = 0.035$  (and assuming a wind optical depth  $\tau = 1$  and a gas-to-dark matter mass fraction  $f_0 = 0.2$ ). With  $v_w/c$  set to a constant to draw this line, it has a slope  $M_{\text{BH}} \propto \sigma^5$ , the usual expectation for energy-conserving feedback. The numerical value of  $v_w/c$  then sets the intercept, and the value that we have applied is in fact the median of a *distribution* of wind speeds that we have estimated individually for every galaxy in Gültekin et al. (2009).

These are all quiet, non-active galaxies and bulges. But if their black hole masses were frozen in as part of the feedback process clearing ambient gas from the protospheroids, and if this feedback was energy-driven, then equation (4.16) can be used to infer the SMBH wind speeds in the past, when the galaxies were young and active. For each point in the left-hand panel of Figure 4.2, we have taken the measured values of  $M_{\text{BH}}$  and  $\sigma$  (and set  $\tau = 1$ ,  $f_0 = 0.2$ ) to solve equation (4.16) for  $v_w/c$ . The results are shown as the normalised histogram in the right-hand panel of Figure 4.2. The arrow there points to the median speed,  $v_w/c = 0.035$ . The minimum is  $v_w/c = 0.005$ , and the maximum (with Circinus excluded) is  $v_w/c = 0.23$ .<sup>2</sup> Uncertainties in the  $v_w/c$  values follow from the uncertainties in  $M_{\text{BH}}$  and  $\sigma$  tabulated by Gültekin et al. , and the median errorbar,  $\Delta(v_w/c) \simeq \pm 0.02$ , is also shown in Figure 4.2.

It is often reported that power-law fits to  $M_{\text{BH}}-\sigma$  data return exponents that are

---

<sup>2</sup>Applying this procedure to Circinus gives  $v_w/c \simeq 1.2$  for that galaxy. In this case, the published SMBH mass estimate would have to be higher by a factor of  $\gtrsim 4$  (for the same  $\sigma$ ) or the stellar velocity dispersion lower by a factor  $\approx 1.3$  (for  $M_{\text{BH}}$  fixed) to bring the inferred wind speed down to  $v_w/c \lesssim 0.3$ .

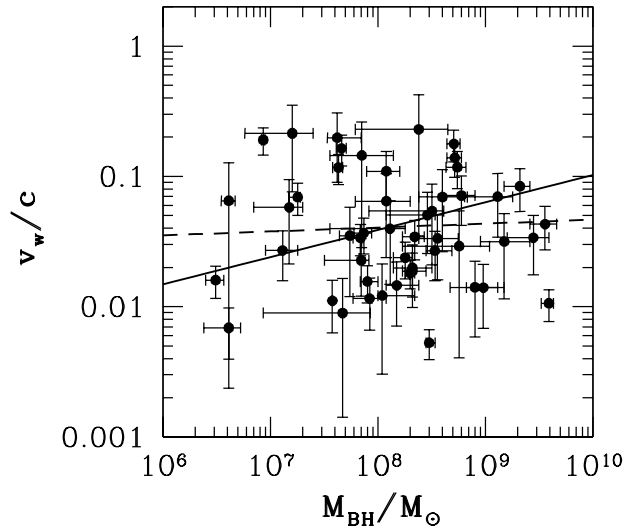


Figure 4.3: Inferred  $v_w/c$  vs. observed  $M_{\text{BH}}$  for the normal early-type galaxies and bulges in Gültekin et al. (2009), with  $v_w/c$  obtained from equation (4.16) for each  $(M_{\text{BH}}, \sigma)$  measurement. The solid line shows the correlation  $v_w \propto M_{\text{BH}}^{0.2}$ , which could explain the slope of the best-fit power-law  $M_{\text{BH}}-\sigma$  relation according to Gültekin et al. The dashed line shows the weaker correlation  $v_w \propto M_{\text{BH}}^{0.03}$ , suggested by the steeper power-law fit to  $M_{\text{BH}}$  versus  $\sigma$  by Ferrarese & Ford (2005).

closer to 4 than to 5; and, as we noted in §4.2, even a weak correlation between black hole mass and wind speed could result in an  $M_{\text{BH}}-\sigma$  relation from energy-conserving feedback having a slope  $< 5$  (equation [4.17]). Thus, Figure 4.3 plots our inferred  $v_w/c$  for the Gültekin et al. spheroids against their  $M_{\text{BH}}$  values.

The fitted  $M_{\text{BH}}-\sigma$  relation of Ferrarese & Ford (2005; their equation [20]) is  $M_{\text{BH}} \propto \sigma^{4.86 \pm 0.43}$ . Taking this power at face value, our equation (4.17) implies, roughly,  $v_w \propto M_{\text{BH}}^{0.03 \pm 0.09}$ . This scaling is drawn as the dashed line in Figure 4.3. On the other hand, Gültekin et al. (2009) quote  $M_{\text{BH}} \propto \sigma^{4.12 \pm 0.37}$  for a fit to the galaxies in their sample minus Circinus (see the note in their Table 1). Putting this into equation (4.17) above implies  $v_w \propto M_{\text{BH}}^{0.2 \pm 0.1}$ , which is illustrated by the solid line in Figure 4.3. Either of these relations between  $v_w$  and  $M_{\text{BH}}$  appears consistent with the data; alternatively,

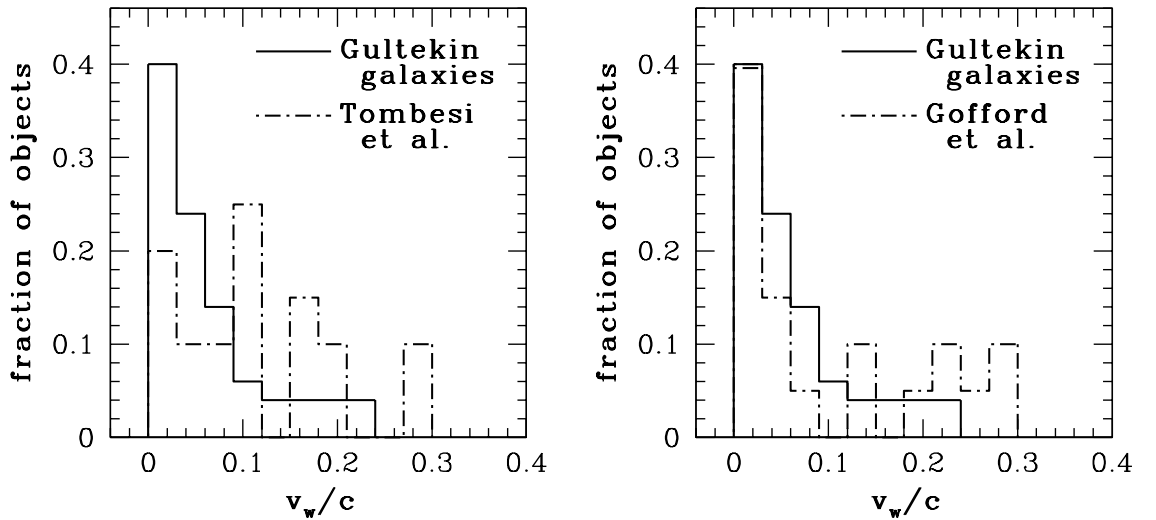


Figure 4.4: Distribution of model (past) SMBH wind velocities for the normal galaxies in Gültekin et al. (2009) (solid lines), compared to the observed distributions of  $v_w/c$  in local AGN, in samples measured by Tombesi et al. (2011) (dashed line in the left-hand panel) and by Gofford et al. (2013) (dashed line in the right-hand panel).

neither is obviously required by the data. In fact, the Spearman rank-correlation coefficient for these  $(v_w, M_{\text{BH}})$  numbers is just  $s = -0.03$ , with a significance of only  $\simeq 15\%$ . Any correlation that there might be between  $v_w$  and  $M_{\text{BH}}$  is simply so weak as to be swamped by the scatter in the  $M_{\text{BH}}-\sigma$  data. This is not really surprising but is, of course, bound up with the well-known fact of the small *intrinsic* scatter in the  $M_{\text{BH}}-\sigma$  relation.

Our analysis of the  $M_{\text{BH}}-\sigma$  data has essentially interpreted the scatter in it (i.e., the spread of  $\log M_{\text{BH}}$  at a given  $\log \sigma$ ) as the result of variations in SMBH wind speeds around an average  $v_w/c \simeq 0.035$ . However, the histogram in Figure 4.2 and the spread of the points in Figure 4.3 have not been corrected in any way for measurement errors in  $M_{\text{BH}}$ , which work to broaden the true, error-free distributions. To attempt any correction is not in the scope of this work. But it is worth noting that the standard deviation of our  $\log(v_w/c)$  values is  $\epsilon \approx 0.4$  dex, as against an rms errorbar of

$\Delta \log(v_w/c) \approx 0.1$  dex (which is dominated by the uncertainties in  $\log M_{\text{BH}}$ ). This implies that there is indeed some real width to our  $v_w/c$  distribution, which is rightly comparable to the intrinsic scatter in the observed  $M_{\text{BH}}-\sigma$  relation ( $\epsilon_0 \approx 0.44$  dex, according to Gültekin et al. 2009).

In any case, the main and most robust result here is our value for the median black hole wind speed,  $v_w/c = 0.035$ . This not only gives a very credible fit of a simple energy-driven feedback model to the  $M_{\text{BH}}-\sigma$  relation; it is also similar to the typical speeds of nuclear outflows in samples of nearby, currently active galaxies having no overlap with the Gültekin et al. sample of quiescent early types and bulges.

## 4.4 Observed AGN outflow velocities

Highly ionised, “ultra-fast” outflows have been observed from the centres of many local active galactic nuclei since the prototypes of the phenomenon were found by Pounds et al. (2003) and Reeves, O’Brien & Ward (2003). These outflows are very massive and have high kinetic powers of the order needed, in simple scenarios of the type discussed in this chapter, for the clearing of gaseous protogalaxies by SMBH-powered winds. As pointed out originally by King (2003), they appear to be an observable, present-day analogue of the processes that may have worked to establish the  $M_{\text{BH}}-\sigma$  relation among now-inactive galaxies.

Two recent studies, by Tombesi et al. (2011) and Gofford et al. (2013), give the velocities for samples of 20 and 21 AGN outflows respectively, with 6 sources in common. We can now compare the distributions of these observed outflow speeds to the distribution that we inferred in §4.3 for SMBH wind speeds in the past, in the normal spheroids that define the  $M_{\text{BH}}-\sigma$  relation.

Figure 4.4 shows this comparison, with the AGN outflow velocity distribution from Tombesi et al. (2011) in the left-hand panel, and with that from Gofford et al. (2013) in the right-hand panel. In each panel, the solid-line histogram is that from Figure 4.2 above, obtained from equation (4.16) assuming that the black holes in the

Gültekin et al. (2009) galaxies were just able to drive energy-conserving supershells to the escape speeds of their dark-matter haloes. The dashed histograms represent the AGN data.

The most striking aspect of Figure 4.4 is the basic agreement, to within factors of a few at worst, in the typical  $v_w/c$  of these different samples of galaxies: our median  $v_w/c = 0.035$  for the normal early-type galaxies, versus a median  $v_w/c = 0.1$  for the AGN outflows of Tombesi et al. (2011) and a median  $v_w/c = 0.056$  for the AGN of Gofford et al. (2013). The overall ranges (i.e., the maxima) of the wind speeds are also very similar. These facts are remarkable as much for the simplicity of the model we have used to estimate  $v_w/c$  in the normal galaxies, as for the complete disconnect between the Gültekin et al. galaxy sample and the Tombesi et al. or Gofford et al. AGN samples.

To be sure, the distributions as they stand in Figure 4.4 are not identical. Kolmogorov-Smirnov (KS) tests return a formal probability of only  $P_{\text{KS}} \simeq 0.3\%$  that our distribution of  $v_w/c$  for the Gültekin et al. galaxies is drawn from the same parent distribution as the Tombesi et al. sample, and  $P_{\text{KS}} \simeq 25\%$  for equality between our  $v_w/c$  values and the Gofford et al. sample. The main reason for this appears to be the relatively small numbers, in the present sample, of normal galaxies with inferred  $v_w/c \gtrsim 0.1$ —or, conversely, a dearth of AGN (in the Tombesi et al. sample especially) with slower  $v_w/c \lesssim 0.1$ .

Whatever shortcomings our very simple analysis might have, it requires that normal galaxies with “underweight” black holes falling significantly below the mean  $M_{\text{BH}} - \sigma$  relation have higher-than-average  $v_w/c$ . If several such galaxies were to be added to the Gültekin et al. sample, they could fill out the high-velocity tail of our model  $v_w/c$  distribution. As for the AGN, it is not clear how selection effects, observational biases or limitations due to instrumentation may have either affected the measurement of relatively slow outflows, or perhaps even prevented their inclusion in studies designed to focus on “ultra-fast” systems. It is also worth noting that the probability that the  $v_w/c$  measurements of Tombesi et al. and Gofford et al. are drawn from the same parent distribution is a formally inconclusive  $P_{\text{KS}} \simeq 28\%$ —the same as in the comparison

between the Gofford et al. distribution of  $v_w$  for their AGN and ours for the normal galaxies. As such, it is not clear that any of the data are yet sufficient to allow a robust comparison at a very detailed level between distributions of observed SMBH wind speeds and those inferred from any model. This makes it even more noteworthy that the median of the  $v_w$  distribution we have obtained in this work lies within a factor  $\approx 1.5$ –3 of the median  $v_w$  of two different observed distributions.

Ultimately, our results are encouraging for the general idea that there is a parallel between the strong nuclear outflows found in local AGN and the kind of black hole feedback that is routinely assumed to have been a key part of galaxy formation and the establishment of the  $M_{\text{BH}}-\sigma$  relation. They also lend support to the relevance of energy-driven feedback specifically, and to the simple sort of modelling that we have applied to assess its role quantitatively.

## 4.5 Summary

We have looked at the behaviour of energy-conserving supershells of swept-up ambient gas driven into isothermal protogalaxies by black hole winds. At large radii, such shells tend to a constant coasting speed,  $v_\infty$ , that depends on the black hole mass,  $M_{\text{BH}}$ , the black hole wind speed,  $v_w$ , and the velocity dispersion of the halo,  $\sigma_0$ . For a shell to coast at the escape speed of a truncated isothermal halo (i.e.,  $v_\infty = 2\sigma_0$ ) requires  $M_{\text{BH}} v_w \propto \sigma_0^5$  as in equations (4.15) and (4.16).

We applied this escape condition for energy-conserving feedback to the observed  $M_{\text{BH}}-\sigma$  relation for the sample of quiescent early-type galaxies and bulges of Gültekin et al. (2009). We used equation (4.16) to infer the black hole wind speed that each galaxy would have had during an active phase if our simple model is to account for the measured value of  $M_{\text{BH}}$  in the galaxy, given its observed  $\sigma$ . In this approach, scatter in the observed  $M_{\text{BH}}-\sigma$  relation directly reflects a distribution of wind speeds from the SMBHs in the protogalaxies. We compared the distribution of wind velocities we obtained for the normal galaxies in Gültekin et al. to the observed distributions of

outflow velocities in two different samples of local AGN (Tombesi et al. 2011; Gofford et al. 2013). The distributions are strikingly similar. Most notably, the median of our inferred wind velocities,  $v_w = 0.035c$ , is within a factor  $\approx 1.5$ –3 of the median of the observed distribution of wind speeds of both Tombesi et al. ( $v_w = 0.1c$ ) and Gofford et al. ( $v_w = 0.056c$ ).

## 4.A Terminal speeds of energy-driven shells

In McQuillin & McLaughlin (2013) we derived the large radius coasting speed of an energy-driven shell in an isothermal halo, taking into account the gravity of the dark matter. Here, we compare our results to other derivations of energy-driven coasting speeds, in particular Silk & Rees (1998), King (2005), King et al. (2011) and Faucher-Giguère & Quataert (2012).

Silk & Rees (1998) give the velocity of a shell driven by a quasar wind into an isothermal halo as

$$v_s = \left( \frac{f_w L_{\text{Edd}} 8\pi^2 G}{f_0 \sigma^2} \right)^{1/3} \quad (4.20)$$

where they have taken the wind luminosity to be a fraction  $f_w$  of the Eddington luminosity, with  $f_w = \dot{M}_{\text{out}} v_w^2 / L_{\text{Edd}}$ . By expressing  $L_{\text{Edd}}$  in terms of  $\dot{M}_{\text{Edd}}$ , in our notation we find

$$f_w = \eta^{-1} \left( \frac{\dot{M}_{\text{out}}}{\dot{M}_{\text{Edd}}} \right) \left( \frac{v_w}{c} \right)^2 = \tau \left( \frac{v_w}{c} \right) \quad (4.21)$$

Then, for the coasting speed in equation (4.20) to equal the escape speed of the halo requires

$$M_{\text{BH}} v_w = \tau^{-1} \frac{\kappa f_0}{4\pi^3 G^2} \sigma^5 \quad (4.22)$$

which has the scaling we expect, though a different normalisation than our equation (4.15), which includes the effects of the dark matter that are not included in the Silk & Rees (1998) analysis. Equation (4.22) gives an  $M$ – $\sigma$  relation

$$\left( \frac{M_{\text{BH}}}{10^8 M_\odot} \right) \left( \frac{v_w}{c} \right) = 7.7 \times 10^{-5} \tau^{-1} \left( \frac{\sigma}{200 \text{ km s}^{-1}} \right)^5 \quad (4.23)$$

which is  $\sim 3$  orders of magnitude below our result.

If we use the energy-driven  $M$ - $\sigma$  relation derived from Silk & Rees (1998) to infer wind speeds for the galaxies in the Gültekin et al. (2009) sample, we find a median wind velocity of just  $v_w \sim 4 \times 10^{-5} c$ , far below the observed medians of  $0.1 c$  from Tombesi et al. (2011) and  $0.056 c$  from Gofford et al. (2013).

King (2005) and King, Zubovas & Power (2011) look at energy-driven outflows only in the specific case that the black hole has reached the critical  $M_\sigma$  mass during an momentum-driven phase and then switched to an energy-driven regime. They also assume that  $\dot{M}_{\text{out}} \simeq \dot{M}_{\text{acc}}$  so that  $\tau \sim 1$  implies  $v_w/c \sim \eta \simeq 0.1$ . Then, in our notation they are looking at the case  $\widetilde{M}_{\text{BH}} \widetilde{v}_w = 150$ , which is greater than the constraint required for escape. In this case, equation (4.13) gives a terminal shell speed  $v_\infty \approx 4.4\sigma_0$ , far above the escape speed of an isothermal halo.

Faucher-Giguère & Quataert (2012) present in their appendix energy conservation conditions for self similar outflows. They assume that half of the kinetic energy injected by the black hole goes into the kinetic motion of the swept up gas. They take this approximation from Weaver et al. (1977) who solve the energy equation  $dE = dU - PdV$  (which neglects the work against gravity), and find  $U = (5/11)L_{\text{in}}t$ . Applying the density profile of an SIS to their results gives a shell speed of

$$v_s = \left( \frac{9\pi G^2}{f_0 \kappa \sigma_0^2} \tau M_{\text{BH}} v_w \right)^{1/3} \quad (4.24)$$

where  $\tau$  has the same definition as in our calculations when the AGN luminosity is equal to the Eddington luminosity. Requiring the shell velocity to equal the escape speed of the halo gives

$$M_{\text{BH}} v_w = \tau^{-1} \frac{8f_0 \kappa \sigma_0^5}{9\pi G^2} \quad (4.25)$$

which again has the scaling we expect, though a different normalisation than our result. This gives and  $M$ - $\sigma$  relation

$$\left( \frac{M_{\text{BH}}}{10^8 M_\odot} \right) \left( \frac{v_w}{c} \right) = 2.7 \times 10^{-3} \tau^{-1} \left( \frac{\sigma}{200 \text{ km s}^{-1}} \right)^5 \quad (4.26)$$

which is a factor of  $\sim 2.5$  below our relation. When using this relation to calculate

winds speeds for the Gültekin et al. (2009) galaxies we find a median wind speed of  $\sim 10^{-3}c$ , which is again below the median observed velocities of  $\sim 0.056c$  and  $\sim 0.1c$ .

## 5 Energy-driven Outflows in Non-isothermal Galaxies

In Chapter 4 we looked at purely energy-driven outflows in dark matter haloes modelled as singular isothermal spheres. We found that if a shell can reach large radius without stalling it will coast at a finite speed that depends on the black hole mass, the velocity dispersion and the black hole wind speed. By requiring the shell coasting speed to equal the escape speed of the halo we found an  $M_{\text{BH}}-\sigma$  relation of the form  $M_{\text{BH}}v_w \propto \sigma^5$ . Using this relation, we inferred the distribution of wind speeds that a sample of now quiescent galaxies would have had during an active phase. These wind speeds are in good agreement with observed wind speeds in local AGN, with a median of  $v_w = 0.035 c$ , which is within a factor  $\sim 1.5 - 3$  of the median observed wind speed of  $v_w = 0.1 c$  and  $v_w = 0.056 c$  (Tombesi et al. 2011; Gofford et al. 2013).

In the case of the purely momentum-driven outflows considered in Chapter 3, we identified several key differences in the analyses between outflows modelled in isothermal spheres and in non-isothermal haloes. As in the energy-driven case, we found that momentum-driven shells in an isothermal halo coast at a constant speed at large radius. When considering such outflows in non-isothermal haloes, we found that if the shell can reach large radius without stalling then it will always accelerate and eventually exceed the escape speed of the halo. This can be done with a CMO mass less than the mass required to drive a shell to the escape speed of an isothermal halo.

With this in mind, it is of interest to look at the effects of relaxing the isothermal assumption for energy-driven outflows.

## 5.1 Equation of motion

We recall that the equation of motion of shell moving outwards into the dark matter halo of a protogalaxy is

$$\frac{d}{dt} [M_g(r)v(r)] + \frac{GM_g(r)}{r^2} [M_{\text{BH}} + M_{\text{DM}}(r)] = 4\pi r^2 P, \quad (5.1)$$

where for an energy-driven outflow  $P$  is the thermal pressure that drives the shell, which satisfies the energy equation

$$\frac{d}{dt} \left[ \frac{4}{3} \pi r^3 \frac{P}{\gamma - 1} \right] = \dot{E} - P \frac{d}{dt} \left[ \frac{4}{3} \pi r^3 \right] - \frac{GM_g(r)v(r)}{r^2} [M_{\text{BH}} + M_{\text{DM}}(r)]. \quad (5.2)$$

Here,  $\gamma$  is the ratio of specific heats and  $\dot{E} = \tau(v_w/c)(L_{\text{Edd}}/2)$  is the kinetic energy flux of the wind (equation [4.9]).

As in Chapter 3, we write  $M_g(r) = f_0 h(r) M_{\text{DM}}(r)$ , where  $f_0$  is the fiducial gas fraction ( $\sim 0.2$ ) and  $h(r)$  is a function that describes how the gas traces the dark matter. Also as in the case of momentum-driven shells in non-isothermal haloes, we refer all masses, radii and velocities to the peak of the circular speed curve,  $V_c^2 = GM_{\text{DM}}(r)/r$ . Recalling §3.5.1 (equations [3.19] - [3.24]), we denote the location of the peak in the circular speed curve by  $r_{\text{pk}}$  and the value  $V_c^2(r_{\text{pk}}) \equiv V_{c,\text{pk}}^2$ . We define the characteristic velocity dispersion  $\sigma_0^2 \equiv V_{c,\text{pk}}^2/2$  to define unique mass and radius units  $M_\sigma$  and  $r_\sigma$ . We then also have that  $\tilde{V}_{c,\text{pk}}^2 = 2$  and  $\tilde{M}_{\text{DM}}(\tilde{r}_{\text{pk}}) \equiv \tilde{M}_{\text{pk}} = 2\tilde{r}_{\text{pk}}$ . We define  $x = r/r_{\text{pk}}$  and we introduce a dimensionless mass profile  $m(x)$  so that  $\tilde{M}_{\text{DM}}(x) \equiv \tilde{M}_{\text{pk}} m(x)$ , where by construction  $\tilde{M}_{\text{DM}}(x=1) \equiv \tilde{M}_{\text{pk}}$  and  $m(x=1) = 1$ .

We use equation (5.1) to eliminate  $P$  from (5.2). Combining this with the above definitions, the equation of motion of an energy-driven shell in any non-isothermal dark matter halo with a singly peaked circular speed curve is

$$\begin{aligned} & \frac{d^2}{dx^2} [h^2 m^2 \tilde{v}^2(x)] + \left( \frac{3(\gamma - 1)}{x} + \frac{hm(x)}{x} \frac{d}{dx} \left[ \frac{x}{hm(x)} \right] \right) \frac{d}{dx} [h^2 m^2 \tilde{v}^2(x)] \\ & + 4 \frac{hm(x)}{x^2} \left( m^2(x) \frac{dh}{dx} + 2hm(x) \frac{dm}{dx} + \frac{\tilde{M}_{\text{BH}}}{\tilde{M}_{\text{pk}}} h(x) \frac{dm}{dx} + \frac{\tilde{M}_{\text{BH}}}{\tilde{M}_{\text{pk}}} m(x) \frac{dh}{dx} \right) \\ & = 6(\gamma - 1) \frac{hm(x) \tilde{M}_{\text{BH}} \tilde{v}_w}{\tau} x \tilde{v}(x) - 4(6\gamma - 7) \frac{h^2 m^2(x)}{x^3} \left[ m(x) + \frac{\tilde{M}_{\text{BH}}}{\tilde{M}_{\text{pk}}} \right] \end{aligned} \quad (5.3)$$

This form of the equation of motion allows us to select any dark matter mass profile that has a single peak in its circular speed curve and also allows for the segregation of gas and dark matter, though we focus on the case where  $h(x) \equiv 1$ . In general equation (5.3) must be solved numerically for a given dark matter profile. In §5.1.2 - 5.1.4 we will look at the solutions of equation (5.3) with the dark matter profiles of Hernquist (1990), Navarro, Frenk & White (1996, 1997) and Dehnen & McLaughlin (2005).

### 5.1.1 Velocity fields at small radius

As in our analysis of the limiting behaviour of momentum-driven shells in a non-isothermal halo in §3.4.1.1, in the limit of small radius, we can assume to leading order that

$$m(x) \rightarrow Ax^p, \quad (x \ll 1) \quad (5.4)$$

where  $p > 1$  as we are considering haloes that are shallower than isothermal in the centre. Defining  $\tilde{q}^2 \equiv m^2(x)\tilde{v}^2(x)$ , equation (5.3) for the motion of an energy-driven shell in a non-isothermal halo becomes at small radius

$$\begin{aligned} \frac{d^2\tilde{q}^2}{dx^2} + \frac{(1-p+3[\gamma-1])}{x} \frac{d\tilde{q}^2}{dx} + 4A^2px^{2p-3} \left[ 2Ax^p + \frac{\tilde{M}_{\text{CMO}}}{\tilde{M}_{\text{pk}}} \right] \\ + 4(6\gamma-7)A^2x^{2p-3} \left[ Ax^p + \frac{\tilde{M}_{\text{CMO}}}{\tilde{M}_{\text{pk}}} \right] = 6(\gamma-1)\tilde{M}_{\text{CMO}}\tilde{v}_w \frac{A^2x^{2p-1}}{\tilde{q}}. \end{aligned} \quad (5.5)$$

We assume that at small radius  $\tilde{q}^2$  tends to a power law of the form:

$$\tilde{q}^2 \rightarrow C + B_1x^\beta + B_2x^{2\beta} + \mathcal{O}(x^{3\beta}), \quad (5.6)$$

so that  $C \equiv m^2(0)\tilde{v}^2(0)$ . Then we have

$$\begin{aligned} \frac{d\tilde{q}^2}{dx} &= \beta B_1x^{\beta-1} + 2\beta B_2x^{2\beta-1} + \mathcal{O}(x^{3\beta-1}) \\ \frac{d^2\tilde{q}^2}{dx^2} &= \beta(\beta-1)B_1x^{\beta-2} + 2\beta(2\beta-1)B_2x^{2\beta-2} + \mathcal{O}(x^{3\beta-1}) \\ \tilde{q}^{-1} &= C^{-1/2} \left( 1 - \frac{1}{2} \frac{B_1}{C} x^\beta + \left[ \frac{1}{2} \frac{B_2}{C} + \frac{3}{8} \frac{B_1^2}{C} \right] x^{2\beta} + \mathcal{O}(x^{3\beta}) \right). \end{aligned} \quad (5.7)$$

Substituting these expansions into equation (5.5) and equating the leading terms gives

$$\tilde{q}^2(x) \equiv m^2(x) \tilde{v}^2(x) \longrightarrow C - \frac{4A^2}{2p-1} \frac{\tilde{M}_{\text{CMO}}}{\tilde{M}_{\text{pk}}} \frac{(p+6\gamma-7)}{[p-1+3(\gamma-1)]} x^{2p-1} \quad (5.8)$$

As for energy-driven shells in an isothermal halo, a shell moving from  $x = 0$  must have a large enough initial momentum to keep  $m^2(x) \tilde{v}^2(x) > 0$  if it is to reach large radius and escape. Equation (5.8) gives the initial condition we use to start our numerical integrations to solve equation (5.3) for the dark matter haloes of Hernquist (1990), NFW and Dehnen & McLaughlin (2005) in the following sections.

### 5.1.2 Hernquist model haloes

The first specific non-isothermal halo we consider is that of Hernquist (1990). As has been discussed previously (§3.4.2), in our notation referring all masses, radii and velocities to the peak of the rotation curve, the mass profile of a Hernquist sphere is given by

$$\tilde{M}_{\text{DM}}(x) = \tilde{M}_{\text{pk}} \frac{4x^2}{(1+x)^2} \equiv \tilde{M}_{\text{pk}} m(x) \quad (5.9)$$

In the limit of small radius,  $m(x) \rightarrow 4x^2$ , so  $A = 4$  and  $p = 2$  in equation (5.8), and

$$\tilde{v}^2 \longrightarrow \frac{C}{16} x^{-4} - \frac{4}{3} \frac{\tilde{M}_{\text{BH}}}{\tilde{M}_{\text{pk}}} \frac{(6\gamma-5)}{(3\gamma-2)} x^{-1}, \quad (x \ll 1) \quad (5.10)$$

which is the initial condition we use in our numerical integration of equation (5.3) for the motion of a shell in a Hernquist halo.

Figure 5.1 shows the velocity fields,  $v^2(r)$ , that solve equation (5.3) for the Hernquist (1990) dark matter profile with  $\tilde{M}_{\text{pk}} = 4000$ . This corresponds to  $M_{\text{pk}} \sim 2 \times 10^{12} M_{\odot}$  in a halo with  $\sigma_0 = 200 \text{ km s}^{-1}$  and recalling  $\tilde{M}_{\text{pk}} = 2\tilde{r}_{\text{pk}}$ , this gives  $r_{\text{pk}} \sim 100 \text{ kpc}$ . Each panel of Figure 5.1 shows solutions with  $\tilde{M}_{\text{BH}} \tilde{v}_{\text{w}} = 0.45, 2.7$  and 22 for a range of initial momenta (i.e., a range of  $C$  values). All solutions have  $\tilde{v}_{\text{w}} = 45$ , corresponding to  $v_{\text{w}} = 0.03c$  for  $\sigma_0 = 200 \text{ km s}^{-1}$ , so that  $\tilde{M}_{\text{BH}} = 0.01, 0.06$  and 0.49 in each case.

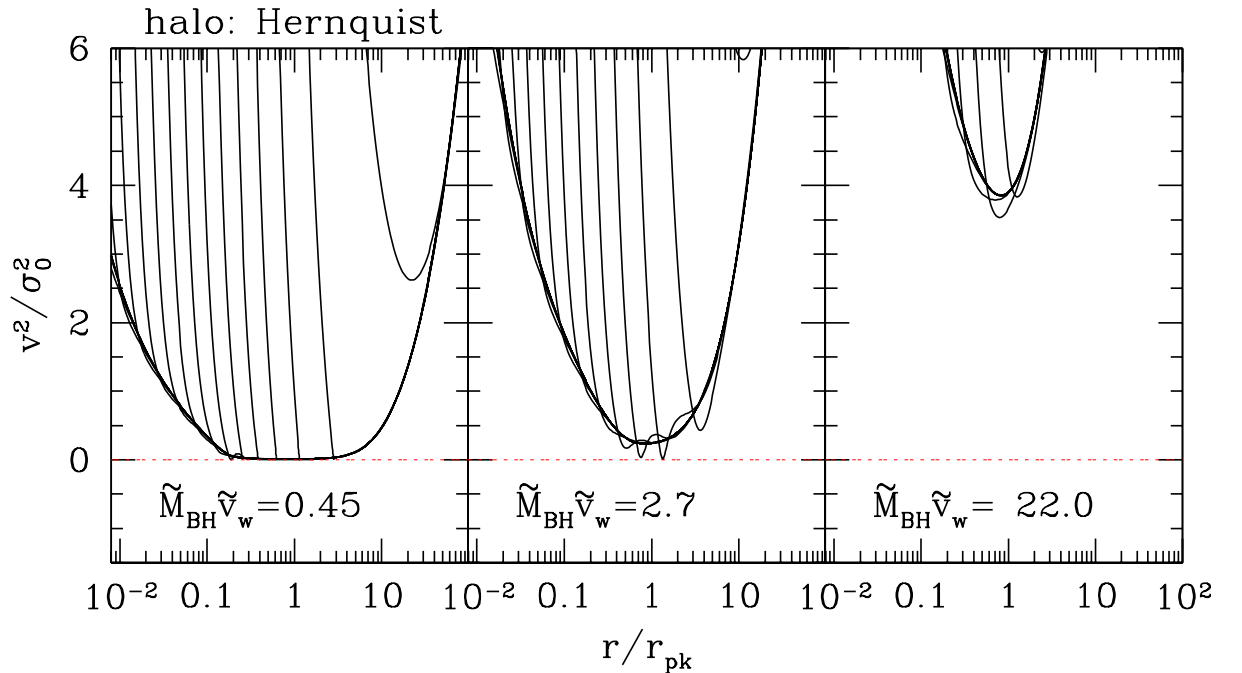


Figure 5.1: Velocity fields for energy-driven shells in a Hernquist (1990) dark matter halo with a spatially constant gas fraction and  $\tilde{M}_{\text{pk}} = 4000$ , which corresponds to a halo with  $M_{\text{pk}} \sim 2 \times 10^{12} M_{\odot}$  and  $r_{\text{pk}} \sim 100$  kpc for  $\sigma_0 = 200$  km s $^{-1}$ . Each panel shows solutions with  $\tilde{M}_{\text{BH}} \tilde{v}_w = 0.45, 2.7$  and  $22$  for an range of initial momenta. In each case,  $\tilde{v}_w = 45$ , corresponding to an outflow velocity of  $0.03 c$  for  $\sigma_0 = 200$  km s $^{-1}$ , so that  $\tilde{M}_{\text{BH}} = 0.01, 0.06$  and  $0.49$ .

The left-hand panel of Figure 5.1 shows solutions with  $\tilde{M}_{\text{BH}} \tilde{v}_w = 0.45$ . Most of these represent shells that stall and are unable to escape. Shells with small initial momenta (i.e.,  $C \ll 1$ ) are formally able to escape, though their velocities are near zero for much of their evolution. From  $x = 0.5$  to  $x = 1$ , corresponding to a distance of  $\sim 50$  kpc, the shell travels at  $\sim 0.1 \sigma_0 \sim 20$  km s $^{-1}$ , so it takes  $\sim 3 \times 10^9$  yrs to reach the peak of the rotation curve. It is notable that this minimum velocity is comparable to the coasting speed of an energy-driven shell in an isothermal halo driven by this  $\tilde{M}_{\text{BH}} \tilde{v}_w$ , where  $\tilde{v}_{\infty} \sim 0.1$  (equation [4.13] with  $\tilde{M}_{\text{BH}} \tilde{v}_w = 0.45$ ). The same is true

for momentum-conserving outflows where the minimum velocities of shells with small initial momenta in a non-isothermal halo are comparable to the large radius coasting speed of a momentum-driven shell driven by the same CMO mass in an isothermal halo. The uppermost curve in the left-hand panel represents the escape of a shell with significant velocity at all radii, though this is only a formal result as it represents a shell with  $v \sim 10^6 c$  at a radius of  $\sim 1\text{pc}$ .

The middle panel of Figure 5.1 shows solutions with  $\widetilde{M}_{\text{BH}} \widetilde{v}_w = 2.7$ . We can see here that although some solutions come close to  $\widetilde{v} = 0$ , all solutions represent shells that are in principle able to escape. The minimum velocity of shells with small initial momenta is comparable to the coasting speed in an isothermal halo where  $\widetilde{v}_\infty \simeq 0.5$  for  $\widetilde{M}_{\text{BH}} \widetilde{v}_w = 2.7$ . Curves with this minimum velocity represent shells that begin the acceleration that allows them to escape at  $x \sim 1$ . Shells with larger initial momenta can begin to accelerate at radii smaller than this but still at large radii in the halo.

Finally, the right-hand panel of Figure 5.1 shows solutions with  $\widetilde{M}_{\text{BH}} \widetilde{v}_w = 22$ . Here we see that all solutions represent shells that easily escape to large radius. Again, solutions with small initial momenta have minimum velocities comparable to the coasting speed in the isothermal case,  $\widetilde{v}_\infty = 2$  for  $\widetilde{M}_{\text{BH}} \widetilde{v}_w = 22$ , the condition for the escape from a truncated isothermal halo.

In all three cases, as with momentum-driven shells in non-isothermal haloes, if the shell can reach large radii without stalling then it will accelerate and eventually exceed the escape speed of the halo. In a Hernquist halo  $m(x) \rightarrow 4$  at large radius, and in a similar way to §5.1.1. we can find the large radius speed by assuming  $\widetilde{q}^2(x)$  follows a power law of the form

$$\widetilde{q}^2 \longrightarrow x^\beta [B_1 + B_2 x^{-1} + B_3 x^{-2} + \mathcal{O}(x^{-3})] . \quad (5.11)$$

Substituting this expansion and its derivatives into equation (5.3) for the motion of an energy-driven shell, with  $m(x) = 4$  we find the large radius speed of the shells tends to

$$\widetilde{v}^2 \longrightarrow \left[ \frac{96(\gamma - 1)\widetilde{M}_{\text{BH}} \widetilde{v}_w}{2\gamma + 2/9} \right]^{2/3} \frac{x^{2/3}}{16} , \quad (x \gg 1) \quad (5.12)$$

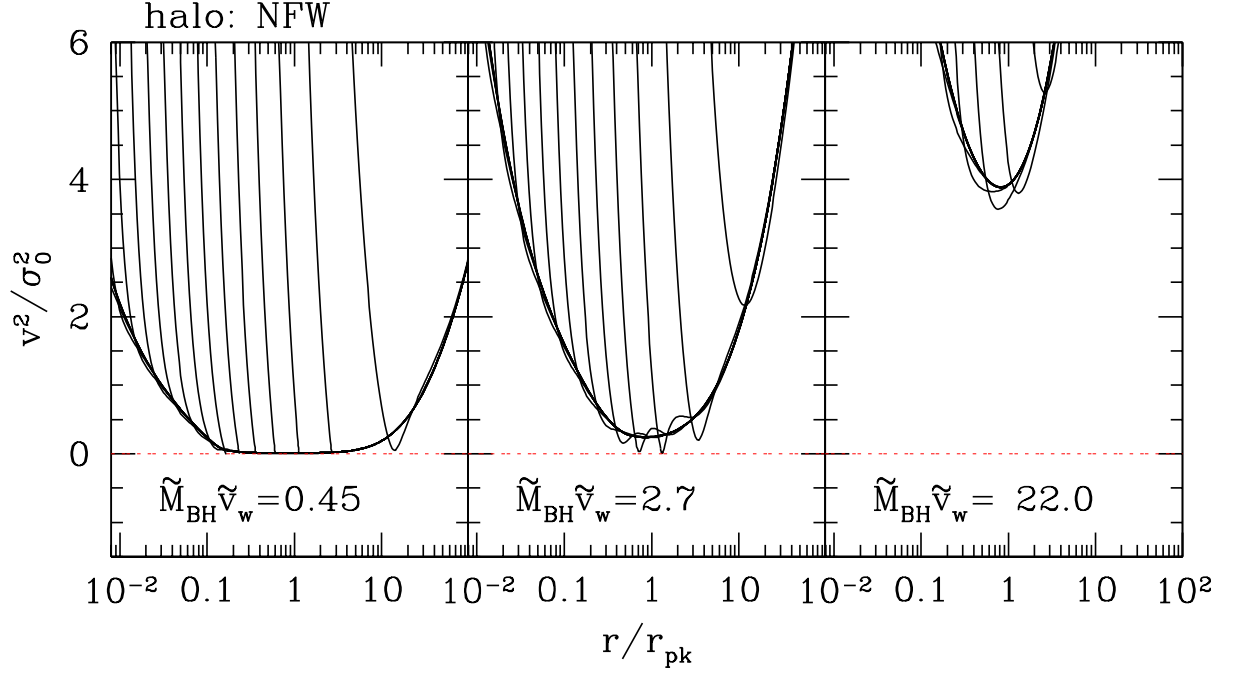


Figure 5.2: Velocity fields for energy-driven shells in an NFW dark matter halo with a spatially constant gas fraction and  $\widetilde{M}_{\text{pk}} = 4000$ . Each panel shows solutions with  $\widetilde{M}_{\text{BH}} \widetilde{v}_w = 0.45$ , 2.7 and 22 and a range of initial momenta. In each case,  $\widetilde{v}_w = 45$ , corresponding to an outflow velocity of  $0.03 c$  for  $\sigma_0 = 200 \text{ km s}^{-1}$ , so that  $\widetilde{M}_{\text{BH}} = 0.01$ , 0.06 and 0.49. The radius unit  $r_{\text{pk}} \simeq 100 \text{ kpc}$ .

so that, again as in the case of momentum-driven outflows, all shells tend to the same large radius  $v(r)$ , independent of the initial conditions (i.e., the value of  $C$ ).

### 5.1.3 NFW model haloes

We look next at the dark matter density profile of Navarro, Frenk & White (1996, 1997; NFW), which has the mass profile (§3.4.3)

$$\widetilde{M}_{\text{DM}}(x) = \widetilde{M}_{\text{pk}} \frac{\ln(1 + \mathcal{R}x) - \mathcal{R}x/(1 + \mathcal{R}x)}{\ln(1 + \mathcal{R}) - \mathcal{R}/(1 + \mathcal{R})} \equiv \widetilde{M}_{\text{pk}} m(x) \quad (5.13)$$

where  $\mathcal{R} = 2.16258$ . At small radii, the dimensionless mass profile,  $m(x)$ , tends to

$$m(x) \longrightarrow \frac{\mathcal{R}^2 x^2}{2} \left[ \ln(1 + \mathcal{R}) - \frac{\mathcal{R}}{1 + \mathcal{R}} \right]^{-1} \quad (x \ll 1) \quad (5.14)$$

Then, from equation (5.8) with  $A = [\mathcal{R}^2/2][\ln(1 + \mathcal{R}) - \mathcal{R}/(1 + \mathcal{R})]$  and  $p = 2$ , the velocity field at small radius tends to

$$\tilde{v}^2 \longrightarrow \frac{4C}{\mathcal{R}^2} \left[ \ln(1 + \mathcal{R}) - \frac{\mathcal{R}}{1 + \mathcal{R}} \right]^2 x^{-4} - \frac{4 \widetilde{M}_{\text{BH}} (6\gamma - 5)}{3 \widetilde{M}_{\text{pk}} (3\gamma - 2)} x^{-1}, \quad (x \ll 1) \quad (5.15)$$

which is the initial condition we use in our numerical integration of equation (5.3) for an NFW halo.

Figure 5.2 shows the velocity fields that solve equation (5.3) in an NFW dark matter halo with  $\widetilde{M}_{\text{pk}} = 4000$ . The panels from left to right show  $\widetilde{M}_{\text{BH}} \tilde{v}_{\text{w}} = 0.45$ , 2.7 and 22. All three panels have  $\tilde{v}_{\text{w}} = 45$ , corresponding to an outflow velocity of  $v_{\text{w}} = 0.03c$  for  $\sigma_0 = 200 \text{ km s}^{-1}$ , so that  $\widetilde{M}_{\text{BH}} = 0.01, 0.06$  and  $0.49$ .

Figure 5.2 is qualitatively similar to Figure 5.1 for velocity fields in a Hernquist dark matter halo. The left-hand panel, with  $\widetilde{M}_{\text{BH}} = 0.01$  shows many solutions which stall (i.e.,  $\tilde{v} = 0$ ) at finite radius, some that escape but have near zero velocities for much of their evolution and one that accelerates when it is at a significant velocity. This solution is again a formal result which is not physically possible ( $v \sim 10^6 c$  at 1pc). The shell that escapes is slow moving and again takes a considerable amount of time to reach the peak of the rotation curve, at least  $\sim 3 \times 10^9$  yrs. The middle panel, with  $\widetilde{M}_{\text{BH}} = 0.06$  shows solutions which represent all shells escaping, though some come close to stalling. The right-hand panel of Figure 5.2 shows solutions with  $\widetilde{M}_{\text{BH}} \tilde{v}_{\text{w}} = 22$ , the critical value in the isothermal case, which all escape easily.

As in the Hernquist halo, shells with small initial momenta have minimum velocities that are comparable to the coasting velocity of shells driven by the same  $\widetilde{M}_{\text{BH}} \tilde{v}_{\text{w}}$  in an isothermal halo, which is analogous to the momentum-driven outflows considered in Chapter 3. These shells begin to accelerate near the peak of the rotation curve, whereas shells with higher initial momenta can begin to accelerate at smaller radii.

Again, as in the case of momentum-driven outflows, all shells accelerate if they can reach large radius without stalling. At large radius the NFW mass profile diverges logarithmically, but the solutions are qualitatively similar to those in a Hernquist halo and we can see from Figure 5.2 that all shells that reach large radius tend to the same  $v(r)$ , regardless of the initial conditions.

#### 5.1.4 Dehnen & McLaughlin model haloes

The last specific non-isothermal dark matter profile we consider is that of Dehnen & McLaughlin (2005) which, in our dimensionless units, has the mass profile (§3.4.4)

$$\widetilde{M}_{\text{DM}} = \widetilde{M}_{\text{pk}} \left( \frac{20}{11} \right)^5 \left( \frac{\frac{11}{9} x^{4/9}}{1 + \frac{11}{9} x^{4/9}} \right)^5 \equiv \widetilde{M}_{\text{pk}} m(x) \quad (5.16)$$

In the limit of small radius  $m(x) \rightarrow (20/9)^5 x^{20/9}$ . From equation (5.8) with  $A = (20/9)^5$  and  $p = 20/9$ , the velocity field of the shell tends to

$$\widetilde{v}^2 \rightarrow C \left( \frac{9}{20} \right)^{10} x^{-40/9} - \frac{36 \widetilde{M}_{\text{BH}}}{31 \widetilde{M}_{\text{pk}}} \frac{(6\gamma - 43/9)}{(3\gamma - 16/9)} x^{-1}, \quad (x \ll 1) \quad (5.17)$$

which, as in the Hernquist and NFW haloes, is the initial condition we use in our numerical integration of equation (5.3) for Dehnen & McLaughlin (2005) haloes.

Figure 5.3 shows the velocity fields that satisfy equation (5.3) for the dark matter profile of Dehnen & McLaughlin (2005) with  $\widetilde{M}_{\text{pk}} = 4000$ . As previously, each panel shows solutions with  $\widetilde{v}_{\text{w}} = 45$ ,  $\widetilde{M}_{\text{BH}} = 0.01, 0.06$  and  $0.49$  and for a range of  $C$  values

Figure 5.3 is similar to Figures 5.1 and 5.2. The left panel, which has  $\widetilde{M}_{\text{BH}} \widetilde{v}_{\text{w}} = 0.45$  shows many solutions that stall at finite radius. Those with small initial momenta are technically able to escape though their velocities are near zero for much of their evolution and it takes at least  $\sim 3 \times 10^9$  yrs to reach the peak of the rotation curve. It takes larger values of  $C$  to be able to escape with velocity much larger than zero at all radii in this case but this gives unphysically large velocities at small radii ( $v \sim 10^6 c$  at radii of order 1pc). The middle panel, with  $\widetilde{M}_{\text{BH}} \widetilde{v}_{\text{w}} = 2.7$ , shows that all shells are able to escape to large radius, though some come close to stalling. The right-hand panel

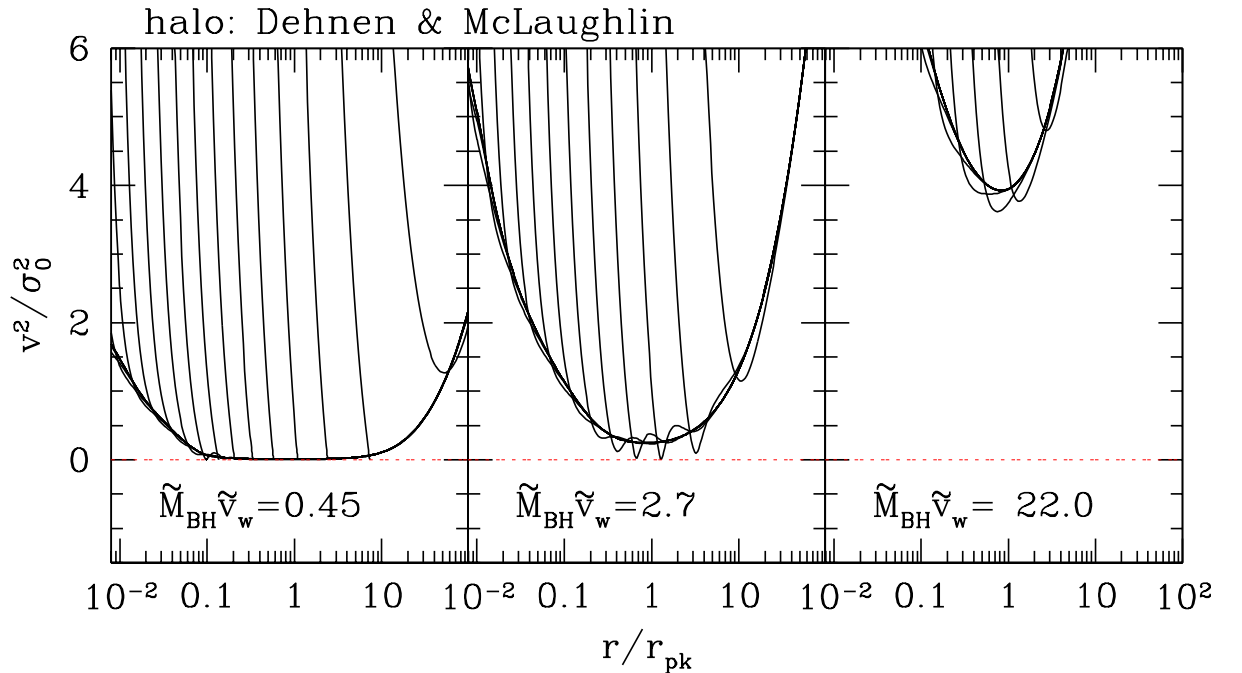


Figure 5.3: Velocity fields for energy-driven shells in a Dehnen & McLaughlin (2005) dark matter halo with a spatially constant gas fraction and  $\widetilde{M}_{\text{pk}} = 4000$ . Each panel shows solutions with  $\widetilde{M}_{\text{BH}} \widetilde{v}_w = 0.45$ , 2.7 and 22 and a range of initial momenta. In each case,  $\widetilde{v}_w = 45$ , corresponding to an outflow velocity of  $0.03 c$ , so that  $\widetilde{M}_{\text{BH}} = 0.01$ , 0.06 and 0.49. The radius unit  $r_{\text{pk}} \simeq 100\text{kpc}$ .

shows solutions with  $M_{\text{BH}} = 22$ , the critical case in an isothermal halo, and all shells are easily able to escape. Again, as in the Hernquist and NFW haloes, shells with small initial momenta have minimum velocities that are comparable to the large radius coasting speed of shells driven by the same  $\widetilde{M}_{\text{BH}} \widetilde{v}_w$  in an isothermal halo. These shells begin to accelerate close to the peak in the rotation curve though shells with larger initial momenta can start to accelerate at smaller radii.

In the limit of large radius in a Dehnen & McLaughlin (2005) halo,  $m(x) \rightarrow (20/11)^5$ . In the same way as with the Hernquist model halo, we find that at large

radius the shell velocity tends to

$$\tilde{v}^2 \longrightarrow \left[ \frac{6(20/11)^{10} \widetilde{M}_{\text{BH}} \tilde{v}_{\text{w}}}{2\gamma + 2/9} \right]^{2/3} x^{2/3}, \quad (x \gg 1) \quad (5.18)$$

which again is independent of the initial conditions.

## 5.2 Wind speeds and the $M$ – $\sigma$ relation

In all three of the specific haloes we considered above we found that energy-conserving feedback can be driven to escape with  $\widetilde{M}_{\text{BH}} \tilde{v}_{\text{w}} \sim 2.7$ , giving an  $M$ – $\sigma$  relation of the form

$$\left( \frac{M_{\text{BH}}}{10^8 M_{\odot}} \right) \left( \frac{v_{\text{w}}}{c} \right) \simeq 8.20 \times 10^{-3} \frac{1}{\tau} \left( \frac{f_0}{0.2} \right) \left( \frac{\sigma}{200 \text{ km s}^{-1}} \right)^5, \quad (5.19)$$

which is a factor  $\sim 8$  below the relation we derived for energy-driven outflows in isothermal haloes, if  $\sigma_0 = V_{\text{c,pk}}/\sqrt{2}$ .

In the same manner as Chapter 4, we can use equation (5.19) to infer the wind speeds a sample of now quiescent galaxies would have had during an active phase. Applying equation (5.19) to the 51 galaxies in the Gültekin et al. (2009) sample gives a distribution of wind speeds with a median of  $\sim 0.004c$ , which is about an order of magnitude below the median in the isothermal case.

As in the analyses of Chapters 3 and 4, these results are for time-independent winds from black holes. A black hole mass and wind speed of  $\widetilde{M}_{\text{BH}} \tilde{v}_{\text{w}} \sim 2.7$  is able to drive an energy-conserving shell to escape, but it takes a considerable amount of time to drive the shell from the halo, during which the black hole mass is growing. This means that the black hole mass observed in a now quiescent galaxy is expected to be larger than the mass that originally drove the shell to escape, i.e., larger than the “critical” mass in equation (5.19), which with the corresponding wind speed, allows for the escape of energy-conserving feedback.

By integrating  $v(r)$  to find  $r(t)$  for a shell driven by  $\widetilde{M}_{\text{BH}} \tilde{v}_{\text{w}} = 2.7$ , we find the time it takes a shell to reach the peak of the rotation curve, which is approximately

where a shell with a small initial momentum (i.e., small  $C$ ) starts to accelerate, is  $\sim 7 \times 10^7$  yrs. This is equivalent to  $\sim 1.5$  Salpeter times so that the black hole mass has grown by a factor  $\sim e^{1.5} \simeq 4.5$  when the shell begins the acceleration that allows it to escape. We note that the time it takes an energy-driven shell to reach  $r_{\text{pk}}$  is much shorter than a momentum-conserving shell driven by the same black hole mass, which takes  $\sim 7 - 8$  Salpeter times to reach the same radius in the halo.

In the momentum-driven case, the growth of the black hole throughout the motion of the shell implies that the  $M$ - $\sigma$  relation derived in that case is a lower limit to observed relations, as the black hole could grow up to a factor  $\sim e^{7-8}$  times more massive when the shell escapes. As discussed in §3.5.2, this difficulty could be compensated for by two effects: 1) if black holes grow from much smaller seeds than a momentum-driven shell may already be at large radius when the black hole reaches the critical mass, and 2) if the shell transitions to an energy-driven phase, the thermal expansion of the shocked wind will cause the shell to accelerate, reducing the time it takes to escape.

In the energy-driven case we have to consider the dependence of the  $M$ - $\sigma$  relation on the wind velocity. If the black hole has grown a factor  $\sim e^{1.5}$  times more massive than the critical mass by the time the shell escapes, then applying equation (5.19) directly to the observed black hole masses and velocity dispersions of Gültekin et al. (2009) leads to smaller inferred wind speeds. If we say the black holes in the Gültekin et al. sample have grown a factor of  $\sim 5$  above the critical black hole mass then the wind speeds inferred by equation (5.19) would be a factor of  $\sim 5$  higher, giving a median wind speed of  $\sim 0.02 c$  which is comparable to observed wind speeds in local AGN ( $v_w \sim 0.1 c$  Tombesi et al. 2011;  $v_w \sim 0.056 c$  Gofford et al. 2013).

These considerations highlight the need for a fully time-dependent treatment of the self-regulated feedback scenario so that the SMBH can be allowed to grow and the corresponding increase in kinetic energy flux of the wind (recall  $\dot{E} \propto M_{\text{BH}} v_w$ ) can be included in the equation of motion of the shell.

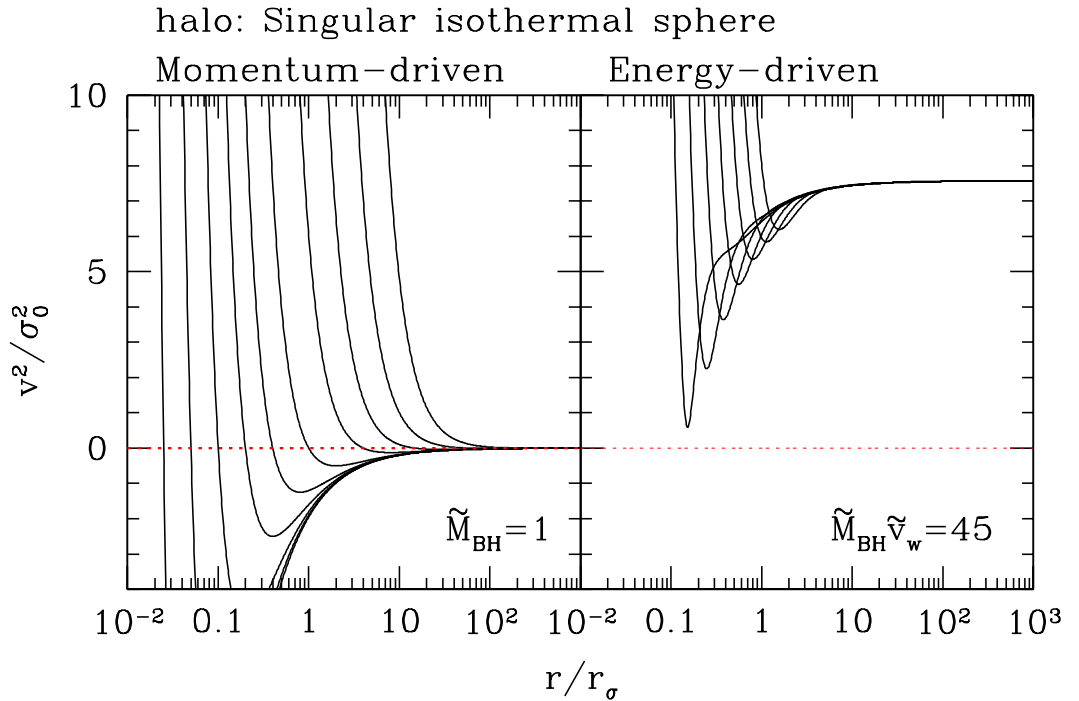


Figure 5.4: Velocity fields for momentum- (*left panel*) and energy-driven (*right panel*) shells in an isothermal halo for a range of initial momenta. In both cases  $\tilde{M}_{\text{BH}} = 1$  and for the energy-driven outflows  $\tilde{v}_w = 45$ , corresponding to a wind speed of  $\sim 0.03c$  for  $\sigma_0 = 200 \text{ km s}^{-1}$ . The radius unit  $r_\sigma \sim 50 \text{ pc}$  in a halo with  $\sigma_0 = 200 \text{ km s}^{-1}$ .

### 5.3 Momentum and energy-driven outflows

As discussed in Chapter 2, it is generally expected that an initially momentum-driven shell will transition to an energy-driven regime. The idea behind a transition in an isothermal halo is that it will cause the momentum-driven shell to accelerate to the higher coasting speed of an energy-driven shell. This could help to alleviate the difficulty identified by Silk & Nusser (2010) of driving the shell to the escape speed of an isothermal halo, which requires a black hole three times more massive than the critical  $M_\sigma$  mass.

The latter issue is partly resolved by considering outflows in non-isothermal haloes. As we saw in Chapter 3, momentum-driven outflows in non-isothermal haloes will always accelerate if they can reach large radius without stalling and eventually exceed the escape speed of the halo. However, as a transition is expected, it is still of interest to consider the effects it could have on the  $M$ - $\sigma$  relations.

First, we look briefly at the plausibility of a transition in an isothermal halo when the black hole is at the  $M_\sigma$  mass, which is the scenario envisioned by King et al. (2011) and Zubovas & King (2012). Figure 5.5 shows the momentum- (left panel) and energy-driven (right-panel) solutions for shells driven by  $\widetilde{M}_{\text{BH}} = 1$  and  $\widetilde{v}_w = 45$  in an isothermal halo.

As we know from Chapter 3, the coasting speed of a momentum-driven shell at large radius with  $\widetilde{M}_{\text{BH}} = 1$  is formally zero, so all solutions represent shells that stall at some finite radius. For a transition to be successful in this case the shell must become energy-driven before it stalls in the momentum-driven phase. For a wind speed of  $0.03c$ , the shell is only momentum-driven to  $r \lesssim 1 \text{ pc} \sim 0.02r_\sigma$  (equation [2.39]) and can transition to energy-driving at  $r \gtrsim 11 \text{ pc}$ , depending on the shell velocity. From our analysis in §3.5.1 we know that for a shell driven by  $\widetilde{M}_{\text{BH}} = 1$  to stall beyond  $r \sim 10 \text{ pc} \sim 0.2r_\sigma$  requires  $C > 0.4$ , several examples of which are shown in Figure 5.4. In these cases the shell could transition to an energy-driven phase where the large radius coasting speed is  $\widetilde{v}_\infty = 2.75$ , which is sufficient for the escape of the shell.

Thus, a transition to energy-driving when  $\widetilde{M}_{\text{BH}} = 1$  is possible and would allow the shell to reach the escape speed of an isothermal halo. Escape for smaller black hole masses would become increasingly more difficult as higher initial momenta would be required to keep the shell from stalling before the transition is made. For  $\widetilde{M}_{\text{BH}} \lesssim 0.49$ , escape would be impossible without black hole growth as the shell would not be able to reach the escape speed of the halo in the energy-driven phase. In non-isothermal haloes where both momentum- and energy-driven shells accelerate at large radius, this may not be a problem. As such, we now look at the possibility of transitions in non-isothermal haloes.

As discussed in Chapter 3 and above, the solutions to equations (3.25) and (5.3)

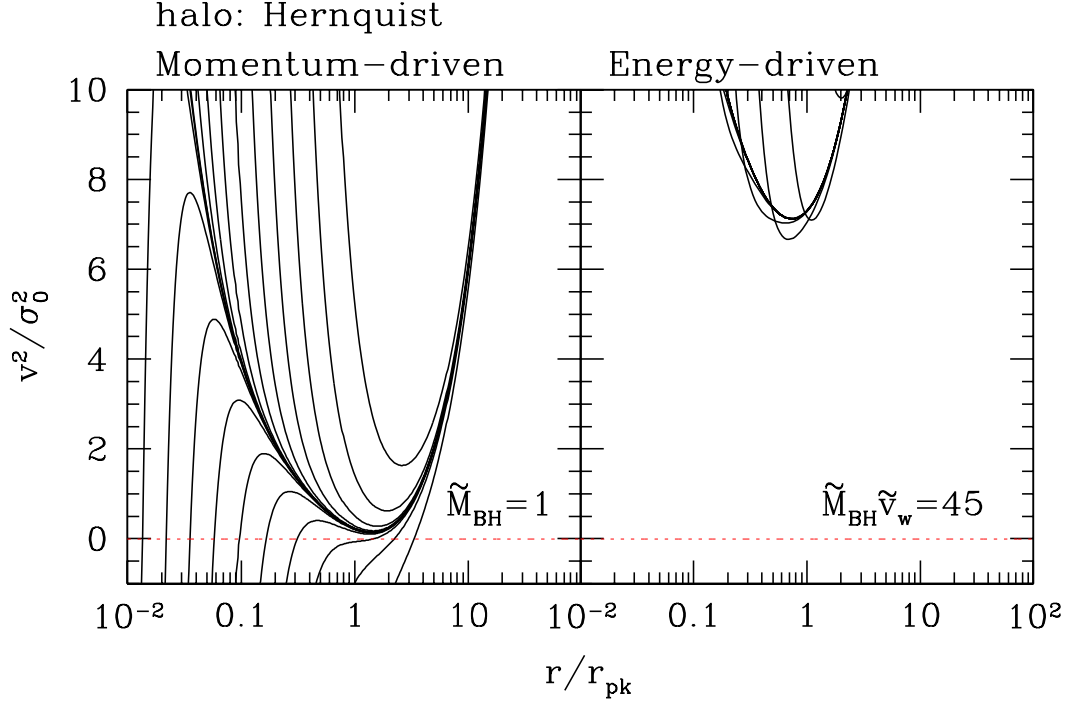


Figure 5.5: Velocity fields for momentum- (*left panel*) and energy-driven (*right panel*) shells in a Hernquist halo with  $\tilde{M}_{\text{pk}} = 4000$  for a range of initial momenta. In each case,  $\tilde{M}_{\text{BH}} = 1$  and for the energy-driven outflows  $\tilde{v}_w = 45$ , corresponding to a wind speed of  $\sim 0.03 c$  for  $\sigma_0 = 200 \text{ km s}^{-1}$ .

for the motion of momentum- and energy-driven shells are qualitatively similar in the different halo types that we consider. As such, in this discussion we shall use solutions in a Hernquist halo as an example.

We consider again the case of shells driven by a black hole mass  $\tilde{M}_{\text{BH}} = 1$  and wind speed  $\tilde{v}_w = 45$ . Figure 5.5 shows the velocity fields  $v^2(r)$  of momentum-driven shells (*left panel*) and energy-driven shells (*right panel*) in a Hernquist halo with  $\tilde{M}_{\text{pk}} = 4000$ .

We can see immediately that as in the case of outflows in an isothermal halo, the velocities of the momentum-driven shells are far below the energy-conserving shells driven by the same black hole mass. Thus, as in the isothermal case, a transition from

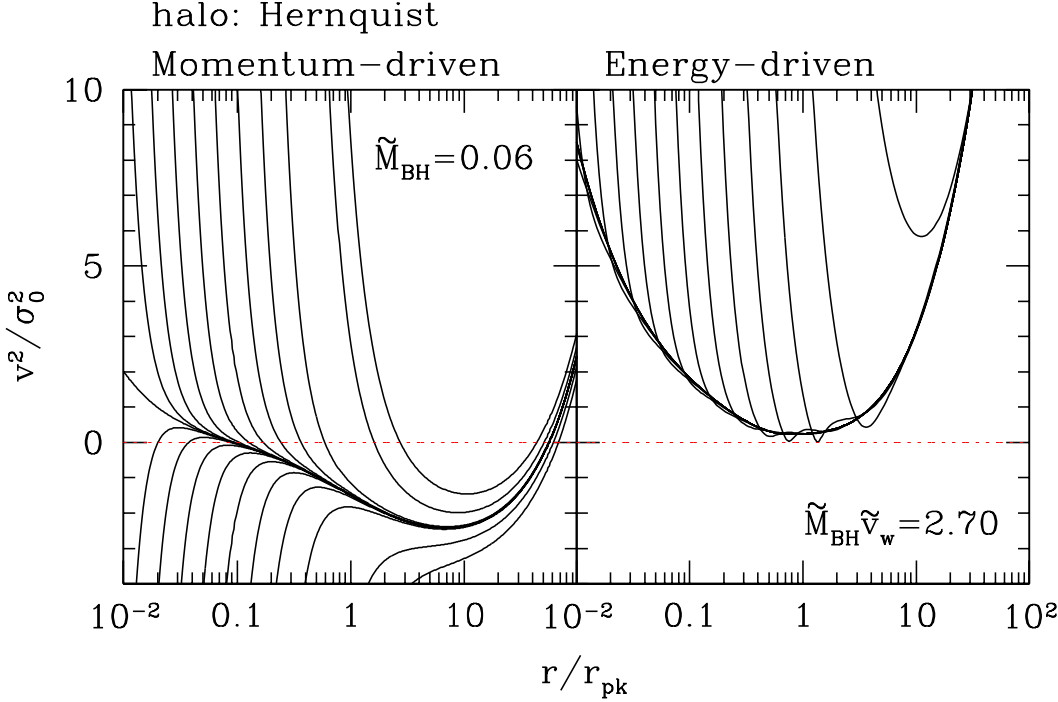


Figure 5.6: Velocity fields for momentum- (*left panel*) and energy-driven (*right panel*) shells in a Hernquist halo with  $\tilde{M}_{\text{pk}} = 4000$  for a range of initial momenta. In each case,  $\tilde{M}_{\text{BH}} = 0.06$  and for the energy-driven outflows  $\tilde{v}_w = 45$ , corresponding to a wind speed of  $\sim 0.03 c$  for  $\sigma_0 = 200 \text{ km s}^{-1}$ .

momentum- to energy-driving would cause the shell to accelerate. Though a transition is not necessary to ensure the escape of an initially momentum-driven shell in this case, as  $\tilde{M}_{\text{BH}} \simeq 1$  is sufficient to drive a momentum-conserving shell to escape in a halo with  $M_{\text{pk}} \gg M_\sigma$ , it would reduce the time it takes for the shell to escape the halo and thus reduce the amount by which the black hole can grow before the shell escapes.

In order to escape after a transition, the conditions for the escape of the shell during the energy-driven phase must be met. In non-isothermal haloes we found that the feedback can escape for  $\tilde{M}_{\text{BH}} \tilde{v}_w \simeq 2.7$ , which with  $\tilde{v}_w = 45$  corresponds to  $\tilde{M}_{\text{BH}} = 0.06$ . Figure 5.6 shows the momentum- (*left panel*) and energy-driven (*right panel*)

solutions in this case.

As we expect for  $\widetilde{M}_{\text{BH}} < 1$  in the momentum-driven case, the shells all stall at a finite radius. As in the isothermal case with  $\widetilde{M}_{\text{BH}} = 1$ , for the shell to escape the transition to energy-driving must occur before the shell stalls. The earliest stall occurs at  $\sim 0.1r_{\text{pk}} \sim 10 \text{ kpc}$ , which is well beyond the radius at which the shell becomes energy-driven (Chapter 2, equation [2.40]). It is therefore possible for an initially momentum-driven shell with  $\widetilde{M}_{\text{BH}} = 0.06$  to transition to an energy-driven regime that drives the shell to escape.

If the initial momentum-driven phase does set the  $M_{\text{BH}}-\sigma$  relation, as suggested by King (2005) and Zubovas & King (2012), then this would give

$$M_{\text{BH}} = 2.73 \times 10^7 M_{\odot} \left( \frac{f_0}{0.2} \right) \left( \frac{\sigma_0}{200 \text{ km s}^{-1}} \right)^4 \quad (5.20)$$

which is a factor  $\sim 4-5$  below the  $M_{\text{BH}}-\sigma$  relation of Gültekin et al. (2009) in normalisation, and an order of magnitude below McConnell & Ma (2013) who find a steeper slope than Gültekin et al. As with the discussion above, we would expect a relation such as equation (5.20) to be a lower limit to the observed relation because we have not considered the growth of the black hole in the time it takes for the shell to escape and establish the  $M-\sigma$  relation.

## 5.4 Summary

We have looked at the effect on energy-driven outflows of relaxing the assumption that dark matter haloes are described by isothermal spheres.

In the isothermal case (Chapter 4), we found that shells that can reach large radius will coast at a finite speed. In the non-isothermal haloes discussed here, we find that the energy-driven shells that make it to large radius will accelerate. This is analogous to the case of momentum-driven shells, which coast at large radius in isothermal haloes and accelerate in non-isothermal haloes.

In each of the three specific non-isothermal haloes that we have considered

(Hernquist 1990; Navarro, Frenk & White 1996, 1997; Dehnen & McLaughlin 2005), with  $\widetilde{M}_{\text{pk}} = 4000$  we found that all energy-driven shells escape when  $M_{\text{BH}} v_w \simeq 2.7 f_0 \kappa V_{c,\text{pk}}^4 / (4\pi G^2)$  (equation [5.19]). Using this relation to infer black hole winds speeds for the galaxies in the Gültekin et al. (2009) sample gives a median wind velocity of  $v_w \sim 0.004 c$ , which is an order of magnitude below the median velocity found in the isothermal case (Chapter 4). However, it takes approximately 1.5 Salpeter times for the shell to reach the peak of the rotation curve where it begins to accelerate. This means the black hole mass grows by a factor of  $\sim 4 - 5$  by the time the shell escapes so observed black hole masses are that much larger than the mass that sets the  $M_{\text{BH}} - \sigma$  relation. This simple argument suggests that the wind speeds would be a factor  $\sim 4 - 5$  higher, i.e., a median of  $v_w \sim 0.02 c$ , than inferred by a direct application of equation (5.19) to the Gültekin et al. (2009) sample, which is in agreement with the median of observed wind speed distributions, as discussed in Chapter 4.

We have also discussed the effect of a transition from a momentum- to energy-driven outflow. We found that it may be possible for an initially momentum-conserving outflow driven by a black hole mass of just  $M_{\text{BH}} = 0.06 M_\sigma$  to escape if a transition to energy-driven occurs. By equation (2.40) from Chapter 2, the change to energy-driving would occur long before the shell stalls in the momentum-driven phase. With a wind speed  $v_w = 0.03 c$  and  $M_{\text{BH}} = 0.06 M_\sigma$ , the energy-driven phase would allow the shell to reach large radii and accelerate, eventually exceeding the escape speed of the halo. If the momentum-driven phase establishes the  $M_{\text{BH}} - \sigma$  relation (as suggested by King 2005; Zubovas & King 2012), then  $M_{\text{BH}} = 0.06 M_\sigma$  would give an  $M_{\text{BH}} - \sigma$  relation that is a factor of a few below the relation observed by Gültekin et al. (2009). The same time-dependent considerations discussed above imply that this would be a lower limit to the observed relation.

Both these points, the black hole growth and the transition scenario, highlight the need for a fully time-dependent treatment of the self-regulated feedback scenario, as we will discuss in Chapter 6.

## 6 Summary and Discussion

### 6.1 Summary

Most massive galaxies harbour supermassive black holes (SMBHs) at their centres while less massive galaxies are host to massive nuclear star clusters (NCs). As discussed in Chapter 1, the properties of these central massive objects (CMOs: either an SMBH or an NC) are observed to correlate with properties of their host galaxies. The main aim of this work has been theoretical derivations of the  $M_{\text{CMO}}-\sigma$  relation, a tight correlation observed between the CMO mass,  $M_{\text{CMO}}$ , and the stellar velocity dispersion,  $\sigma$ , of the the host galaxy spheroid (i.e., the bulge of a spiral galaxy or the whole of an elliptical galaxy).

We have looked in detail at the dynamics of swept-up shells driven from galaxy nuclei by steady winds from CMOs. In Chapter 2 we reviewed general outflow physics, which allowed us to address the question of whether outflows from CMOs are energy- or momentum-driven. We showed that in the case the CMO is an NC the outflow may be momentum-driven out to several tens of kiloparsecs in its host galaxy. Conversely, when the CMO is a black hole the outflow is initially momentum-driven but may quickly transition to an energy-driven regime which could dominate most of its evolution. As such, we have looked at the cases when the shell is purely momentum-driven and when the shell is purely energy-driven.

In Chapter 3 we looked at the  $M-\sigma$  relation that results from purely momentum-driven outflows, particularly applicable to NC driven outflows. Momentum-driven  $M-\sigma$  relations have been derived previously by several authors (e.g, Fabian 1999; King 2003, 2005; Murray et al. 2005; McLaughlin et al. 2006; Silk & Nusser 2010), though only in analytic detail in the case that the host galaxy is modelled as a singular isothermal sphere (SIS). Our main aim in this Chapter was to investigate the effect on the  $M-\sigma$  relation of relaxing the assumption that dark matter haloes are described by SISs.

We began by revisiting the case of a momentum-driven outflow in a galaxy mod-

elled as an SIS. We showed that in this case the shell tends to a constant coasting speed at large radii which is dependent on the CMO mass and the velocity dispersion of the halo. The large radius coasting speed is non-zero when the CMO is above the critical mass

$$M_{\text{crit}} = M_{\sigma} \equiv \frac{\kappa f_0}{\lambda \pi G^2} \sigma_0^4 \simeq 4.56 \times 10^8 M_{\odot} \lambda^{-1} \left( \frac{f_0}{0.2} \right) \left( \frac{\sigma_0}{200 \text{ km s}^{-1}} \right)^4, \quad (6.1)$$

where  $f_0$  is a fiducial gas fraction ( $\approx 0.2$ ),  $\sigma_0$  is the velocity dispersion that characterizes an SIS and the parameter  $\lambda \sim 1$  for SMBHs or  $\lambda \simeq 0.05$  for NCs. This is the same as the critical CMO mass that has been derived previously (King 2005; McLaughlin et al. 2006), which gives  $M_{\text{CMO}}-\sigma$  relations that lie a factor of a few above the observed relations. However, we showed that in a galaxy modelled as an isothermal sphere this critical mass is necessary but not sufficient to drive the swept-up shell to large radii, which also depends on the initial momentum of the shell when it is close to the CMO. Furthermore, for the large radius coasting speed of the shell to exceed the escape speed of a truncated isothermal halo actually requires  $M_{\text{CMO}} > 3M_{\text{crit}}$ , giving  $M_{\text{CMO}}-\sigma$  relations an order of magnitude above the observed relations, which is essentially the objection raised by Silk & Nusser (2010) to CMOs being the sole contributors in establishing the  $M-\sigma$  relations.

In more realistic dark matter haloes, which have a single peak in their circular speed curve,  $V_c^2(r) = GM_{\text{DM}}(r)/r$ , we found that if a momentum-driven shell can reach large radius without stalling, then it will accelerate and eventually exceed the escape speed of the halo, negating part of the problem with the SIS analysis. The CMO mass then needs to be large enough to drive the shell to the radius where it begins to accelerate. In any dark matter halo with a single peak in  $V_c^2(r)$ , *any* momentum-driven shell, regardless of the initial momentum, can be driven to escape when the CMO is above the critical mass

$$M_{\text{crit}} = M_{\sigma} \left[ 1 + \left( \frac{M_{\sigma}}{M_{\text{pk}}} \right) + \mathcal{O} \left( \frac{M_{\sigma}^2}{M_{\text{pk}}^2} \right) \right]. \quad (6.2)$$

The mass unit  $M_{\sigma}$  is now defined as

$$M_{\sigma} \equiv \frac{\kappa f_0}{\lambda \pi G^2} \frac{V_{\text{c, pk}}^4}{4}, \quad (6.3)$$

where  $V_{c,\text{pk}}$  is the peak value of the circular speed and  $M_{\text{pk}}$  is the mass of dark matter inside this peak. Unlike in the SIS case, this critical mass is by itself sufficient for the escape of any purely momentum-driven shell.

In the limit that  $M_{\text{pk}}$  is much larger than  $M_\sigma$ , equation (6.2) gives a relation between the CMO mass and the peak circular speed of the dark matter halo:

$$M_{\text{CMO}} = 1.14 \times 10^8 M_\odot \lambda^{-1} \left( \frac{f_0}{0.2} \right) \left( \frac{V_{c,\text{pk}}}{200 \text{km s}^{-1}} \right)^4, \quad (6.4)$$

which is within a factor of a few of correlations observed between  $M_{\text{CMO}}$  and the large-scale circular speed,  $V_{c,a}$ , which at large radius probes the distribution of dark matter that dominates the galaxy potential (Volonteri et al. 2011).

In Chapter 4 we considered purely energy-driven outflows from SMBHs, as an initially momentum-driven shell may transition to energy-driven at radii comparable to the sphere of influence of the black hole. We considered the case of energy-driven outflows in a galaxy modelled as an SIS and as in the momentum-driven case, we found that the shell coasts at a constant speed at large radii. By requiring the coasting speed to equal the escape speed from a truncated SIS, we found that the escape of the swept-up shell depends on the black hole mass, the velocity dispersion and the black hole wind speed as

$$[M_{\text{BH}} v_w]_{\text{crit}} = 22 \frac{\kappa f_0}{\pi G^2} \sigma_0^4, \quad (6.5)$$

where the equality holds for a ratio of the specific heats  $\gamma = 5/3$ .

We took a sample of quiescent early-type galaxies and bulges, from the compilation of Gültekin et al. (2009), with measured black hole masses and velocity dispersions and used equation (6.5) to infer the black hole wind speeds these galaxies would have had when they were active. We found a remarkable agreement between our distribution of black hole wind speeds and the distributions of wind speeds observed in local AGN. In particular, our median outflow velocity,  $v_w = 0.035c$ , is in good agreement with the medians of observed distributions,  $v_w = 0.05c$  for Gofford et al. (2013) and  $v_w = 0.1c$  for Tombesi et al. (2011).

In Chapter 5 we looked at the effect of relaxing the isothermal assumption for purely energy-driven outflows. As with momentum-driven outflows, we found that if an

energy-driven outflow in non-isothermal halo can reach large radii then it will accelerate and eventually exceed the escape speed of the halo. In the three specific haloes that we considered with  $M_{\text{pk}} = 4000 M_{\sigma}$  (suitable for a Milky Way sized halo) and  $\sigma_0 = V_{\text{c, pk}}/\sqrt{2}$ , we found that the feedback can escape when  $M_{\text{BH}} v_w \gtrsim 2.7 \kappa f_0 \sigma_0^5 / (\pi G^2)$ . If we apply the same process as in Chapter 4 to infer a distribution of wind speeds for the Gültekin et al. (2009) galaxies then we find a median wind speed of just  $0.004 c$ , which is an order of magnitude below the median in the isothermal case. We do expect this to be a lower limit because we have only considered time-independent outflows. By integrating to find  $r(t)$ , we found that it takes a shell driven by this black hole mass and wind speed  $\sim 1.5$  Salpeter times to reach the peak of the rotation curve where it begins to accelerate. The observed black hole mass would then be a factor  $\sim 4 - 5$  times larger than the mass that sets the  $M_{\text{BH}} - \sigma$  relation. Conversely, applying this escape condition directly to the Gültekin et al. (2009) sample results in smaller outflow velocities by the same factor of  $\sim 4 - 5$ .

We also discussed the effects of a transition from momentum- to energy-driving. In the case of outflows in an isothermal halo, the coasting speed in the energy-driven phase is higher than for a momentum-driven shell. A transition from momentum- to energy-driven would cause the shell to accelerate to the higher coasting speed. If the conditions in the energy-driven phase satisfy the escape criteria then the shell could escape.

In the non-isothermal case the shell will accelerate at large radii when momentum- or energy-driven but the same applies, the shell must satisfy the escape condition for energy-driven outflows when it has made the transition. The minimum black hole mass and wind speed that allow the escape of energy-conserving feedback in the haloes we have considered are  $M_{\text{BH}} = 0.06 M_{\sigma}$  and  $v_w = 0.03 c$ . We found that it is possible for a shell driven by a black hole mass  $M_{\text{BH}} = 0.06 M_{\sigma}$  to transition from momentum- to energy-driving before the shell stalls in its momentum-driven phase. The shell would then accelerate to the higher speed of an energy-driven outflow and eventually escape the halo. If the initial momentum-driven phase establishes the  $M_{\text{BH}} - \sigma$  relation, then  $M_{\text{BH}} = 0.06 M_{\sigma}$  gives an  $M_{\text{BH}} - \sigma$  relation a factor of a few below the relation compiled

by Gültekin et al. (2009). Again, we would again expect this to be a lower limit as we have not considered the growth of the black hole in the time it takes the shell to escape the halo.

## 6.2 Momentum- versus energy-driven outflows

We have considered the  $M$ - $\sigma$  relations that result from either purely momentum- or purely energy-driven outflows. We showed in Chapter 2 that for outflows driven by SMBH winds the shell is initially momentum-driven, as shown by King (2003), but that it can become energy-driven within tens of parsecs (cf. Zubovas & King 2012). In the NC case we found that the outflow is momentum-driven out to several tens of kiloparsecs, in the same way as McLaughlin et al. (2006). However, for either CMO type the radius inside which the shocked wind cools efficiently (equation [2.30] for NCs, equation [2.39] for SMBHs), and the radius at which the shell becomes energy-driven (equation [2.31] for NCs, equation [2.40] for SMBHs) are quite sensitive to the wind velocity.

In the black hole case, we calculated the radius where the shell becomes energy-driven using a shell speed of  $v_s \sim \sigma_0 \sim 200 \text{ km s}^{-1}$  and a wind speed of  $v_w = 0.03c$ , the median of our distribution of wind speeds inferred from the Gültekin et al. (2009) galaxies in Chapter 4, and found the shell is energy-driven beyond

$$r_s \simeq 11 \text{ pc} \left( \frac{v_s}{200 \text{ km s}^{-1}} \right)^{-1} \left( \frac{M_{\text{BH}}}{10^8 M_\odot} \right) \left( \frac{v_w}{0.03c} \right)^2 \left( \frac{v_e}{0.85c} \right)^2, \quad (6.6)$$

which is similar to the sphere of influence of a  $10^8 M_\odot$  black hole in a halo with velocity dispersion  $\sigma = 200 \text{ km s}^{-1}$ ,  $r_{\text{inf}} = GM_{\text{BH}}/\sigma^2 \simeq 10.8 \text{ pc}$ .

This radius is dependent on the wind speed and the inverse of the shell speed, so that a faster wind speed or slower shell speed would lead to the shell becoming energy-driven at a larger radius.

For example, Zubovas & King (2012) find that the shell becomes energy-driven at  $r \sim 520 \text{ pc}$  when the wind speed is  $\sim 0.1c$  and the shell velocity equals the momentum-

driven coasting speed of King (2003; equation [14],  $v_s = [G L_{\text{Edd}} / (2 f_0 \sigma_0^2 c)]^{1/2}$ , which is  $\sim 130 \text{ km s}^{-1}$  for  $M_{\text{BH}} = 10^8 M_{\odot}$  and  $\sigma = 200 \text{ km s}^{-1}$ ). The use of the momentum-driven coasting speed is not entirely appropriate because, before the shell becomes energy-driven, it goes through a partially radiative phase during which it conserves neither momentum nor energy (Koo & McKee 1992; Faucher-Giguère & Quataert 2012). We also note that the coasting speed from King (2003) does not include the gravitational effects of the dark matter. Zubovas & King (2012) also note that the radius where the shell becomes energy-driven is dependent on the wind velocity, which is observed to vary between  $\sim 0.03 c$  and  $\sim 0.2 c$  (e.g., Tombesi et al. 2011; Gofford et al. 2013), leading to variations between  $\sim 10 \text{ pc}$  and  $\sim 500 \text{ pc}$  from equation (6.6).

Due to the difference in cooling processes and a slower wind speed, in the nuclear cluster case the radius out to which the shocked gas cools efficiently and the radius where the shell becomes energy-driven are strongly dependent on the inverse of the wind velocity ( $r \propto v_w^{-6.5}$  and  $r \propto v_w^{-5.5} v_s^{-1}$  respectively), so faster wind speeds lead to the shell becoming energy-driven sooner.

With this in mind, it is important to consider the effect on the  $M$ - $\sigma$  relation of an outflow that switches from initially momentum-driven to an energy-driven regime.

A transition from a momentum- to energy-driven outflow has been invoked as a way of reducing the normalisation of the theoretical  $M$ - $\sigma$  relation from momentum-driven outflows in isothermal spheres, while preserving the  $M_{\text{CMO}} \propto \sigma^4$  scaling (King 2003, 2005; Power et al. 2012), though more recent compilations of the observed  $M$ - $\sigma$  relation for black holes favour a slope of  $\sim 5$  rather than  $\sim 4$  (McConnell & Ma 2013; see §6.3). For nuclear clusters, where the observed  $M$ - $\sigma$  relation has a slope closer to  $\sim 4$  (Ferrarese et al. 2006), such an effect could help to bring the theoretical relation more in line with observations.

The idea behind a transition is that when the CMO is at the critical mass that establishes the  $M$ - $\sigma$  relation (equation [6.1]), the switch to energy-driving causes the shell to accelerate to a higher speed because of the thermal expansion of the shocked wind region, which could drive the shell to escape.

We have found that energy-driven shells have velocities higher than momentum-conserving shells driven by the same black hole mass. For example, in an SIS a momentum-driven shell will coast at  $2\sigma_0$  when the black hole has a mass  $3M_\sigma$ , whereas an energy-conserving shell driven by the same black hole mass and a wind speed  $v_w = 45\sigma_0$  will coast at  $\sim 4.23\sigma_0$ .

Furthermore, during the momentum-driven phase a CMO with a mass less than  $M_{\text{crit}}$  could drive the shell to the radius where the transition occurs. Then the switch which causes the shell to accelerate and escape occurs for a CMO mass less than  $M_{\text{crit}}$ , hence reducing the normalisation of the predicted  $M$ - $\sigma$  relation. The switch to energy-driving and acceleration of the shell to a higher coasting speed could also help overcome the fact that a CMO mass  $\geq 3M_{\text{crit}}$  is required to drive a momentum-driven shell to a coasting speed that equals (or exceeds) the escape speed of an isothermal halo.

One caveat with this scenario is that after the transition the CMO mass and wind speed must be sufficient to drive the energy-conserving shell to escape. As we showed in Chapter 4, energy-driven shells coast at a constant speed at large radius in isothermal dark matter haloes. If the product of CMO mass and wind speed is too small,  $< 22f_0\kappa\sigma^5/(\pi G^2)$  (equation [6.5]), then even with a transition to energy-driving the shell will not reach the escape speed of a truncated isothermal sphere. For a wind speed of  $0.03c$ , this corresponds to a CMO mass  $\simeq 0.49M_\sigma$ . If the CMO mass in the momentum-driven phase were less than this, then after a transition the shell would still not be able to achieve the escape velocity of the halo. Moreover, during the momentum-driven phase we know that all shells driven by this mass would stall (see §3.3), and those with initial momenta near zero could stall before the transition occurs. Interesting though,  $M_{\text{BH}} = 0.5M_\sigma$  gives an  $M$ - $\sigma$  relation that is very close to the observed relation of Gültekin et al. (2009).

Part of this issue could be resolved by considering shells that are driven into non-isothermal haloes. Whether momentum- or energy-driven, if a shell can reach large radius in a non-isothermal halo without stalling it will always accelerate and eventually exceed the escape speed of the halo. Then the shell just has to transition to energy-driven before it stalls.

In Chapter 5, we looked at the momentum- and energy-driven solutions for shells driven by the same black hole mass into a non-isothermal halo. We found that as in the isothermal case, the velocity of an energy-driven shell is much higher than a momentum-driven shell driven by the same black hole mass. In the non-isothermal haloes that we considered (Hernquist 1990; NFW; Dehnen & McLaughlin 2005; all with  $M_{\text{pk}} = 4000 M_\sigma$ ), energy-driven feedback can escape with  $M_{\text{BH}} = 0.06 M_\sigma$  and  $v_w = 45\sigma_0$ . We found that momentum-driven shells would reach the radius at which they transition to energy-driven before they would stall. Thus momentum-driven feedback from a black hole with a sub-critical mass could still escape if the transition to energy-driven occurs.

It is unclear in this scenario how long the outflow has to be momentum-driven to preserve the  $M_{\text{CMO}} \propto \sigma^4$  scaling that results from purely momentum-driven outflows, which is perhaps appropriate to the nuclear cluster case (see also §6.3). If, as we have found, nuclear cluster driven outflows are momentum-conserving to radii of several tens of kiloparsecs, i.e., beyond the effective radius inside which  $\sigma$  is measured, then we would expect  $M_{\text{NC}} \propto \sigma^4$  as momentum-driving dominates the evolution of the outflow. We recall that the radius at which a shell driven by a nuclear star cluster becomes energy-driven is

$$r_s \simeq 70 \text{ kpc} \left( \frac{\lambda}{0.05} \right) \left( \frac{M_{\text{CMO}}}{10^8 M_\odot} \right) \left( \frac{v_w}{300 \text{ km s}^{-1}} \right)^{-5.5} \left( \frac{v_s}{200 \text{ km s}^{-1}} \right)^{-1} \left( \frac{Z}{Z_\odot} \right)^{0.6}. \quad (6.7)$$

If the wind speed is higher than our fiducial value of  $300 \text{ km s}^{-1}$ , then the outflow becomes energy-driven at a smaller radius, for example, if  $v_w \sim 500 \text{ km s}^{-1}$  then the outflow is energy-driven beyond a radius of  $\sim 1.5 \text{ kpc}$ , for  $v_w \sim 800 \text{ km s}^{-1}$  the outflow is energy-driven for  $r \gtrsim 75 \text{ pc}$ . Given this, it is not immediately obvious which phase of feedback dominates the evolution of an outflow driven by a nuclear cluster and hence sets the  $M_{\text{NC}}-\sigma$  scaling.

We found that outflows from black holes can be momentum-driven inside  $\sim 0.26 \text{ pc}$  and can become energy-driven at  $\sim 11 \text{ pc}$ , which is of the order of the sphere of influence of a  $10^8 M_\odot$  black hole in a halo with velocity dispersion  $200 \text{ km s}^{-1}$ . In this case, we presume energy-driving will dominate the evolution of the outflow resulting in

an  $M$ - $\sigma$  relation where  $M \propto \sigma^5$ , which is in better agreement with the most recently compiled  $M_{\text{BH}}$ - $\sigma$  relation. However, if the wind speed is higher then the shell becomes energy-driven at a larger radius, such as the case considered by Zubovas & King (2012) who find the shell is momentum-driven inside  $\sim 500$  pc when the wind speed is  $\sim 0.1 c$ .

If we consider a galaxy with an effective radius  $r_e \sim 2$  kpc, which is the radius inside of which  $\sigma$  is measured, that is described as an isothermal halo, the gas mass inside this radius is  $\sim 7 \times 10^9 M_\odot$ . If the shell becomes energy-driven at  $r = 11$  pc (as for  $v_w = 0.03 c$ ) then the shell mass is  $\sim 4 \times 10^7 M_\odot$ , which is only 0.5% of the mass inside the effective radius. If the shell becomes energy-driven at the larger radius of  $r = 120$  pc (as for  $v_w = 0.1 c$ ) then the shell mass at the transition is 6% of the mass inside the effective radius. In either case, most of the gas will be swept-up when the shell is energy-driven, which will presumably have an effect on the observed  $M_{\text{BH}}$ - $\sigma$  relation. In the nuclear cluster case with  $v_w = 300 \text{ km s}^{-1}$ , all of the mass inside  $r_e$  would be swept-up during a momentum-driven phase, leading to  $M_{\text{NC}} \propto \sigma^4$ .

As discussed in Chapter 5, if a shell driven by a black hole quickly transitions to an energy-conserving regime, it takes  $\sim 1.5$  Salpeter times for the shell to reach the peak of the rotation curve where it begins the acceleration that allows it to escape. During this time the black hole would grow a factor  $\sim 4 - 5$  times more massive, meaning  $\sim 80\%$  of its mass is gained during an energy-driven phase. This could mean that energy-driving is the dominant feedback mechanism and the  $M_{\text{BH}} \propto \sigma^4$  scaling from the initial momentum-driven phase may not be preserved.

Silk & Nusser (2010) object to a transition from momentum- to energy-driven outflows based on their own analysis of the cooling rate of the shocked wind region. They note that if momentum-driven feedback from the black hole alone is to clear the galaxy of gas, the resulting  $M_{\text{BH}}$ - $\sigma$  relation is an order of magnitude above the observed relation. They propose that additional momentum input from star formation triggered by the outflow is the key to establishing the  $M$ - $\sigma$  relation. However, as noted by several authors (e.g., Zubovas & King 2012), Silk & Nusser appear to have calculated the cooling rate of the shocked ambient material using the cooling function of Sutherland & Dopita (1993), which we used to calculate the cooling rate of the shocked

wind in the nuclear cluster case. This cooling function, which includes various atomic process but no relativistic effects (see §2.3.1) extends to temperatures  $\sim 10^7 - 10^8$  K. This is below the shock temperature in the black hole case ( $T \sim 10^9$  K, equation [2.32]), so such a cooling function may not be suitable in this case. Even so, it is still important to note that additional sources of momentum input, such as positive feedback from star-formation which could be triggered by the outflow, could be an effective way of reducing the normalization of the  $M-\sigma$  relation.

In a more detailed analysis of the cooling of high velocity shocked winds in AGN, Faucher-Giguère & Quataert (2012) show that the electrons and protons can be decoupled for long enough timescales that the shocked material actually forms a two-temperature plasma which greatly effects the cooling rate. As long as the shocked gas does not become substantially mixed with cooler gas, Faucher-Giguère & Quataert find that inverse Compton scattering is the dominant cooling process, though the electron energy is lower than we assumed in Chapter 2 (cf. King 2003) because of the two-temperature effects. They find that the cooling time can be longer by a factor of  $\gtrsim 10 - 100$  compared to if the electrons and protons have the same temperature at all times. This suggests that the cooling of the shocked wind is less efficient than we have assumed and thus that the outflow becomes energy-driven at even smaller radii than we found.

Faucher-Giguère & Quataert (2012) show that the cooling is inefficient in a wide range of circumstances (varying wind velocities and the density of the ambient medium), meaning energy-driving may be the dominant form of feedback in more scenarios than previously thought.

### 6.3 Observed $M-\sigma$ relations

The question of whether it is momentum- or energy-driven feedback that establishes the  $M-\sigma$  relation couples with the discussion of the slope of the observed relations.

The most recent compilation of the  $M_{\text{NC}}-\sigma$  relation by Scott & Graham (2013)

suggests that nuclear clusters follow a much shallower relation than the  $M_{\text{NC}} \propto \sigma^{4.27 \pm 0.61}$  found by Ferrarese et al. (2006). Scott & Graham suggest a relation of the form  $M_{\text{NC}} \propto \sigma^{2.11 \pm 0.31}$  which does not seem to fit with the theoretical  $M$ – $\sigma$  relations that result from either momentum- or energy-driven feedback. However, the Scott & Graham sample, which builds on that of Ferrarese et al. (2006), includes several galaxies that also host SMBHs. The masses of these black holes fall within the data that define the  $M_{\text{BH}}$ – $\sigma$  relation of McConnell & Ma (2013). In these cases, we suggest it is the mass of the dominant component (if not the sum of black hole and nuclear cluster masses) that needs to be considered for the  $M$ – $\sigma$  relation. We discuss this further in §6.5.

In the black hole case Gültekin et al. (2009) report  $M_{\text{BH}} \propto \sigma^{4.24 \pm 0.41}$ , which seems in line with the  $M$ – $\sigma$  relation that results from momentum-driven feedback, though we noted in Chapter 4 (equation [4.17]) that energy-driven outflows can imply an  $M_{\text{BH}}$ – $\sigma$  relation with a slope less than 5 if  $M_{\text{BH}}$  and  $v_w$  are correlated by even a very weak power. More recently, with a larger sample including several updated masses from the Gültekin et al. (2009) sample, McConnell & Ma (2013) found the much steeper  $M_{\text{BH}} \propto \sigma^{5.64 \pm 0.32}$ , which seems to favour the energy-driven scenario.

Zubovas & King (2012) suggest that there are actually three different  $M_{\text{BH}}$ – $\sigma$  relations for different galaxy types in different environments. The three relations correspond to spiral galaxies with evolved bulges, ellipticals in cluster centres and field ellipticals. Their results also imply a fourth  $M_{\text{BH}}$ – $\sigma$  relation for cluster spirals, though they note that such galaxies are expected to be rare due to high merger probabilities. Each of these  $M_{\text{BH}}$ – $\sigma$  relations has a slope  $\sim 4$  but each has a slightly different normalisation.

Figure 6.1 shows the  $M_{\text{BH}}$ – $\sigma$  relation of McConnell & Ma (2013) and the short-dashed (blue) lines show the four separate  $M_{\text{BH}}$ – $\sigma$  relations proposed by Zubovas & King (2012) which are for (from top to bottom) cluster ellipticals, field ellipticals, cluster spirals and field spirals.

The effect of combining of these individual  $M$ – $\sigma$  relations may be to increase the slope of the observed relation, though the exact slope would depend on the numbers of galaxies in each group.

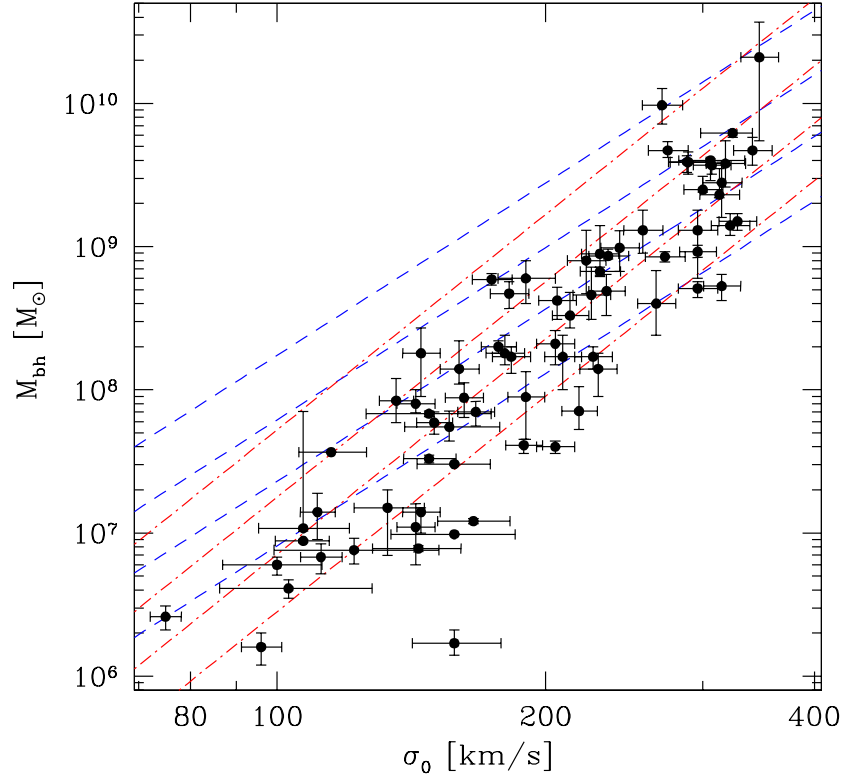


Figure 6.1: The points show the data that define the  $M_{\text{BH}}-\sigma$  relation of McConnell & Ma (2013). The short-dashed (blue) lines show the four  $M_{\text{BH}}-\sigma$  relations suggested by Zubovas & King (2012), which from top to bottom represent cluster ellipticals, field ellipticals, cluster spirals and field spirals. The dot-dashed (red) lines show our  $M_{\text{BH}}-\sigma$  relation for energy-driven outflows in an isothermal halo with  $v_w = 0.03c$  [equation (6.5)] for the same galaxy types and environments considered by Zubovas & King (2012).

McConnell & Ma (2013) do consider the  $M_{\text{BH}}-\sigma$  relations for the sub-samples of early- and late-type galaxies and they find that the black hole masses in the early-type galaxies are about two times more massive than in late-type galaxies at the same velocity dispersion, as suggested by Zubovas & King (2012). However, for each of the early- and late-type galaxies they find  $M_{\text{BH}} \propto \sigma^{5.20 \pm 0.36}$  and  $M_{\text{BH}} \propto \sigma^{5.01 \pm 1.16}$ , which is steeper than the relations suggested by Zubovas & King (2012).

The  $M_{\text{BH}} \propto \sigma^4$  relations of Zubovas & King (2012) are established by an initial momentum-driven phase of the outflow, as discussed above. The different intercepts in their relations come from two considerations. First is the consequence of a major merger which can trigger star-formation and a burst of quasar activity which could clear the remaining gas from galaxy so it becomes a red-and-dead elliptical. They find it takes approximately 2 Salpeter times to clear the gas after a merger, meaning the black hole mass can grow to  $\sim 7.5M_\sigma$  in these galaxies. The second is the result of either gas depletion from star-formation or gas replenishment in galaxy clusters. Both of these affect the gas fraction,  $f_0$ , in the galaxy, which affects the normalisation of the resulting  $M_{\text{BH}}-\sigma$  relations. Zubovas & King estimate that gas depletion by star-formation leads to a gas fraction a factor  $\sim 2.5$  below that cosmic value  $f_0 = 0.16$ . This implies that in field spiral galaxies, where internal gas depletion dominates, we might expect the black hole mass to be a factor  $\sim 2.5$  lower than the predicted value. In the cluster environment, Zubovas & King suggest that gas replenishment from cooling flows can balance the depletion from star formation at gas fractions  $\sim 0.2$ , preserving the predicted value of the  $M-\sigma$  relation.

None of these considerations is dependent on the outflow being momentum-driven. If the outflow quickly transitions to an energy-driven phase each of these effects could result in three (possibly four)  $M_{\text{BH}}-\sigma$  relations with slopes of  $\sim 5$ , as shown by the dot-dashed (red) lines in Figure 6.1, which again from top to bottom represent cluster ellipticals, field ellipticals, cluster spirals and field spirals. These relations are closer to those found by McConnell & Ma (2013) for the sub-samples of early- and late-type galaxies, and they could combine to give a relation steeper than 5, again in agreement with McConnell & Ma.

## 6.4 Galaxy outflows

In our analysis we have focussed on the scaling relations that result from momentum- or energy-conserving feedback from CMOs. Recent observations show that AGN can

also drive galaxy-scale outflows, which can be connected to the self-regulated feedback scenario.

Such large-scale outflows are observed to have velocities of  $\sim 1000 \text{ km s}^{-1}$  at radii of  $\sim 2 - 3 \text{ kpc}$  (e.g., Rupke & Veilleux 2011). In simulations of major mergers Debuhr, Quataert & Ma (2012) study the effects on the host galaxy of AGN winds. With an initial wind velocity of  $\simeq 10000 \text{ km s}^{-1} = 0.03 c$ , they find that the wind sweeps up the ambient gas leading to a large-scale outflow with a velocity of  $\sim 1000 \text{ km s}^{-1}$ .

As discussed above, it is generally agreed that at large radii the shells driven by AGN feedback are energy-conserving. In Chapter 4 we showed that energy-driven shells in an isothermal halo will coast at a constant speed at large radius. If the product of the black hole mass and black hole wind speed is high enough then such shells can be driven to escape the halo, resulting in a galaxy-scale outflow which could be linked to the observed large-scale outflows. For energy-driven outflows in an isothermal halo with  $\sigma_0 = 200 \text{ km s}^{-1}$  to have velocities of  $\sim 1000 \text{ km s}^{-1}$  on kiloparsec scales requires  $M_{\text{BH}} v_w \simeq 200 M_\sigma \sigma_0$  (from  $\tilde{v}_\infty = 5$  in equation [4.13]). For a wind speed of  $0.03 c$ , this implies a black hole mass of  $M_{\text{BH}} \sim 4 M_\sigma$ , or for a higher wind speed of  $0.1 c$ ,  $M_{\text{BH}} \sim 1.5 M_\sigma$ . If the large-scale outflow were momentum-driven, to reach a large radius velocity of  $\sim 1000 \text{ km s}^{-1}$  in an isothermal halo would require  $M_{\text{BH}} \sim 12 M_\sigma$  (equation [3.12]).

Energy-driven shells in a non-isothermal halo will accelerate at large radius if they can avoid stalling and will eventually exceed the escape speed of the halo. This again would result in a galaxy-scale outflow which could be linked with observations. At radii of the order a few kpc, energy-driven outflows in non-isothermal haloes have not begun the acceleration that allows them to escape but could have velocities of  $\sim 1000 \text{ km s}^{-1}$  (see e.g., Figure 5.1). Whether a such a shell would escape or stall at some large radius in the halo depends on the value of  $M_{\text{BH}}$  and  $v_w$  that drive the shell.

King et al. (2011) note that when these massive outflows are observed there is often little or no AGN activity (e.g., Tremonti, Moustakas & Diamond-Stanic 2007). In order to understand the connection between the massive outflow and its possible origin, King et al. looked in detail at the behaviour of an energy-driven shell when the

AGN switches off. They consider an energy-driven shell in an isothermal halo that is driven by a black hole at the critical  $M_\sigma$  mass (equation [6.1]). After  $10^6$  yrs the AGN switches off and the shell is driven outwards by the residual thermal pressure in the shocked wind region. King et al. find the shell can expand for  $\sim 10$  times longer than the original driving time, which could explain why massive outflows are sometimes observed when there is little nuclear activity.

If the residual pressure in the shocked gas were insufficient to drive the shell, it could stall at large radius in the galaxy halo. This could provide an explanation for large gas reservoirs observed at large radii in galaxies (e.g., Tumlinson et al. 2011) and gas reservoirs seen in simulations (e.g., Stinson et al. 2012), a point noted by Sharma & Nath (2013).

Sharma & Nath (2013) consider winds driven by energy and mass injection from multiple supernovae, as well as momentum injection due to radiation from a central black hole. They only include momentum input from the black hole and they do not include cooling of the wind in their analysis. Sharma & Nath consider energy/momentum injection for a central region, which for the SNe winds could be connected to a nuclear cluster. They do note that other star clusters distributed throughout the galaxy would provide additional momentum input, though modelling the additional feedback is beyond the scope of their work.

They find that the feedback from supernovae and AGN operate effectively in low and high mass galaxies respectively. In an intermediate mass range ( $10^{11.5} - 10^{12.5} M_\odot$ ) winds from quiescent star forming galaxies cannot escape but are still driven to large radius in the halo. As noted above, this could provide an explanation for large gas reservoirs observed at large radii in galactic haloes.

## 6.5 Co-existing SMBHs and NCs

In Chapter 1 we presented the observed  $M-\sigma$  relations for black holes and nuclear star clusters (Figure 1.3). The nuclear clusters from Ferrarese et al. (2006) follow a

similar but offset relation to the  $M$ - $\sigma$  relation defined by the most recent black hole compilation of McConnell & Ma (2013). When including the nucleated galaxies from Scott & Graham (2013), the slope of the  $M_{\text{nc}}-\sigma$  relation becomes much shallower, with  $M_{\text{NC}} \propto \sigma^{2.11 \pm 0.31}$ . A relation of this form does not seem to fit with either the momentum- or energy-driven scenarios that we have considered. However, as we noted in Chapter 1 (§1.1.3), several of the galaxies from the Scott & Graham sample also harbour SMBHs in their nuclei.

Figure 6.2 shows the  $M$ - $\sigma$  relations for SMBHs (McConnell & Ma 2013; filled grey circles, solid grey line) and for the nuclear clusters of Ferrarese et al. (2006; open grey circles, dotted grey line). The (red) squares show the galaxies of Scott & Graham (2013) that host both a nuclear cluster and an SMBH. The open (red) squares show the masses of the nuclear clusters that appear to reduce the slope of the  $M_{\text{nc}}-\sigma$  relation from  $\sim 4$  to  $\sim 2$ . However, the black holes masses in these galaxies, shown by the filled (red) squares, fall amongst the data that define the black hole  $M$ - $\sigma$  relation of McConnell & Ma (2013).

This raises the question of whether it is the nuclear cluster, the black hole or the combination of the two that sets the  $M$ - $\sigma$  relations in these galaxies where the two types of CMO co-exist.

In their analysis of the  $M_{\text{NC}}-\sigma$  relation in isothermal haloes, McLaughlin et al. (2006) address the point that nuclear clusters are rarely observed in massive galaxies. They argue that in the self-regulated feedback scenario the shell must become energy-driven before it reaches the virial radius of the galaxy so that it can accelerate and escape. They find  $R_{\text{vir}} \approx 540 \text{ kpc} (1+z)^{-1.1} (\sigma/200 \text{ km s}^{-1})$  from the relations of Bryan & Norman (1998), which when combined with the radius at which the shell becomes energy driven (equation [6.7]) implies that this only works for nuclear clusters in haloes with  $\sigma \lesssim 160 \text{ km s}^{-1}$ . For typical nuclear clusters that are  $\sim 5 \text{ Gyr}$  old,  $z = 0.5$  and this becomes  $\sigma \lesssim 130 \text{ km s}^{-1}$ . In isothermal haloes with velocity dispersions higher than this a shell driven by a nuclear cluster reaches the virial radius before it transitions to the energy-driven phase that allows it to escape, so it cannot achieve the blow out that sets the  $M$ - $\sigma$  relation. However, we have shown that both momentum-

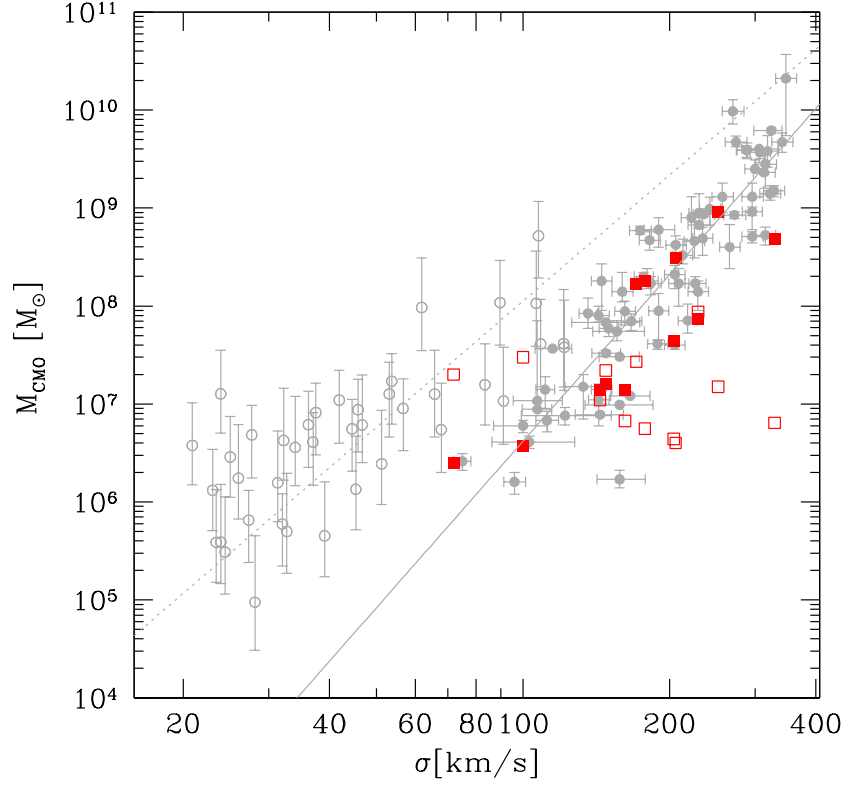


Figure 6.2: The mass of the central object,  $M_{\text{CMO}}$ , plotted against the velocity dispersion,  $\sigma$ , of the galaxy bulges averaged within the effective radius,  $R_e$ . The filled (grey) circles represent SMBHs from the compilation of McConnell & Ma (2013) and the solid (grey) line shows their best fit. The open (grey) circles show the nuclear clusters from Ferrarese et al. (2006) and the dotted (grey) line shows their best fit to their data. The (red) squares represent galaxies from the compilation of Scott & Graham (2013), which host both NCs and SMBHs. The open (red) squares show the nuclear cluster masses and the filled (red) squares show the black hole masses in the Scott & Graham (2013) sample.

and energy-driven shells in non-isothermal haloes are able to accelerate at large radius, overcoming this difficulty.

Nayakshin, Wilkinson & King (2009) discuss the observation that most nuclear clusters have masses  $\lesssim 10^8 M_\odot$  while SMBHs often have masses  $\gtrsim 10^8 M_\odot$ . They suggest

that this change over from nuclear cluster to SMBH dominated galaxies reflects a competition between the NC and SMBH feedback. When one of these objects reaches their  $M-\sigma$  mass it drives away the gas fuelling its growth and the growth of its ‘competitor’. This then leaves the competitor underweight with respect to its  $M-\sigma$  mass.

In detail, Nayakshin et al. (2009) rely on the different timescales on which the black holes and nuclear clusters evolve. The black hole growth is governed by the Salpeter timescale

$$t_{\text{Salp}} = \frac{M_{\text{BH}}}{\dot{M}_{\text{Edd}}} = \frac{M_{\text{BH}} \eta c^2}{L_{\text{Edd}}} = 4.5 \times 10^7 \text{ yr} \left( \frac{\eta}{0.1} \right). \quad (6.8)$$

This is a lower limit as the timescale will increase if the black hole is accreting at a sub-Eddington rate.

Star formation occurs on the free-fall or dynamical time of the system

$$t_{\text{dyn}} = \frac{r_s}{\sigma} = 4.9 \times 10^6 \text{ yr} \left( \frac{r_s}{\text{kpc}} \right) \left( \frac{\sigma}{200 \text{ km s}^{-1}} \right)^{-1} \quad (6.9)$$

where  $r_s$  and  $\sigma$  are the scale length and velocity dispersion of the bulge. Whether this dynamical time is applicable to nuclear clusters on scales  $\lesssim 10\text{pc}$  is unclear, especially given the debate over their formation mechanism, as discussed in Chapter 1. In this case, Nayakshin et al. (2009) estimate the dynamical time as a function of velocity dispersion using the observed scaling relations  $L-r_s$  and  $L-\sigma$  where  $L$  is the total luminosity of stellar spheroid. These relations are projections of the two-dimensional plane occupied by stellar spheroids in the space defined by  $L$ ,  $r_s$  and  $\sigma$ , known as the Fundamental Plane.

By relating the dynamical time to the velocity dispersion, Nayakshin et al. (2009) find  $t_{\text{Salp}} > t_{\text{dyn}}$  in bulges with  $\sigma \lesssim 150\text{km s}^{-1}$  so that the nuclear cluster evolves more quickly than the black hole. In this case feedback from the NC clears the gas from the nucleus cutting off fuel to the SMBH. In larger bulges with  $\sigma \gtrsim 150\text{km s}^{-1}$  they find  $t_{\text{Salp}} < t_{\text{dyn}}$ . In this case the black hole grows quickly to its  $M-\sigma$  mass and while nuclear clusters may also exist in the nucleus their feedback becomes negligible and they are underweight in the bulge.

This scenario fits with the galaxies in the Scott & Graham (2013) sample which host both an SMBH and a nuclear cluster. Figure 6.2 shows that in galaxies with  $\sigma \gtrsim 150 \text{ km s}^{-1}$  the black holes in the Scott & Graham data (filled red squares) lie on the  $M$ - $\sigma$  relation defined by the McConnell & Ma (2013) data, while the nuclear clusters (open red squares) are underweight with respect to the  $M$ - $\sigma$  relation of Ferrarese et al. (2006). For the two galaxies with  $\sigma \lesssim 150 \text{ km s}^{-1}$ , though the black hole masses do fall on the  $M_{\text{BH}}$ - $\sigma$  relation of McConnell & Ma, they are less massive than nuclear clusters which lie on the  $M_{\text{NC}}$ - $\sigma$  relation of Ferrarese et al.

As such, it is not really appropriate to define an  $M_{\text{NC}}$ - $\sigma$  relation that includes these underweight nuclear clusters from galaxies where self-regulated feedback from an SMBH is likely to be setting the  $M$ - $\sigma$  relation.

## 6.6 Open questions and future work

Our results predict relations between CMO masses and the properties of the dark matter haloes of their host galaxies. In comparing our predicted relations to the observed relations we have associated the velocity dispersion,  $\sigma_0$ , with the observed stellar velocity dispersion,  $\sigma_{\text{eff}}$ , and the peak circular speed of the dark matter halo,  $V_{\text{c,pk}}$ , with the asymptotic circular speed,  $V_{\text{c,a}}$ . By doing so we find that our relations that result from momentum-driven outflows lie a factor  $\sim 3 - 4$  above the observed  $M_{\text{BH}}$ - $\sigma$  relation of Gültekin et al. (2009) and the  $M_{\text{BH}}$ - $V_{\text{c,a}}$  relation of Volonteri et al. (2011). The  $M$ - $\sigma$  relation that results from energy-driven feedback is within a factor of a few of the most recent compilation of the  $M_{\text{BH}}$ - $\sigma$  relation of McConnell & Ma (2013).

However, it is important to find the correct relations between the theoretical and observed quantities which will be dependent on the choice of dark matter halo. The theoretical quantities we use are three dimensional. It would be of interest to calculate how quantities such as the 3D velocity dispersion translates to observable, line-of-sight velocity dispersion and the effect this might have on the predicted  $M$ - $\sigma$  relation.

We, like other authors, have also assumed that the gas traces the dark matter

directly, though our general equations of motion allow for the segregation of gas and dark matter through the function  $h(r)$ , which describes how the gas traces the dark matter. The gas in a galaxy will cool and condense to become more centrally concentrated than the dark matter. In comparison to our model the swept-up shell in this case would be more massive at a given small radius which could make it more difficult for the CMO to drive it to escape. On the other hand, for a shell of a given mass there would be less dark matter inside than in our model where the gas traces the dark matter directly, which could make it easier to escape. A detailed treatment of the case when  $h(r) \neq 1$  would be required to find out whether the expected scalings for momentum- and energy-driven feedback would survive.

As mentioned previously, additional sources of momentum input could be important in establishing the  $M$ - $\sigma$  relation, such as from star formation triggered by the outflow, as proposed by Silk & Nusser (2010) who object to a transition to energy-driving. Although they also do not consider energy-driving, Sharma & Nath (2013) have noted that feedback from star clusters distributed through the galaxy could also have an effect on the galaxy outflow, though such a mechanism cannot be modelled analytically. This kind of positive feedback would aid in the escape of the shell and possibly reduce the CMO mass required to drive the shell to escape.

The self-regulated feedback scenario would certainly benefit from a fully time-dependent treatment, which could address several issues. Firstly, we have assumed the CMO mass and associated wind thrust remain constant throughout the motion of the shell. Zubovas & King (2012) consider the case of a wind speed  $v_w \simeq 0.1c$  and a black hole that has grown to the critical mass in equation (6.1) during a momentum-conserving phase and then switches to an energy-driven regime. When in the energy-driven phase they allow the black hole mass to grow at the Eddington rate for two Salpeter times, then the SMBH becomes inactive. In the case of a shell moving out into an isothermal galaxy they find that the shell velocity is almost constant, only increasing in response to the black hole growth. For this  $M_{\text{BH}}$  and  $v_w$ , in the time-independent case we find the shell coasts at  $\sim 4.23\sigma_0$ , which is  $\sim 900\text{km s}^{-1}$  in a halo with  $\sigma = 200\text{km s}^{-1}$ . This appears to be consistent with Zubovas & King whose Figure

1 (left column, middle and bottom panels) shows a shell in an isothermal with a velocity that reaches  $\sim 900\text{km s}^{-1}$  and slowly increases until the AGN switches off.

If SMBHs grow from smaller seeds, then a swept up shell may already be at large radius by the time the SMBH reaches the critical mass that allows the shell to escape. Then it is a question of how much more can the SMBH grow before the shell is driven to escape. Also in this kind of scenario, the black hole growth and increasing wind thrust could prevent a momentum-conserving shell driven by a low mass black hole from stalling before it can become energy-driven, perhaps reducing the normalisation of the  $M$ - $\sigma$  relation.

In the nuclear cluster case we have assumed that the feedback from the cluster is instantaneously ‘switched on’ and stays on. As in the black hole case, we have also assumed that the associated wind thrust remains constant throughout the motion of the shell. It could be that initially the feedback has to build up to the constant value that we have used throughout our analysis. If this is the case, the wind can begin to sweep up and drive out a shell before it reaches the constant wind thrust value. The feedback of the nuclear cluster is also limited by the lifetime of the stars that contribute to the superwind. As the cluster evolves the wind thrust will be reduced and the creation of more massive stars would be required to maintain a roughly constant wind thrust. As in the black hole case, it may be that additional feedback from star formation aids the escape of the shell. In a time-dependent treatment, the detailed evolution of the cluster could be applied, allowing us to better estimate a short fall in the momentum required to drive the shell to escape. Including a detailed treatment of the cooling processes would also allow us to identify any change to an energy-driven regime and whether, as is argued in the simpler case of constant wind thrust, a transition could alleviate some of this difficulty.

A key question in the self-regulated feedback scenario is still whether the outflow conserves momentum or energy. The on going discussion regarding the slope of the observed  $M$ - $\sigma$  relations (e.g., for nuclear clusters: Ferrarese et al. 2006; Scott & Graham 2013; for black holes Gültekin et al. 2009; McConnell & Ma 2013) adds to the uncertainty in the feedback mechanism.

A time-dependent analysis including the detailed cooling in both the nuclear cluster and the black hole case would allow further investigation into the driving mechanism of the shell in each case. This would also address some of the other issues discussed above such as the time-dependence and lifetime of the wind thrust. By translating the relations derived in such an analysis into observable quantities would allow us to see how close the self-regulated feedback scenario comes to describing the observed  $M$ - $\sigma$  relations.

# Publications

## Refereed

McQuillin R. C., McLaughlin D. E., 2012, MNRAS, 423, 2162, '*Momentum-driven feedback and the  $M-\sigma$  relation in non-isothermal galaxies*'.

McQuillin R. C., McLaughlin D. E., 2013, MNRAS, 434, 1332, '*Black hole wind speeds and the  $M-\sigma$  relation*'.

## Conference Proceedings

McQuillin R. C., McLaughlin D. E., 2012, ASPC, 460, 256, '*Momentum-driven feedback and the  $M-\sigma$  relation in non-isothermal galaxies*', proceedings of *AGN Winds in Charleston* held October 2011.

## Bibliography

- Baade W., Minkowski R., 1954, ApJ, 119, 206
- Baade W., Minkowski R., 1954, ApJ, 119, 215
- Baade W., 1944, ApJ, 100, 147
- Babul A., Rees M. J., 1992, MNRAS, 255, 346
- Baes M., Buyle P., Hau G. K. T., Dejonghe H., 2003, MNRAS, 341, L44
- Bautista M. A., Dunn J. P., Arav N., Korista K. T., Moe M., Benn C., 2010, ApJ, 713, 25
- Binggeli B., Sandage A., Tammann G. A., 1985, AJ, 90, 1681
- Binggeli B., Tammann G. A., Sandage A., 1987, AJ, 94, 251
- Binney J., Tremaine S., 2008, Galactic Dynamics, Princeton University Press, Second Edition edition
- Böker T., Laine S., van der Marel R. P., Sarzi M., Rix H.-W., Ho L. C., Shields J. C., 2002, AJ, 123, 1389
- Böker T., Sarzi M., McLaughlin D. E., van der Marel R. P., Rix H.-W., Ho L. C., Shields J. C., 2004, AJ, 127, 105
- Bothun G. D., Mould J. R., 1988, ApJ, 324, 123
- Bryan G. L., Norman M. L., 1998, ApJ, 495, 80
- Bullock J. S., Kolatt T. S., Sigad Y., Somerville R. S., Kravtsov A. V., Klypin A. A., Primack J. R., Dekel A., 2001, MNRAS, 321, 559
- Burkert A., 1995, ApJL, 447, L25

- Burstein D., 1982, *ApJ*, 253, 539
- Caldwell N., Bothun G. D., 1987, *AJ*, 94, 1126
- Cappellari M., Bacon R., Bureau M., Damen M. C., Davies R. L., de Zeeuw P. T., Emsellem E., Falcón-Barroso J., Krajnović D., Kuntschner H., McDermid R. M., Peletier R. F., Sarzi M., van den Bosch R. C. E., van de Ven G., 2006, *MNRAS*, 366, 1126
- Carollo C. M., Stiavelli M., de Zeeuw P. T., Mack J., 1997, *AJ*, 114, 2366
- Carollo C. M., Stiavelli M., Mack J., 1998, *AJ*, 116, 68
- Castor J., McCray R., Weaver R., 1975, *ApJL*, 200, L107
- Côté P., Blakeslee J. P., Ferrarese L., Jordán A., Mei S., Merritt D., Milosavljević M., Peng E. W., Tonry J. L., West M. J., 2004, *ApJS*, 153, 223
- Côté P., Piatek S., Ferrarese L., Jordán A., Merritt D., Peng E. W., Hasegan M., Blakeslee J. P., Mei S., West M. J., Milosavljević M., Tonry J. L., 2006, *ApJS*, 165, 57
- Côté P., Ferrarese L., Jordán A., Blakeslee J. P., Chen C.-W., Infante L., Merritt D., Mei S., Peng E. W., Tonry J. L., West A. A., West M. J., 2007, *ApJ*, 671, 1456
- Debuhr J., Quataert E., Ma C.-P., 2012, *MNRAS*, 420, 2221
- Dehnen W., McLaughlin D. E., 2005, *MNRAS*, 363, 1057
- Dehnen W., McLaughlin D. E., Sachania J., 2006, *MNRAS*, 369, 1688
- Dopita M. A., Sutherland R. S., 2003, *Astrophysics of the Diffuse Universe*, Springer, First Edition edition
- Dubinski J., Carlberg R. G., 1991, *ApJ*, 378, 496
- Emsellem E., van de Ven G., 2008, *ApJ*, 674, 653

- Fabian A. C., 1999, MNRAS, 308, L39
- Faucher-Giguère C.-A., Quataert E., 2012, MNRAS, 425, 605
- Ferguson H. C., Sandage A., 1989, ApJL, 346, L53
- Ferguson H. C., Sandage A., 1990, AJ, 100, 1
- Ferrarese L., Ford H., 2005, Sp. Sci. Rev., 116, 523
- Ferrarese L., Merritt D., 2000, ApJL, 539, L9
- Ferrarese L., 2002, ApJ, 578, 90
- Ferrarese L., Côté P., Dalla Bontà E., Peng E. W., Merritt D., Jordán A., Blakeslee J. P., Haşegan M., Mei S., Piatek S., Tonry J. L., West M. J., 2006, ApJL, 644, L21
- Filippenko A. V., Ho L. C., 2003, ApJL, 588, L13
- Gebhardt K., Bender R., Bower G., Dressler A., Faber S. M., Filippenko A. V., Green R., Grillmair C., Ho L. C., Kormendy J., Lauer T. R., Magorrian J., Pinkney J., Richstone D., Tremaine S., 2000, ApJL, 539, L13
- Gerhard O., Kronawitter A., Saglia R. P., Bender R., 2001, AJ, 121, 1936
- Ghez A. M., Salim S., Weinberg N. N., Lu J. R., Do T., Dunn J. K., Matthews K., Morris M. R., Yelda S., Becklin E. E., Kremenek T., Milosavljevic M., Naiman J., 2008, ApJ, 689, 1044
- Gofford J., Reeves J. N., Tombesi F., Braitto V., Turner T. J., Miller L., Cappi M., 2013, MNRAS, 430, 60
- Graham A. W., Spitler L. R., 2009, MNRAS, 397, 2148
- Gültekin K., Richstone D. O., Gebhardt K., Lauer T. R., Tremaine S., Aller M. C., Bender R., Dressler A., Faber S. M., Filippenko A. V., Green R., Ho L. C., Kormendy J., Magorrian J., Pinkney J., Siopis C., 2009, ApJ, 698, 198

- Haehnelt M. G., Natarajan P., Rees M. J., 1998, MNRAS, 300, 817
- Harms R. J., Ford H. C., Tsvetanov Z. I., Hartig G. F., Dressel L. L., Kriss G. A., Bohlin R., Davidsen A. F., Margon B., Kochhar A. K., 1994, ApJL, 435, L35
- Hernquist L., 1990, ApJ, 356, 359
- Ho L. C., 2007, ApJ, 668, 94
- Hodge P. W., 1963, AJ, 68, 691
- Hodge P. W., 1973, ApJ, 182, 671
- Jennison R. C., Das Gupta M. K., 1953, Nature, 172, 996
- Jordán A., Blakeslee J. P., Côté P., Ferrarese L., Infante L., Mei S., Merritt D., Peng E. W., Tonry J. L., West M. J., 2007, ApJS, 169, 213
- King A. R., Pounds K. A., 2003, MNRAS, 345, 657
- King A., 2003, ApJL, 596, L27
- King A., 2005, ApJL, 635, L121
- King A. R., 2010, MNRAS, 408, L95
- King A. R., Zubovas K., Power C., 2011, MNRAS, 415, L6
- Koo B.-C., McKee C. F., 1992, ApJ, 388, 103
- Kormendy J., Bender R., 2011, Nature, 469, 377
- Kormendy J., Richstone D., 1995, Annu. Rev. Astron. Astrophys., 33, 581
- Kormendy J., Bender R., Cornell M. E., 2011, Nature, 469, 374
- Kronawitter A., Saglia R. P., Gerhard O., Bender R., 2000, A&AS, 144, 53

- Lamers H. J. G. L. M., Cassinelli J. P., 1999, *Introduction to Stellar Winds*, Cambridge University Press, First Edition edition
- Longair M. S., 2011, *High Energy Astrophysics*, Cambridge University Press, Third Edition edition
- Magorrian J., Tremaine S., Richstone D., Bender R., Bower G., Dressler A., Faber S. M., Gebhardt K., Green R., Grillmair C., Kormendy J., Lauer T., 1998, *AJ*, 115, 2285
- McConnell N. J., Ma C.-P., 2013, *ApJ*, 764, 184
- McLaughlin D. E., King A. R., Nayakshin S., 2006, *ApJL*, 650, L37
- McMillan P. J., 2011, *MNRAS*, 414, 2446
- McQuillin R. C., McLaughlin D. E., 2012, *MNRAS*, 423, 2162
- McQuillin R. C., McLaughlin D. E., 2013, *MNRAS*, in press
- Merrifield M. R., Forbes D. A., Terlevich A. I., 2000, *MNRAS*, 313, L29
- Merritt D., Ferrarese L., 2001, *MNRAS*, 320, L30
- Milosavljević M., 2004, *ApJL*, 605, L13
- Monaco P., Salucci P., Danese L., 2000, *MNRAS*, 311, 279
- Murray N., Quataert E., Thompson T. A., 2005, *ApJ*, 618, 569
- Navarro J. F., Frenk C. S., White S. D. M., 1996, *ApJ*, 462, 563
- Nayakshin S., Wilkinson M. I., King A., 2009, *MNRAS*, 398, L54
- Ostriker J. P., Peebles P. J. E., Yahil A., 1974, *ApJL*, 193, L1
- Padovani P., Burg R., Edelson R. A., 1990, *ApJ*, 353, 438

- Phillips A. C., Illingworth G. D., MacKenty J. W., Franx M., 1996, *AJ*, 111, 1566
- Pounds K. A., Reeves J. N., King A. R., Page K. L., O'Brien P. T., Turner M. J. L., 2003, *MNRAS*, 345, 705
- Redman R. O., Shirley E. G., 1938, *MNRAS*, 98, 613
- Reeves J. N., O'Brien P. T., Ward M. J., 2003, *ApJL*, 593, L65
- Rossa J., van der Marel R. P., Böker T., Gerssen J., Ho L. C., Rix H.-W., Shields J. C., Walcher C.-J., 2006, *AJ*, 132, 1074
- Rubin V. C., Ford W. K. J., Thonnard N., 1980, *ApJ*, 238, 471
- Rupke D. S. N., Veilleux S., 2011, *ApJL*, 729, L27
- Salpeter E. E., 1964, *ApJ*, 140, 796
- Sandage A., Binggeli B., 1984, *AJ*, 89, 919
- Sargent W. L. W., Young P. J., Lynds C. R., Boksenberg A., Shortridge K., Hartwick F. D. A., 1978, *ApJ*, 221, 731
- Schneider P., 2006, *Extragalactic Astronomy and Cosmology*, Springer, First Edition edition
- Scott N., Graham A. W., 2013, *ApJ*, 763, 76
- Seth A., Agüeros M., Lee D., Basu-Zych A., 2008, *ApJ*, 678, 116
- Seyfert C. K., 1943, *ApJ*, 97, 28
- Sharma M., Nath B. B., 2013, *ApJ*, 763, 17
- Shields J. C., Walcher C. J., Böker T., Ho L. C., Rix H.-W., van der Marel R. P., 2008, *ApJ*, 682, 104
- Silk J., Nusser A., 2010, *ApJ*, 725, 556

- Silk J., Rees M. J., 1998, *A&A*, 331, L1
- Stinson G. S., Brook C., Prochaska J. X., Hennawi J., Shen S., Wadsley J., Pontzen A., Couchman H. M. P., Quinn T., Macciò A. V., Gibson B. K., 2012, *MNRAS*, 425, 1270
- Sturm E., González-Alfonso E., Veilleux S., Fischer J., Graciá-Carpio J., Hailey-Dunsheath S., Contursi A., Poglitsch A., Sternberg A., Davies R., Genzel R., Lutz D., Tacconi L., Verma A., Maiolino R., de Jong J. A., 2011, *ApJL*, 733, L16
- Sutherland R. S., Dopita M. A., 1993, *ApJS*, 88, 253
- Tombesi F., Cappi M., Reeves J. N., Palumbo G. G. C., Braitto V., Dadina M., 2011, *ApJ*, 742, 44
- Tombesi F., Cappi M., Reeves J. N., Nemmen R. S., Braitto V., Gaspari M., Reynolds C. S., 2013, *MNRAS*, 430, 1102
- Tremaine S., Gebhardt K., Bender R., Bower G., Dressler A., Faber S. M., Filippenko A. V., Green R., Grillmair C., Ho L. C., Kormendy J., Lauer T. R., Magorrian J., Pinkney J., Richstone D., 2002, *ApJ*, 574, 740
- Tremonti C. A., Moustakas J., Diamond-Stanic A. M., 2007, *ApJL*, 663, L77
- Tumlinson J., Thom C., Werk J. K., Prochaska J. X., Tripp T. M., Weinberg D. H., Peebles M. S., O'Meara J. M., Oppenheimer B. D., Meiring J. D., Katz N. S., Davé R., Ford A. B., Sembach K. R., 2011, *Science*, 334, 948
- Volonteri M., Natarajan P., Gültekin K., 2011, *ApJ*, 737, 50
- Walcher C. J., van der Marel R. P., McLaughlin D., Rix H.-W., Böker T., Häring N., Ho L. C., Sarzi M., Shields J. C., 2005, *ApJ*, 618, 237
- Weaver R., McCray R., Castor J., Shapiro P., Moore R., 1977, *ApJ*, 218, 377
- Wehner E. H., Harris W. E., 2006, *ApJL*, 644, L17

Yu Q., Tremaine S., 2002, MNRAS, 335, 965

Zubovas K., King A. R., 2012, MNRAS, 426, 2751